MIXING CHARACTERISTICS AND MECHANICAL PROPERTIES OF CAST Al (Mg)—Al$_2$O$_3$ PARTICULATE COMPOSITE

A THESIS

submitted in fulfilment of the
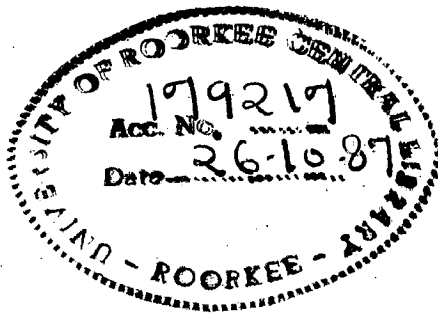requirements for the award of the degree
of
DOCTOR OF PHILOSOPHY
in
METALLURGICAL ENGINEERING

By

PRAKRITI KUMAR GHOSH

DEPARTMENT OF METALLURGICAL ENGINEERING
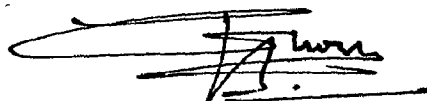UNIVERSITY OF ROORKEE
ROORKEE-247 667 (INDIA)

July, 1986

CANDIDATE'S DECLARATION

I hereby certify that the work which is being presented in the thesis entitled 'MIXING CHARACTERISTICS AND MECHANICAL PROPERTIES OF CAST Al(Mg)-Al$_2$O$_3$ PARTICULATE COMPOSITE' in fulfilment of the requirement for the award of the degree of Doctor of Philosophy, submitted in the Department of METALLURGICAL ENGINEERING of the University is an authentic record of my own work carried out during a period from March 1983 to July 1986 under the supervision of Dr. S.Ray.

The matter embodied in this thesis has not been submitted by me for the award of any other degree.

Dated: July 14th, 1986

(PRAKRITI KUMAR GHOSH)

This is to certify that the above statement made by the candidate is correct to the best of my knowledge.

(S.RAY)
READER
DEPTT OF METALLURGICAL ENGINEERING,
UNIVERSITY OF ROORKEE,
ROORKEE-247 667 U.P.

A B S T R A C T

Aluminium alloy particulate composites have received wide spread attention from the technologists due to its improved specific strength (strength/unit weight) and stiffness especially at elevated temperatures. A number of processes have been tried so far to fabricate these particulate composites but the foundry technique has been considered as a more direct and simpler one as compared to other techniques used. However, the primary difficulties in making cast composites by the vortex method are to attain a significant retention of particles, their homogeneous distribution in the matrix and reproducible characteristics. The maintenance of suitable mixing conditions during agitation of a partially solid aluminium alloy is necessary to surmount the present difficulties. However, no systematic investigation of the parameters influencing the mixing had been undertaken.

The mechanical properties of the compocast particulate composites are very much sensitive to the volume fraction of porosity, the particle content, their shape, size and distribution in the matrix. The shape, size and the distribution of porosity can not be fully controlled during the casting process. It is common practice to correlate the mechanical properties of the cast materials directly to the volume fraction of porosity. However, the role of particle porosity interaction in cast particulate composites influencing its mechanical properties at ambient and elevated temperatures have not been clearly understood.

In this study an effort has been made to optimise the mixing parameters for the incorporation of alumina particles in partially solid aluminium alloy melt so as to achieve the maximum incorporation of the particles and a homogeneous distribution. The role of porosity in reducing the ambient and elevated temperature strength of the cast particulate composites has been investigated with the help of a phenomenological model and the experimental results. The adverse contribution of porosity on the strength has been estimated in the cast composites having different volume fraction of alumina particles with narrow and broad spectrum of sizes. The projected ultimate tensile strength at zero porosity level has been determined with the help of the model. The effect of porosity content on the engineering fracture strain of the composites containing different levels of alumina content has been found out at ambient and elevated temperatures.

The detailed perspective of the problem under investigation has been introduced in chapter 1. The critical review of the literature on the variations of vortex method used for making cast particulate composite e.g., liquid metal process, partially solid melt process (compocasting) have been explained in chapter 2. The chapter 2 also contains a review of the mechanical properties of the composites.

In chapter 3 the experimental method used to study the relevant process parameters influencing the fabrication of particulate composite in the vortex method and the procedure for characterisation of the mechanical properties have been

described. The particulate composites have been prepared by adding pre-heated (1072K) alumina particles of narrow and wide spectrum of sizes from the top to the vortex of the vigorously agitated freshly alloyed aluminium-4wt.%Mg alloy at a given holding temperature. The slurry has been cast through bottom pouring and the ingot has been quenched by spraying water on it. The chemical composition of the composites has been determined by spectrographic analysis. The volume fraction of alumina particles and the porosity in each casting has been estimated by determining density by weight loss method and point counting under optical microscope. The impact of process parameters like the holding temperature of the melt, the speed of stirring, the size and the position of the impeller inside the melt on the retention of alumina particles in the cast composites and its porosity content has been investigated. Flat four blade impellers of different sizes have been used. The microstructures of the cast composites have been studied under optical microscope with a view to determine the roles of various process parameters. The particle-matrix interface has been of particular interest for observations under scanning electron microscope (SEM). The composites have been analysed by X-ray diffraction to detect products of interfacial reaction between the particles and the alloy.

Mechanical properties of the composites have been investigated under tension at ambient and elevated temperatures by taking samples from different positions of the ingots. The volume fraction of alumina and the porosity content of each

specimen have been determined. The effects of true strain and porosity on the nucleation and growth of voids during testing under tension at ambient temperature have been estimated under SEM. The fractured, surface of the specimens have been investigated under SEM.

Chapter 4 deals with the influence of holding temperature, stirring speed, the diameter and the position of the impeller on the particle retension, porosity content and the particle-matrix interface in the cast composites. The retention of alumina particles in the cast composites has been found to increase with the decrease in melt temperature between the liquidus (915K) and the solidus (875K) temperature of Al-4wt.%Mg alloy for a given stirring speed, diameter and position of the impeller. However at the holding temperature below 883K the casting of the slurry has been found extremely difficult. The retention of alumina particle in the partially solid alloy at 900K has been found to increase initially with the increase in the stirring speed, the diameter and the position of the impeller from the bottom of the crucible 'upto a certain value followed by a decrease with further increase in the values of these parameters. The optimum values of the stirring speed, the diameter of the impeller and the position of the impeller for the maximum retention of alumina particles (~ 12.5 wt.%) in the partially solid aluminium alloy at a temperature of 900K have been found as ~ 16 revolution.s^{-1}, 0.63D and 0.81H respectively where D is the diameter of the melt surface at rest and H is the height of the melt at rest from the bottom of the crucible. A deviation in mixing parameters from the

optimum value has been found to result in a significant clustering of alumina particles in the matrix. The various features of the retention of alumina particles in the matrix resulting from different mixing conditions are evident from the micrographs of different castings.

The analysis of the mixing process carried out with the help of a model expression correlating the various parameters of a concentrically agitated liquid system influencing the liquid profile in the vessel shows that in all the choices of process parameters in this work the impeller surface has been exposed except during mixing at the holding temperature of 883K. The exposing of the impeller has been found to play a helpful role in retaining the particles in the agitated slurry. However, the retention of particles has been found to be controlled by the radius of the cylindrically rotating zone (c.r.z.), r_c, which increases with the increase in the diameter of the impeller at a given holding temperature. The retention of particles in the slurry increases so long as r_c remains below r_3, the radius of the central region of the impeller excluding the blades. In case of low holding temperature of 883K a large retention of alumina inside the melt without any exposure of the impeller may have been possible due to mechanical entrapping of the particles.

The influence of the holding temperature, the stirring speed, the diameter and the position of the impeller inside the melt on the microstructures observed at the bottom and the

top of the castings show that under all the combinations of mixing parameters a tendency to form a dendritic microstructure is always there especially at the top of the ingot. The extent of the dendritic growth at the top of the ingot has increased with a reduced holding temperature, stirring speed and size of the impeller. During pouring the stirring was on and the slurry from the central regions of the crucible has come out first through the bottom hole of the crucible followed by the slurry from the side of the crucible wall which may have undergone a limited dendritic growth in the boundary layer. In the composites fabricated at a lower holding temperature of 883K the zones of coarse dendrite and large primary solid particles have been observed having no alumina particles entrapped in this region.

An examination of microstructure also reveals a reacted layer at the boundry of the alumina particles. The thickness of this reacted layer reduces with an increase in the stirring speed and the holding temperature. It has been attributed to detachment of the reacted layer from particle (caused by stirring) due to its viscous liquid nature. This effect is reduced with a reduction of the stirring speed. Lower fluidity at a lower holding temperature also counters the tendency of detachment. The reacted layers are of irregular shape in the composite and often cracks during solidification as it has been observed in the microstructures under scanning electron microscope.

The cold model experiments have been conducted with water and poorly wetting plastic beads to observe visually the role of stirring speed and the size of the impeller on the particle retention. It has been noticed that the deviation of these parameters from the optimum level cause either non-immersion or rejection of the particles and sometimes, even accumulation of the particles at the bottom of the impeller. The observations of the cold model experiments have been found to be in qualitative agreement with the results obtained in the cast composites.

The porosity in the composites has been found to increase initially with the increase in stirring speed, the diameter of the impeller and its distance from the bottom of the crucible upto a certain value followed by a decrease with a further increase in these process variables. However, the porosity of the composites has always been found to increase with the decrease in holding temperature of the melt. It is interesting to note that the porosity in the composites increases linearly with the level of retention of alumina. The increase in porosity in a composite is accompanied with a larger inhomogeneity in the distribution of particles. The scanning electron microscopic observation on the microstructures of the composites shows the presence of pores primarily at the boundry of the primary solid particles. Some pores have also been observed inside the primary solid particles.

The influence of porosity and alumina content on the mechanical properties of compocast Al-4wt.%Mg + alumina particulate composites at ambient and elevated temperatures are presented in chapter 5. The contribution of porosity on the reduction of the strength of the composite at various levels of alumina content has been expressed as a linear function of porosity with two experimentally determined parameters, σ_0 , the ultimate tensile strength at zero porosity and α , a weakening factor, as

$$\sigma_p / \sigma_0 = 1 - \alpha P$$

where, σ_p is the tensile strength of the composite at the volume percent porosity P, in the composite.

At ambient temperature the weakening effect of porosity expressed as α has been found to decrease significantly with the increase in alumina content (with wide spectrum of sizes) of the composite upto ~ 7 vol.%. But the rate of reduction slows down at higher alumina levels in the composite. With α , the corresponding values of σ_0 also follow a similar trend of reduction with an increase in the alumina content. For a given alumina content the increase in average particle size from 22 μm to 115 μm has been found to push the value of α a little up followed by a significant decrease with a further increase in the particle size upto 195 μm. However, the increase in average particle size from 22 μm to 195 μm has always been found to reduce the value of σ_0 . The behaviour of the curve for σ_0 versus alumina content of the composite

obtained with the help of model equation has been found in agreement to the trend of variation in ultimate tensile strength of a composite with its alumina content for a given level of porosity.

The role of porosity on the engineering fracture strain, e_f, of the composite has been found to increase almost linearly with the inverse of porosity beyond a critical level of porosity. The fracture of the composite within this linear regime of high porosity content has been caused primarily by the growth and coalescence of the existing pores along with some nucleated voids in the matrix as evident from scanning electron micrographs. In the region of lower porosity beyond the critical level the fracture of the composite is possibly dominated by the nucleation of voids by particle debonding and their coalescence. The wide spread debonding has been reflected in the observed serrations in tensile stress-strain curve of the composite. The critical level of the inverse of porosity below which the linear behaviour of e_f versus P^{-1} is observed increases with the decrease in alumina content of the composite and the composite having higher alumina content shows a linear behaviour upto a lower e_f value. This may have been due to lower strain for void nucleation, ϵ_N, caused by a decrease in particle content has resulted into new voids assuming a primary role in the fracture of composites with high alumina content.

At elevated temperatures of 473 K and 573 K the weakening factor, α , has been found to decrease with an increase in the

volume fraction of alumina in the composite similar to that observed at ambient temperature. But, here, α is more sensitive to the alumina content of the composite. The weakening factor in a composite increases significantly with the increase of temperature but this effect gradually reduces with an increase in the alumina content of the composite. Finally, in a composite having $\sim$ 10.3 Vol.% alumina the weakening factor, α , reduces with an increase in the temperature. The tensile strength at zero porosity level, σ_0, of the composite estimated at elevated temperatures has been found to reduce with the increase of alumina content upto a certain level ($\sim$ 9 vol.%) similarly as it has been observed at ambient temperature. In contrast to the observations at the ambient temperature a sharp fall of σ_0 has been observed at higher alumina contents at the elevated temperature of 473K and 573K. The σ_0 of a composite of a given alumina content does not vary significantly with the increase in temperature upto about 473K but drops sharply with a further increase in temperature. This reduction in tensile strength at zero porosity, σ_0, is attributed to dynamic recrystalisation of the matrix under tensile deformation. The tendency to recrystallisation has been found comparatively more in the matrix around the alumina particles which may have caused a sharp fall in σ_0 at a higher alumina level of about 10 Vol.%.

An increase in the porosity level has been found to reduce the engineering fracture strain, e_f, of a composite at elevated temperature and this effect is more pronounced

at higher particle content of the composite. At a given porosity level the engineering fracture strain of a composite decreases with an increase in the temperature. At elevated temperatures the fracture of the composite has been marked by the growth and coalescence of voids at the boundary of primary solid particles and the recrystalised zones.

ACKNOWLEDGEMENT

also very much due to Mr. M.C.Vaish for neat tracing and drawing work and to Mr. Jamshed Ali for neatly typing of the thesis.

Special thanks are due to Mrs Mita Ghosh my wife for providing an efficient assistance and encouragement at every step in compilation work of this thesis.

Last but not the least, I express my gratitude to all my friends, relatives, parents and in-laws who have shown patience and keen interest in my work and contributed directly or indirectly towards this achievement.

Dated: JULY 14ᵗʰ, 1986.   (PRAKRITI KUMAR GHOSH)

LIST OF FIGURES

Fig.No.	Title	Page No.

LIST OF TABLES

NOMENCLATURE

ρ_s	Density of α -solid particles in partially solid Al-4 wt.% Mg alloy.
ρ_L	Density of the liquid Al-4 wt.% Mg alloy.
ρ_{slurry}	Average density of the partially solid Al-4 wt.% Mg alloy.
ρ_{Al-Mg}	Density of Al-4 wt.% Mg.
$\rho_{Al_2O_3}$	Density of Alumina powder.
ρ_{mes}	Density of particulate composite as measured.
ρ_{Th}	Theoretical density of particulate composite.
ρ_S'	Density of solid particles.
ρ_1'	Density of liquid in mixing vessel.
r	Radius measured from the axis of the impeller.
v	Liquid velocity in mixing vessel.
g	Acceleration due to gravity.
w	Weight of unit volume of liquid.
ω	Angular velocity.
c	Constant.
τ	Viscous force.
N_f	Critical agitator speed.
N	Impeller speed (r.p.m.)
n	Impeller speed (r.p.s.)
d	Impeller diameter
r_1	Radius of impeller
R_e	Reynolds number

H'	Impeller head
D'	Diameter of a cylindrical vessel
r_2	Radius of a cylindrical vessl
p'	Power consumption in mixing
C_O	mean alloy composition
T_L	Liquidus temperature
T_I	Initial temperature
T_H	Holding temperature
T_S	Solidus temperature
e	Electronic charge
ez	Ionic charge
s	Effective radius of the ion
D	Diameter of the crucible at the surface of the slurry
h	Height of the impeller from the bottom of the crucible
V	Volume of liquid in the vessel
r_c	Radius of the cylindrically rotating zone (C.R.Z.)
H	Depth of the slurry at rest in the crucible
h'	Depth of the impeller from surface of the slurry
t'	Thickness of the impeller
A_O	Initial cross sectional area of the tensile specimen
A_f	Final cross sectional area at different regions of the gauge length after fracture of specimen
η	Co-efficient of viscosity

η_{slurry}	Co-efficient of viscosity of the partially solid Al-4 wt.% Mg
θ	Contact angle
γ_{SV}	Solid-Vapour interfacial tension
γ_{LV}	Liquid-Vapour interfacial tension
γ_{LS}	Liquid-solid interfacial tension
W_A	Work of adhesion
σ_l	Surface tension of liquid
x	Reacted layer thickness
t	Residence time of alumina particles in the slurry
a	Constant
n'	Constant
d_p	Pressure difference
$\emptyset$	The volume fraction of primary solid particles in partially solid Al-4 wt.% Mg alloy
$V_{Al_2O_3}$	Volume fraction of alumina in the composite
V_v	Volume fraction of void in the composite
V_a	Volume fraction of void+volume fraction of alumina in the composite
V_{Al-Mg}	Volume fraction of matrix in the composite
$W_{Al_2O_3}$	Weight fraction of alumina in the composite
e	Engineering strain
ϵ	True strain
ϵ_N	True strain for void nucleation
ϵ_c	Uniform strain of the composite

σ_{disl}	Stress rise due to dislocation pile up
σ_{ah}	Increase in strength due to heat treatment
σ_{comp}	Predicted strengthening of the composite
$\sigma_{m\epsilon}$	Strength of the matrix at the failure strain of composite
β	Constant
ρ_1	Average dislocation density
ΔT	Under cooling
σ_m'	Hydrostatic stress
σ_{loc}	Local dislocation density
ν	Poisson's ratio of matrix
ν^*	Poisson's ratio of particle
β'	Ratio of Young's modulus of particle to that of matrix
σ_{loc}	Local stress
γ	Surface energy per unit area
r_4	Minor semi-axis of an ellipsoidal void
r_5	Major semi-axis of an ellipsoidal void
$\dot{r}_4$	Rate of increase of r_4
$\dot{r}_5$	Rate of increase of r_5
$\sigma_{m'}$	Mean stress
$\dot{\gamma}_a$	Factor describes the amplification of the growth rate of void relative to the strain rate of the matrix.
σ_c'	True tensile stress
σ_o'	Constant

ϵ_m	Uniform strain of the matrix
ϵ_p	Uniform strain of the particle
ϵ'_p	True tensile plastic strain
e_f	Engineering fracture strain at ambient temperature
e'_f	Elevated temperature engineering fracturestrain
d_v	Diameter of void
d_p	Diameter of particle
t_v	Thickness of void
$2\theta_2$	Angle of diffraction
$\bar{d}$	Interplanner spacing
λ	Wave length of X-ray
E_C	Young's modulus of the composite
E_A	Young's modulus of phase A
E_B	Young's modulus of phase B
V_A	Volume fraction of phase A
V_B	Volume fraction of phase B
σ_{yc}	Yield stress of the composite
σ_c	Theoretical ultimate tensile strength of a ccmposite
G_m	Shear modulus of the matrix
G_p	Shear modulus of the particle
d_1	Average particle diameter
b	Burger's vector of the matrix dislocation
c'	Constant
c''	Constant

$\dot{\epsilon}$ Tensile strain rate

$\bar{\epsilon}$ Average strain rate

ϵ_g Strain required for growth of void

σ_p Ultimate tensile strength of the composite containing P% porosity.

σ_o Ultimate tensile strength of pore free composite

α Weakening factor

R_p Radius defining weakened zone

r_p' Average effective radius of pore on a planar section

n_1 Constant

k Constant

σ_m'' Stress in region unaffected by pore

P_c Critical porosity level

P Porosity (volume percent)

R Average cell radius

N_A Number of pores per unit area

R_v Average effective radius of pore

F Tensile force acting on a specimen

$f(r')$ Functional form of the force carried out by unit area of the material

m	Generalized moment
s	Effective radius of ion
θ', θ''	Limiting values of θ
α'	Angle between the horizontal surface of the substrate and the direction of γ_{LS}
α''	Limiting value of α'
ΔG_T	Gibb's free energy
a_{Mg}	Value of equilibrium
p_{O_2}	Partial pressure of oxygen
ρ'	Density of liquid
z	Height of a point on the liquid profile at the top from the bottom of the vessel.
z_o	Height of the lowest point of the liquid profile at the top from the bottom of the vessel.
σ_{sg}	Subgrain component of strengthening
σ_{wh}	Increase in the stress due to work hardening between the yield stress and ultimate tensile strength.
C'	Constant
$\alpha-$	Phase

C O N T E N T S

CHAPTER 1

GENERAL INTRODUCTION

A heterogeneous mixture of two or more homogeneous phases bonded together and having its own distinctive properties unobtainable in either of the phases individually is known as composite material. Thus, the composite materials are physically combined, intimately bonded compatible materials to form an integral structure possessing some unique properties.

The history of man-made composite materials dates back to ancient materials technologies of early civilizations. They used laminated bows for extra strength, mixtures of straw and mud for building bricks, forged wrought iron and steel to make sabres, dispersed platinum in gold and silver. These are the excellent examples of composite materials known to ancient peoples.

Conscious efforts to develop composites have started relatively recently. A number of composites have been developed with improved wear resistance, fatigue characteristics and the "Specific" values (values/unit weight) of strength and stiffness especially at elevated temperature. These unique properties have nominated these composite materials to a wide range of applications in cutting tool production, air craft and space activities and ground transportation.

About 200 composite components with a high specific strength/weight ratio have been so far been introduced in air crafts or helicopters in the past few years and no significant degradation has been observed in residual strength even after 5 years of service [1]. The necessity of a material offering high strength to-weight or stiffness-to-density ratio even at elevated temperature has indicated the potential of aluminium alloys as an ideal matrix material for this class of composite. Various aluminium alloy composites have a promising future for various applications in large light weight structures in the civil, aerospace and transportation industries. In aluminium base composites alumina has been found ideal as a reinforcing material since both of these materials are physically and chemically compatible at the projected service temperature of the resultant composite [2].

Modern composite materials can be broadly classified into two groups as fibre and particulate composites. The fibre composite materials consist of reinforced second phase having a length/diameter ratio greater than one. The size of the fibrous second phase varies from a fraction of a micron to several mils in diameter and its volume concentration in the matrix may increase from a few percent to greater than 70%. The types of fibre composites available are unidirectional continuous fibre reinforced composites, unidirectional short (discontinuous) fibre reinforced composites and randomly oriented short fibre reinforced composites. The fibres are usually uniformly dispersed throughout the composite. In continuous fibre composites the fibres act as a primary load bearing constituent where the function

of the matrix is only to transmit load to the reinforcing fibres. However in short fibre composites the strengthening mechanism is somewhat different.

In particulate composites the second phase particles having a length/diameter ratio or approximately one are reinforced and uniformly distributed in the matrix. The particulate composites differ from dispersion strengthened materials by the larger size of the dispersoid exceeding 1.0 μm with the volume concentration as high as 30%. Unlike dispersion strengthened materials where the matrix acts as the only load bearing constituent and the strength of the matrix is increased in proportion to the effectiveness of the dispersoid to act as a barrier to the motion of matrix dislocations. In particle reinforced composites the matrix and the dispersed particles both share the load. Because of non-directionality in mechanical properties and for ease of fabrication into various shapes [3-8] the particulate composites have attracted widespread attention for a number of applications. In conventional dispersion strengthening alloys prepared by casting methods, the dispersion of second phase (amount, size and shape) in the matrix is governed by thermodynamic considerations hence the opportunities for strengthening the alloys by dispersion of second phase is restricted by a limit. In particulate composite materials it is easily possible to control the amount and morphology of the second phase particles to a great extent by choosing a suitable manufacturing process and its parameters. The range of attainable properties may thus be wider in particulate composites.

The production of metal based particulate composites
has been tried from two principal approaches, one is the Powder
Metallurgy and the other is by Foundry Technique. Mechanical
mixing [9-11] of two comminuted phases by means of mixing and
blending in ball mills, colloid mills or blenders followed by
compaction, sintering or hot pressing and consolidation by metal
working such as hot rolling, forging and especially extrusion
are the powder metallurgical approach for introducing fine or
coarser particles in the matrix of a particle strengthened
component. Inspite of the simplicity of this process the
technique has some inherent problems [12] of inferior dispersion
or distribution due to adherence and clustering or agglomeration
depending on the size and the physical nature of the
particles.

In a comparative study [13] between powder metallurgy
and other competitive processes for the mass production of
structural parts it has been observed that the powder metallurgy
process is economically preferable for components weighing 20
to 200 gms. From the point of energy consumption the advantage
of powder metallurgical process over other competitive processes
is doubtful [13]. A comparison of the potential and the
limitations of sintering and foundry technology reveals [14]
that for manufacturing of complex precision parts with high
dimensional accuracy the foundry technique is more advantageous
than powder metallurgy specially when die casting can be employed.

Fabrication of metal base composites by foundry technique has been persued over a decade now. This is a more direct and simpler process than other energy intensive techniques for making isotropic composite materials by homogeneous dispersion of short fibres or particles in molten metal or alloy [15]. Several variations have been applied in Foundry technique for the production of particulate composites [16] such as Vortex method [17-23], blowing of reducible oxide and high melting point materials in molten aluminium [24], infiltration method [19,25], blowing of oxygen in molten aluminium [26]. Out of these processes the vortex method has drawn a considerable attention since the process offers a reasonable extent of control over the incorporation of particles in the composite and the application of the process for making various size of products are comparatively easier in this method.

The incorporation of non-metallic particulate materials in to the melt by vortex method has been done in two different ranges of temperature (a) above the melting point of the matrix alloy called liquid metal process [17,20-22,27], and (b) between the liquidus and solidus temperature of the matrix alloy called compocasting process [18,28-31]. In the liquid metal process the particulate composites are produced by adding particles into the vortex formed in vigorously agitated molten metals or alloys followed by gravity diecasting [21,22] of the slurry. Compocasting process has been developed by using the rheological behaviour of partially solid metals or alloys, where the short fibres

or particles are incorporated into the semi-solid slurry through

the vortex formed on its surface due to vigorous stirring.
The resulting slurry is cast by various methods [17,32]. In
some cases the particle incorporated slurry/solidified composite
obtained by compocasting process are reheated to above their
liquidus temperature and simultaneously cast by gravity die
casting [28] or pressure die casting processes [18,27,31,33].
The use of pressure die casting system has been found effective
in the production of particulate composites by a newer process
[34] named Thixocasting. Here the partially solidified slurries
are cast in preforms and subsequently cut into appropriate charges
for casting. The individual charges are then rapidly reheated
to the partially solid range and are fed to a cold chamber die
casting machine to recast under pressure. The reheated preforms
behave as a soft solid and only assume their fluid like properties
when sheared at gate entry and flows smoothly into the die without
excessive turbulence.

The major problems encountered in production of
particulate composites by vortex method can be accounted as
follows. The difficulties in the incorporation of large amounts of
non-metallic particles in molten metals or alloys is due to
their poor wettability in the melt [18,28]. In addition, it
is difficult to obtain homogeneous distribution of particles
in these cast composites [18,20,35]. The formation of porosity
in cast particulate composites, especially under vortex method,
is a serious obstacle for achieving the desired mechanical proper-
ties. Lastly, the most important aspect which has engaged attention

in composite technology is to obtain a strong bonding between the reinforcing particles and the matrix.

The difficulties mentioned above in the production of particulate composites by foundry technique are largely dependent on the physical and chemical nature of the particle, temperature of the melt and the mixing conditions in the vortex method. The maintenance of an optimum mixing condition in the production of cast composites by vortex method is very important for incorporation, retention and distribution of particles or short fibres inside the melt. However a systematic investigation of the parameters influencing the mixing process of the particles in molten metal has not yet been undertaken.

In this investigation an effort has been made to optimise the mixing parameters for incorporation of alumina particles in partially solid Al-4.0wt.%Mg alloy so as to achieve the maximum incorporation with a homogeneous dispersion. The effect of holding temperature of the melt on the incorporation of particles under a given mixing condition has been studied. The porosity content of the cast particulate composites obtained at different mixing conditions have also been estimated in an effort to understand the process of air entrapment in vortex method under a given mixing condition.

In the present study the effects of size and volume fraction of alumina particles with narrow and wide spectrum of sizes respectively, on the tensile strength of Al-4.0wt.%Mg-alumina com-pocast particulate composite at ambient temperature have been

investigated. The effect of volume fraction of particles on the elevated temperature tensile strength of Al-4wt.%Mg-alumina compocast particulate composite has also been studied. The effect of temperature on the tensile strength has been evaluated in the composites having a definite amount of alumina. The contribution of porosity in reducing the ambient and elevated temperature tensile strength of the composite at given levels of alumina content and at different temperatures have been determined to project the ultimate tensile strength at zero porosity level. The role of porosity on the initiation of fracture in these composites has been examined both at ambient and elevated temperatures.

CHAPTER 2

REVIEW OF LITERATURE

2.1   INTRODUCTION

The desirable properties of a particulate composite considerably depend on the characteristics of the matrix and the particles, particle-matrix bonding and its strength, amount of particles and their distribution in the matrix and the presence of flaws in the matrix or at the particle-matrix interface. Besides the selection of the matrix and the particles all other aspects of a composite mentioned above are to a great extent linked with the fabrication process of the composite.

The mechanical properties of a composite at ambient and elevated temperature are the most important criteria controlling its performance in any application. The strength of a particulate composite is related to (a) the deformation characteristics of the matrix, particles and their interface, (b) shape, size, amount and distribution of particles in the matrix, and, (c) the interactions between the particles and the flaws like porosity and voids in the matrix.

The earlier studies carried out on the vortex method of making particulate/short fibre composites and on various other aspects related to this field have been examined in this

chapter to determine the present state of knowledge about this process. Mechanical properties of the particulate composites analysed by several investigators have also been reviewed. In this regard the plastic behaviour and fracture characteristics of particulate composites related to the size, shape, distribution and volume fraction of particles and the nucleation, growth and coalescence of voids have been surveyed.

2.2 FABRICATION OF CAST PARTICULATE COMPOSITES BY VORTEX METHOD

For fabrication of cast particulate composites selection of suitable reinforcing material wettable by the matrix is always essential. Wetting of non-metallic particles by molten metals and homogeneous distribution of particles in the matrix are the two most important factors involved in successful fabrication of particulate composites by vortex method. The promotion of wetting can be facilitated physically or chemically and it is a function of the physical and the chemical characteristics of the particle-matrix interface. The interface activities are largely governed by the parameters of the fabrication process, such as pretreatment of the particle, chemical composition of the melt, melt temperature, residence time of the particles inside the melt etc. The behaviour of the melt and the mixing parameters involved in stirring of melt have been found to play a significant role on the extent of retention and distribution of particles inside the melt. Howwever, the solidification of the slurry also influences the distribution of particles in the composites.

The presence of porosity and voids are considered as major flaws in the matrix of a composite. The cast composites are very much prone to develop these defects which damage its mechanical properties and reduce reliability. To avoid the formation of these defects a number of ways have been tried which make the composite casting process more critical and costly.

2.2.1   THE WETTING OF THE PARTICLES AND PARTICLE-MATRIX BONDING

A satisfactory wetting between the non-metallic reinforced materials and the matrix in a composite is of primary importance to achieve any improvement in the mechanical properties over that of the matrix. The interfacial bond strength is largely dependent on the surface phenomena like wetting and chemical reactions. The understanding of interface interaction of a metal-ceramic system is important also for designing an effective fabrication technique of composite.

The wetting is explained by the well known criterion of contact angle between the melt and the solid second phase. For a solid-liquid wetting the contact angle, θ, defined as the angle included between the tangent to the surface of a liquid and the tangent to the surface of the solid at any point along their line of contact, must be less than $90°$. Complete wetting is obtained at $\theta = 0°$ and wetting is absent at $\theta > 90°$. The wetting is described conveniently in terms of a sessile drop on a substrate as shown in Fig. 2.1 (a). The contact angle is determined by the balance of the interfacial tension between
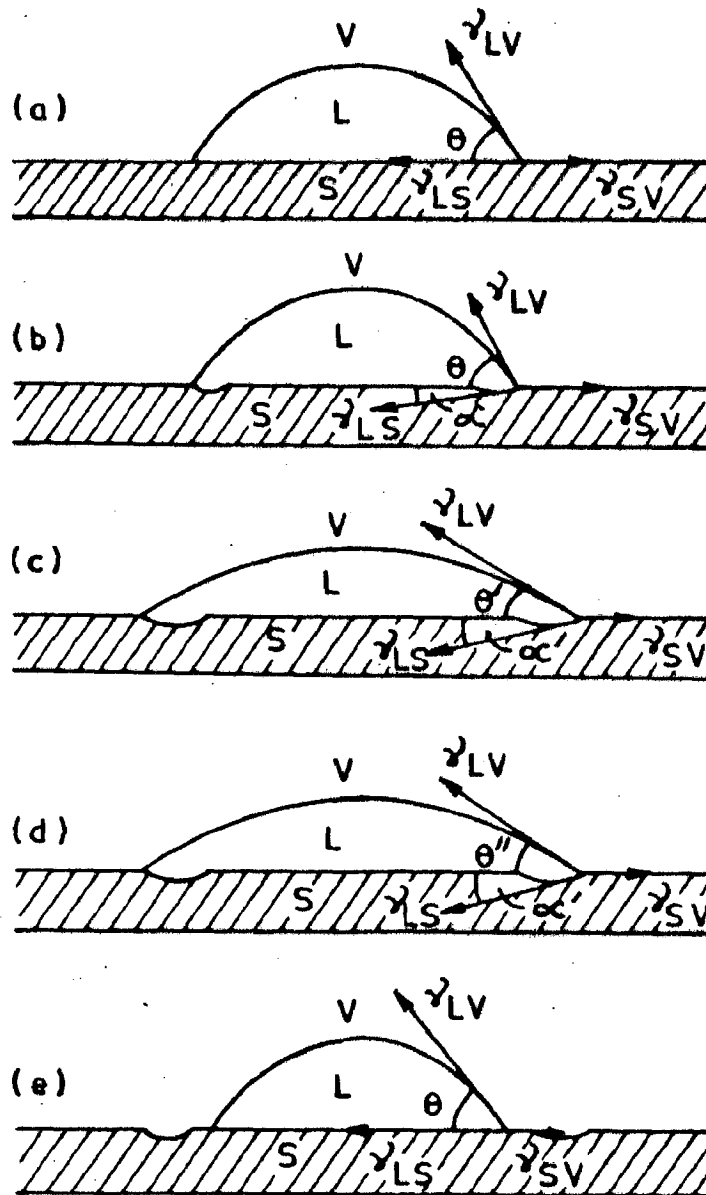
FIG. 2.1 DIAGRAM SHOWING THE RESOLVED FORCES OF INTERFACIAL TENSIONS AT THE PERIPHERY OF THE LIQUID DROP ON A SOLID REACTING SUBSTRATE [47] WITH TIME.

solid-vapour, γ_{SV}, liquid-vapour, γ_{LV}, and liquid-solid, γ_{LS}, surfaces. The condition for equilibrium between these forces is given by the Young equation as,

$$\gamma_{SV} = \gamma_{LV} \cos\theta + \gamma_{LS} \qquad\qquad .. \qquad (2.1)$$

The contact angle in any system can be changed drastically by manipulating a number of factors of physical and chemical nature, such as temperature of the system, the presence of surface active elements in the liquid and the surface coating of the solid.

(a)   Promotion of Physical Wetting .

Physical wetting between a solid and a liquid under close contact is induced by adhesion, which depends on wettability. Wetting is dependent on the energy of solid-liquid, solid-vapour and liquid-vapour interfaces. The decrease of interface energy always improves wetting and some time it may also be achieved by a decrease in the liquid surface tension. The surface tension of a number of molten alkaline earth metals has been found to decrease with the increase of temperature following a linear relationship [36].

Though a substantial amount of literature and reliable data are available for surface tension and surface chemistry of the aqueous and other liquid systems, but very little work has been carried out in metal-ceramic system. In a metal-oxide system the energy of interaction (adhesion) can be estimated as the work of adhesion, W_A , when

$$W_A = \sigma_1 (1 - \cos\theta) \qquad .. \qquad (2.2)$$

where, σ_1 is the surface tension and θ is the angle of contact. The work of adhesion has been observed to vary with the temperature, the affinity of the liquid metal for oxygen and the free energy of formation of the wetted oxide. The angle of contact, θ, decreases with increasing temperature, the increasing affinity of the wetted metal for oxygen and the decreasing stability of the wetted oxide. Ermenko has been observed [37] that higher electrical conductivity of the oxides containing greater number of free electrons and holes provide better wetting of oxides by liquid metal confirming the conclusions from the electron theory of adsorption [38,39,40].

In a system of high surface energy like metal (liquid)-oxide (solid) if the necessary wettability is not ensured under a given condition, the addition of some surface active element in the liquid is advantageous [37,41]. The introduction of some surface active elements in a melt decreases its surface tension and enhances the wettability. Whether the impurity element will act as a positive or negative modifier in modification of surface tension of a liquid is determined by the energetic properties of the molecules, which is explained by a quantity called generalized moment [42]. The generalized moment, m, is a physical quantity determined mainly by two properties of a molecule such as the average electrical moment of the atoms and their dimensions. For ionic and metallic liquids the generalized moment is expressed as

$$m = ez/s \qquad\qquad \cdots \qquad (2.3)$$

where, e is the electronic charge, ez is the ionic charge and s is the effective radius of the ion. With the help of the values of generalized moment the energetic properties of a metal such as its surface tension, surface activity, activity coefficient and consequently all the basic thermodynamic properties can be determined to a first approximation. The generalized moment permits one to arrange all the ions of the different metals in a series, each of the successive members of which is weaker energetically than the preceeding one. So all the metals having a position at the right hand side of the metal chosen will act as a surface active element or positive modifier to it since the ions of the latter one is weaker than the ions of the first metal [43]. The positive modifiers lead to the formation of an adsorbed film on the grains of the aggregate and their preferential concentration at the interface reduces the surface energy, γ_{LS}, thus, promoting wetting according to the Gibbs adsorption concept [37].

However, even in case of poor wetting at the metal-oxide boundry the energy of interaction (adhesion) has been found [44] to be of the order of 1000 ergs/cm^2. Conversion of this energy to molar work of adhesion gives a value of several tens of kilo calories. This is impossible to obtain by Van der Waals forces alone which, of course, are always present there. Thus, as the only possible reason to provide such a high interface energy it was inferred that there is a chemical interaction at the boundry of seperation between metal and oxide [37,44].

(b)   Promotion of Chemical Wetting

The affinity for chemical interaction of a solid with liquid may alter the wetting environment of a liquid-solid system. Chemical attack affects the surface regularity of the solid which changes the direction of the horizontally acting liquid-solid surface tension force by pushing it towards inside of the solid. Thus, the liquid-solid interfacial tension becomes less and it disturbs the condition of equilibirum. To restore the equilibrium θ decreases due to higher γ_{SV} and the liquid spreads over the solid surface.

The alumina (α-Al$_2$O$_3$) in contact with liquid aluminium undergoes a chemical reaction by evolving a volatile oxide Al$_2$O [45]

$$4Al + Al_2O_3 = 3Al_2O \qquad\qquad .. \qquad (2.4)$$

In sessile drop experiments of molten aluminium on alumina plaque the reaction occurs at the periphery of the interface along a ring [46-48]. The reaction occurs at temperatures above about 1208 K and increases with the increase in temperature [49]. Al$_2$O has a low solubility in molten aluminium [50] and being volatile, it increases pressure at the interface. Thus the rate of reaction given in equation (2.4) is governed by the removal of Al$_2$O from the interface.

During chemical reaction between alumina and liquid aluminium at a temperature of about 1223 K and above, γ_{LS} no longer act horizontally [46], rather becomes deflected downwards

at an angle α' as shown in Fig. 2.1(b). The equilibrium between the forces of tension at the interface is disturbed to,

$$\gamma_{SV} > \gamma_{LV} \cos \theta + \gamma_{LS} \cos\alpha' \qquad .. \qquad (2.5)$$

and the drop of liquid aluminium tends to spread outward under the influence of γ_{SV} until a new equilibrium is reached as shown in Fig. 2.1(c).

$$\gamma_{SV} = \gamma_{LV} \cos \theta' + \gamma_{LS} \cos\alpha'' \qquad .. \qquad (2.6)$$

where θ' and α'' are the limiting value of θ and α'. Throughout this period the drop of liquid aluminium looses its mass by evaporation [45] which is faster at temperatures above 1423K, and lowers the contact angle further to θ''. Under this condition the force of interfacial tension satisfies the new condition that,

$$\gamma_{SV} < \gamma_{LV} \cos \theta'' + \gamma_{LS} \cos\alpha'' \qquad .. \qquad (2.7)$$

as shown in Fig. 2.1(d). As a result the drop contracts to a new pseudo-equilibrium position [47,51] having contact angle θ as shown in Fig. 2.1(e), and the process of changing contact angle from $\theta \longrightarrow \theta' \longrightarrow \theta'' \longrightarrow \theta$ is repeated in cycles. However, at a temperature of 1623 K, where this cyclic process has been observed [47] by significant reaction, the contact angle θ of pseudo equilibrium condition has not recovered upto its initial value θ as it is evident in Fig. 2.2. This may be due to the reason that during the first cycle of the process the whole alumina surface in contact with the liquid aluminium has been attacked by the chemical reaction which provides an condition somewhere between equations(2.5) and
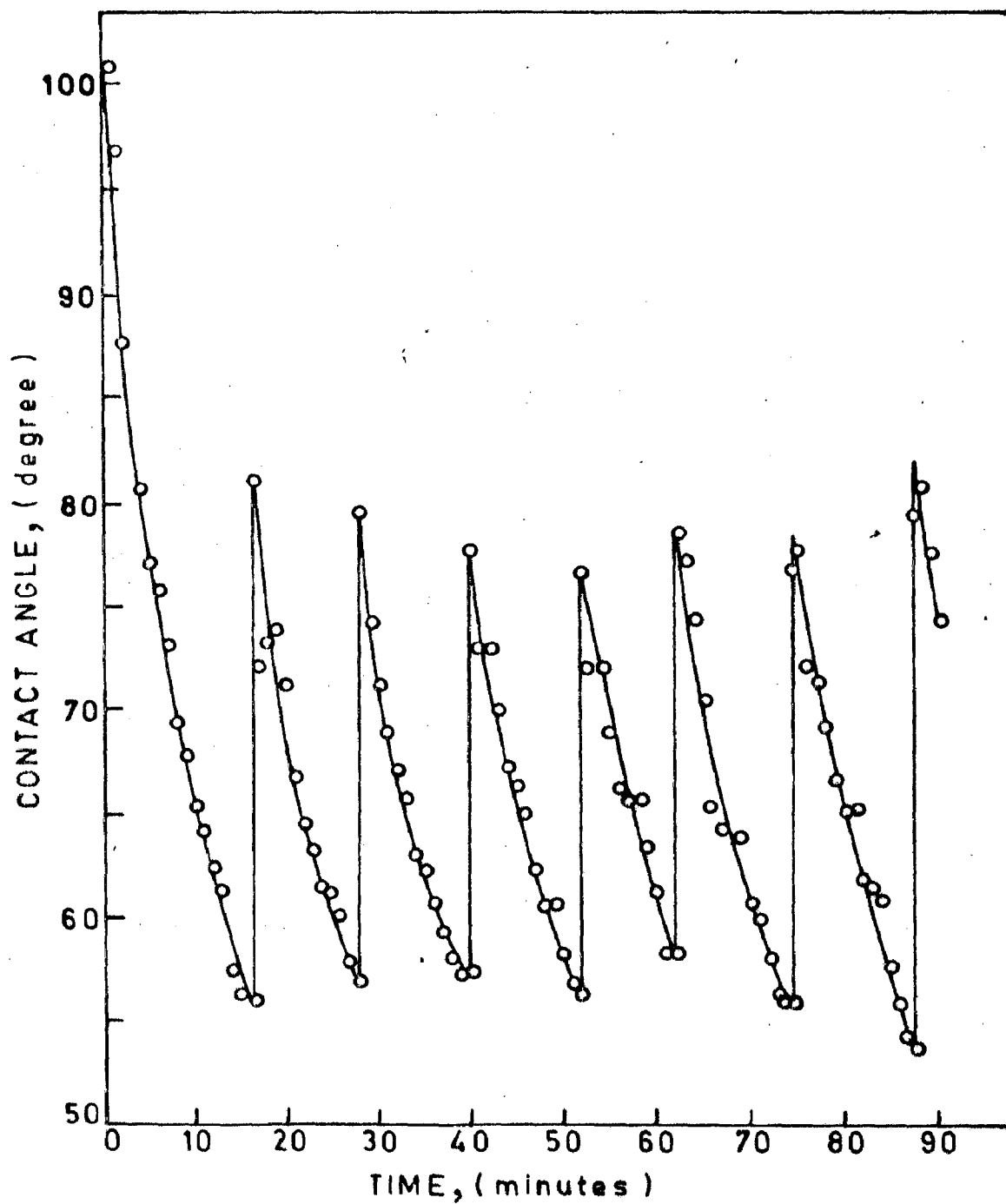
FIG.2.2 ALUMINIUM ON SINGLE-CRYSTAL SAPPHIRE
VARIATION OF CONTACT ANGLE WITH
TIME AT 1623 K [47].

The reduction of contact angle in aluminium α-alumina system is a function of time at a given temperature [48]. The time required to reach the equilibrium decreases with the increase in temperature [47]. In the aluminium - alumina system the contact angle has been found to reduce to a value of $\sim 75°$-$80°$ at temperatures of 1973 K and 1173 K after 10 hours and 4 hours in contact respectively, whereas the contact angle in the same system was sharply decreased to a value of atoms $\sim 55°$ within $\sim$ 17 minutes at a temperature of 1623 K [47]. For obtaining wetting in terms of $\theta < 90°$ at equilibrium, both long contact time at low melt temperature and having a high melt temperature to minimise contact time are not feasible solutions for designing an effective fabrication technique of Al-Al$_2$O$_3$ composite by foundry method. The onset of an interfacial action in commercial Al— α-Al$_2$O$_3$ system, to produce wetting has been found to be significantly enhanced with a rapid increase in contact area, only at temperatures above 1173 K [28,47,49,52]. However, this temperature is fairly high compared to that used in alumnium casting process.

For the production of particulate composite by foundry technique, proper wetting of the incorporated ceramic particles by the melt at the temperature of casting is essential. There are two basic processes for making particulate composite by foundry technique, such as the liquid metal process and compocasting process. In these two processes the casting temperatures used are respectively about 50 K above the liquidus and in the range between the liquidus and the solidus temperatures

of the alloy. To achieve a faster wetting between the non-metallic particles and the matrix surface active agents are used. Here, the modifying action of surface active element cannot be realised purely by the concept of generalised moment as discussed earlier in section 2.2.1(a) rather it can be explained by a chemical concept of the formation of chemical compound or crystalline complexes by reaction [53]. In this case the wetting behaviour may be influenced by the surface active nature of the compound as well as the stability of the compound in solid state [53]. The wetting agents used in a metal - oxide system are the interface active elements having either an affinity for the cation of the oxides (metal ions) or a greater affinity for oxygen than the solvent matrix as measured by the free energy of oxide formation [40,54]. Due to higher affinity for oxygen than the matrix the interface active element reduces the oxide and modify the chemical nature of its surface for promotion of wetting.

The presence of various elements such as sodium (Na), potassium (K), lithium (Li), magnesium (Mg), copper (Cu), nickel (Ni) and rare earth elements in molten aluminium have been found [35,47,49,55-59] useful to enhance the wettability of alumina in it. The elements are detected to concentrate on the alumina surface due to their ability to reduce alumina and induce wetting [27,35,59]. However the improvement in wetting does not always provide a practical solution to composite production process. Highly alkaline element like sodium (Na)

is not favoured because of its immiscibility in aluminium at
all temperature and the unreacted residue requires extra care
for removal [60]. Lithium (Li) in aluminium-alumina system
reacts with alumina and promotes wetting by formation of Li_2O.
$5Al_2O_3$ but the preparation and handling of the alloy as well
as the control of the chemical interaction during composite
production process is difficult [27]. Among all the elements
tried so far copper (Cu) and magnesium (Mg) are primarily
accepted for use as a wetting agent in aluminium-alumina system
due to their capacity to reduce the contact angle [49] and
ease of handling in the composite production process. The
thermodynamic analysis [28] of the possible reactions of alumina
with Mg or Cu given in Table 2.1. The table shows that magnesium
may undergo a number of chemical reactions reducing the surface
layer of alumina [28,49] to produce solid magnesium oxide
(MgO) and magnesium aluminate ($MgAl_2O_4$) by the following
reactions.

$$3[Mg] + <Al_2O_3> \quad = \quad 3<MgO> + 2[Al] \quad .. \quad (2.8)$$

$$[Mg] + 4/3<Al_2O_3> \quad = \quad <MgAl_2O_4> + 2/3[Al] \quad (2.9)$$

$$[Mg] + 2[Al] + 2(O_2) = \quad <MgAl_2O_4> \quad .. \quad (2.19)$$
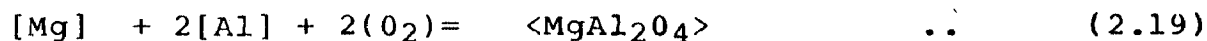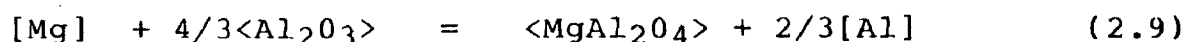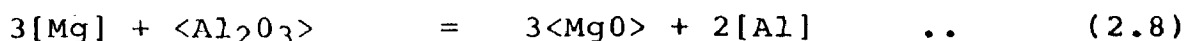
Symbols : [in solution]; <solid>; (gas)

The chances of MgO formation by reaction of magnesium
with alumina following the equation 2.8 is more at higher
concentration of magnesium in the melt [28]. The equilibrium

TABLE 2.1

FREE ENERGY CHANGES FOR THE REACTIONS OF INTEREST IN $Al-Mg-Al_2O_3$ AND $Al-Cu-Al_2O_3$ SYSTEM (ΔG_T KJ/Mole)[28]

Reaction	Nominal alloy composition			
	2%Mg	4%Mg	8%Mg	4.5%Cu
$2[Al] + 3/2(O_2) = <Al_2O_3>$	-1388	-1391	-1401	-1388
$[Mg] + \frac{1}{2}(O_2) = <MgO>$	-508	-509	-512	-
$[Cu] + \frac{1}{2}(O_2) = <CuO>$	-	-	-	-29
$2[Cu] + \frac{1}{2}(O_2) = <Cu_2O>$	-	-	-	-13
$<MgO> + <Al_2O_3> = <MgAl_2O_4>$	-28	-28	-28	-
$[Mg] + 4/3<Al_2O_3> =$				
$\quad <MgAl_2O_4> + 2/3[Al]$	-39	-43	-52	-
$[Mg] + 2[Al] + 2(O_2) =$				
$\quad <MgAl_2O_4>$	-1888	-1915	-1962	-
$3[Mg] + <Al_2O_3> =$				
$\quad 3<MgO> + 2[Al]$	-33	-46	-73	-
$[Cu] + \frac{1}{2}(O_2) + <Al_2O_3> =$				
$\quad <CuAl_2O_4>$	-	-	-	-30
$[Cu] + 2[Al] + 2(O_2) =$				
$\quad <CuAl_2O_4>$	-	-	-	-1467
$[Cu] + [Al] + (O_2) =$				
$\quad <CuAlO_2>$	-	-	-	-756
$<CuAlO_2> + \frac{1}{2}<Al_2O_3>+\frac{1}{4}(O_2)=$				
$\quad <CuAl_2O_4>$	-	-	-	-16

Symbols : <Solid>, (gas), [In solution]

activity of magnesium for reaction (2.8) indicates that at a magnesium concentration of 4-8 wt.% in the bulk alloy the MgO becomes more stable than alumina where the values of equilibrium a_{Mg} for nominal alloy compositions 4 wt.% and 8 wt.% are 0.135 and 0.040 respectively and the estimated activities of magnesium in the enriched liquid were 0.018 and 0.050 respectively. This is in agreement with the observations of the large transformation of alumina particles into MgO during the fabrication of a particulate composite by adding alumina particles into liquid Al-14 wt.% Mg alloy [35].

In oxidation mechanism study [61] of molten Al-10 wt.% Mg alloy it has been observed that a low temperature around 973 K favours primarily the formation of MgO but an amount of magnesium aluminate ($MgAl_2O_4$) is also formed. However, at higher temperatures of around 1073 K the situation is reversed and magnesium aluminate is primarily formed.

The formation of magnesium aluminate on the reinforced alumina in Al-Mg alloy melt is of great interest to the technologists as it can provide a stable reacted layer on alumina and enhances its wettability in molten alloy. The thermodynamic calculations given in Table 2.1 and Table 2.2 show the possibility of formation of magnesium aluminate in a system having alumina and magnesium at a temperature between 873 K to 923 K by reactions (2.9), (2.10) and any of the following reactions [28,61].

TABLE 2.2

REACTIONS OF THE FORMATION OF MgO AND MgAl$_2$O$_4$, AND THE

GIBB'S ENERGIES FOR THEIR FORMATIONS [55]

Reaction	$\triangle$ G kJ		
	923K	1023K	1123K
[Mg] + ½(O$_2$) = <MgO>	-28.9	-28.3	-27.7
[Mg] + 2[Al] + 2(O$_2$) = <MgAl$_2$O$_4$)	-108.6	-106.1	-106.0
<MgO> + 2[Al] + 3/2(O$_2$) =			
<MgAl$_2$O$_4$>	-79.7	-77.7	-76.0
<MgO> + <Al$_2$O$_3$> = <MgAl$_2$O$_4$>	-0.574 (at 803 K)		

Symbol : <Solid>, (gas), [In solution]

$$\langle MgO \rangle \ + \ 2[Al] \ + \ 3/2(O_2) \ = \ \langle MgAl_2O_4 \rangle \qquad .. \qquad (2.11)$$

$$\langle MgO \rangle \ + \ \langle Al_2O_3 \rangle \qquad \qquad = \ \langle MgAl_2O_4 \rangle \qquad \qquad .. \qquad (2.12)$$
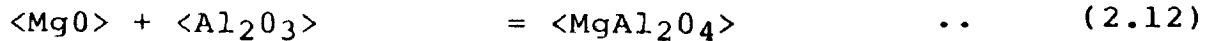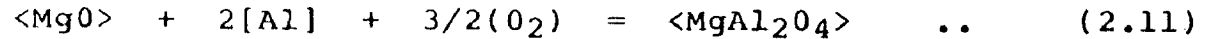
For a low magnesium content upto about 4 wt.% in the aluminium alloy the formation of magnesium aluminate by reaction of magnesium with alumina is energetically more favourable [28]. The formation of magnesium aluminate by direct reaction of alumina with magnesium following the reaction (2.9) requires a larger quantity of alumina in the reaction where alumina is expected to be heavily consumed giving rise to a thick reacted layer of magnesium aluminate in it. In discontinuous fibre reinforced aluminium alloy composite, produced by incorporation of alumina fibre in vigorously agitated partially solid Al-4wt.%Mg alloy, no heavily reacted layer on fibre or a degradation of fibre has been observed [28] after allowing a long contact time ($\sim$ 2 hours) between fibre and the slurry. This indicates the limitation of reaction (2.9) for the production of magnesium aluminate in the above process. However the reaction (2.9) cannot be ignored in the production of particulate composites where a large quantity of incorporated alumina particles are readily available to react with magnesium for the formation of magnesium aluminate. There is also a strong possibility for magnesium to react with fine alumina particles formed inside the Al-Mg alloy melt by oxidation of aluminium leading to the reaction (2.10). The equilibrium partial pressure of oxygen (p_{O_2}) for reaction (2.10) has been estimated [28] to be

of the order of 10^{-50}. In the vortex method of fabrication
of particulate or short fibre composite the vigorous agitation
of Al-Mg melt provide a high possibility to introduce enough
gas bubbles to rise the p_{O_2} inside the melt above this level.

Thus under this process magnesium aluminate may form as fine
particles [61] by reactions (2.9) and (2.10). During stirring
of the melt there is a high possibility of collision between
these fine magnesium aluminate and the incorporated alumina
particles, where fine magnesium aluminate may adhere on alumina
particles in order to reduce the surface energy of dispersion
and subsequently grow on it.

The MgO is produced in Al-Mg-Al$_2$O$_3$ system by reaction
(2.8) and may also form by the following reaction,

$$[Mg] + \tfrac{1}{2}(O_2) = \langle MgO \rangle \qquad\qquad .. \qquad\qquad (2.13)$$

due to high affinity of Mg to react with readily available
oxygen in the melt. Available MgO may take part in reactions
(2.11) and (2.12) and produce magnesium aluminate. MgO fines
or particles react with molten aluminium in presence of readily
available oxygen (reaction 2.11) or may react with fine alumina
particles produced by direct oxidation of the melt (reaction
(2.12)), thus magnesium aluminate is produced as discrete
particles or may form on reinforcing alumina using it as a
suitable substrate. There is also a possibility of MgO
reacting directly with incorporated alumina to produce a
continuous layer of magnesium aluminate following the reac-
tion (2.12). But a further growth of the layer requires

magnesium to diffuse through this layer for subsequent reaction and thus the reaction must be sluggish.

Thermodynamically the formation of alumina, magnesium oxide (MgO) and magnesium aluminate are likely to be competitive processes and significantly depend on the magnesium content of the alloy as discussed earlier in this section. In partially solid slurry the formation of magnesium aluminate will be relatively sluggish as the rate of formation of magnesium aluminate is more dependent on temperature than that of MgO [61]. Thus, initially the melt will be having a high MgO content subsequently the MgO reacts again and the magnesium aluminate can form by reactions (2.11) and (2.12).

The kinetics of growth of interaction layer thickness (μm), x, on alumina estimated by the growth law

$$x = at^{n'} \qquad \qquad .. \qquad (2.14)$$

where, t is the residence time (min) of alumina in the molten alloy. a and n' are the positive constants, and have been found [28] to increase with the increase in magnesium addition upto 4 wt.% in aluminium. The estimated values of n' for 2,4 and 8 wt.% magnesium have been found to be 0.57, 0.59 and 0.38 respectively. Thus for making aluminium alloy alumina composite the presence of magnesium upto about 4 wt.% in aluminium is useful.

(c)   Promotion of Wetting By Coating of Particles

Precoating of ceramic particles improves its wettability in liquid metals. The particles are coated with the elements which are readily wettable by the liquid metal matrix. The coating of ceramic particles are carried out by electroless deposition or sputtering techniques. Electroless coating of copper and nickel on oxide, carbide and graphite particles as well as on mica flakes improve their wetting in liquid aluminium [16,21,62,63]. Nichrome and duplex coating of Ti-Ni and physically attached sputtered coatings of Ni(Ti), Ni(Cr) and 1020 carbon steel on alumina fibre also improve its wetting behaviour in liquid aluminium [64-67].

Though the precoating on nonwettable ceramic particle is successful for increasing the incorporation of particles and fibers in liquid aluminium, still the use of this process is restricted due to certain limitations. Inspite of sufficient wetting, precoated particles may not provide a strong interface due to the nature of physical attachment. Discontinuity in coating on the particle interrupt the uniform wetting. Most of the coating may cause debonding unless the fabrication time is short enough to prevent the dissolution of the coated layer in the liquid matrix. During fabrication of composites by incorporation of coated ceramic particles in liquid aluminium the fabrication time is required to be controlled within a time period of the order of few minutes [28]. Moreover the use of precoating of ceramic particles in composite production by foundry technique make the process costlier due to involvement of extra step of coating.

(d)   Particle Matrix Bonding

The performance of a composite is governed by the interfacial bond strength developing as a result of wetting and chemical reaction between the matrix and the reinforced material. The strength of composite is achieved by transfer and distribution of load from the matrix to the reinforcing entity through a strong interface between the two. Mechanical locking and physical adherence cannot provide an interface strong enough for this purpose.

Under close contact of two interacting dissimilar materials bonding occurs by donor-acceptor interaction. The reaction leading to the formation of a transition region containing new reaction products provide a strong bond between two dissimilar materials [68]. The greatest coherency is established between the components of a composite with the formation of a chemical bond at their interface which provides the strongest interface.

Aluminium oxide (Al_2O_3) has been found to react with many divalent transition metal oxides and forms aluminates having a crystal structure similar to mineral spinels. The reacted layers of spinels have a high potential to form strong bonds between metal and ceramics [69-72]. Thus the presence of magnesium, copper, zinc or iron in Aluminium - alumina system may provide a strong bond between alumina and the matrix since they can form aluminate under appropriate conditions. Out of these elements magnesium and copper have been favoured in

composite fabrication process by foundry technique due to their
easy application in the process [28]. The presence of magnesium
as an interface active element in aluminium alloy - alumina
system is more widely used than the addition of copper, because
the reaction product magnesium aluminate is more stable than
copper aluminate ($CuAl_2O_4$). The copper aluminate decomposes
into alumina and CuO at the heat treating temperatures for
Al-Cu alloy matrix [28], thus the interfacial bond containing
copper aluminate is not suitable for providing the strength
of the composite at elevated temperature.

2.2.2   PRODUCTION OF COMPOSITE

In the production of a cast composite by vortex method
the particles are introduced in the molten alloy through the
vortex and thus, an effective utilisation of the process can
be achieved after having an understanding over the behaviour
of the vortex under different process parameters. In a
concentrically agitated vessel the process parameters such
as the size of the impeller, the position of the impeller,
the speed of stirring etc. primarily control the flow pattern
of the liquid and influence the mixing of solid particles inside
the liquid.

During the fabrication of cast composites the control
of the holding temperature of the alloy, an effective addition
of the wetting agent and the pretreatment of the solid particles

play significant roles on the retention of particles in the casting. Development of porosity in the cast composites produced by vortex method is considered as the most hazardous aspect of this process. A number of efforts so far have been put forward to control or minimise the porosity in the composite.

In this section an effort has been made to review the observations of the earlier investigators on the following aspects related to the production of cast composites by vortex method.

a) Mixing criteria under the vortex method

b) Fabrication process

c) Porosity in the composites produced by the vortex method.

(a) Mixing Criteria Under Vortex Method

In a mixing process by rotating a concentric impeller inside a liquid as shown in Fig. 2.3, a vortex forms at the center of the liquid surface due to establishment of a pressure difference between the inner and the outer surface of the liquid. By momentum balance the pressure difference, dp, in a given liquid of density, 'ρ'', can be expressed as

$$dp/\rho' = v^2/r \, dr \qquad \qquad .. \qquad (2.15)$$

where, r, is the radial co-ordinate measured from the axis of the impeller and v is the liquid velocity. By expressing equation (2.15) in terms of w = ρ'/g. the weight of unit volume of
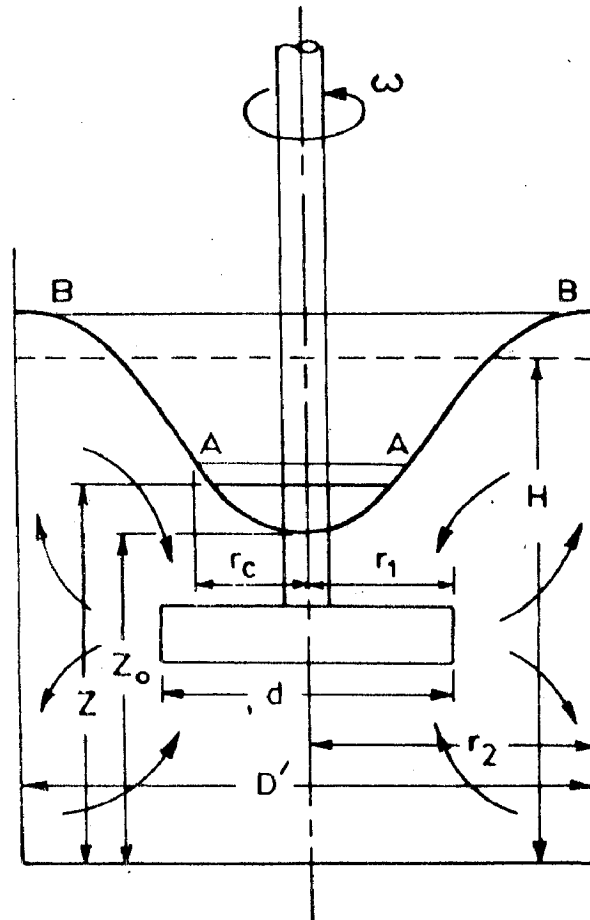
FIG.2.3 SCHEMATIC DIAGRAM OF LIQUID FLOW
IN A CYLINDRICAL MIXING VESSEL.

the liquid.

$$dp/w = v^2/gr\,dr \qquad\qquad .. \qquad (2.16)$$

As per Bernouli-theorem the condition for free vortex is

$$dp/w + v\,dv/g = 0 \qquad\qquad .. \qquad (2.17)$$

By solving equations (2.16) and (2.17) and integrating we find

$$vr = c \qquad\qquad .. \qquad (2.18)$$

where, c, is a constant. The characteristic of vortex is largely dependent on the viscosity of the liquid. The viscous force, τ , acting on an unit surface of the liquid of cofficient of viscosity, η , is expressed as

$$\tau = -\eta\,dv/dr \qquad\qquad .. \qquad (2.19)$$

Differentiating equation (2.18) with respect to, r, and substituting the value in equation (2.19) we get

$$dv/dr = -c/r^2 \qquad\qquad .. \qquad (2.20)$$

Therefore, $\tau = \eta\,c/r^2$ $\qquad\qquad .. \qquad (2.21)$

It shows that the viscous shear stress is inversely proportional to r^2. Thus, towards the center of rotation τ becomes very large and as per equation (2.18) the velocity reaches a very high value. According to Bernoulli's theorem this increase in velocity causes a decrease of pressure which is minimum at the center and a sucking action takes place at this region. Again around the center the viscosity of the liquid is maximum and the liquid rotates at a constant angular velocity, ω , like a solid cylinder of radius r_c ,

without shear. This is ∩ forced vortex region. Thus we get
a combined vortex condition in mixing process where,

$$r \leqslant r_c; \quad v = r\omega \qquad \qquad \text{..} \qquad (2.22)$$

$$r \geqslant r_c; \quad v = \omega \, r_c^2/r \qquad \qquad \text{..} \qquad (2.23)$$

The circumferential velocity distribution curve of an agitating liquid given in Fig. 2.4 depicts [73] that a velocity difference between the impeller and the liquid, shown by the curves (AA'-AA"), always exists in a cylindrical mixing vessel where 0AA' is the circumferential velocity of the impeller and 0AA" is the same for the liquid. The circumferential velocity of the liquid has been found to be maximum at a distance r_c where the sucking takes place due to lower pressure. The velocity difference between the impeller and the liquid accelerates the liquid and controls the discharge from the impeller.

The value of r_c can be evaluated by the following procedure.

The liquid level H before agitation of liquid can be expressed in terms of liquid volume, V, and the radius, r_2, of the cylindrical container as

$$H = v/\pi \, r_2^2 \qquad \qquad \text{..} \qquad (2.24)$$

During stirring the volume of liquid is expressed as [73]
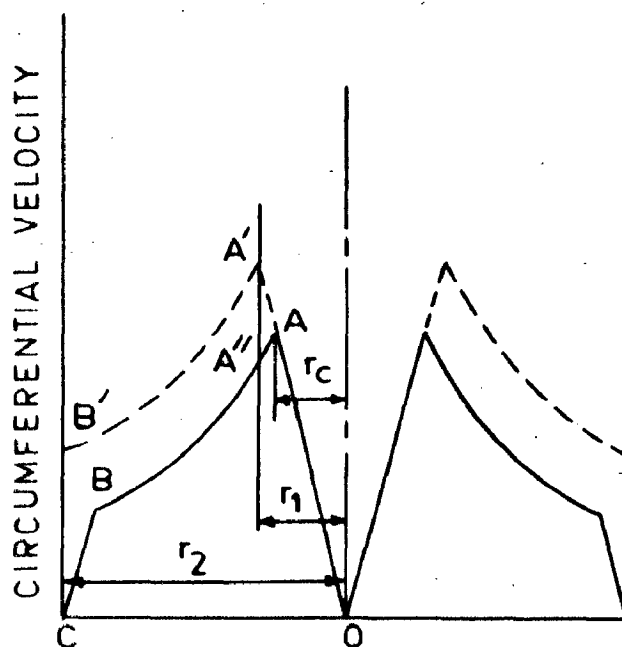
FIG.2.4 CIRCUMFERENTIAL VELOCITY DISTRI-
BUTION IN AN AGITATED CYLINDRICAL
VESSEL [73]

$$V = z_o \pi r_2^2 + \pi(\omega^2/4g) r_c^4 + \pi (\omega^2/g) r_c^2(r_2 - r_c^2)$$

$$- \pi(\omega^2 r_c^4/g) \ln(r_2/r_c) \qquad \qquad .. \qquad (2.25)$$

where, z_o is the height of the lowest point of the liquid profile at the top from the bottom of the vessesl. By substituting the equation (2.25) in the equation (2.24) one gets,

$$\left\{ (H-z_o)/r_2^2 \right\} (g/\omega^2) = y^2 - y^4 \left\{ 2.303 \log(1/y) + 0.75 \right\} .. (2.26)$$

where, $y = r_c/r_2 \leqslant 1$

The value of ω is estimated as

$$\omega = 2n\pi \qquad \qquad .. \qquad (2.27)$$

where, n is the stirring speed measured in revolution per second.

The flow of liquid in a cylindrical vessel is characterised by the dimensionless Reynold's number, R_e, given as[73]

$$R_e = d^2 n \rho'/\eta \qquad \qquad .. \qquad (2.28)$$

where, ρ' is the density of the liquid, d is the diameter of the impeller and η is the coefficient of viscosity of the liquid. For a given R_e the value of r_c/r_1 is estimated as [73]

$$R_e/(10^3 + 1.6 R_e) = r_c/r_1 \qquad \qquad .. \qquad (2.29)$$

where, r_1 is the radius of the impeller. Thus, for a given mixing system and the speed of the stirrer one can calculate the Reynold's number from eqn.(2.28)which,in turn, decides the value of

r_c/r_1. From the value of r_c/r_1 one can compute the value of r_c/r_2 and substitute it in equation (2.26) to get the corresponding value of Z_o.

The state of flow in a cylindrical vessel is complicated and there exists violent turbulence near the impeller blades. For simplicity one may assume that the tangential flow is predominant and there exists a combined vortex type flow as discussed above. It has been observed [74] that in an agitated vessel the forced vortex zone or cylindrically rotating zone (C.R.Z.) prevails in a range within 70% of the impeller diameter and a quasi-free vortex zone in the outer part of it when the impeller rotates in water. With an increase in the viscosity of the agitated liquid, the radius of the forced vortex (r_c) is reduced and finally becomes zero at the transitional viscosity from turbulent to laminar ranges. This transition has a considerable influence on the discharge flow of the liquid from the impeller.

During the flow of liquid in a cylindrical vessel at $R_e \leqslant 10$ the liquid around an impeller has a laminar movement with the impeller rotation and the liquid distant from the impeller remains stagnant. The tangential velocity of liquid flow in a region close to the impeller is large and is extremely small at a distance from the impeller. Thus, the centrifugal effect due to impeller rotation becomes negligible and the discharge flow has been found [74] to be weak. In order to

prevent the occurrence of the stagnant zone the use of large size impeller has been preferred. When the R_e increases to ten or more the centrifugal force due to impeller rotation is no longer negligible and the discharge flow has been found to increase abruptly which contributes to the transfer of the angular momentum to a distant part of the liquid. However though the mixing is greatly improved in this region still stagnant domains, of doughnut shape, appear near the upper and lower parts of the impeller. A further increase of R_e to several hundred, the flow around the impeller becomes turbulent. In this condition the discharge flow has been found to reach a maximum and the stagnant zones totally disappear. This is a transition range where both the turbulent and laminar flow coexist. The liquid apart from the impeller shows a laminar behaviour having a small rotational speed. Thus the velocity difference between the liquid and the impeller is so large that the centrifugal effect is predominant. More increase of R_e spreads out the turbulence and finally engulfs all the regions in the liquid. When the flow becomes turbulent and approaches a completely turbulent state, a combined vortex has been found to be established. At the R_e beyond 10^3 the tangential flow becomes predominant and a weak, secondary circulation flow has been found to overlap in an unbaffled vessel.

The tangential velocity component is almost proportional to the distance, r, from the center within the forced vortex zone (CRZ), but is nearly inversely proportional to r outside.

The equations for estimation of tangential velocity, v_t, written as

$$v_t = r\omega \quad ; \quad r_c > r \gg 0 \qquad \qquad .. \qquad (2.30)$$

$$v_t r^{0.8} = \text{Constant; when } D/2 > r > r_c \qquad .. \qquad (2.31)$$

where, ω is the angular velocity. These equations have been found [74] to follow the observed data closely.

The flow patterns of liquid at various agitator speeds are similar with the exception of flow near the central zone of the liquid surface. Therefore the absolute flow velocity may be assumed to increase in proportion to the impeller speed. The maximum tangential velocity $v_{t(max)}$ is equal to $2\pi N r_c$ where N is the speed of the impeller. The radius of C.R.Z. (forced vortex), r_c, which plays a significant role on flow pattern, has been found to be a function of the ratio of impeller diameter, d, to the vessel diameter, D, and of the Reynolds number, R_e. The r_c is nearly zero at the transition Reynolds number and becomes larger with the increase in R_e until finally it reaches a constant value in the completely turbulent range.

The tangential velocity components are high relative to radial and axial components. They are almost symmetrical to the impeller axis and also to the plane of the impeller rotation. The radial velocity component moves towards the vessel wall in the vicinity of the thickness of the impeller and outside this region it moves towards the agitator shaft. Due to the axial velocity component the liquid moves upwards

from the level of the impeller at the vessel wall and in part of the zone above the impeller. The liquid again returns to the impeller annularly . The discharge flow in the region where the radial velocity component moves towards the vessel wall, sucks liquid in from out side, strikes the vessel wall, turns upwards (or downward), generates the axial flow, inverts to a radial direction and finally flows down axially. These flow patterns characterised as a secondary circulation flow has been shown in Fig. 2.5[74].

In case of agitation of solid particles inside liquid in a cylindrical vessel the solid particles have been found to deposit at the bottom when the agitator speed is low and the particles have been fluidized when the agitator speed reaches a certain critical value N_f. When the density of solid particles are small and the impeller is set at a height of higher than 30% of the liquid depth from the bottom of the vessel the particles have been found to accumulate at the center of the bottom. However, the setting of the impeller near the bottom of the vessel has been found to fluidize the particles. When the density of solid is small the N_f is smaller in the above case. When the density of the solid particles is large and the diameter of the particle is small, the N_f for fluidization of particles has been found to be smaller in case of the setting of the impeller near the bottom of the vessel than the N_f has been observed during placing of the impeller away from the bottom. The correlation of N_f with the
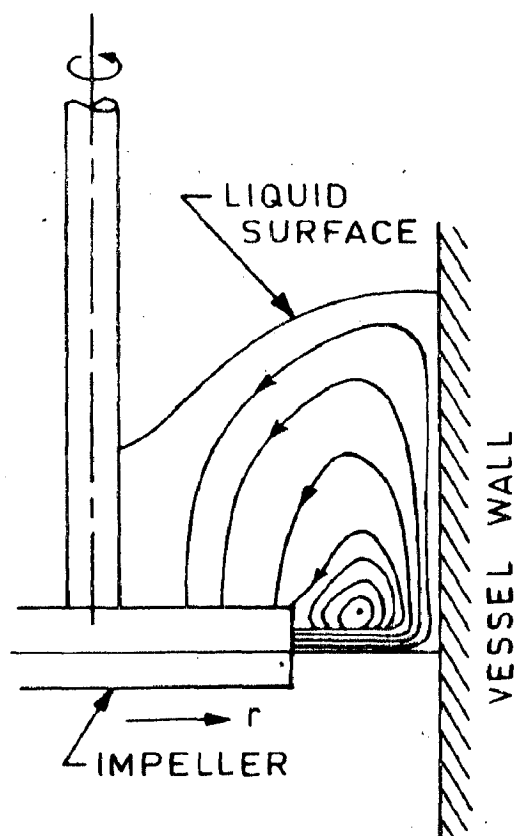
FIG. 2.5 FLOW PATTERN OF SECONDARY CIR-
CULATION FLOW [74].

factors having influence on it is expressed as [75],

$$N_f = K'D'^{-2/3} d_p^{1/3} [(\rho_s' - \rho_l')/\rho_l']^{2/3} (\eta/\rho_l')^{-1/9} (V_p'/V_p'')^{0.7} \quad .. \quad (2.32)$$

where, ρ_s' and ρ_l' are the densities of the solid and the liquid respectively, d_p is the diameter of the particle, η is the viscosity of the liquid, V_p' is the bulk volume of the particles measured in a measuring cylinder and V_p'' is the true volume calculated from the weight and its true density. The ratio V_p'/V_p'' is a correction term for the shape of the particles. The proportionality constant K' is a function of the shape of the bottom of the vessel, the impeller diameter, the position of the impeller, the number of blades, the blade width and the blade angle. The correlation of N_f given in equation (2.32) is applicable only upto a certain concentration of solid in the liquid ($\sim$ 0.105 kg/litre) beyond which the value obtained from equation (2.32) has to be corrected. The procedure of correction is complicated and may be applicable for all types of impellers. The ratio of increase in N_f with the increase of solid charged, also differs with the difference in density and size of particles.

The optimisation of impeller diameter at a given stirring speed is very much important for fluidization of the solid particles in both the central and peripheral parts of the vessel. When the impeller diameter is too small, the solid particles have been found [75] to remain suspended at the periphery of the vessel even at a speed when there is no

deposition in the center. When the impeller diameter is too large, the solid particles have been found to remain undispersed in the center of the vessel bottom. The value of the optimum diameter of impeller has been found to vary with the impeller width, blade angle, number of blades, density of solid particles and the shape of the bottom of the vessel. But the optimum diameter of the impeller has not been found to be influenced by the impeller height or liquid depth.

In case of liquid depth to vessel diameter ratio is larger than 1.0, usually the uniform suspension of particles does not result. Thus a liquid depth smaller than the vessel diameter has been recommended [75]. For uniform suspension of solid particles in an agitated vessel Rushton [76] has suggested that an impeller height of about one sixth of the liquid depth from the vessel bottom is preferable.

In the vortex method of fabrication of particulate composite the particles are directly added to the vortex formed on the vigorously stirred molten alloy. The success of the process depends on the introduction and the retention of particles inside the molten alloy. In vortex method the incorporation of a given particle in a given molten alloy depends primarily on the stirring speed, the impeller size and the position of the impeller which determines the fluidisation of solid particles in the molten alloy. The impeller blades designed to move very close to the walls of the crucible and positioned and just below the surface of the

melt has been reported [27] to be helpful for the introduction of short fibre into the melt due to the high shear rate.

The majority of the studies discussed above for mixing of solid particles in a concentrically agitated vessel are carried out for getting a uniform suspension and fluidisation of solids in a fluid. In all these studies the incorporation of solids in the liquid with the help of sucking through the vortex has not been aimed and the vortex formation has always been avoided. Thus the observed data of these studies for various mixing parameters are of limited relevence in the foundry technique of making particulate composites. So far no systematic investigation of the process parameters influencing the mixing of solid particles in molten alloy has been undertaken. It is imperative to study these aspects to achieve reproducibility in the characteristics of the cast composites and to carry out an optimisation of the process parameters for the development of this process.

(b)   Fabrication Process

The two widely used methods for the fabrication of particulate composites by foundry technique, such as liquid process and compocasting process are discussed below.

In liquid process [17,20-22,27] the liquid metals or alloys are vigorously stirred at a holding temperature of about 50 K above the melting or the liquidus point and the

particles are put into the vortex formed at the surface of the liquid during stirring. After the addition of particles stirring is continued for a certain time and then, the slurry is cast at the holding temperature as mentioned above.

In compocasting process [18, 28-31] the particulate composites are prepared with the help of rheological behaviour of the alloys. In this process the liquid alloy of a given composition, C_O, is allowed to cool down from an initial temperature, T_I, upto its liquidus temperature, T_L. A vigorous stirring of the solidifying melt is employed during further cooling of the slurry from the liquidus temperature down upto a suitable holding temperature, T_H, somewhere within the semisolid region in between liquidus and solidus temperature, T_S, of the alloy as shown schematically in Fig. 2.6. At the holding temperature the particulate materials are added to the vortex formed on the surface of the slurry and the stirring continues further for a certain time, t. Then the slurry is cast in a permanent mould by gravity die casting [17], squeeze casting [32], or pressure die casting method [17]. A variation of the compocasting process has been tried where the temperature of the slurry containing non metallic particles was raised to a temperature above the T_L and subsequently cast by gravity or pressure die casting process [18,27,28,31,33].

During compocasting one has to maintain sufficient fluidity of the slurry for its smooth flow at every
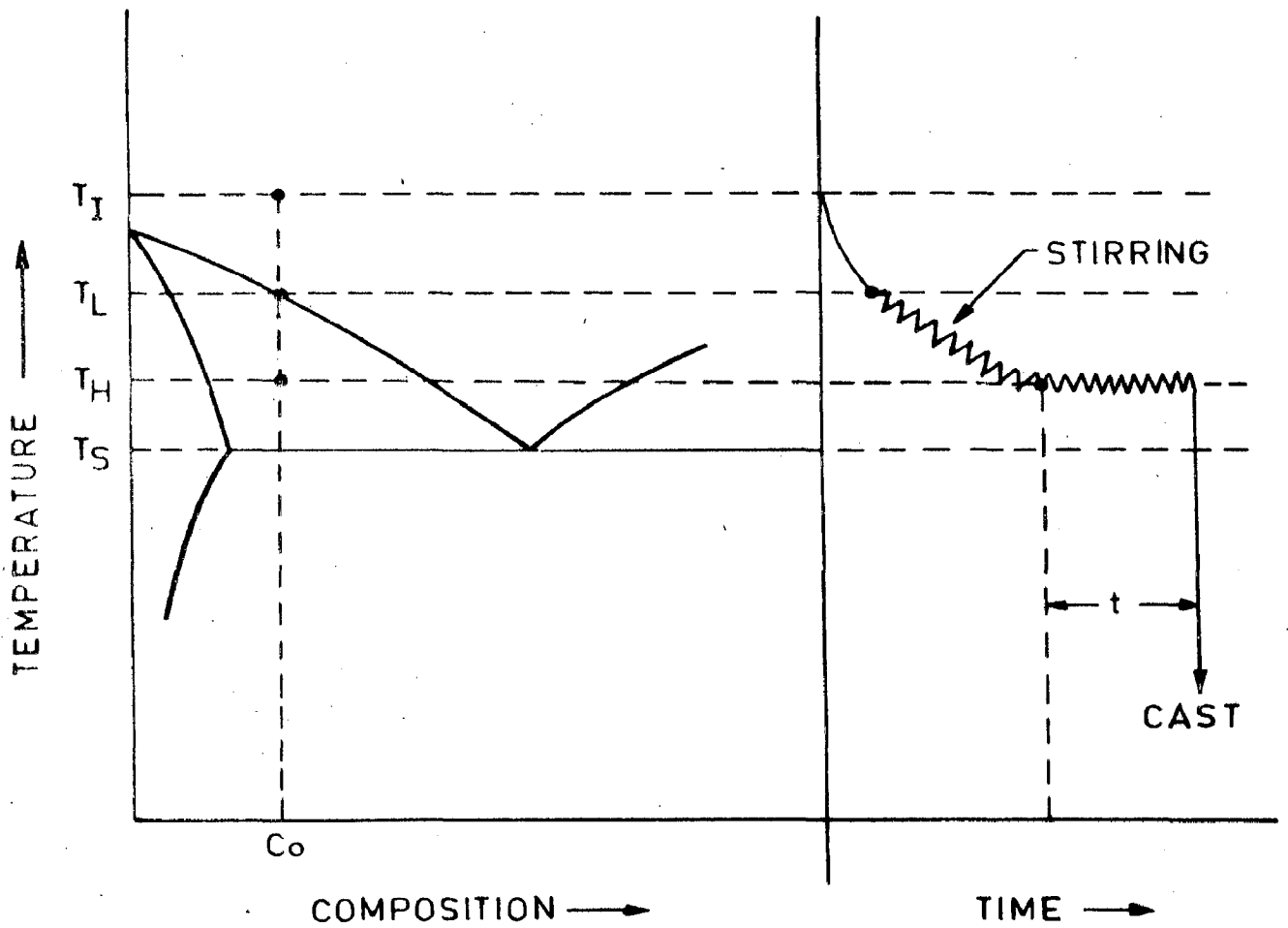
FIG.2.6 SCHEMATIC REPRESENTATION OF THE
CONDITIONS FOR COMPOCASTING IN A
BINARY EQUILIBRIUM DIAGRAM.

corner of an intricate mould. Vigorous and continuous stirring of the melt from liquid state to a semisolid state under a slow rate of cooling, retains the required fluidity for casting up to a volume fraction of about 0.5 of primary solid [77,78]. However, the incorporation of particulate materials in a partially solid slurry increases its viscosity further which may create difficulties in casting. Thus, a careful maintainance of the process parameters such as holding temperature, speed of stirring and other mixing parameters, at an optimum level is very much important for ease of casting in the compocasting technique.

The vortex method of fabrication of particulate or short fiber composites has been employed to various metals and alloys [17-22,62,79] of tin, zinc, copper and aluminium. A large variety of nonmetallic/ceramic materials such as anthracite, mica, glass, graphite, silicon carbide (SiC), magnesium oxide (MgO), alumina (Al_2O_3) of the size ranges about 1 - 200 μm have been used [17,18,33] as reinforcing material.

A review of earlier works for making particulate composites by vortex method reveals that the main difficulties associated with this process are the retention and incorporation of poorly wetting materials in the melt. The nonmetallic particles have been found to be rejected to the melt surface of aluminium and its alloys when they are added to the melt at temperatures above the liquidus [17,20]. The rejection of

particles by the melt leads to a segregation of particles at the top of an ingot and also results into an inhomogeneous distribution of particles in its matrix. The distribution of alumina particles (10-200 μm size) in aluminium and Al-11.8% Si alloy has been found to improve [20] by lowering the holding temperature of the melt from 1023K to 973K. This may have been achieved since the particles experience a resistance to floating due to an increase in the viscosity of the melt. When the particles are added in vigorously agitated partially solid slurry the added particles collide with the particles of the α-solid phase imparting kinetic energy and momentum in random directions. Thus the residence time of the particles in the slurry is enhanced [31,33] due to successive collisions. The increased residence time permits the particles to be well interacted with the slurry for providing sufficient wetting and thereby enhances the incorporation of particles even up to a level of about 30wt%. The use of compocasting has been found to be an effective process for production of particulate or short fibre composite having a large amount of particles or short fibres in it [8,28,31,33]. However, the high residence time of the particles inside the slurry may sometimes result in the form of a reacted layer like spinel formed on the incorporated alumina [33] particles in the Al-Mg alloy improving its bond strength.

The successive collisions between primary solid particles and the added particles give rise to a better mixing of the slurry followed by a homogeneous distribution

of particles in the matrix. However, sometimes it has been reported that there has been difficulties in obtaining a homogeneous distribution of particles in the matrix. Mehrabian et.al. [18] has observed that alumina particles of size 3 μm are homogeneously distributed in the aluminium - 4% Cu - 0.75% Mg composite when it has been reheated to above the liquidus temperature and cast in a die under a pressure of 100 psi. The inconsistency in the observed distribution of particles by different investigators may be attributed to the variation in mixing conditions. In the earlier studies of making composites by foundry technique, maintenance of suitable mixing conditions has been found important for incorporation and distribution of particles or short fibres inside the melt [8,27]. However, during fabrication of particulate composite by incorporating particles in vigorously stirred partially solid slurry it has been noticed that the particles of sizes greater than 5 μm are distributed homogeneously in the composite while the particles about 1 μm in size show a tendency to cluster in the matrix [31,33].

During fabrication of particulate composites by adding particles in molten metals or alloys, the distribution of particles in the matrix may also be affected by the solidification process inside the mould. While making aluminium alloy - alumina particulate composite by the liquid process the alumina particles of sizes about 80 μm have been found [35] to segregate in the interdendritic regions of similar size. The higher heat content of alumina particles and its

lower thermal conductivity results in a higher temperature of the particles relative to that in the matrix and so the advancing dendritic tips melt and preventing particle entrapment. Thus, during freezing of the composite slurry the alumina particles are generally rejected by the solid-liquid interface. In compocasting processes the solidification of the slurry does not affect the distribution of particles in the matrix significantly due to its characteristic solidification pattern.

During addition of ceramic particles in the melt a high thermal shock, due to large temperature differences between the melt and the particle have been observed [35] resulting in cracking the particles radially from the centre of the particles to the surface. Preheating of ceramic particles at a temperature of the order of the melt or higher, before addition to the melt may reduce the possibility of cracking by minimising the thermal shock.

In section 2.2.1(b) it has been observed that the presence of magnesium in molten aluminium improves its ability to wet ceramic materials and thus, enhances the incorporation of particles in the melt/slurry. Magnesium in the melt may be provided either by melting aluminium-magnesium alloy or by adding magnesium freshly in molten aluminium. For successful retention of nonmetallic materials like mica in molten aluminium Mehrabian et.al.[18] has claimed it necessary to add magnesium freshly in the melt. The alumina particles and short fibres may

be incorporated in the molten aluminium magnesium alloy. However, it has been observed [35] that it is possible to retain a larger amount of alumina in the casting by fresh addition of magnesium in the aluminium melt as compared to the molten Al-Mg alloy. It is also interesting to note that the increase in time elapsed between magnesium addition and the addition of alumina particles beyond 30 seconds decreases the amount of alumina particles incorporated in the casting [35]. However, the exact role of the freshly added magnesium on the incorporation of alumina particles in the aluminium melt has not yet been clearly understood.

After addition of ceramic particles in the melt the time required for isothermal mixing of the slurry before casting has been varied in number of investigations. The effect of different mixing time on the interaction of ceramic particles with the molten matrix and their retention in the slurry have been studied for a period ranging between 2-30 minutes [17, 18, 28]. Levi and his co-workers [28] has observed that a relatively short residence time of 10 minutes is sufficient for alumina to interact with partially solid Al-Mg alloy matrix.

Preheating of ceramic particles at temperatures similar to or higher than the melt temperature before addition to the melt has been found to enhance the amount of incorporation [80]. Preheating of particles drive out

the adsorbed and crevice gases from the particles. Thus after incorporation of preheated ceramic particles inside the melt, their contact and interaction with the matrix become much more assured due to the absence of the envelope of released gases from the particles and thus, enhances their incorporation inside the melt.

(c)   Porosity in the Composites Produced by Vortex Methods

A high level of porosity or void in the composites produced by foundry technique can be considered as a characteristics of this process. The amount of porosity in the composite is enhanced with the increased disolution of gases in the melt. During solidification of a slurry the particles impose a considerable hindrance to the passage of the evolved gases and promotes porosity in the composite produced by vortex method as discussed below.

Due to the presence of a negative pressure difference at the centre of the vortex as described in section 2.2.2(a). There is suction of air bubbles inside the melt. These air bubbles may get entrapped by the particles in the slurry. The gases in the crevices of the particles also enter the slurry. The exposure of the fresh melt surface continuously to the atmosphere due to turbulance, enhances the dissolution of gases in the melt.

The pick up of gases by the melt from the normal atmosphere can be minimised by carrying out the vortex method, making particulate composite in vacuum [81] or

in an inert atmosphere [18,27,28]. The other way to minimise the amount of dissolved gases in the slurry is by degassing the slurry with the help of some suitable gas purging. However, the degassing of the slurry by purging has not always been found suitable. In Al-5% Si-2% Fe alloy at temperature above the liquidus the ceramic particles have been found to be rejected by the melt during purging by chlorine gas [17]. This may have happened due to the alteration of interfacial energy between the particles and the melt in presence of chlorine. However, no significant rejection of ceramic particle by the molten aluminium alloy has been observed during nitrogen purging, but it has not been found as efficient as chlorine [17,27]. The adsorbed or crevice gass in the particle or moisture etc. can be minimised by preheating the particles before addition to the melt [80]. In an attempt [82] to prepare isotropic composite - materials in space by dispersion of short fibres and/or particles in molten metal matrix the degassing of the slurry has been carried out by moving the gas bubbles with the unidirectional solidification front.

Despite all these efforts it is practically very difficult and costly to prepare pore-free composites by foundry technique. Thus, in production of cast composites one has to reconcile with an amount of porosity in the composite affecting its properties adversely.

2.3   MECHANICAL PROPERTIES OF PARTICULATE COMPOSITE

The particulate composites are prepared by incorporating load bearing second phase particles in a matrix to modify its mechanical properties. In a number of cases the second phase particles may have occurred in the matrix due to transformed phase, insoluble impurities or inclusions, where the material has not been originally designed as particulate composite. These second phases, impurities or inclusions exert a considerable influence on the fracture characteristic of the material also. The mechanical properties of the particulate composite largely depend on the deformation characteristics of the matrix (continuous phase) and the particles (discontinuous phase) dispersed in the matrix. Thus, for the purpose of examining the mechanical properties of the particulate composites these materials are divided into four basic classes-

(i) brittle matrix-ductile particle

(ii) brittle matrix-brittle particle

(iii) ductile matrix-ductile particle, and

(iv) ductile matrix-brittle particle.

In this section the existing concepts on the fracture behaviour of plastically deformable composites having brittle or ductile particle in ductile matrix have been examined to evaluate its mechanical properties.

2.3.1 TENSILE PROPERTIES OF PARTICULATE COMPOSITE

The tensile properties of a composite depend on the mechanical behaviour of its components under a given condition of loading. At the initial stages of loading of a two phase composite, both the phases are elastically deformed. For a prediction of the elastic properties of the two phase composite two simple limiting models of rule-of-mixture are used [83-84]. The first one is a direct rule-of-mixtures where,

$$E_C = E_A V_A + E_B V_B \qquad \qquad (2.33)$$

E_C, E_A and E_B are the Young's modulus of the composite and the phases A and B respectively. V_A and V_B are the volume fraction of phase A and phase B respectively. Equation (2.33) represents an isostrain condition of the two phases and predicts the upper limit estimate of the Young's modulus of the composite. The other one is the inverse rule-of-mixture and estimates the lower limit of the Young's modulus as given by

$$E_C = E_A E_B / (E_A V_B + E_B V_A) \qquad \qquad (2.34)$$

Equation (2.34) represents an isostress condition of the two phases approached in particle reinforced composites.

The strength of a composite is dependent on the plastic behaviour of its phases. Beyond the elastic limit of a composite the matrix deforms plastically while the

strengthening phase may deform elastically or plastically under the stress constraints imposed by virtue of continuity with the matrix. Thus, the strength of$_\lambda$ a particulate composite is to be considered from two different angles such as the composite ⟨⟩ having deformable or undeformable particles in the matrix.

In presence of deformable particules the composite may undergo an extensive plastic deformation. The stress necessary to impart extensive ductility to these composites is identical to the flow stress of dispersed phase under the stress state present in the composite. Thus the stress initiating gross plastic flow is independent of the volume concentration of the particles and their mean free path [85]. The yield stress of the composite, σ_{yc} , under a matrix constraint sufficient to develop stress to deform the particles is expressed [84] as

$$\sigma_{yc} = [\frac{G_m G_p b}{C'}]^{\frac{1}{2}} \qquad .. \qquad (2.35)$$

where, G_m and G_p are the shear moduli of matrix and particle respectively, b is the Burger's vector of the dislocations piled up against the particle and C' is a constant. The expression does not show any relation of σ_{yc} with the geometry of the particle and the inter particle spacing.

The larger class of particulate composites are prepared by dispersing undeformable particles in the matrix which do not deform prior to fracture. The presence of these

rigid particles impart high strength to the composite but it reduces ductility below that of the matrix alone. These particles are generally brittle materials such as oxides, carbides and intermetallic phases.

The yield strength of the composite, σ_{yc}, containing non-deformable particles can be expressed as [84]

$$\sigma_{yc} = [\ \frac{G_m G_p b}{C'' \lambda_1}\ ]^{\frac{1}{2}} \qquad\qquad (2.36)$$

where, λ_1 is the interparticle spacing and C'' is a constant. λ_1 is a function of mean particle diameter, d_1, and the volume fraction of the particles, V_p, as

$$\lambda_1 = \tfrac{1}{2}d_1\ [\sqrt{\frac{2\pi}{3V_p}} - \sqrt{8/3}\ ] \qquad\qquad (2.37)$$

d_1 is expressed as

$$d_1 = \sqrt{3/2}\ 1 \qquad\qquad (2.38)$$

where, 1 is the mean linear intercept of a random particle distribution. The equation (2.37) shows that the yield strength of these composites increases with a decrease in the interparticle distance, λ_1. However, below a certain value of λ_1 the yield strength of the composite decreases due to the nucleation of cracks at weak particle-matrix boundaries.

The basic concepts of composite strengthening as given by the theories of continum mechanics and the results obtained by the earlier investigators [83,86,87], have shown a good agreement between the theory and experimental value for composites containing well aligned perfectly bonded fibres or platelets having no voids. As per Piggott [86] the theoretical ultimate tensile strength, σ_c, of a composite reinforced by platelets can be estimated as

$$\sigma_c = \sigma_{m\epsilon} \, SV_p/4 + V_m \, \sigma_{m\epsilon} \qquad .. \qquad (2.39)$$

where, the aspect ratio, $S = 2L/t_1$, L is the length of the long axis of the platelets, t_1 is the thickness of the platelets, V_p is the volume fraction of platelets, V_m is the volume fraction of matrix and $\sigma_{m\epsilon}$ is the strength of the matrix at the failure strain of the of the composite. However, when these concepts were applied to the data obtained from heat treated composite of 6061 aluminium alloy containing discontinuous silicon carbide, the agreement has not been found satisfactory [88,89]. The observed ultimate tensile strength of the composite was beyond the 20% deviation proposed by Piehler [90] from the values predicted by the rule – of – mixtures. The higher observed strength of these composites has been attributed [88] to (i) a relatively higher rate of work hardening of the matrix (ii) the strengthening of the matrix in the presence of short fibers or particles leading to the formation of a high general dislocation density, and (iii) polygonization into very small sub-grains. The mechanism of strengthening

of particulate composites developed in the context of various materials having the configuration of a particulate composite are discussed below.

Mileiko [91] followed by Garmong and Thompson [92] have developed the concept of the mechanical properties of a composite consist of two ideally bonded ductile phases. The model considers the fibre composite under a tension parallel to the axis of the fibres. The theory of Mileiko [91] relating the strength and ductility of the two ductile components to the mechanical properties of the composite is based upon the application of plastic instability criteria to the composite under the following assumptions :

(i) the relationship between the true stress and true strain for both the composite and its components can be expressed as $\sigma = K \epsilon^n$, where σ is the true stress, ϵ is the true strain and, K and n are the constants,

(ii) equal strain in both the phases, and

(iii) the flow stress of the composite can be estimated by the law of mixtures.

Though the theory of Mileiko has been developed for fibre composites yet Davies has estimated [93,94,95], the changes in tensile strength and ductility in a dual phase steel as a function of volume fraction of martensite islands and found this theory satisfactory. Following the theory of Mileiko, the relation between the tensile strength,

σ_c, the true uniform strain ϵ_c and the volume fraction of the particle, V_p, has been expressed [94], as

$$V_p = \cfrac{1}{1 + \beta' \cfrac{\epsilon_c - \epsilon_p}{\epsilon_m - \epsilon_c} \epsilon_c^{\epsilon_p - \epsilon_m}} \qquad \qquad .. \qquad (2.40)$$

where,

$$\beta' = \frac{\sigma_p}{\sigma_m} \frac{\epsilon_m^{\epsilon_m}}{\epsilon_p^{\epsilon_p}} \frac{\exp \epsilon_p}{\exp \epsilon_m} \qquad \qquad .. \qquad (2.41)$$

σ_p = tensile strength of the particle

σ_m = tensile strength of the matrix

ϵ_p = uniform strain of the particle

ϵ_m = uniform strain of the matrix

The tensile strength of the composite is given by

$$\sigma_c = V_p \lambda' \sigma_p + (1 - V_p) \lambda'' \sigma_m \qquad \qquad .. \qquad (2.42)$$

where,

$$\lambda' = (\epsilon_c / \epsilon_p)^{\epsilon_p} \exp(\epsilon_p - \epsilon_c) \qquad \qquad .. \qquad (2.43)$$

and,

$$\lambda'' = (\epsilon_c / \epsilon_m)^{\epsilon_m} \exp(\epsilon_m - \epsilon_c) \qquad \qquad .. \qquad (2.44)$$

Koo et al.[96] suggests the requirement of modification of rule-of-mixture

$$\sigma_c = \sigma_m + (\sigma_p - \sigma_m)V_p \qquad \qquad .. \qquad (2.45)$$

where,

σ_m is the stress in the matrix at the ultima

tensile strain of the particles, σ_p is the tensile strength of the particle and V_p is its volume fraction, by including some factors related to the dislocation hardening of the matrix and the geometry and distribution of second phase. Öström [97] has analysed the work of Davies [93,95] using the deformation model for two phase materials given by Mileiko [91]. The model is simple and promising but he did not find it reliable for two phase material because the theories [91,93-95] overlook the distribution and the geometry of the phases. Thus it is also necessary to have a knowledge of how stress and strain develop in the two phases during deformation of the composite.

A number of theories have been proposed for determination of strength of the dispersion-strengthened alloys modifying Orowan's original concept. The theories have been developed on the basis of the observations of a steep rise in dislocation density in these alloys with strain. In his work-hardening theory of dispersion-strengthed alloy Ashby [98,99] assumes that the work-hardening occurs due to interaction of the primary, glide dislocations with the secondary dislocation loops which intersect the slip plane. The secondary loops or forest dislocations arise from the relaxation of the large stress generated by primary dislocation loops in and immediately around the particles. Ashby envisages that during straining of a composite material there forms a plastic 'shell' around the particles which spread outwards filling the volume of the matrix between

the particles with secondary dislocations which in general, intersect the primary slip system.

For moving a dislocation by overcoming the above obstackles at a given true strain, ϵ_t and volume fraction of particles, V_p, in dual phase steel, the requirement of true stress estimated [100] as

$$\sigma_c' - \sigma_0' = K'' \; G_m \sqrt{\frac{bV_p \epsilon_t}{0.41d_1}} \qquad \qquad .. \qquad (2.46)$$

where, σ_c' is true tensile stress, σ_0' is a constant related to the initial flow stress, G_m is the shear modulus of the matrix, b is the Burger's vector of the matrix dislocations, d_1 is the average particle diameter and K" is a constant.

Differentiation of equation (2.46) with respect to true strain may give the work hardening rate

$$\frac{d\sigma_c'}{d\epsilon_t} = 0.78 K'' \; \frac{G_m b^{1/2}}{\epsilon_t^{1/2}} \sqrt{\frac{V_p}{d_1}} \qquad \qquad .. \qquad (2.47)$$

Brown and Stobbs[110] further modified the equation (2.47) by including the contribution of internal stress to hardening as

$$\sigma_c' - \sigma_0' = M^{3/2} [K_2 G_m \sqrt{\frac{48bV_p \epsilon_p'}{\pi d_1}} + (\frac{16\pi b}{K_2^2 \epsilon_p' d_1})^{1/8}$$

$$K_2 G_m V_p \sqrt{\frac{16 \; b \epsilon_p'}{\pi d_1}} \;] \qquad \qquad .. \qquad (2.48)$$

where, ϵ'_p is the true tensile plastic strain, K_2 is a constant and, M is the Taylor's factor. The plastic strain ϵ'_p is related to the true strain ϵ_t as

$$\epsilon_t = \epsilon'_p + \frac{\sigma'_c}{E} \qquad \qquad .. \qquad (2.49)$$

where E is the Young's modulus. The contribution of elastic deformation on total strain is negligible, thus $\epsilon_t \simeq \epsilon'_p$. The term $(16 \, \pi \, b/K_2^2 \, \epsilon'_p d_1)^{1/8}$ of equation (2.48) always gives a value close to unity [101], and varies slowly with ϵ'_p and d_1. So equation (2.48) can be written as

$$\sigma'_c - \sigma'_0 = A\sqrt{\frac{\epsilon_t V_p}{d_1}} + BV_p\sqrt{\frac{\epsilon_t}{d_1}} \qquad .. \qquad (2.50)$$

where,

$$A = M^{3/2} \, K_2 G_m \sqrt{48b/\pi}$$

$$\qquad \qquad \qquad \qquad \qquad \qquad .. \qquad (2.51)$$

$$B = M^{3/2} \, K_2 G_m \sqrt{16b/\pi}$$

The work hardening rate obtained by differentiating equation (2.59) with respect to ϵ_t can be expressed as

$$\frac{d \, \sigma'_c}{d \, \epsilon_t} = \frac{A}{2\sqrt{\epsilon_t}}\sqrt{\frac{V_p}{d_1}} + \frac{B}{2\sqrt{\epsilon_t}}V_p\sqrt{\frac{1}{d_1}} \qquad .. \qquad (2.52)$$

For a given value of V_p the equation (2.52) can be written as

$$\sigma'_c = \sigma'_0 + A''\sqrt{1/d_1} \qquad \qquad .. \qquad (2.53)$$

The equation shows a linear relationship between the σ'_c and $d^{-\frac{1}{2}}$ with a slope A". However, it cannot be plotted because of the unknown constant σ'_o. Lanzilloto and Piekering [102] has observed that the work hardening rate increases with an increase in the volume fraction of the particles and also, with a decrease in the particle size.

In the above models the discrepancies have been observed between the predicted and the experimental values of the rate of work hardening and are attributed to the deformation of the particles at a higher strain level and also, to the decohesion of the particle-matrix interface. Thus the assumption of compatible deformation between the phases to maintain matrix particle continuity is no longer tenable at these higher strains and so ~~in this level of strain~~ the theory is no longer applicable.

In transmission electron microscopic observations on the microstructure of heat treated composite of 6061 aluminium alloy containing SiC, Arsenault and Fisher [88] has observed the presence of high dislocation density of the order of $2 \times 10^{10}/cm^2$ in the matrix around the short fibres and the particles. Arsenault [89] proposed a model equation for estimation of ultimate tensile strength, σ_c of the dislocation strengthened composite as

$$\sigma_c = \sigma_{disl} + \sigma_{sg} + \sigma_{wh} + \sigma_{comp} + \sigma_{ah} \quad .. \quad (2.54)$$

where,

$$\sigma_{disl} = \beta \, G_m \, b \, \rho^{\frac{1}{2}} \quad .. \quad (2.55)$$

β is a constant approximately equal to unity, G_m is the shear modulus of the matrix, b is the Burger's vector, ρ is the average dislocation density, σ_{sg} is the subgrain component of strengthening, σ_{wh} is the increase in the stress due to work hardening between the yield stress and the ultimate tensile strength, σ_{ah} is the increase in strength due to heat treatment and σ_{comp} is the strengthening of the composite predicted by equation (2.39). The value estimated by equation (2.54) has been found to be in good agreement to the experimental ultimate tensile strength values [89].

2.3.2   DUCTILE FRACTURE OF COMPOSITES

The ductile fracture of crystalline solids occurs by the formation of cracks under excessive plastic deformation. The initiation of cracks in a solid is created by the crystal defects which are attributed to the forces like tensile, compressive, shear and hydrostatic being developed from different nature of stress and strain fields. Thus to realise the fracture mechanism in a composite it is essential to have a knowledge about the stress and strain fields in the matrix and around the reinforced component of a composite.

The ductile fracture mechanism is in general considered by three interconnected stages as, the nucleation of microvoids, the void growth and their linkage or coalescence.

(a)   Void Nucleation

For void nucleation at the interface of solid particles in a particulate composite two necessary criteria have been proposed namely, stress criterion and energy criterion [101, 103-105].

As per the stress criterion proposed by Ashby[99] the void nucleates at the interface if the stress at that place exceeds its fracture stress. According to the theory proposed by Tanaka et al. [106] the void nucleation takes place in a plastically deforming matrix under uniaxial tension. The critical void nucleating strain, ϵ_N, at the interface of a soft particle ($\beta' < 1$) is given as,

$$\epsilon_N \geqslant [\frac{(7-5\nu)(1+\nu^*) + (8-10\nu)(1+\nu)\beta'}{10(7-5\nu)}]^{\frac{1}{2}} \quad .. \quad (2.56)$$

where, ν and ν^* are the Poisson's ratio of the matrix and the particle respectively and β' is the ratio of Young's modulus of the particle to that of the matrix. For hard particles ($\beta' > 1$), the ϵ_N is expressed as

$$\epsilon_N \geqslant [\frac{(7-5\nu)(1+\nu^*) + (8-10\nu)(1+\nu)\beta'}{10(7-5\nu)\beta'}]^{\frac{1}{2}} \quad .. \quad (2.57)$$

For nucleation of a void at the interface the normal stress at the particle matrix interface must exceed a critical

value, σ_c , which is expressed as

$$\sigma_c = \sigma_{loc} + \sigma'_m \qquad \qquad .. \qquad (2.58)$$

where, σ_{loc} is the local stress and σ'_m is the hydrostatic stress. σ_{loc} is determined by local dislocation density, ρ_{loc} , at the particle. Assuming $\sigma_{loc} \propto \sqrt{\rho_{loc}}$ the void nucleation strain, ϵ_N , is expressed as

$$\epsilon_N^{\frac{1}{2}} = 1/H'(\sigma_c - \sigma'_m) \qquad \qquad .. \qquad (2.59)$$

where, H' is a constant. According to the

~~As per~~ energy criterion concept the nucleation of void can take place when it is energetically favourable as

$$E_1 > E_2$$

where, E_1 and E_2 are the total energy of the specimen before and after void nucleation respectively.

During plastic deformation of the ductile matrix large internal stresses are developed around the non-deformable large ~~enough~~ particles due to the entangled secondary dislocations, the movement of which reduces the stress. The internal stress is characterised by a dimensionless parameter, ϵ_p^*, which is equal to the strain when the internal stress is balanced by the local flow stress developed due to work hardening of the matrix and becomes zero.

Nucleation of a void releases the internal stress along with the elastic stress and the total energy released has been termed as elastic energy. When the released elastic

energy is more than the requirement of energy for the creation of a new surface, the void nucleation is energetically favourable. According to Brown and Stobbs [101] the critical strain required for the nucleation of void, ϵ_N, can be expressed as

$$\epsilon_N \geqslant \frac{3\gamma}{G_p\, b} \qquad\qquad .. \qquad (2.60)$$

where, γ is the surface energy per unit area and G_p is the shear modulus of the particle.

For void nucleation, Tanaka et al.[106] proposed a theory based upon a strain energy calculation in and adjacent to the particles. His expression for ϵ_N is different from that of Brown and Stobbs in respect of its dependence on the size of the particle. The nucleation of voids at the particles larger than 200-300 A° in diameter occur at the critical strain which can be derived from the energy criterion [106]. However, the growth of voids with further plastic strain at the interface may be controlled by the stress criterion. Hence the critical strain obtained by the stress criterion may provide the upper limit of strain for the void nucleation [106].

The energy criterion of Brown and Stobbs [101] results in a critical strain for nucleation of void independent of particle size but in the theory of Tanaka [106] it is inversely proportional to the square root of the particle radius. However, both the theories indicate

that smaller particles, satisfy first the stress criterion and then the energy criterion for fracture, in contrast to bigger particles.

Palmer and Smith [107] has observed that at room temperature equiaxed non-deforming particles produces voids after having an uniform elongation under tensile deformation. For a given particle size, the void nucleation strain does not depend remarkably on the volume fraction of the particles. The Edelson et al.[108] and Gurland et al.[109] have observed, at most, a minor effect of particle size or inter particle spacing on the ductility of materials. However, in spheroidized carbon steel Inoue et al.[110] has observed that the amount of strain required to initiate voids increases as the interparticle spacing increases. Palmer and Smith [107] have noticed that within a given specimen larger particles tend to form voids at lower strains than smaller particles. However, Rogers [111] has experienced that not all systems show a marked size dependence. The void nucleating strain has been observed to depend strongly upon the shape and orientation of the particle [112], the adhesion between particles and the matrix []3] and on the impurity addition which lowers the stacking-fault energy and produce a tendency to high stress concentration. It has been noticed [106] that the void can be nucleated in the very early stages of plastic deformation. However, in steels with spheroidized carbides Pickering [114] has been observed to initiate voids in the late stages of plastic deformation.

(b)   Growth and Coalescence of Void

McClintock [115,116] and Rice and Tracey [117] have proposed two elegant solutions for estimation of the expansion of an isolated void in terms of the imposed strain rate. McClintock developed the model for the growth of a cylindrical hole in a hardening plastic matrix. In a non-hardening plastic matrix Rice and Tracey has observed a non-linear relationship between the radial velocity of the void surface and the applied strain field during the growth of a spherical hole. According to their assumption a spherical particle of radius r_0, initiates a void of its own size and subsequently grows to an ellipsoidal shape, elongated in the tensile direction and characterized by its major axis, and minor axis. LeRoy et al.[118] proposed that the minor and major semi-axes r_4 and r_5 respectively of an idealised ellipsoidal void can be related to their rates of increase $\dot{r}_4$ and $\dot{r}_5$ as

$$\dot{r}_5 = r_5 [\, \gamma_a \, \dot{\epsilon}^{\infty}_3 + 0.56 \, \dot{\epsilon}^{\infty}_3 \, \sinh (\frac{3}{2} \frac{\sigma_m{}'}{\sigma_c})] \qquad \qquad .. \qquad (2.61)$$

$$\dot{r}_4 = r_4 [- \frac{\gamma_a}{2} \, \dot{\epsilon}^{\infty}_3 + 0.56 \, \dot{\epsilon}^{\infty}_3 \, \sinh (\frac{3}{2} \frac{\sigma_m{}'}{\sigma_c})] \qquad \qquad .. \qquad (2.62)$$

where, σ_c, is the tensile flow stress of the material which is assumed constant, $\sigma_m{}'$, is the mean stress, $\dot{\epsilon}^{\infty}_3$ is the tensile strain rate at a point remote from the void i.e. the equivalent average strain rate $\bar{\epsilon}$, γ_a is a factor which describes the amplification of the growth rate of the void

relative to the strain rate of the matrix. The expressions for r_5 and r_4 are derived as

$$r_5 = r_0 \exp(D\bar{\epsilon}) \left[2 \exp\left(\frac{3\,\bar{\epsilon}}{2} \right) - 1 \right]^{2/3} \qquad \cdot\cdot \qquad (2.63)$$

$$r_4 = r_0 \exp(D\bar{\epsilon}) \left[2 \exp\left(\frac{3\,\bar{\epsilon}}{2} \right) - 1 \right]^{-1/3} \qquad \cdot\cdot \qquad (2.64)$$

when,

$$D = 0.56 \sinh\left(\frac{3}{2} \frac{\sigma_m'}{\sigma_c} \right) = \tfrac{1}{2}\left[\exp\left(\frac{3}{2} \frac{\sigma_m'}{\sigma_c} \right) - \exp\left(- \frac{3}{2} \frac{\sigma_m'}{\sigma_c} \right) \right]$$

$$\cdot\cdot \qquad (2.65)$$

Failure due to growth of a void possibly takes place by two mechanisms. The material between growing voids becomes thinner with an increasing strain till a necking instability sets in, resulting in a coalescence of the voids and eventual fracture when,

$$r_5 = 3r_5^{crit} \qquad \cdot\cdot \qquad (2.66)$$

The critical size of the void at fracture can be estimated as

$$r_5^{crit} = K\, r_0\, \left(\sqrt{\pi/6v_p} - \sqrt{2/3} \right) \qquad \cdot\cdot \qquad (2.67)$$

where, K is a constant which may be a function of material tested. The fracture of the material takes place when $r_5 \geqslant r_5^{crit}$. The fracture occurs when the void length $2r_5^{crit}$ at an observed fracture strain, ϵ_f, becomes nearly

equal to the planar spacing of voids estimated on the basis of the geometrical criterion for necking. Brown and Embury[119] have proposed that after nucleation the voids grow by plastic extension and as soon as the spacing of neighbouring voids becomes equal to their length, a slip plane can be drawn between the voids, and the plastic constraint caused by the surrounding material preventing local deformation is lost. Once this situation is achieved any further plastic flow is localised in one plane and ductile fracture takes place immediately. In tensile testing the necking occurs well before this geometrical condition is met. Thus, the geometrical condition for the removal of the plastic constraint gives strictly a lower limit to the true strain to fracture, ϵ_f. The geometry of the growth of void and local necking described above is confirmed [120] by scanning electron microscopic observation on ductile fracture. The geometrical criterion proposed above differs from that used by McClintock [115] in regard to the definition of the point of instability. In the treatment by McClintock the onset of necking is attributed to the commencement of a localised shear between the neighbouring voids but in the Brown and Embury model [119] the onset of necking is attributed to the localised collapse between voids by the transition from smooth necking to local fracture.

After nucleation of a void on a particle of radius r_0, a further strain ϵ_g produces a void of length $2r_0$ $(1+ \epsilon_g)$. According to the geometrical consideration for failure by growth of void it is required that this length of void must be

equal to the spacing of neighbouring voids centered in the same plane. The mean planar spacing of spherical particles in a matrix having V_p volume fraction of particle is expressed as

$$2r_0(1+ \epsilon_g) = r_0(\sqrt{\frac{2\pi}{3V_p}} -\sqrt{\frac{8}{3}}) \qquad .. \qquad (2.68)$$

As per the simplified model given by Brown and Embury[119] the strain to fracture, ϵ_f, is the sum of the strain to nucleate the void, ϵ_N, and the further strain required for its growth, ϵ_g, to the critical size can be written as

$$\epsilon_f = \ln \frac{A_0}{A_f} = \ln(1+ \epsilon_g+ \epsilon_N) = \ln(\sqrt{\frac{\pi}{6V_p}} -\sqrt{\frac{2}{3}} + \epsilon_N) \qquad (2.69)$$

The equation(2.69) shows that the true strain to fracture is largely controlled by the volume fraction of particles when it is less than 5%. However, as per equation(2.68), the growth strain becomes zero above a critical volume fraction of particle of 0.159, so that for higher volume fractions of particle the fracture strain is controlled entirely by the nucleation strain plus the final linkage strain, and therefore strongly depends upon particle shape, adhesion and the work hardening rate of the matrix. With a reasonable expectation LeRoy et al.[118] attempted to conceive the ductile fracture process as the void nucleation and void growth are not sequential process, but after nucleation of a first void the nucleation and growth of voids take place simultaneously. Using a linearized form of Rice and Tracy[117] model, Schmitt and Jalinier[121] predicted the growth and change in shape of a spherical void under biaxial state of stress and confirmed his theoretical predictions by experimental observations.

2.3.3   ELEVATED TEMPERATURE STRENGTH OF PARTICULATE COMPOSITE

The tensile behaviour of aluminium alloy particulate composite under short time exposure of about 2 minutes in air at elevated temperatures between 460 K to 682 K is of considerable interest in advanced missile design [122] and other elevated temperature applications. However, a very limited number of work has so far been carried out to understand the effect of elevated temperature on the mechanical properties of particulate composites. Besides the amount, size, shape and distribution of particles in the matrix along with the stability of the particle-matrix bond strength at elevated temperature, the elevated temperature mechanical properties of the matrix is very important. Thus during fabrication of particulate composites the matrix material should be selected carefully. For making aluminium alloy – alumina particulate composite having good elevated temperature property, Al-Mg alloy has received considerable attention because in this composite the reacted layer (consisting of $MgAl_2O_4$) formed at the particle-matrix interface is significantly stable [28] and retains the bond strength at elevated temperature as discussed earlier in section 2.2.1(d). It has also been observed that the decrease in strength of the Al-Mg alloy with increasing temperature is less rapid than that observed in other aluminium alloys due to the formation of magnesium clouds around the dislocations hindering their movement[123].

The failure characteristic of a material under short time exposure at high temperature is so far not very much clear. In an investigation on the high temperature tensile strength and ductility of Co_3Ti alloy Takasugi et al.[124] has observed that the increase in test temperature decreases the work hardening rate of the matrix. They have found that this has been possible due to dynamic recrystalization of the matrix appeared as newly formed small grains during deformation which accomodate the stress concentration resulting into an increase in ductility and decrease in strength at high temperatures. The failure has been caused [124] on the grain boundaries leading to the formation of micro-cracks along grain boundaries where insufficient recrystalization took place. The density of micro-cracks decreases with the distance from the fracture surface as the dynamic recrystalization takes place significantly near the fracture surface [124]. In any material during its tensile deformation at elevated temperature the dynamic recrystalization takes place beyond a certain temperature. At lower temperature the plastic accomodation at the inclusions or particles become more difficult giving rise to the local stress and helps in sooner nucleation of voids [118]. The elevated temperature fracture strain of a material increases with the increase of temperature upto a certain limit followed by a reduction with further rise in temperature as it is observed by LeRoy et al. [118] in spheroidized carbon steel and Takasugi et al.[124] in polycrystalline Co_3Ti.

CHAPTER 3

EXPERIMENTAL WORK

3.1   SELECTION OF MATRIX ALLOY

The chemical composition of the matrix for fabrication of aluminium alloy composite is chosen on the basis of wettability between the matrix and the reinforced ceramic particles. The matrix of Al-4wt.% Mg alloy has been of great interest due to its ability to provide a satisfactory wetting as well as a good bonding strength between the matrix and the alumina particles as discussed earlier in section 2.2.1(b).In Al-4wt.% Mg alloy the gap between the liquidus and solidus temperatures, as shown in Fig. 3.1, is suffi- ciently wide facilitating the application of compo- casting technique for the fabrication of particu- late composite by vortex method. On the basis of the above considerations Al-4wt.% Mg alloy has been selected as a matrix for the fabrication of Al-4wt.% Mg-Al_2O_3 particulate composites in the present inves- tigation.
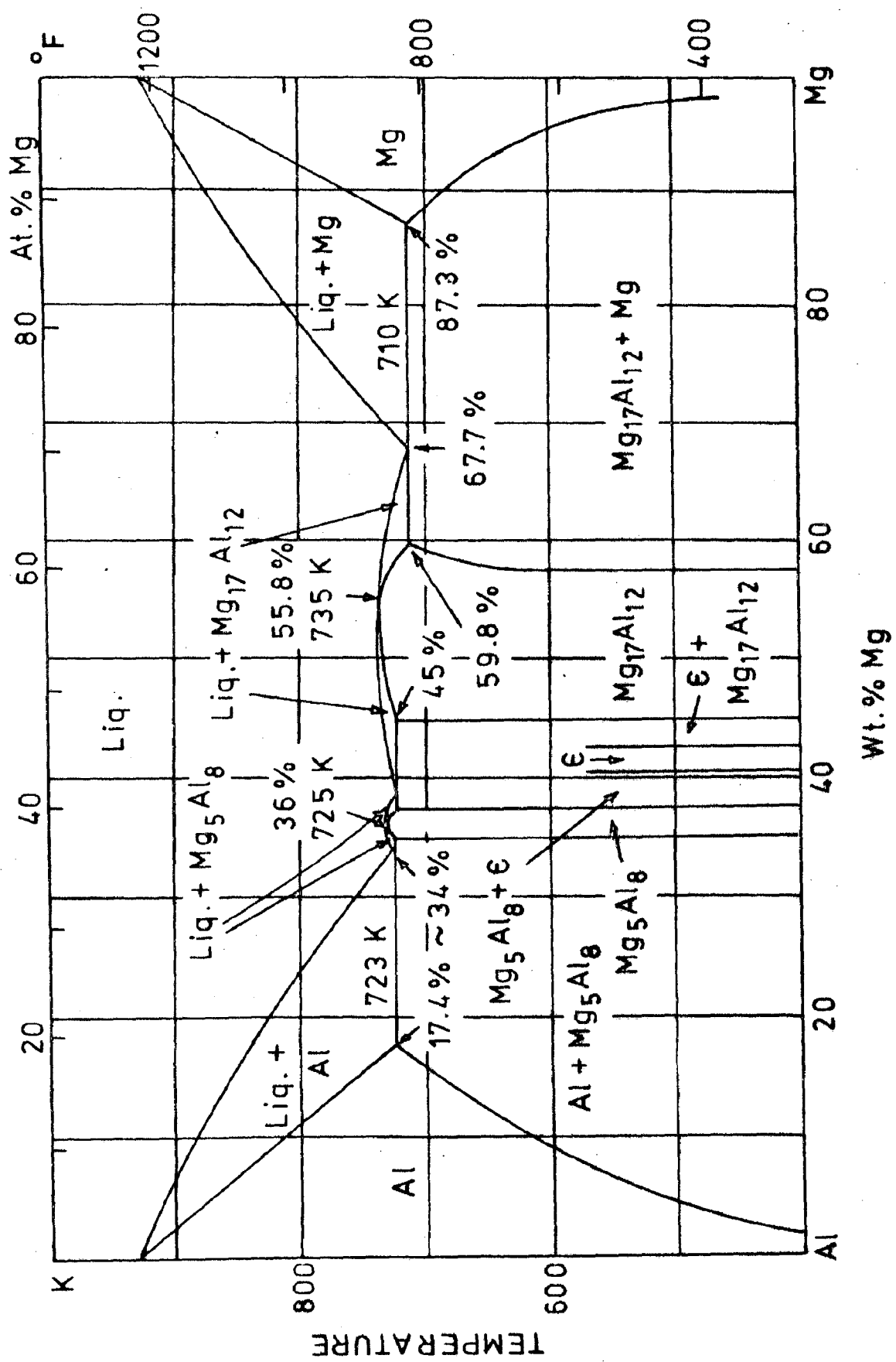
FIG. 3.1 EQUILIBRIUM PHASE DIAGRAM OF AL-Mg SYSTEM [123].

3.2   SELECTION OF PROCESS VARIABLES

In earlier studies related to the making of composites by foundry technique, the maintenance of suitable mixing conditions during the process has been found important. To achieve the maximum incorporation and a homogeneous dispersion of alumina particles in the aluminium alloy slurry, the stirring speed, the size of impeller, the position of impeller inside the slurry and the holding temperature of the melt/slurry were varied in preparing a number of Al-Mg — Al_2O_3 cast particulate composites.

The stirring speeds of 7.5, 9.7, 16, 19, 22.5 and 25 revolutions.s^{-1} were employed.

For optimization of impeller size several impellers with varying diameter, d, were used. As for a given impeller the mixing characteristic depend upon the clearance between the impeller and the wall of the crucible, the size of the impeller was represented by a dimensionless parameter; the diameter ratio d/D, where, D is the diameter of the crucible at the surface of the slurry. The surface diameter of the slurry with the stirrer dipped into it was measured by a divider. In this work the value of diameter ratio, d/D were varied as 0.56, 0.59, 0.63, 0.71, 0.72 and 0.74, where the value of D was maintained at 81 mm.

The position of impeller inside the slurry was varied by adjusting the shaft length of the stirrer. It

has been reported as a dimensionless height ratio, h/H, where, h, is the position of impeller from the bottom of the crucible and, H, is the depth of the slurry at rest in the crucible. The depth of the impeller from the surface of the slurry, h', and the depth of the slurry, H, were estimated by dipping a graduated scale into the melt. The value of h was estimated as

$$h = H - h' \qquad\qquad .. \qquad (3.1)$$

The h/H ratio of 0.54, 0.67, 0.74, 0.81, 0.87, and 0.91 were employed in this investigation. The impeller and its position inside the slurry are schematically shown in Fig. 3.2.

The influence of the holding temperature on the incorporation of alumina particles in the melt/slurry were studied at temperatures of 883, 900, 930, and 958 K. At the holding temperature below 900 K pouring of the slurry was often difficult due to the choking of the hole at the bottom of the crucible.

The investigations on the effect of stirring speed, size of impeller, position of impeller and the holding temperature of the melt/slurry separately on the incorporation of alumina particles in the melt were carried out by varying the relevent parameter while keeping the other three process parameters constant as described below.
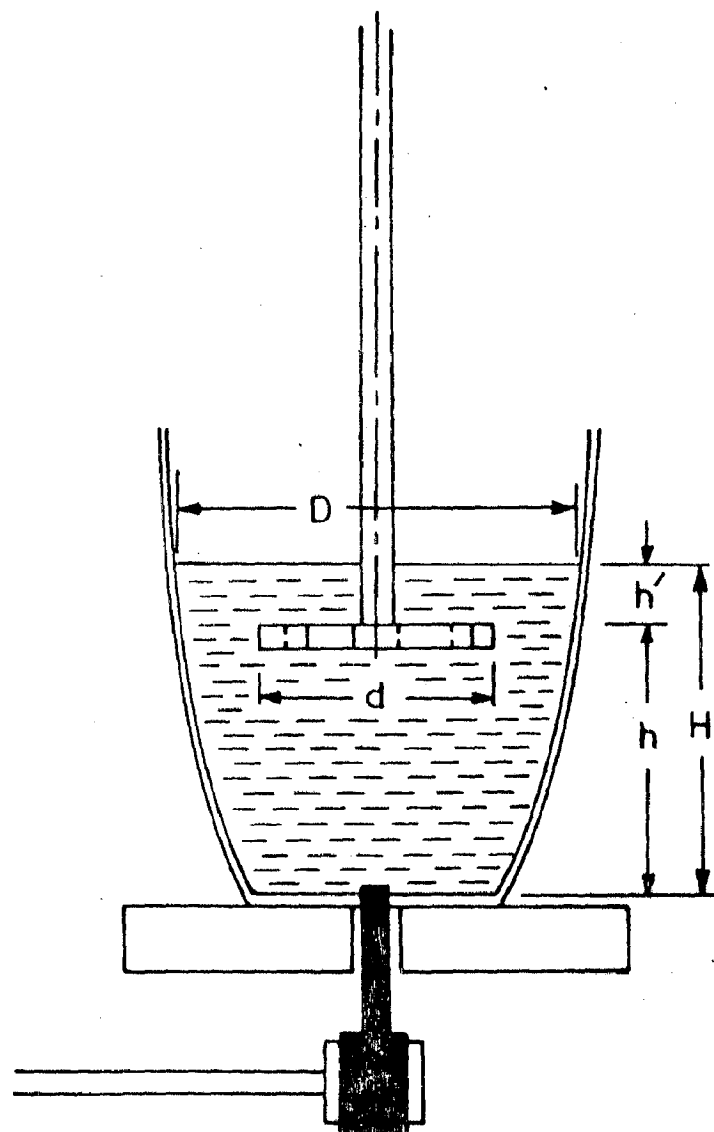
FIG. 3.2 SCHEMATIC PRESENTATION OF THE CRUCIBLE CONTAINING LIQUID MELT AND THE RELATIVE POSITION OF THE STIRRER.

PARAMETER UNDER INVESTIGATION	GIVEN VALUE OF OTHER PROCESS PARAMETERS .
Stirring speed	d/D=0.63; h/H=0.81; 900 K
Size of the impeller	16 revolutions.s^{-1}; h/H=0.81; 900 K
Position of impeller	16 revolutions.s^{-1}; d/D=0.63; 900 K
Holding temperature	16 revolution.s^{-1}; d/D=0.63; h/H=0.81

3.3   CASTING PROCESS

A batch type of compocasting set-up, schematically shown in Fig. 3.3, was used in this investigation. The set-up consists of a melting unit, a stirring arrangement and a bottom pouring system. The melting unit was a resistance heating vertical muffle furnance constructed by winding a 18 SWG Kanthal wire over a muffle of 125 mm x 125 mm x 260 mm size, having a total resistance of 30 ohms. One end of the muffle was open and the other end was closed having a hole in its center. The

FIG. 3.3 SCHEMATIC DIAGRAM OF THE EXPERIMENTAL SET-UP FOR MAKING CAST COMPOSITES.
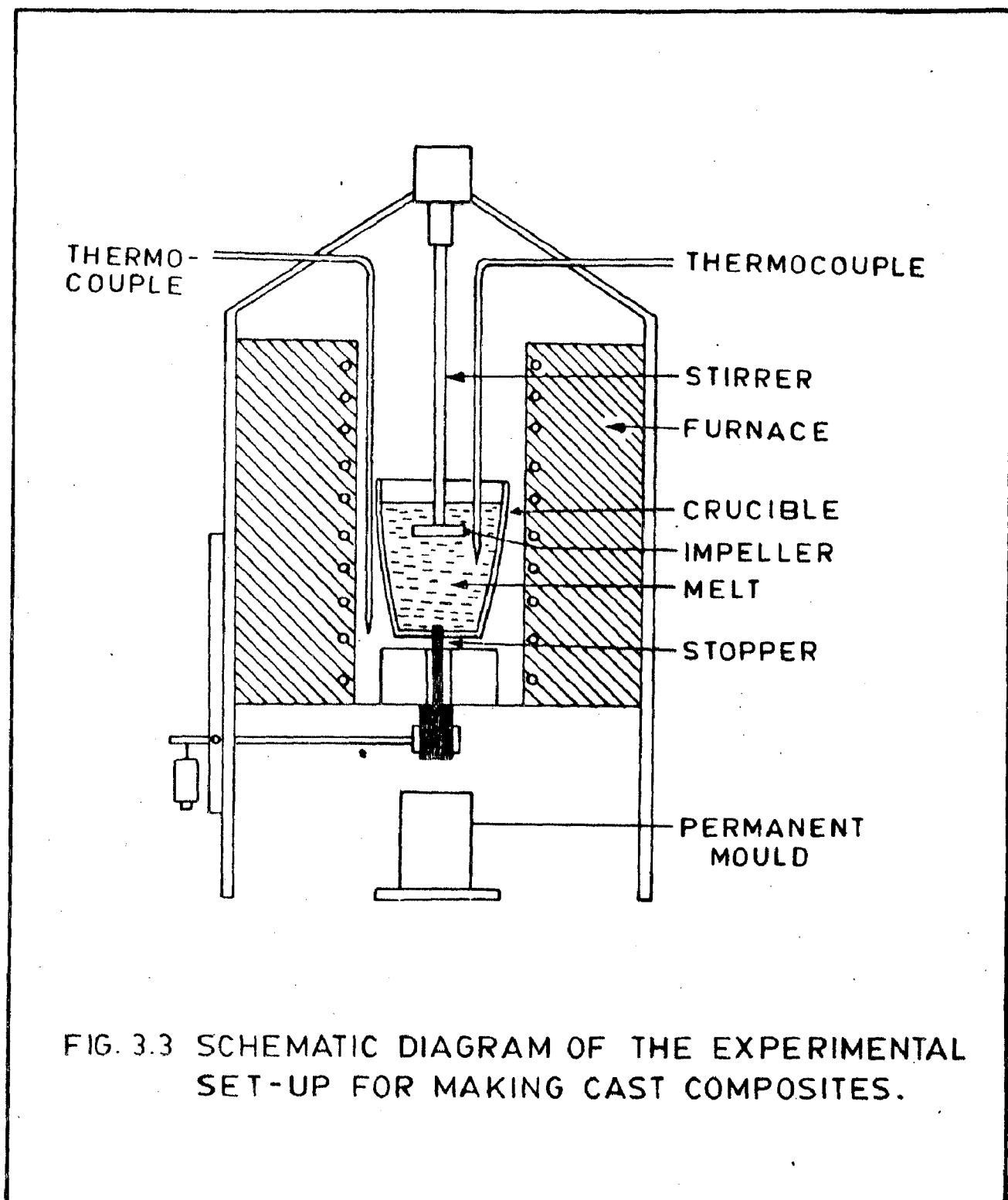
muffle was mounted on a steel frame leaving a sufficient clearance from the floor for placing the mould conveniently right below the furnance. The electrical connection to the furnace was given through an auto transformer to control the power input to the furnance. A $Pt/Pt-13\%Rh$ thermocouple connected to a temperature controller having a range of $0-1600°C$ and a control accuracy of $\pm5°C$ was placed close to the muffle wall to control the temperature of the furnance at a desired level during casting.

For melting of aluminium a graphite crucible having a bottom hole of 12 mm in diameter was placed inside the muffle furnance as shown in Fig. 3.3. The hole was plugged with a graphite stopper inserted through the hole in the bottom of the muffle. The stopper was held in place with the help of a lever arrangement as shown in Fig. 3.3.

A stirrer driven by a 1 HP motor having a maximum rated speed of 66.7 revolution.s^{-1} was used for stirring the melt. The motor of the stirrer was held rigidly over the furnance by a gripping arrangement fixed with the steel frame structure of the set-up. Flat four blade impellers of desired diameters, machined out from 3 mm thick mild steel sheet was fastened at one end of the stirring rod connected to the shaft of the motor. A schematic diagram of the impeller has been shown in Fig. 3.4.
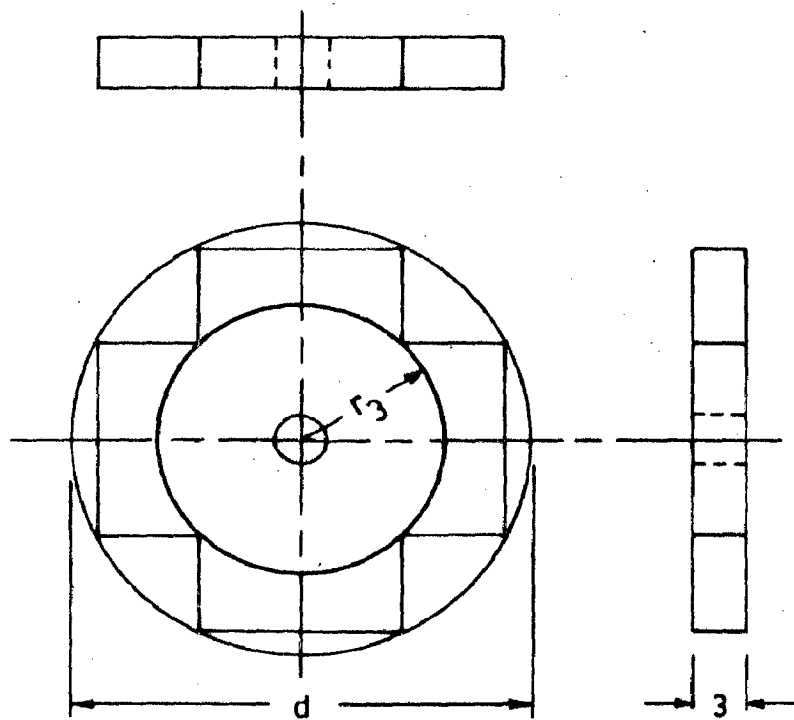
Dimension in mm

FIG. 3.4 SCHEMATIC DIAGRAM OF THE IMPELLER.

About 500 gms of commercially pure aluminium was taken in the graphite crucible inside the furnance and heated upto 1005 K. After melting the temperature of the furnance was allowed to come down by switching off the furnance. The temperature of the melt was continuously measured with the help of a chromel/alumel thermocouple, having a protective sheath, placed inside the melt at a depth of 15-20 mm. The temperature was read out directly in Fahrenheit scale on a Leeds-Northrup No. 8694 potentiometer, with a least count of 2.5°F. The temperature obtained in Fahrenheit scale was converted to Kelvin scale and reported. About 25 g of magnesium lump, with an estimated loss of 20% due to evaporation and burning was covered in an aluminium foil and added to the aluminium melt at temperature about 975K. The surface of the melt was cleaned by skimming. When the melt temperature came down to 20-30 K above the desired holding temperature, the stirrer with impeller preheated to 373 K was introduced into the slurry. The position of the shaft of the stirrer was always kept at the center of the slurry surface. The slurry was vigorously agitated at different speeds as per requirements and the furnance was put on. The alumina particles preheated to 1072 K were added to the vortex formed on the slurry surface during stirring. The particles were added at the rate of 1.66-2.5 g/second to the slurry when the temperature of the slurry was held at the desired temperature. $\alpha-Al_2O_3$ particles used in this investigation

had been supplied by M/S Burgoyne Urbidges & Co., India
and were approximately round in shape as shown in Fig.
3.5. The size analysis of the particles were as mentioned
in Table 3.1. The particles with sizes in a restricted
ranges of (+6, -45) μm, (+53,-75) μm, (+106, -125)μm and
(+180, -212)μm were also used as reinforcing particles
for making particulate composite in a certain phase of
this work. The stirring was continued for 225-240 seconds
after the addition of the particles to the slurry and the
speed of stirring was maintained at a desired level by
regulating the power input to the motor of the stirrer
through an auto transformer. During stirring the speed
was measured continuously with the help of a strobometer
capable of measuring speeds upto 300 revolution.s^{-1}.

After stirring the slurry for a given time as
mentioned earlier the graphite stopper was removed from
the bottom of the crucible and the slurry was poured directly
into a 25 mm x 30 mm x 300 mm permanent split mould kept
below the furnance. The mould was kept as close as possible
to the bottom of the furnance leaving only the necessary
clearence between the two for smooth removal of stopper.
During pouring the stirring was continued. The ingot was
quenched immediately after casting. The holding temperatures
for the purpose of this work were both above and below
the liquidus temperatures of Al-4wt.% Mg alloy matrix as
determined. The liquidus and solidus temperatures of
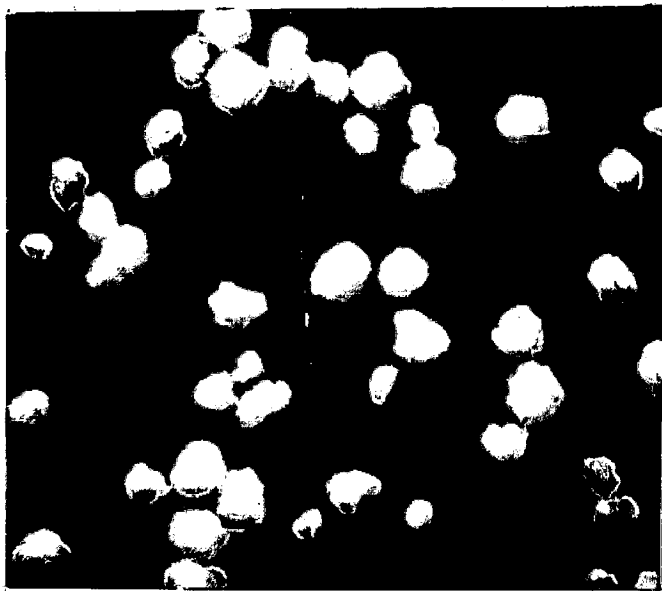
X 50

FIG.3.5 PHOTOMICROGRAPH SHOWING THE ALUMINA
POWDER USED IN THIS INVESTIGATION.

TABLE 3.1

DISTRIBUTION OF VARIOUS SIZES OF PARTICLES IN THE
ALUMINA POWDER USED WITH A BROAD SPECTRUM OF SIZES

	Size of the Alumina particles (µm)								
	+212	+180 -212	+125 -180	+106 -125	+75 -106	+63 -75	+53 -63	+45 -53	-45
Amt. wt.%	0.31	49.37	13.90	31.56	1.87	1.73	0.33	0.15	0.78

Liquidus/ melts the alloy casting are determined The liquidus and solidus temperatures of Al-4wt.% Mg alloy were estimated from standard Al-Mg binary phase diagram as 915 K and 875 K respectively. For each combination of process parameters castings were carried out five to seven times.

The alumina particles having a broad spectrum of sizes were employed during preparation of cast composites using various process parameters under investigation. But to study the effect of the size of particles on the incorporation of alumina inside the melt, the alumina particles of close size ranges were used for making cast composites and the stirring speed of 16 revolution . s^{-1}, the size of impeller, d/D=0.63, the position of impeller, h/H=0.81 and the holding temperature of 900 K were employed.

Some castings with the same composition of aluminium and magnesium as it has been used for matrix alloys were prepared with no addition of alumina particles by following a similar procedure as discussed above. The melt was not stirred and was poured in the similar mould at temperature of 55-65 K above the liquidus. These castings were termed as conventional castings and were used for comparison of properties with those of the particulate composites.

3.4   CHEMICAL ANALYSIS

The chemical composition of the aluminium alloy matrix was estimated with the help of Emission Spectroscopic analysis. The samples of 20 mm x 20 mm x 10 mm size were randomly collected from the composites fabricated in this investigation. The specimens having pointed tips were suitably prepared and mounted. The counter electrode was made of graphite.

The average chemical composition of the matrix are shown in Table 3.2.

3.5   COLD MODEL EXPERIMENT

To study the effect of impeller size and stirring speed on the incorporation of particles inside a liquid through vortex a model experiment for visual observations was also carried out by using plastic beads as particles and water as liquid matrix. The plastic beads with poor wettability and a density lower than water were chosen. Water was taken as a fluid medium in a transparent glass beaker of internal diameter 75 mm. The impellers of three different sizes of d/D as 0.48, 0.66 and 0.82 and of similar design as it has been mentioned earlier, were used for stirring of water. The stirrer having the impeller fixed with its shaft was vertically placed at the center of the liquid with the help of a clamping facility attached to

TABLE 3.2

AVERAGE CHEMICAL COMPOSITION OF MATRIX OF THE COMPOSITES

Material	Chemical composition (wt %)					
	Mg	Fe	Si	Mn	Ti	Al
Al-alloy	4.0 ± 0.2	0.98 ± 0.02	0.3 ± 0.05	0.5 ± 0.1	0.01	bal.

a stand. During all the experiments the height of water inside the beaker and the position of the impeller inside water were kept constant at h/H=0.15. The speed of the stirrer was regulated with the help of an auto-transformer and the stirring speed was measured by using a stroboscope as discussed earlier.

The particles were added to the surface of the water when they floated and then the stirrer was switched on. The stirring speed was raised slowly by a gradual increase in the power input to the stirrer. The same procedure was followed in the experiments using different size of impeller.

The vortex formation and the movement of particles in liquid during stirring were observed. The entire experiment was photographed with the help of a movie camera at a speed of 25 photographs per second.

3.6   METALLOGRAPHY

The scheme of sectioning of the ingot for making the specimens for various metallographic studies has been shown in a schematic diagram in Fig. 3.6. The sections AA' and BB' taken respectively from the top and the bottom of the ingots were used for metallographic examination after preparing the specimens by standard metallographic procedure. The final polishing was carried out on a polishing cloth using polishing grade alumina suspension. After polishing the specimens were cleaned thoroughly with
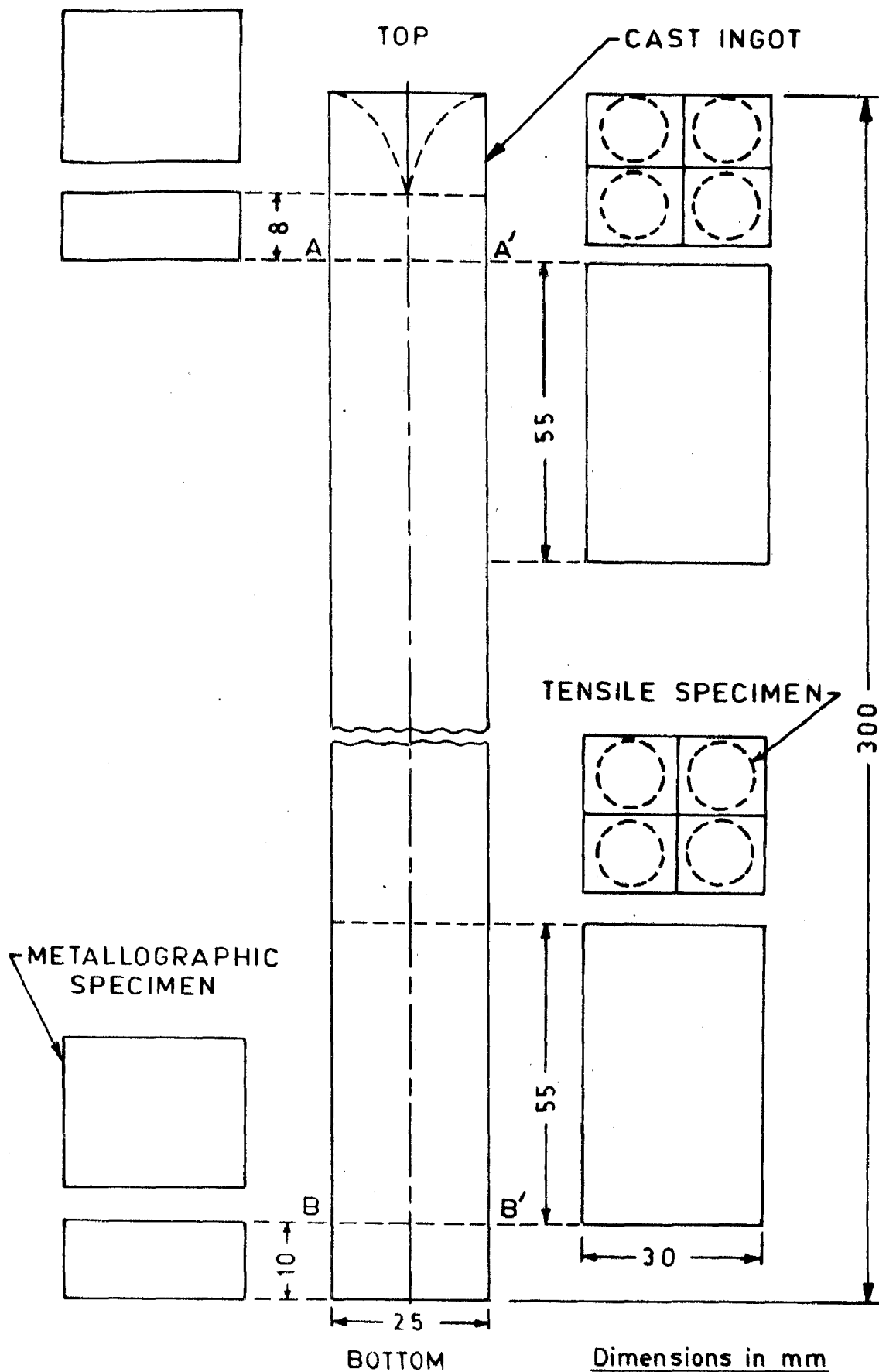
FIG. 3.6 LOCATION OF THE TEST SPECIMENS MACHINEDOUT FROM THE CAST INGOTS.

water and methanol. Then, the specimens were etched with Keller's reagent containing, 2%HF, 3%HCl, 5%HNO$_3$ and water, for 20-30 seconds followed by washing and drying. Polished specimens before and after etching were examined under optical microscope. Typical distributions of alumina particles in aluminium alloy matrix and various microstructural features of all the samples were photographed.

The alumina particles and the voids present in the matrix were observed as dark spots. The area fraction of the particle and voids were measured under optical microscope by 'point counting method'. The magnification in the microscope was so adjusted that a maximum resolution could be obtained and at the same time the condition of not more than one grid-point in one dark spot was satisfied. For each sample 300 such observations were made at random locations. The area fraction of dark spots on the matrix was evaluated dividing the average value of the number of grid points in dark spots by the total number of grid points. The estimation of particle and void content of the cast composite from the area fraction of dark spots is explained latter in section 3.7.

A number of unetched polished specimens obtained from various castings were examined under optical and scanning electron microscopes to study the particle matrix interface. The typical features of the interface was photographed.

A number of tensile specimens after fracture under tensile loading at ambient and elevated temperatures were sectioned longitudinally and prepared by standard metallographic procedure. The specimens etched with Keller's reagent were examined under optical and scanning electron microscopes to study the morphological changes occurring in the specimens during tensile loading. Before etching the polished unetched specimens were examined under SEM to estimate the nucleation of new voids in the matrix with respect to the strain developed in the specimen during tensile loading as discussed later in section 3.8 and 3.9.

3.7 ESTIMATION OF PARTICLE AND VOID CONTENT

The volume fraction of particles and voids present at the bottom and the top of the cast ingot were estimated with the help of observed density of the specimens collected from both the regions. The density of the cast particulate composite, ρ_{mes}, was determined by the usual weight loss method. The density of Al-4wt.% Mg, ρ_{Al-Mg}, was taken [125] as 2.65 g/cm^3. For a random distribution of particles and voids the area fraction of the darks spots was taken as numerically equal to its volume fraction, V_a. The theoretical density, ρ_{Th}, assuming that there are no voids in the composite, is defined as

$$\rho_{Th} = V_a \, \rho_{Al_2O_3} + (1-V_a) \, \rho_{Al-Mg} \qquad \qquad .. \qquad (3.2)$$

where, $\rho_{Al_2O_3}$, is the density of alumina. The value of $\rho_{Al_2O_3}$ for the alumina particles used in this work was measured as 3.012 gms/cm^3. The measured density of the particulate composite can be expressed as

$$\rho_{mes} = (1-V_a)\, \rho_{Al-Mg} + V_{Al_2O_3}\, \rho_{Al_2O_3} \qquad .. \qquad (3.3)$$

where $V_{Al_2O_3}$ is the volume fraction of alumina in the composite. Since V_a includes both voids and alumina particles so,

$$V_a = V_{Al_2O_3} + V_v \qquad\qquad .. \qquad (3.4)$$

where V_v is the volume fraction of void. Combining the equations 3.2, 3.3 and 3.4 the following equation for estimating V_v was obtained as given below.

$$V_v = \frac{\rho_{Th} - \rho_{mes}}{\rho_{Al_2O_3}} \qquad\qquad .. \qquad (3.5)$$

Substituting the value of V_v in equation (3.4), the value of $V_{Al_2O_3}$ was obtained. The unit volume of the Al-Mg alloy — Al$_2$O$_3$ composite having some voids in it, was expressed

$$V_{Al-Mg} + V_{Al_2O_3} + V_v = 1 \qquad\qquad .. \qquad (3.6)$$

where V_{Al-Mg} was the volume fraction of matrix of the composite. Substituting the values of $V_{Al_2O_3}$ and V_v in equation 3.6 the value of V_{Al-Mg} was estimated. The weight fraction of alumina $W_{Al_2O_3}$ in the composite was calculated as

$$W_{Al_2O_3} = \frac{\rho_{Al_2O_3} \, V_{Al_2O_3}}{\rho_{Al_2O_3} \, V_{Al_2O_3} + \rho_{Al-Mg} \, V_{Al-Mg}} \qquad \cdots \qquad (3.7)$$

3.8 ESTIMATION OF VOIDS IN THE MATRIX WITH RESPECT TO STRAIN

The contribution of true strain on nucleation of new voids in the matrix was estimated by observations on polished unetched longitudinal section of fractured tensile specimens under scanning electron microscope. The diameter of the fractured specimen reduced during extension in gauge length under tensile loading at different regions starting from necking area to far from this zone were measured by projecting a marker scale on the image of the specimen as shown in Fig. 3.7. From the value of reduced diameter the final crossectional area, A_f, at different regions were estimated. The true strain, ϵ , of these areas locally were evaluated as

$$\epsilon = \ln \frac{A_o}{A_f} \qquad \cdots \qquad (3.8)$$

where, A_o is the initial crossectional area at gauge length of the tensile specimen before testing as estimated by measuring its diameter with the help of a vernier callipers.

FIG. 3.7 LONGITUDINAL SECTION OF THE FRACTURED SPECIMENS USED FOR THE MEASUREMENT OF THE STRAIN AND THE CORRESPONDING VOID CONTENT UNDER SEM; X 70

The area fraction of voids present on the matrix was measured by point counting method, at every region where the true strain has been evaluated. A 100 mm x 100 mm grid containing 121 points were placed on the image of the specimen at SEM screen and the point counting was carried out by following a similar procedure as mentioned earlier in section 3.6. In every region perpendicular to the longitudinal direction of the specimen, the counting were carried out at 7 random locations. From the point counting the area fraction of void at every location was evaluated as discussed in section 3.6. Averages of the seven values of area fraction of void estimated from the above observations has been presented as the void content of the matrix in a region having a given amount of strain.

3.9   X-RAY DIFFRACTION ANALYSIS OF CAST COMPOSITE

The X-Ray diffraction study was carried out by using powder samples of cast composite in a Philips X-Ray diffraction unit, to identify the various phases formed in the cast Al-Mg — Al_2O_3 particulate composite by chemical interactions during processing. The powder of the sample was prepared and the size of the powder was in the range of 0.15-0.25 mm. The diffractiion study was carried out by using copper target, nickel filter, 20 mA current, 35 KV voltage. The diffraction pattern was automatically scanned under a X-Ray diffractometer model PW 1140/90, for an angle of diffraction $2\theta_2$ from $5°$ to $120°$.

The intensity of diffracted beam against $2\theta_2$ was plotted on a graphical chart where the chart speed and Goniometer speed were maintained as 1 cm/min and 1°/cm respectively. For all the intensity peaks and corresponding value of $2\theta_2$ the value of interplanner spacing, d_2, were estimated from the Bragg law

$$\lambda = 2 \bar{d} \sin \theta_2 \qquad \qquad .. \qquad (3.10)$$

where, λ , is the wave length of X-ray used for diffraction. The value of λ was taken as 1.54 05 for calculation of $\bar{d}$ values. From the calculated values of $\bar{d}$ the phases were identified with the help of ASTM X-ray diffraction data card.

3.10 ESTIMATION OF PARTICLE AND POROSITY CONTENT OF THE TENSILE SPECIMENS

The tensile specimens were collected from the bottom and the top portions of the castings as described in Fig. 3.6. Before conducting the tensile tests the density of each specimen was determined by the weight loss method. The area fraction of the particles and voids in the bottom and the top of the castings were measured on the sections BB' and AA' (Fig. 3.6) of the specimens collected from the bottom and the top of the castings respectively, following the procedure mentioned in section 3.7. From the values of measured density and V_a, the volume fraction of alumina particles and the porosity content of each tensile specimen were estimated following the procedure discussed in sec.3.7.

3.11 MEASUREMENTS OF MECHANICAL PROPERTIES

The mechanical properties of the cast composites were evaluated by carrying out tensile tests at ambient and elevated temperatures. The dimensions of the tensile specimens is given in Fig. 3.8. The tensile specimens were machined out from the bottom and the top of each castings. The tensile tests were performed in a motor driven Hounsfield Tensometer having an arrangement for plotting the load-extension curve. All the tests were carried out on a load scale of 0-500 kg. with matching beam. During testing at ambient temperature the temperature was recorded as 298 K. Before tensile testing the diameter and the gauge length of each specimen were measured.

The elevated temperature tensile properties were determined by carrying out the tensile tests at temperatures of 373 K, 473K, 573 K, and 623 K. The tests were carried out in an electrically heated 155 mm long horizontal tube furnance having a constant temperature zone of 100 mm ± 10 mm. The furnance was connected to the power source through an auto transformer. The specimens were held horizontally inside the furnance with the help of a suitable gripping arrangement maintaining its position at the center of the furnance. Both the ends of the furnance tube were closed properly. The temperature of the furnance was regulated by controlling the power input with the help of the auto transformer. The temperature of the furnance was measured in Fahrenheit scale (presented in Kelvin after
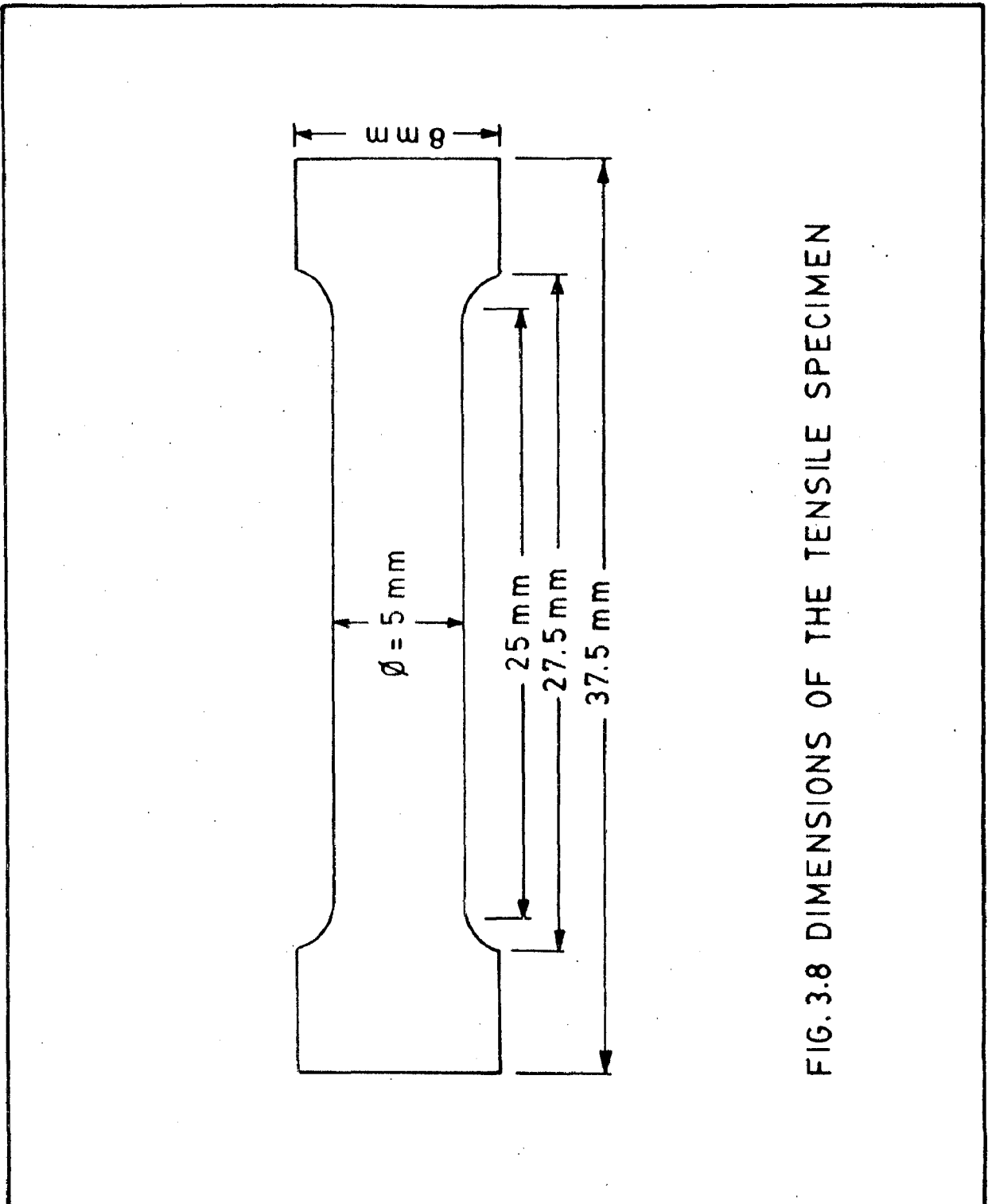
FIG. 3.8 DIMENSIONS OF THE TENSILE SPECIMEN

conversion) with the help of a potentiometer, mentioned earlier in section 3.3, by placing a chromel/alumel thermocouple just by the side of the specimen inside the furnance. The specimens were allowed a soaking for 700 to 750 seconds at the test temperature and then fractured under tension inside the furnance. During soaking and testing the temperature of the furnance was maintained within ± 4 K of the test temperature.

The tensile tests at ambient and elevated temperatures were carried out on the samples containing various amounts of reinforced alumina. For a given alumina content the specimens were collected having different levels of porosity. The ultimate tensile strength of the specimens were evaluated by dividing the maximum tensile force recorded during testing, in kilogram, by the initial crosssectional area of the specimen measured in mm^2. However, the ultimate tensile strength has been reported here after conversion in to MN/m^2. After fracture the increase in gauge length has been measured and the engineering fracture strain, e_f, was estimated as a change in gauge length per unit gauge length. For a number of specimens having various combination of porosity and particle content the load-extension behaviour were recorded with the help of the recorder fitted to the tensile testing machine.

3.12   FRACTOGRAPHY UNDER SCANNING ELECTRON MICROSCOPE

In order to have an understanding about the fracture behaviour of particulate composites, containing different amount of particles and porosity, the fractured surfaces of the tensile specimens were examined under a Philips 501 scanning electron microscope with a maximum rated resolution of 70A°. Small samples from the fractured side of the broken tensile specimens were cut out of its length without any damage to the fractured surface. The samples were collected for specimens fractured under both the ambient and the elevated temperatures, and the samples were fixed carefully on the specimen holder of SEM by using silver paste at the bottom of the specimen. The typical features of the fractured surfaces were photographed.

CHAPTER 4

RESULTS AND DISCUSSIONs: PARTICLE RETENTION AND THE PARTICLE-
MATRIX INTERFACE

4.1   INTRODUCTION

In making alloy particulate composites by foundry
technique three aspects of particle incorporation play an
important role in its successful fabrication - (a) introduction
of the particles inside the slurry (b) retaining the particles
and (c) distribution of particle in the slurry as well as
in the castings after solidification in the mould. In the vortex
method the particles are sucked into the melt through the
vortex formed during stirring but the retention and the
distribution of particles in molten matrix are very much
dependent on the flow pattern in the slurry during stirring,
the amount of solid in the slurry and the flow pattern in
the melt. In this section the effect of various process
parameters on the amount of retention and distribution of
alumina particles in the composite have been presented and
discussed.

The results of the visual observations in cold
model experiments have been presented to gain a qualitative un-
derstanding regarding the role of various mixing parame-
ters on the movement of particles inside the liquid.

The optical microscopic observation on the microstructures of the cast composites prepared under different combinations of process parameters have been discussed with a particular attention on the distribution of particles in the matrix. An effort has also been made to study the role of solidification of the composite slurry on the distribution of alumina particles inside the mould. The formation of porosity in the composites prepared by vortex method is observed as a common hazard due to suction of air through the vortex. The degree of enhancement of porosity in this process of fabrication of particulate composite has been estimated.

The particle-matrix interface is of prime interest in a composite. The interface of alumina and the matrix studied under scanning electron microscope has been presented and the possible interfacial reaction between the particles and the alloy has been discussed on the basis of its products detected by X-ray diffraction technique.

4.2   OPTIMIZATION OF THE PROCESS PARAMETERS FOR PARTICLE INCORPORATION

4.2.1   RESULTS: INFLUENCE OF PROCESS PARAMETERS ON THE RETENTION OF ALUMINA PARTICLES

The retention of alumina particles in the cast composites produced by vortex method depends on the control of a number of process parameters, such as the holding temperature of the melt, the speed of stirring, the position

of the impeller (h/H) and the size of the impeller (d/D).
The parameters h and H indicate the height of the impeller
from the bottom of the crucible and the depth of the melt
at rest in the crucible respectively. The variables d and
D represent the impeller diameter and the diameter of the
crucible at the surface of the slurry respectively. In this
section the role of these process parameters on the retention
of alumina in the composite has been evaluated. An effort
has also been made to determine an optimum level of process
parameters for maximum retention of alumina.

The effect of holding temperature of the melt
on the variation in retention of alumina in the cast composites
has been shown in Fig. 4.1. To assess the homogenety in
distribution of alumina particles in the slurry during mixing,
the alumina content in the top and the bottom of the ingot
were estimated. The alumina retained at the top and at the
bottom of the ingots are indicated in Fig. 4.1 by open
and closed circles respectively. Fig. 4.1 shows that at a
given speed of stirring (16 revolution.s^{-1}), position of
impeller (h/H=0.81) and size of impeller (d/D=0.63), a high
amount of alumina retention in the casting has been achieved
at a holding temperature of 883 K.At this temperature the
retention of alumina at the bottom of the casting has been
found to be comparatively less than that at the top of
the casting as shown in Fig. 4.1 and evident in the micrographs
Fig. 4.2 (i) and Fig. 4.2 (ii) respectively. It has been
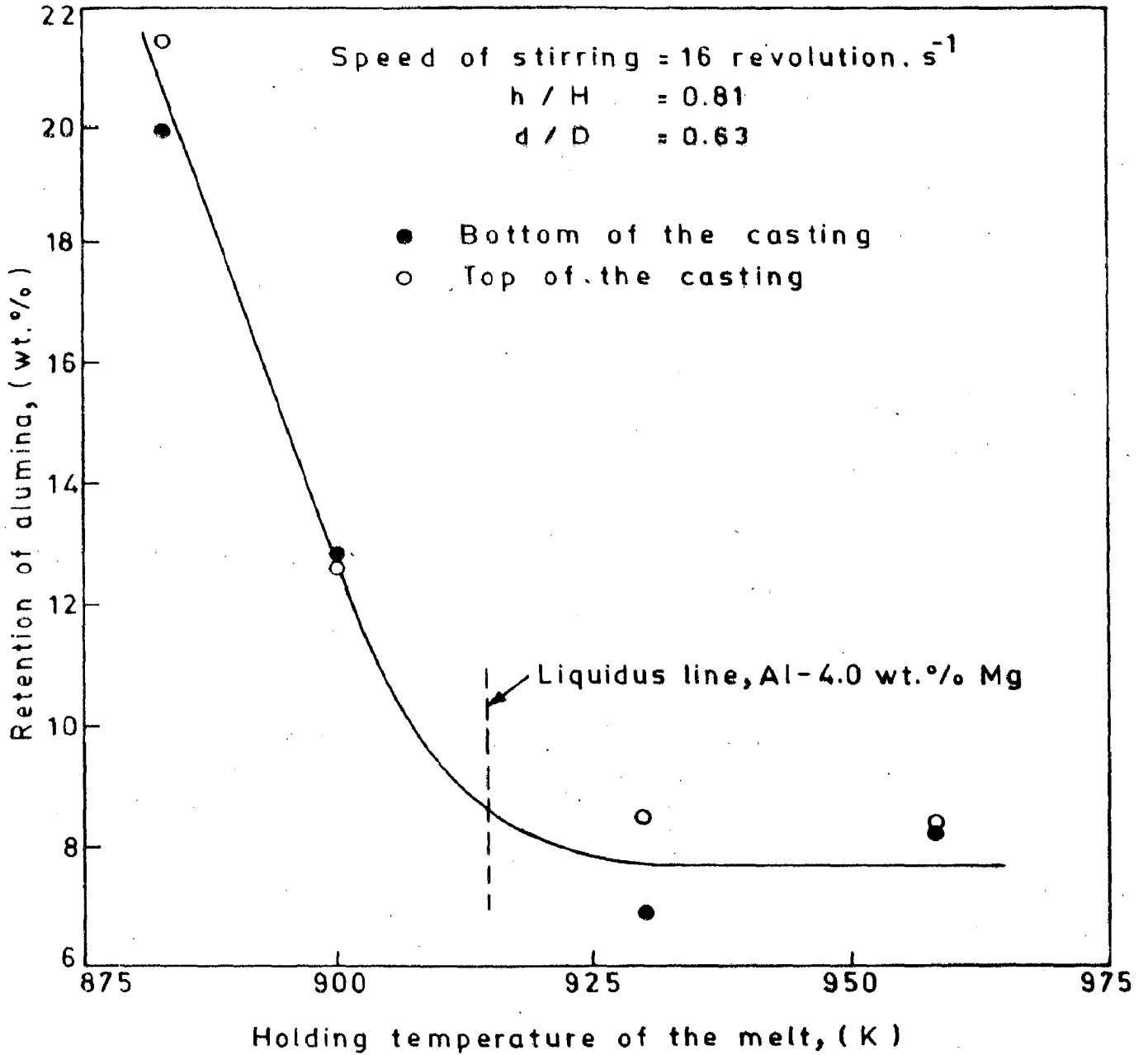
FIG. 4.1 VARIATION IN THE RETENTION OF ALUMINA WITH THE HOLDING TEMPERATURE.

BOTTOM

TOP

(i)   883 K

(ii)   883 K

(iii)   900 K

(iv)   900 K

(v)   958 K

(vi)   958 K

FIG. 4.2 MICROGRAPHS SHOWING THE EFFECT OF HOLDING
TEMPERATURE ON THE RETENTION OF ALUMINA
PARTICLES AT THE TOP AND THE BOTTOM OF THE
CASTINGS; STIRRING SPEED = 16 r.p.s., d/D = 0.63
AND h/H = 0.81; X 60

observed in Fig.4.1 that an increase in the holding temperature of the slurry (900 K) within the range of the solidus and the liquidus temperature of Al-4.0 wt% Mg alloy drastically reduces the retention of alumina particles in the castings. However, at this holding temperature (900 K) no significant difference in alumina content between the bottom and the top of the casting is observed as given in Fig. 4.1 and revealed in the micrographs in Fig. 4.2 (iii) and 4.2 (iv) respectively. Enhancement of holding temperature above the liquidus point (915 K) of the alloy has been found to reduce further the alumina retention in the casting. But at a temperature above the liquidus point a further increase in the holding temperature of the melt to 958 K has not shown any significant effect on the amount of retention of alumina particles in the castings as shown in Fig. 4.1. The retention of alumina particles at the bottom and the top of the casting made at 958 K are shown in the micrographs given in Fig. 4.2 (v) and Fig. 4.2 (vi) respectively.

The amount of alumina particles retained in a partially solid slurry has been found to vary with a variation in the stirring speed under a given mixing condition of h/H=0.81, d/D=0.63 and a holding temperature of 900 K, as shown in Fig. 4.3. At a low stirring speed of 7.5 revolution. s^{-1} a small amount of alumina particles has been found to be retained in the casting. At this stirring speed a comparatively lower amount of alumina particles has been observed at the bottom of the casting than that retained
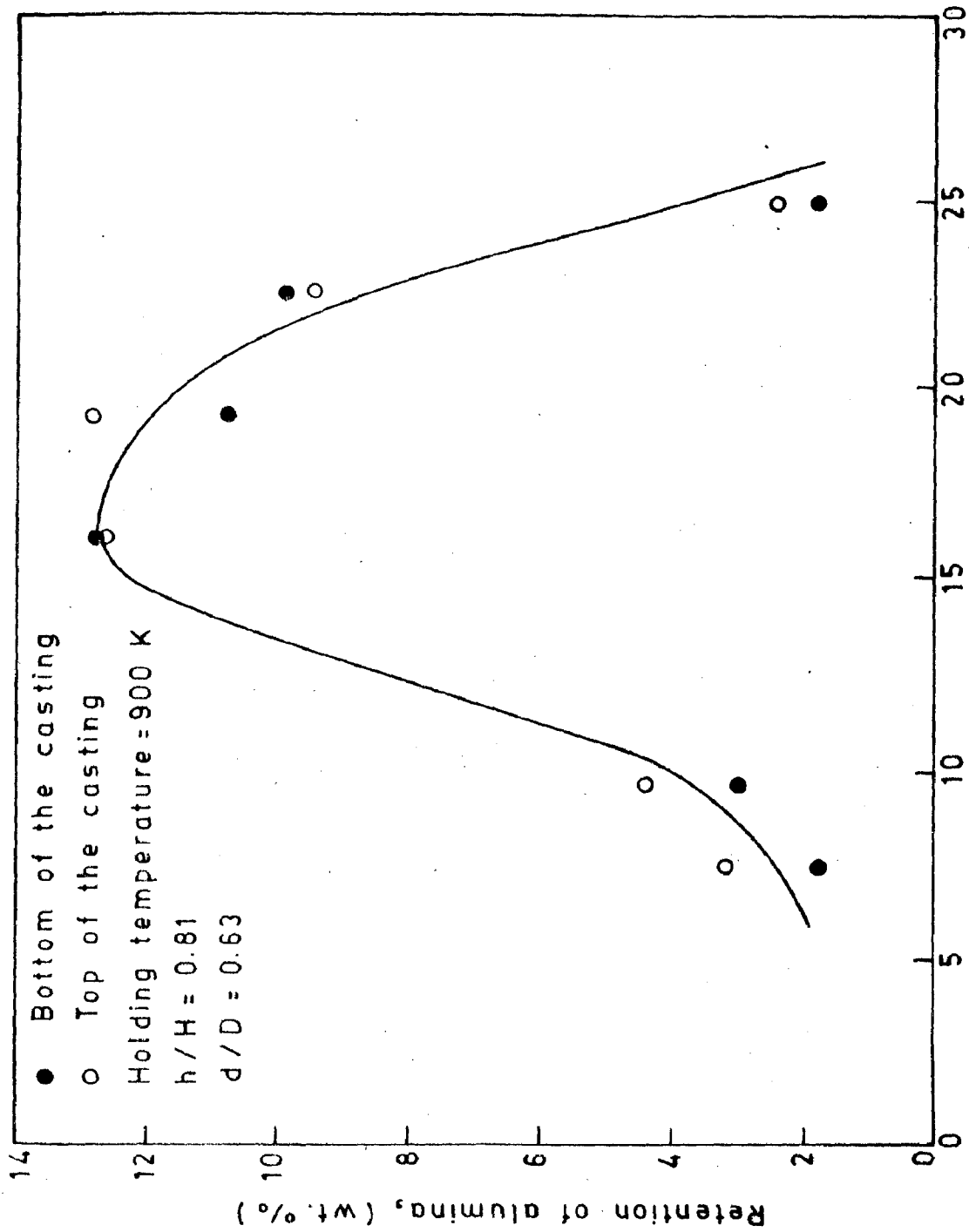
FIG. 4.3 VARIATION IN THE RETENTION OF ALUMINA WITH THE
SPEED OF STIRRING.

at its top as depicted in Fig. 4.3 and revealed in the micrographs Fig. 4.4 (i) and 4.4 (ii) respectively. It is observed that the increase in speed of stirring upto about 16 revolution.s^{-1} increases the retention of alumina in the casting as shown in Fig. 4.3. At this speed of stirring even at the level of maximum retention of alumina particles in the casting no significant difference in retention of the particles between the bottom and the top of the ingot has been observed as shown in Fig. 4.3 and evident in the micrographs Fig. 4.2 (iii) and 4.2 (iv) respectively. A further increase in stirring speed beyond 16 revolution.s^{-1} upto 25 revolution.s^{-1} has reduced the alumina retention in the casting as shown in Fig. 4.3. The micrographs presented in Fig. 4.4 (iii) and Fig. 4.4 (iv) show the alumina retention at the bottom and the top of the casting respectively made at a stirring speed of 23 revelution.s^{-1} where a typical clustering of particles at the top of the casting is revealed in Fig. 4.4 (iv). A very low retention of particles in the bottom and the top of the casting made at the stirring of 25 revolution. s^{-1} as given in Fig. 4.3 are evident in the micrographs shown in Fig. 4.4 (v) and 4.4 (vi) respectively.

The influence of the position (h/H) of the impeller on the variation of the amount of alumina retained in the slurry as shown in Fig. 4.5 indicates that as h increases the extent of retention of alumina also increases until h/H=0.81, while the holding temperature, the speed of stirring

BOTTOM

TOP

(i)   7.5 r. p. s.

(ii)   7.5 r. p. s.

(iii)   23 r. p. s.

(iv)   23 r. p.s.

(v)   25 r. p.s.

(vi)   25 r. p.s.

FIG. 4.4 MICROGRAPHS SHOWING THE EFFECT OF STIRRING
SPEED ON THE RETENTION OF ALUMINA PARTICLES
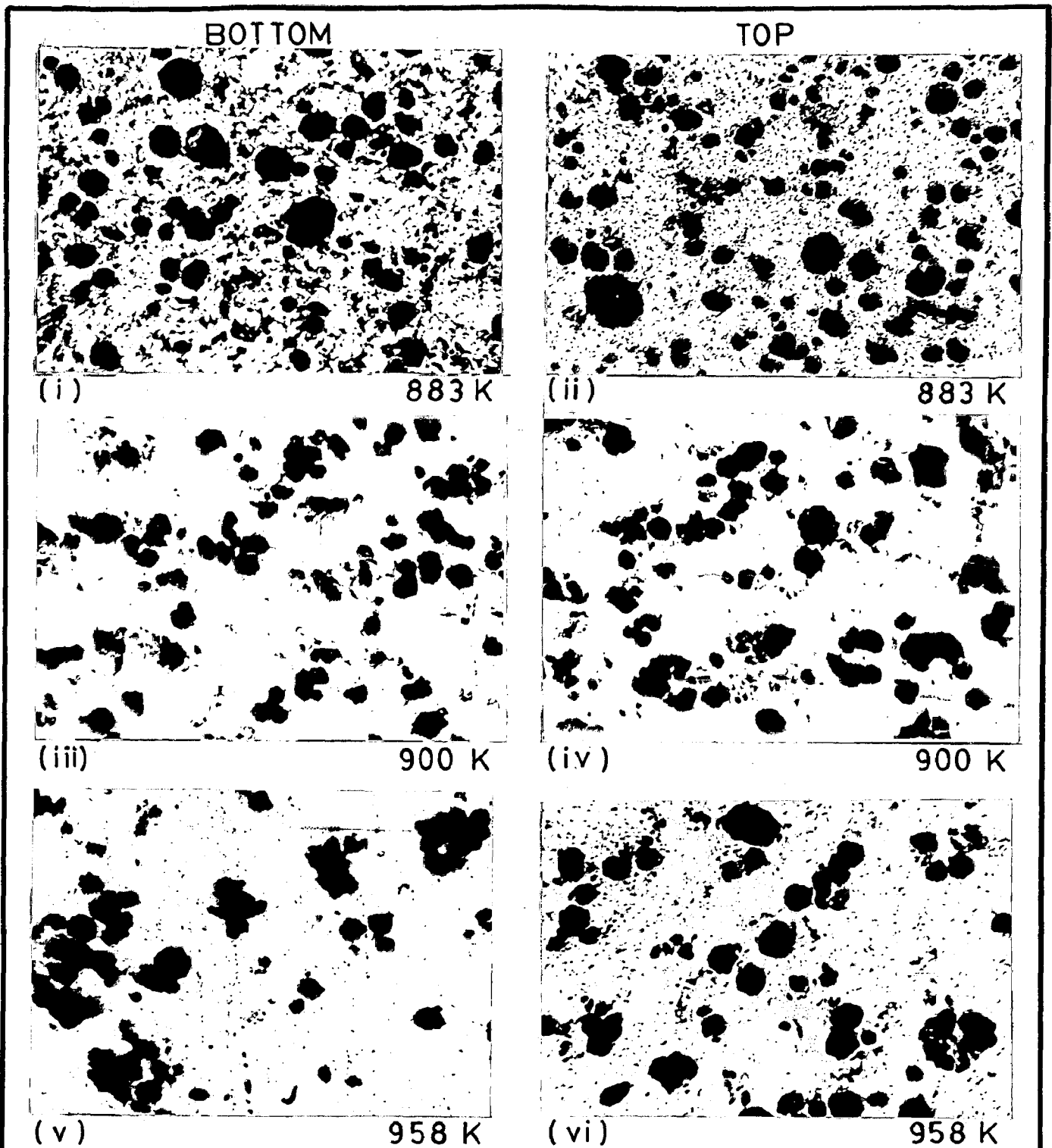AT THE TOP AND THE BOTTOM OF THE CASTINGS;
d/D=0.63, h/H=0.81 AND HOLDING TEMPERATURE
= 900 K; X 60
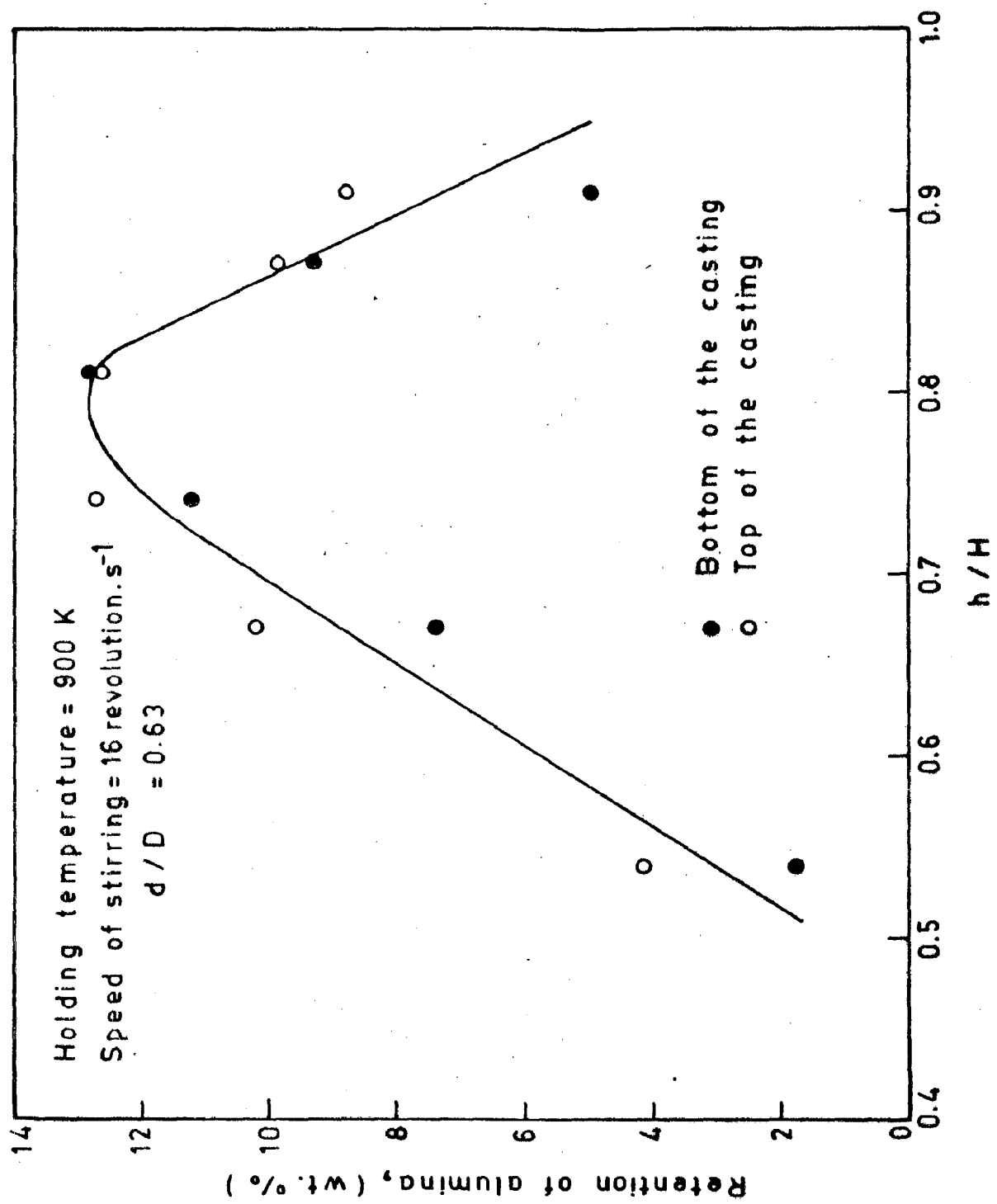
FIG. 4.5 VARIATION IN THE RETENTION OF ALUMINA WITH THE POSITION OF THE IMPELLER.

and the d/D ratio have been kept constant at 900 K, 16 revolution. s^{-1} and 0.63 respectively. But beyond it, the amount of retention drops. The difference in the levels of retention of alumina between the top and the bottom of the castings increases, as one goes away from the optimum position where the extent of retention is maximum. The retention of alumina particles in the bottom and the top of the casting fabricated at h/H = 0.54 where, the holding temperature, speed of stirring and d/D ratio have been kept at 900 K, 16 revolution.s^{-1} and 0.63 respectively, are shown in the micrographs given in Fig. 4.6 (i) and Fig. 4.6 (ii) respectively where a significant tendency of clustering of retained particles at the top of the casting has been marked. However, for a composite made at h/H=0.81 a large retention of alumina particles has been observed in addition to a considerable lower incidence of clustered zone of particles as shown in Fig. 4.2 (iii) and Fig. 4.2 (iv). The decrease in retention of particles in the bottom and the top of the castings with a further increase in the value of h/H to 0.91 have been shown in the micrographs presented in Fig. 4.6 (iii) and Fig. 4.6 (iv) respectively.

In an effort to optimise the size of the impellers, presented as a diameter ratio d/D, a maximum level of retained alumina of 12.78 wt% have been observed (See Fig. 4.7) when the slurry has been stirred with a stirrer having an optimum d/D=0.63. The h/H ratio, the holding temperature and the speed of stirring have been maintained at 0.81, 900 K and

BOTTOM   TOP

(i)   h/H = 0.54   (ii)   h/H = 0.54

(iii)   h/H = 0.91   (iv)   h/H = 0.91
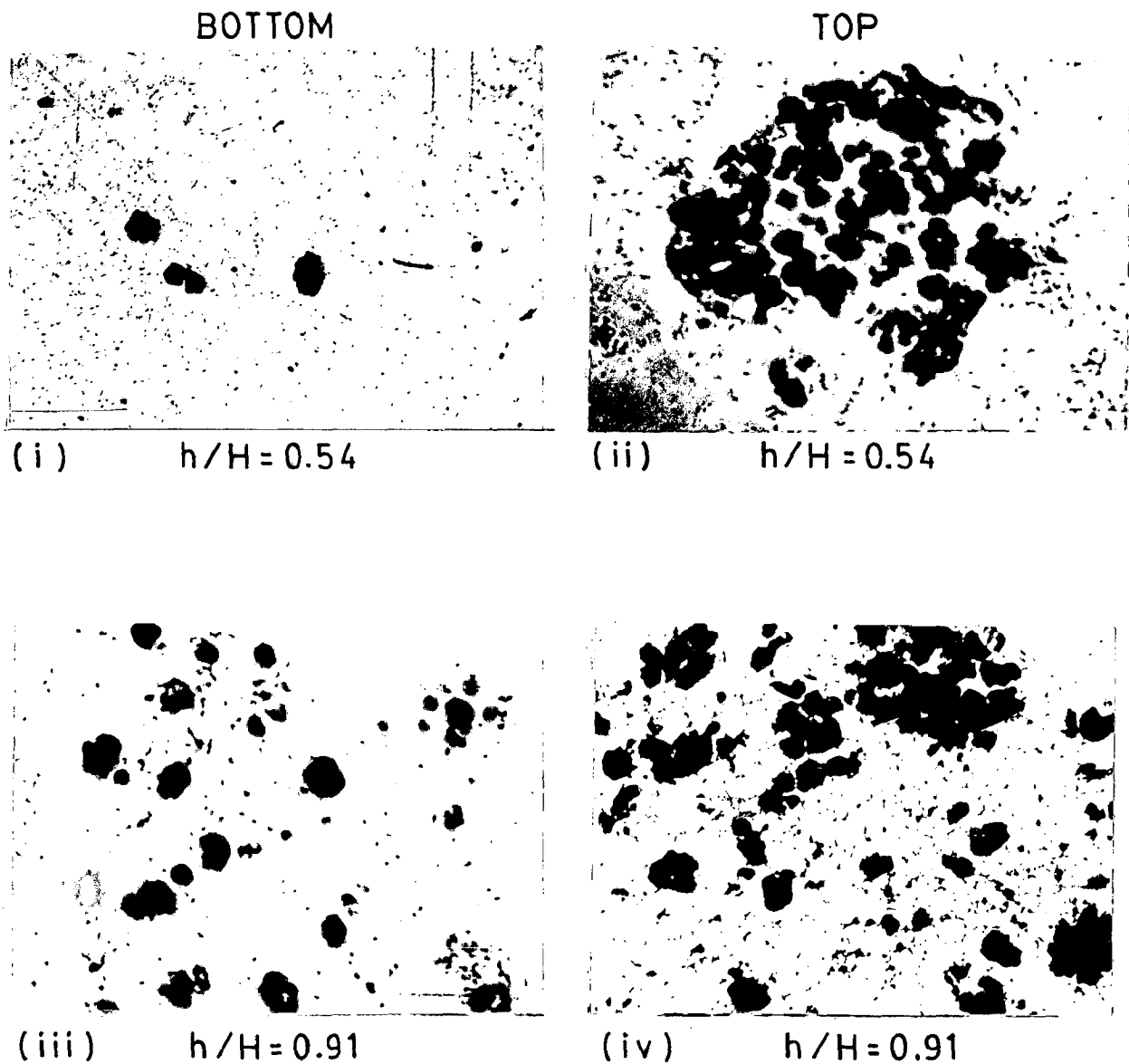
FIG. 4.6 MICROGRAPHS SHOWING THE EFFECT OF POSITION
OF THE IMPELLER INSIDE THE MELT ON THE RE-
TENTION OF ALUMINA PARTICLES AT THE TOP AND
THE BOTTOM OF THE CASTINGS; STIRRING SPEED
=16 r. p. s., d/D = 0.63 AND HOLDING TEMPERATURE
= 900 K; X 60
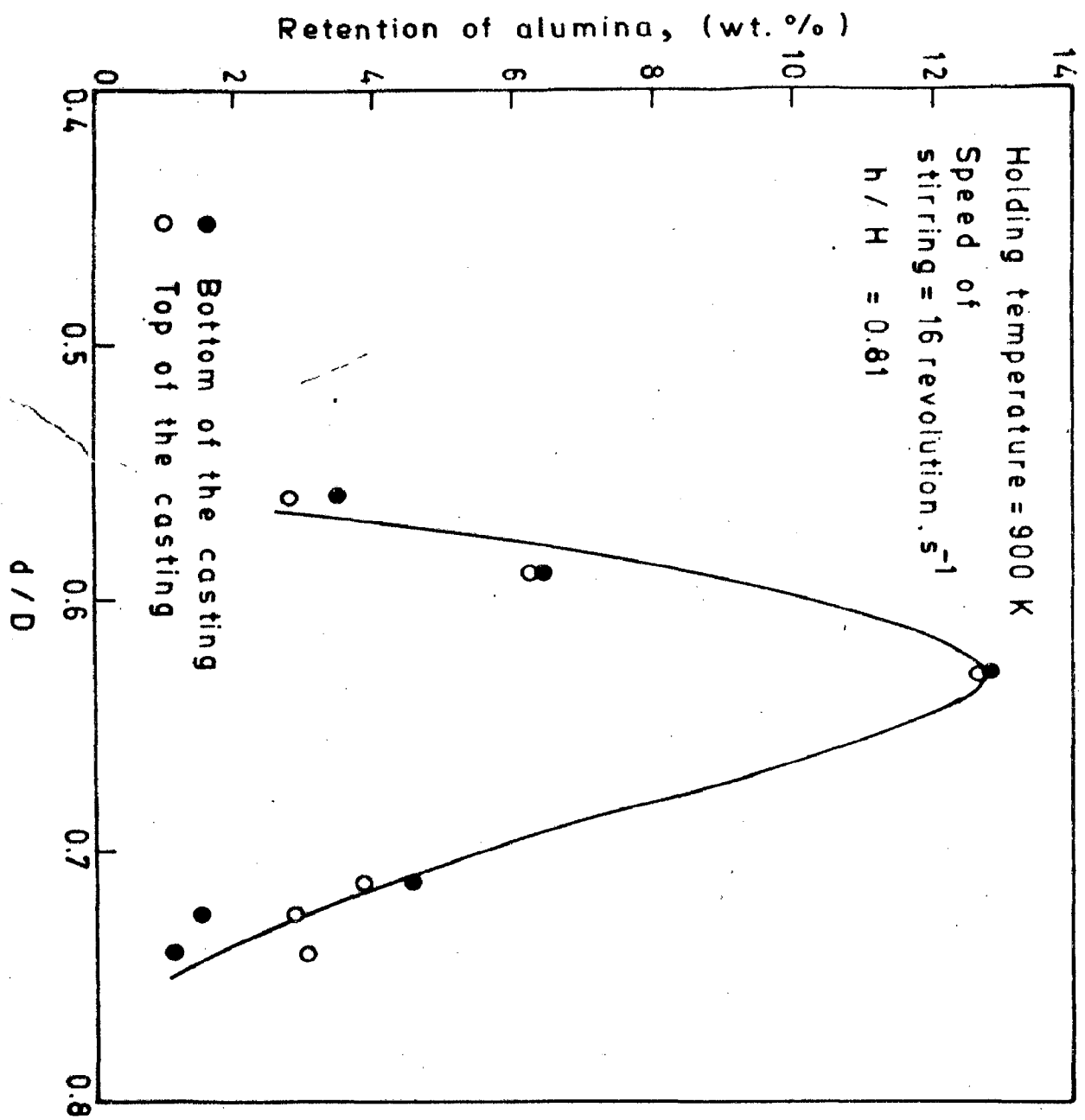
FIG. 4.7 VARIATION IN THE RETENTENTION OF ALUMINA
WITH THE SIZE OF THE IMPELLER.

16 revolution.s^{-1} respectively. The micrographs presented in Fig. 4.2 (iii) and Fig. 4.2 (iv) are showing the retention of alumina particles at the bottom and the top of the casting respectively, fabricated at d/D=0.63 in combination with other mixing parameters as mentioned above. A deviation in d/D ratio at both the sides of the optimum value have been found to reduce significantly the amount of alumina retained in the casting as depicted in Fig. 4.7 and shown in the micrographs given in Figs. 4.8 (i) and (ii) and Figs. 4.8 (iii) and (iv) where the values of d/D have been kept at 0.56 and 0.74 respectively. In the micrographs presented in Figs. 4.8 (i) and (iii) showing the retention of particles at the bottom and the same for the top of the respective castings have been shown in Figs. 4.8 (ii) and (iv). The alumina content in the top and the bottom of the casting has not been found to differ much at a d/D=0.63 as shown in Fig. 4.7 and evident in the micrographs presented in Figs. 4.2 (iii) and (iv). However, a further increase in d/D ratio has caused a relatively small increase in the variation of the extent of retention at the bottom and the top of the casting as observed in Fig. 4.7 and marked in the micrographs presented in Figs. 4.8 (iii) and (iv) respectively.

4.2.2   ·RESULTS: ·POROSITY CONTENT OF THE CASTINGS

The porisity of the cast composites has been found ✓ to vary significantly with a change in process parameters.

BOTTOM

(i)　　　　d/D = 0.56

TOP

(ii)　　　　d/D = 0.56

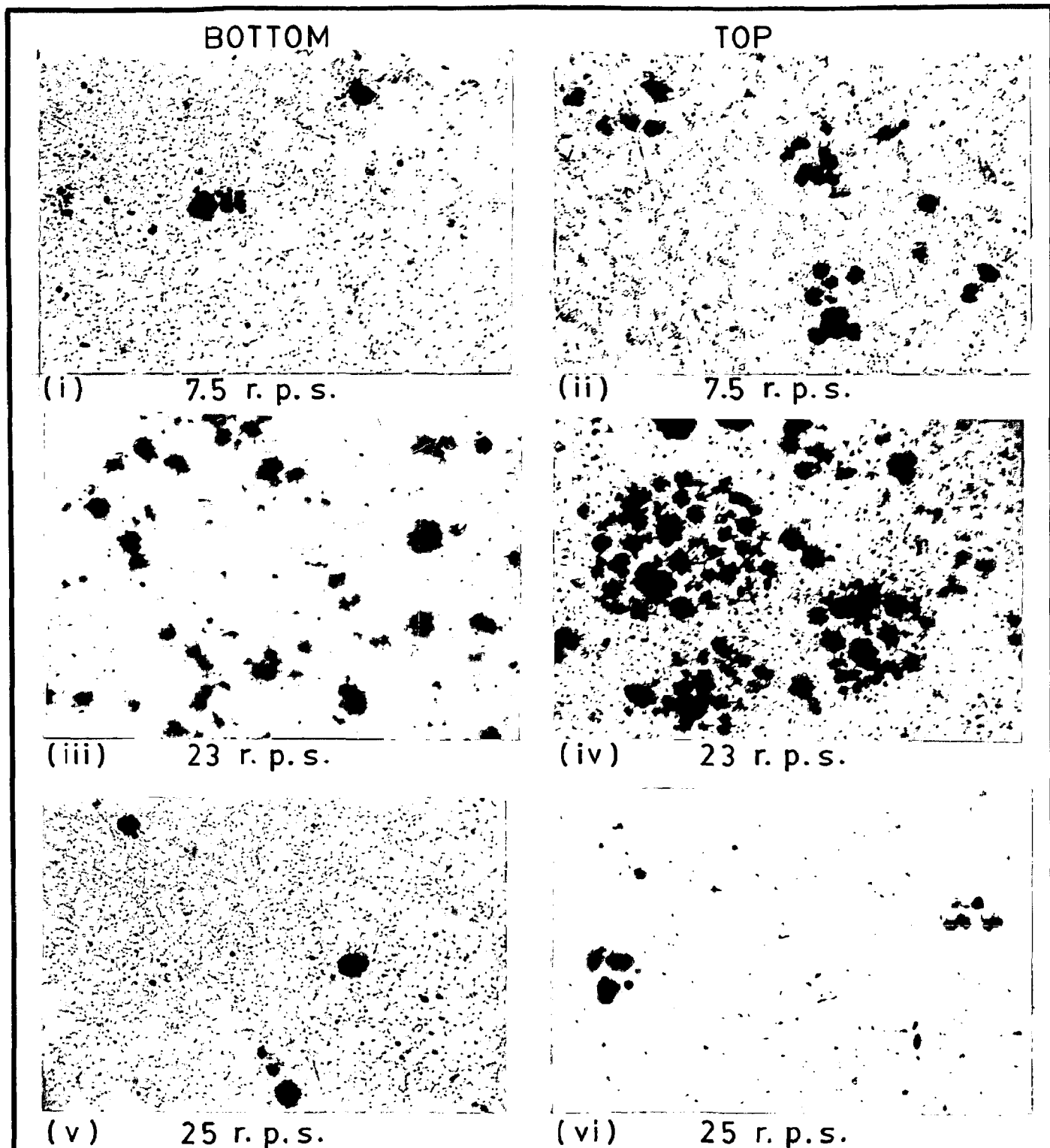(iii)　　　　d/D = 0.74

(iv)　　　　d/D = 0.74
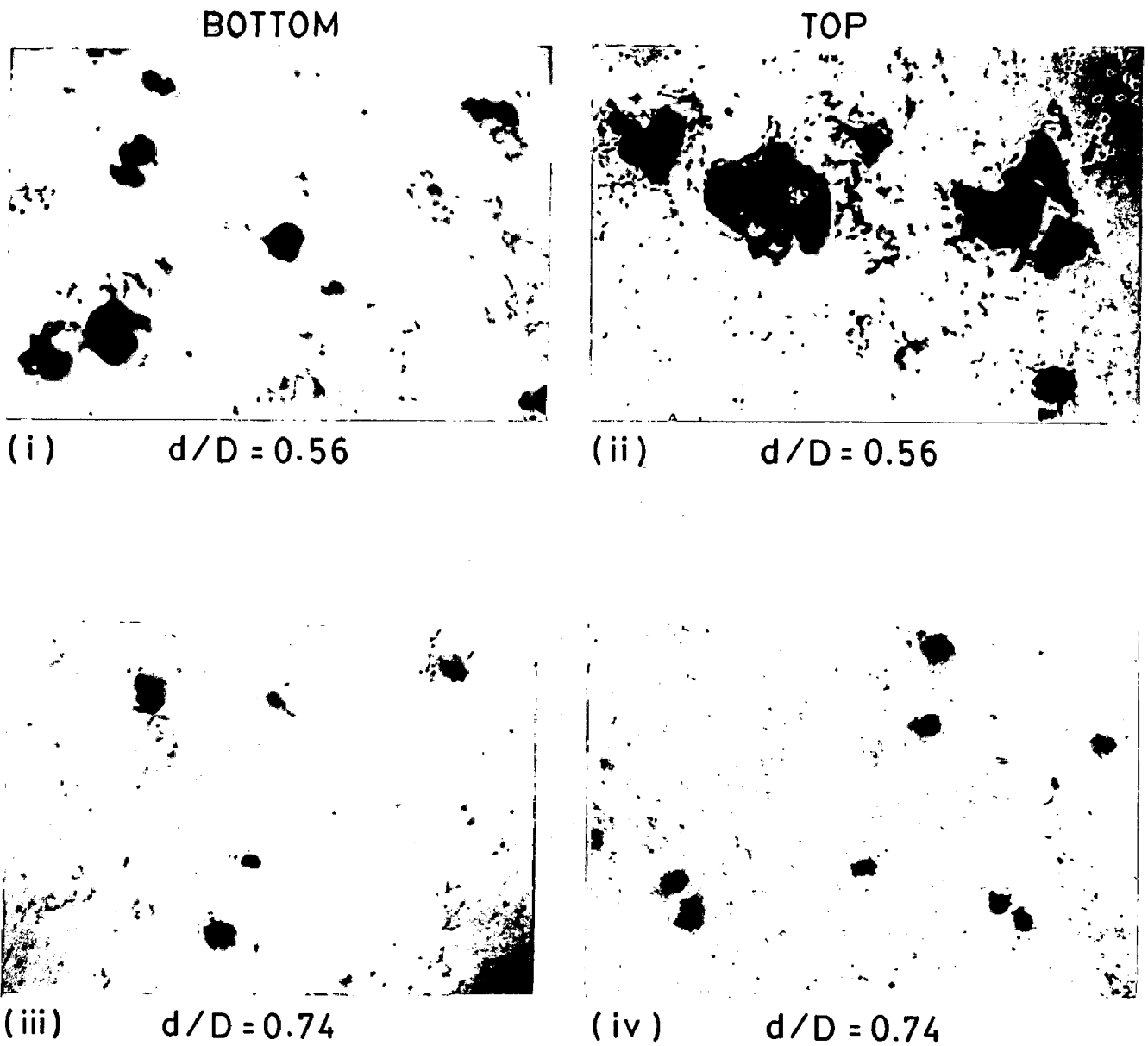
FIG. 4.8 MICROGRAPHS SHOWING THE EFFECT OF THE SIZE
OF THE IMPELLER ON THE RETENTION OF ALUMINA
PARTICLES AT THE TOP AND THE BOTTOM OF THE
CASTINGS; STIRRING SPEED = 16 r. p. s., h/H = 0.81
AND HOLDING TEMPERATURE = 900 K; X 60

Fig. 4.9 shows the effect of holding temperature on the variation in porosity content of the composites when the other process parameters such as the speed of stirring, the h/H value and the d/D value have been fixed at 16 revolution. s^{-1}, 0.81 and 0.63 respectively. It has been observed that when the holding temperature is kept close to the solidus temperature (875 K) of the Al-4.0 wt% Mg alloy a large amount of porosity has been created in the composite. However, the porosity content of the composite has been found to reduce drastically with the increase of the holding temperature within the partially solid region of the alloy. A further increase in holding temperature beyond the liquidus temperature (915 K) of the alloy has not shown any significant effect on the porosity content of the composite.

The increase in the stirring speed upto 19 revolution s^{-1} has been found to increase the porosity content of the composite where the holding temperature, the h/H and the d/D ratios have been maintained at 900 K, 0.81 and 0.63 respectively as shown in Fig. 4.10. The porosity of the composite has come down sharply with further increase in the stirring speed beyond 19 revolution.s^{-1}.

Fig. 4.11 shows that the increase in h/H ratio upto 0.81 gradually increases the porosity content of the composite when the other process parameters like the speed of stirring, holding temperature and d/D ratio remain constant at 16 revolution.s^{-1}, 900 K and 0.63 respectively. However,
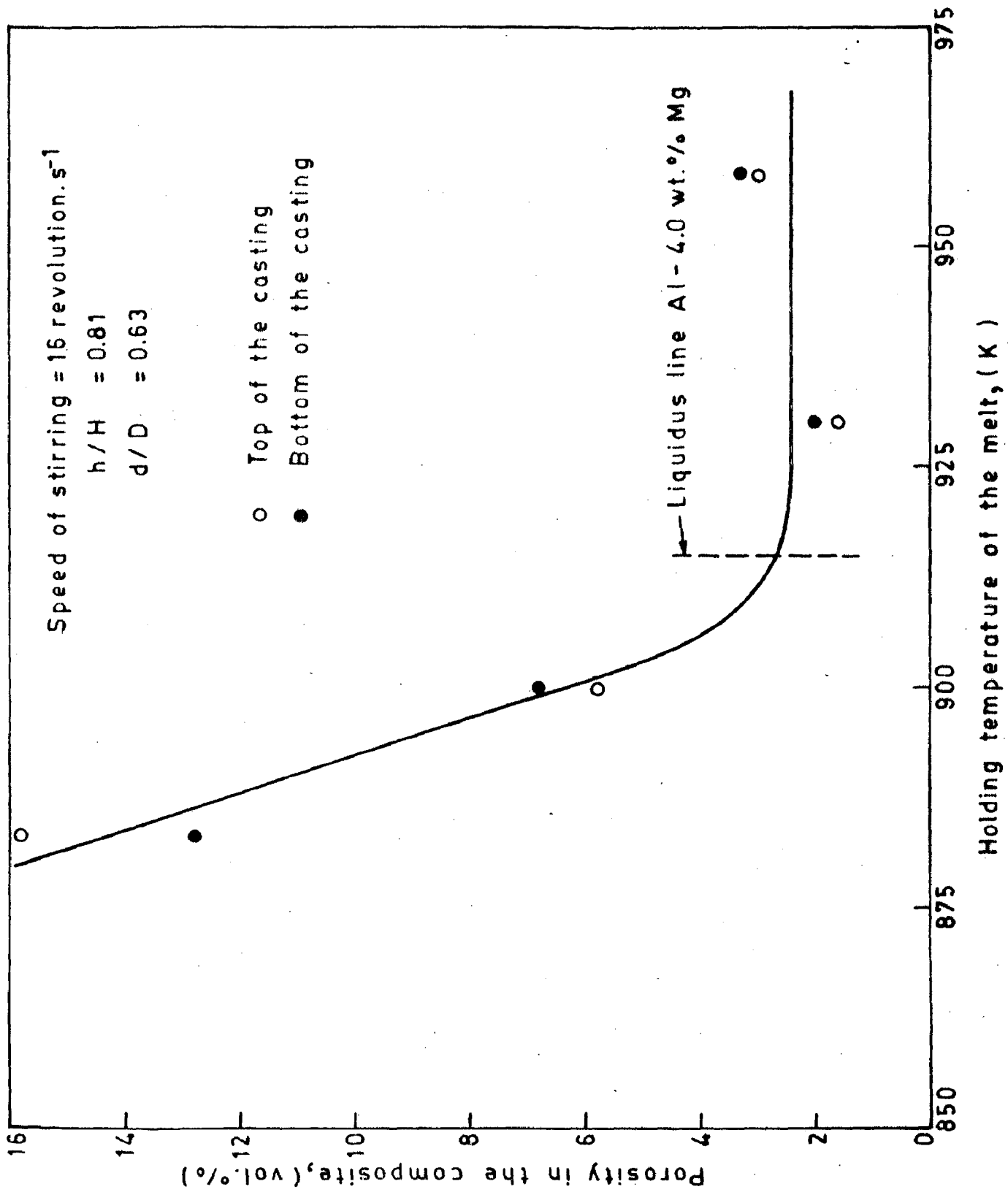
FIG. 4.9 EFFECT OF HOLDING TEMPERATURE ON THE POROSITY CONTENT
IN THE COMPOSITES.
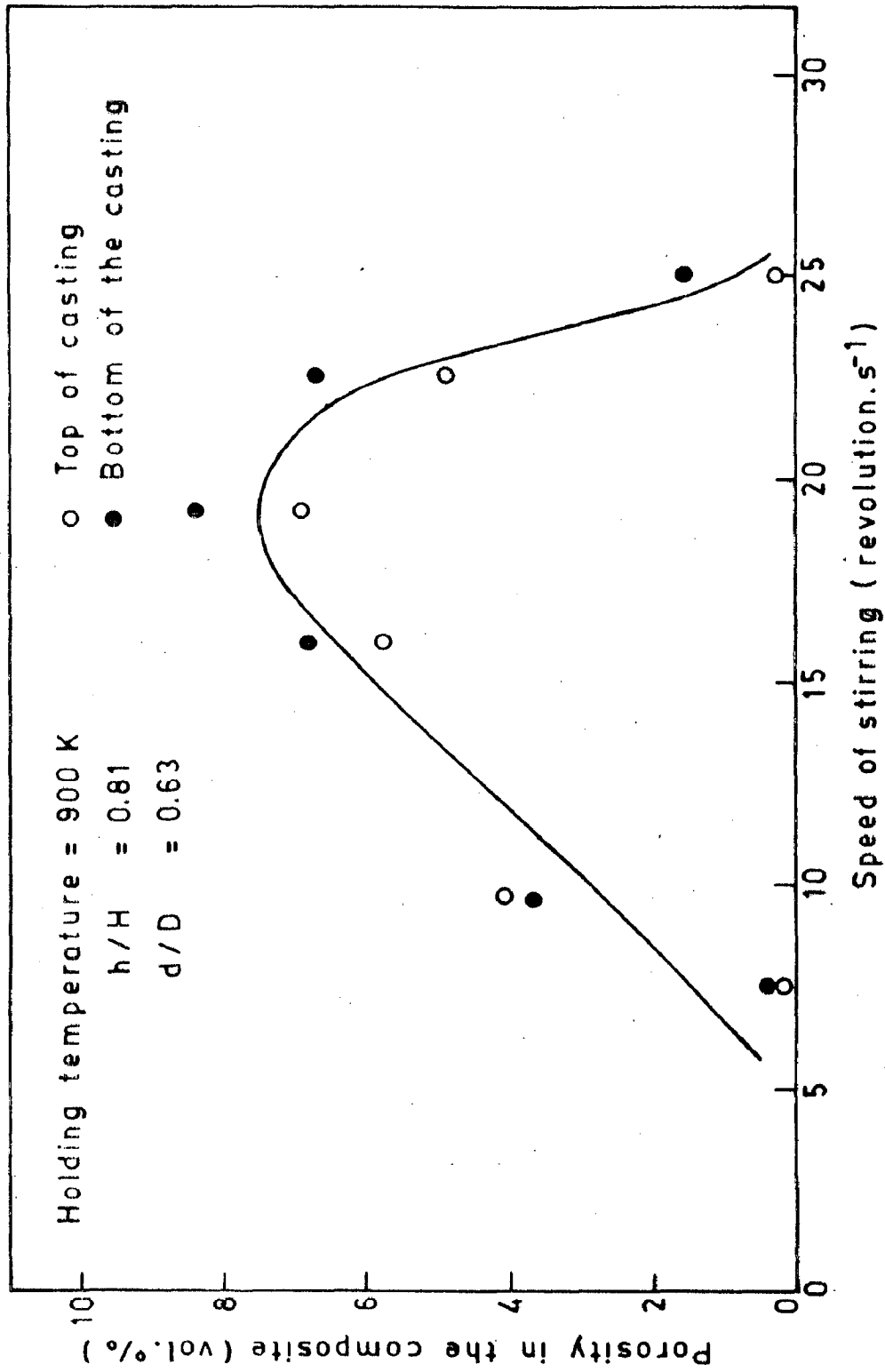
FIG. 4.10 EFFECT OF STIRRING SPEED ON THE POROSITY CONTENT IN THE COMPOSITES.

a further increase in h/H ratio has been found to decrease the porosity level of the composite relatively very fast.

The porosity content of the composite has been found to increase drastically with the increase in d/D ratio of the impeller from 0.56 to 0.63 as shown in Fig. 4.12, when the process parameters such as the holding temperature, the stirring speed and the h/H ratio have been kept constant at 900 K, 16 revolution.s^{-1} and 0.63 and 0.81 respectively. The increase in d/D ratio beyond 0.63 has been found to decrease the porosity level of the composite comparatively slowly.

The scanning electron microscopic observation on the matrix of a typical cast composite has been shown in Fig. 4.13. The figure shows the presence of voids at the boundary of some alumina particles where the rest of the particles are having no such defects. In addition there are porosities in the matrix which are revealed in the microstructure as discussed later.

4.2.3   RESULTS: STUDY OF FLUID PARTICLE BEHAVIOUR IN MODEL EXPERIMENTS

The effect of stirring speed on the distribution of plastic beads in water have been shown in Fig. 4.14, Fig. 4.15 and Fig. 4.16 for the different size of impeller having d/D ratio of 0.82, 0.66 and 0.48 respectively.
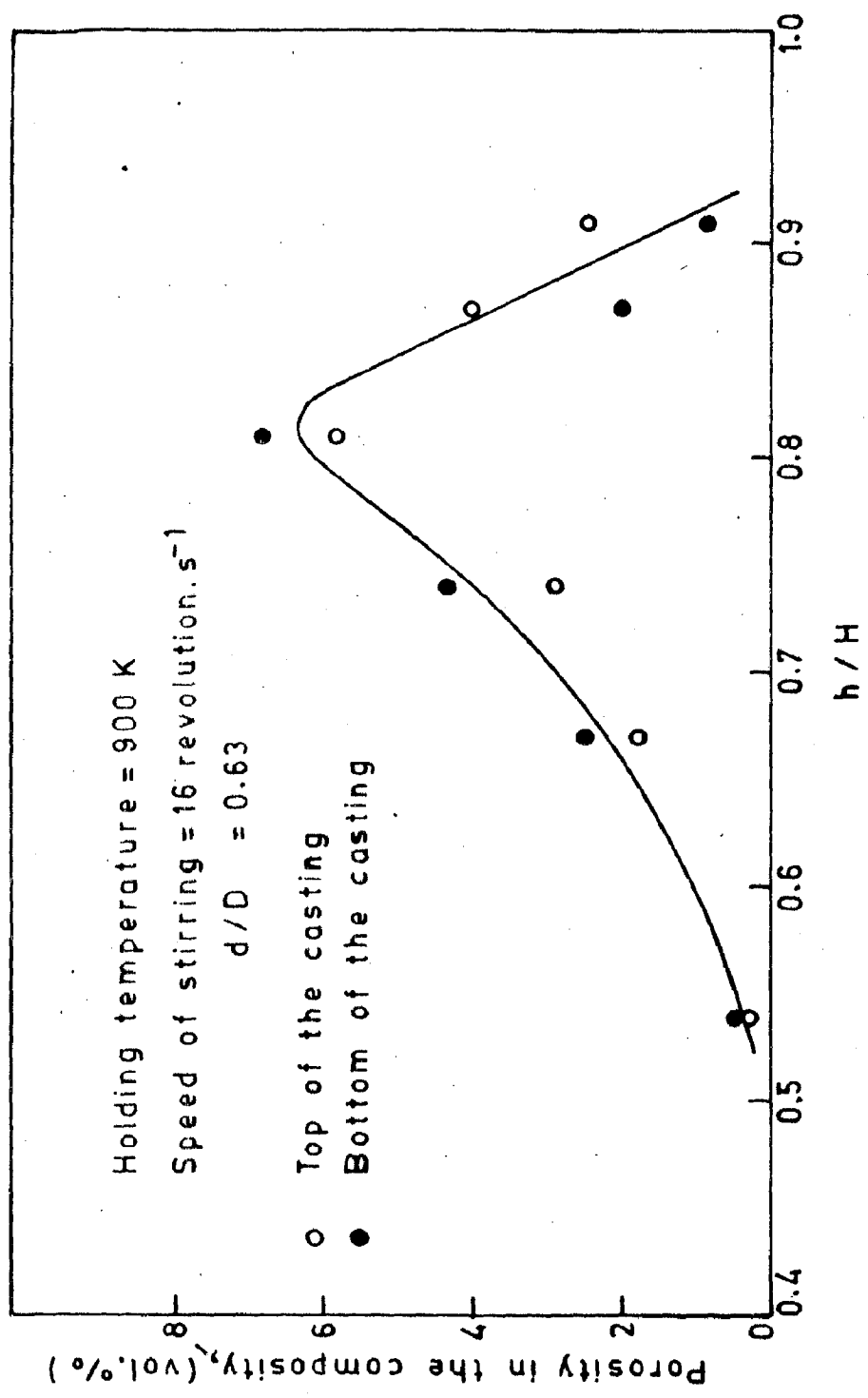
FIG. 4.11 EFFECT OF POSITION OF THE IMPELLER ON THE POROSITY CONTENT IN THE COMPOSITES.

Holding temperature = 900 K

h / H = 0.81

Speed of stirring = 16 revolution.s^{-1}

o   Top of the casting

●   Bottom of the casting

Porosity in the composite,(vol.%)

d/D
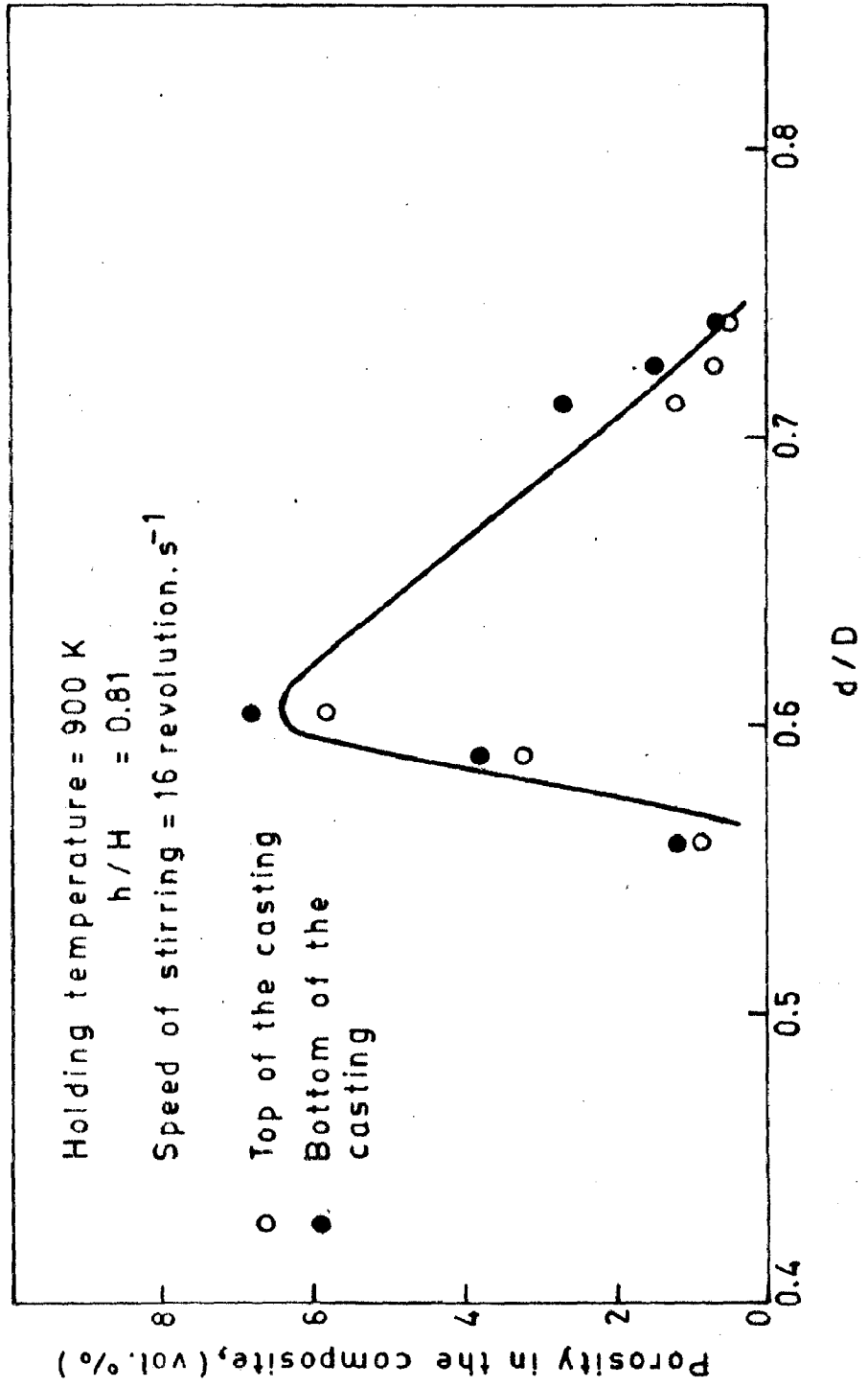
FIG. 4.12 EFFECT OF SIZE OF THE IMPELLER ON THE POROSITY
CONTENT IN THE COMPOSITES.
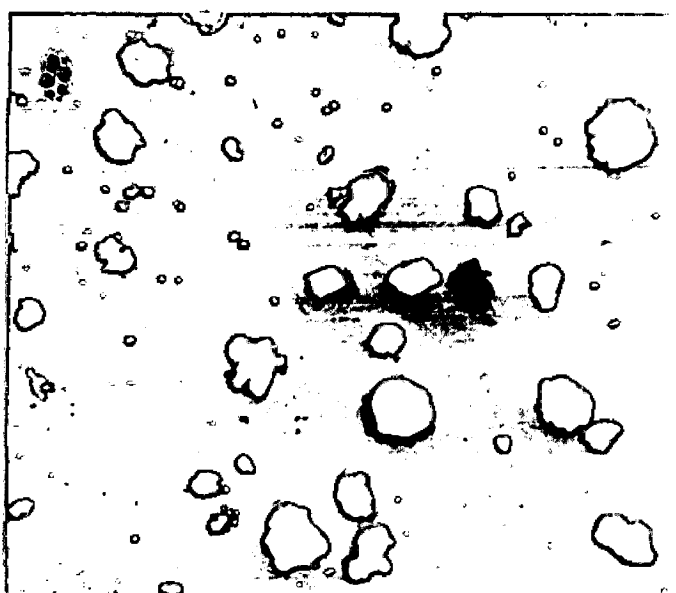
FIG.4.13 SEM MICROGRAPHS SHOWING THE FORMATION OF VOIDS AROUND ALUMINA PARTICLES IN THE AS CAST COMPOSITES; X 60
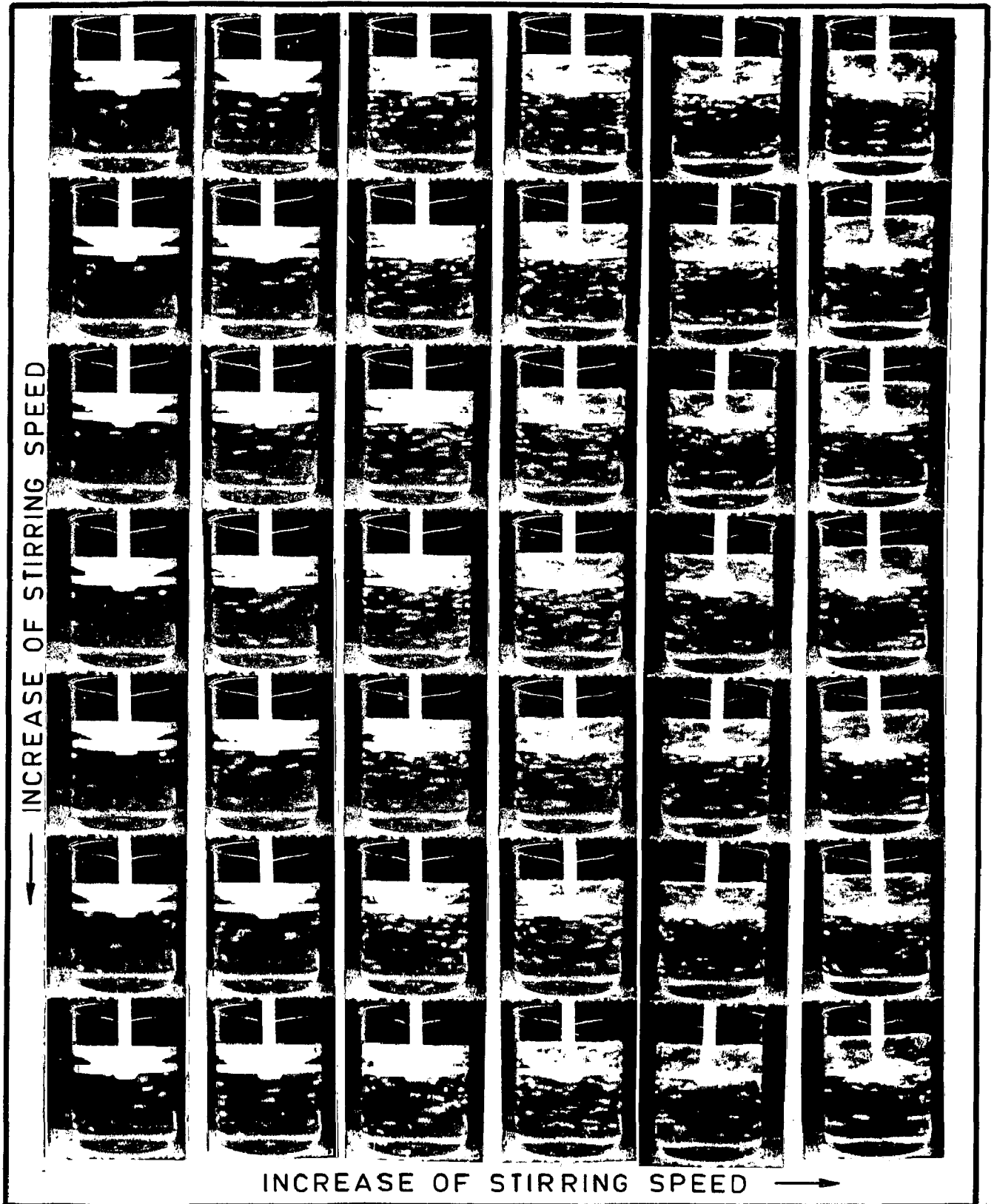
FIG. 4.14 PHOTOGRAPHS SHOWING THE EFFECT OF STIRRING
SPEED ON THE INCORPORATION OF PLASTIC BEADS
IN WATER OBSERVED DURING THE COLD MODEL EX-
PERIMENT WITH AN IMPELLER OF d/D = 0.82
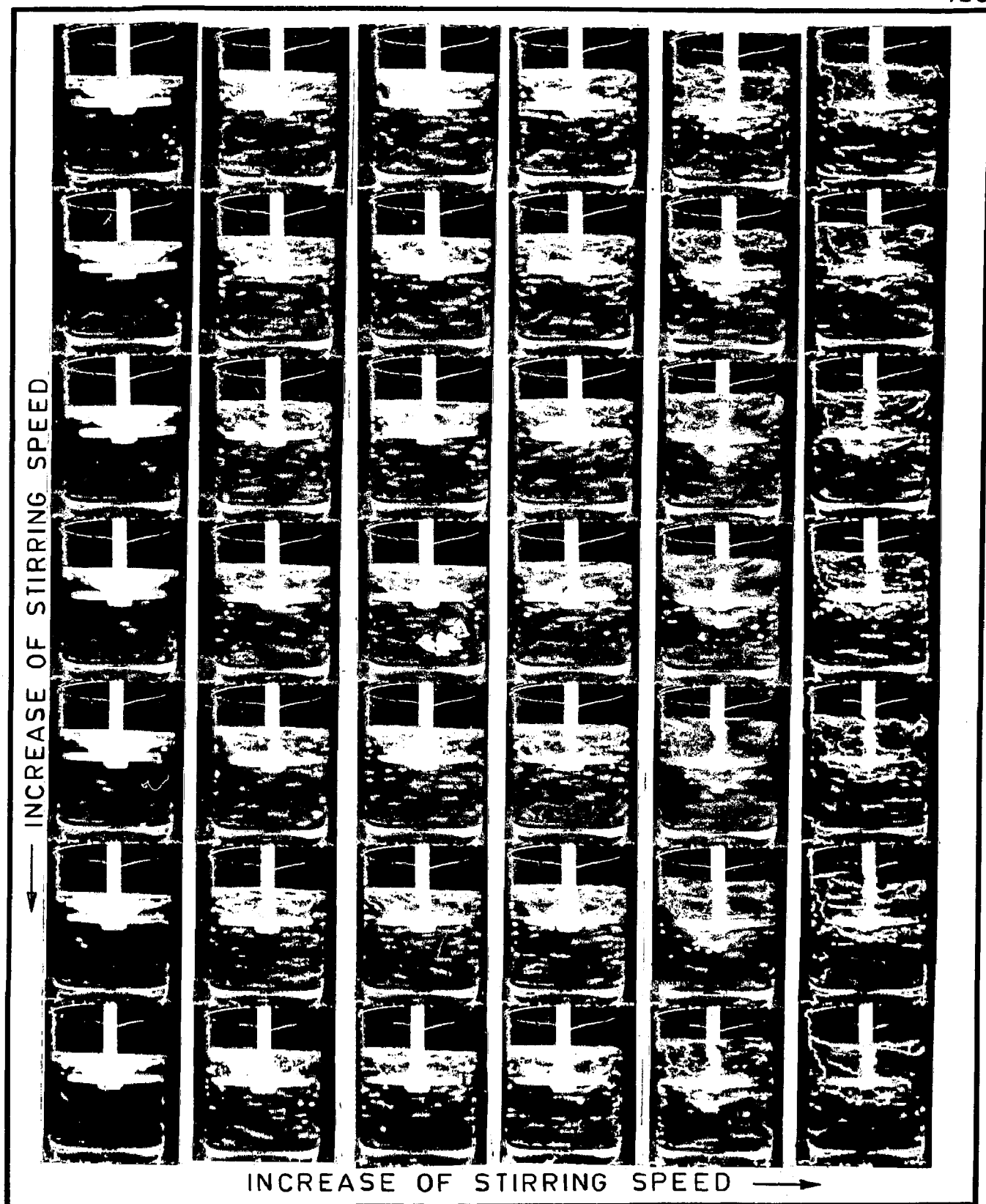
FIG. 4.15 PHOTOGRAPHS SHOWING THE EFFECT OF STIRRING SPEED ON THE INCORPORATION OF PLASTIC BEADS IN WATER OBSERVED DURING THE COLD MODEL EXPERIMENT WITH AN IMPELLER OF d/D = 0.66
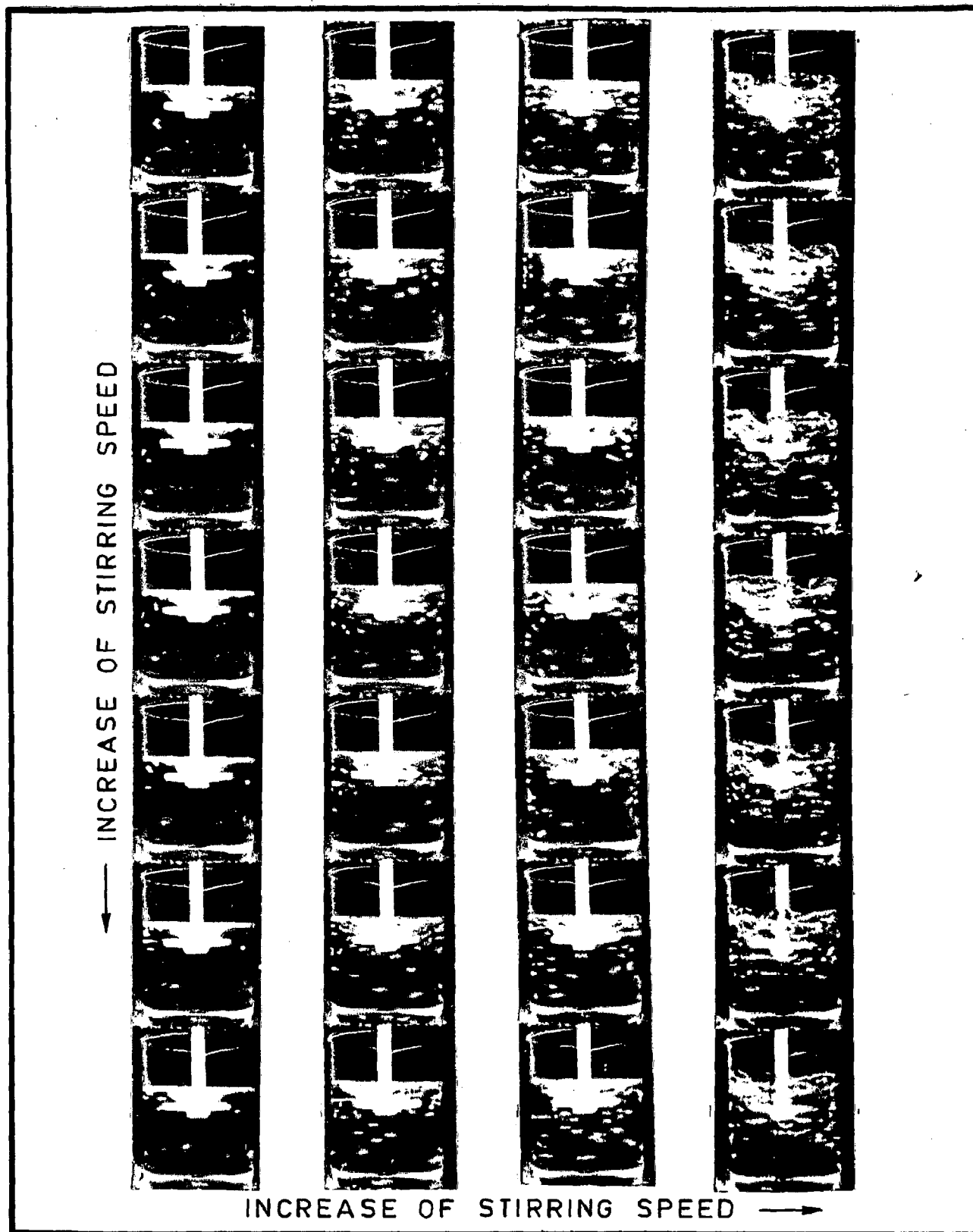
FIG. 4.16 PHOTOGRAPHS SHOWING THE EFFECT OF STIRRING
SPEED ON THE INCORPORATION OF PLASTIC BEADS
IN WATER OBSERVED DURING THE COLD MODEL
EXPERIMENT WITH AN IMPELLER OF d/D = 0.48

Fig. 4.14 shows the behaviour of the plastic beads inside water with increasing stirring speed from rest. The impeller used has a d/D ratio of 0.82. At the beginning of the stirring at a slow speed the beads have been mostly retained on the surface of the vortex. A few beads have been sunk into water during their placement due to higher kinetic energy and these beads have been found inside the water during initial period of stirring at a slow speed. The entry of the beads inside water has been found to initiate when the stirring speed reaches at an optimum value where the impeller surface is just exposed, i.e. the lower surface of the vortex touches the impeller surface. A further increase in stirring speed has increased the incorporation of beads. However, at a very high speed when a substantial part of the impeller surface has been exposed the incorporated beads have been found to accumulate just at the bottom of the impeller minimising the amount of incoorporation of the beads in the liquid medium.

In other two experiments carried out by using the impellers of d/D ratios of 0.66 and 0.48 the same behaviour as reported above have been observed for the incorporation of beads in water with the increase in stirring speed upto a moderate range as shown in Fig. 4.15 and 4.16 respectively. However, at higher speed of stirring with an impeller of d/D=0.66 it has been observed that after achieving the maximum incorporation of beads a further increase in stirring speed

results in pushing the vortex surface below the impeller. The beads have been found to be attracted to and accumulated at this vortex surface below the impeller making the bulk of water free from the beads as shown in Fig. 4.15. The retention and the distribution of the beads inside water has been found comparatively difficult when the stirring has been carried out by the impeller of d/D=0.48. Fig. 4.16 shows that even at a stirring speed when the beads start entering water leaving the vortex, there is a tendency for the beads to move around the wall of the container near the top surface of the liquid and join the vortex surface eventually without being distributed in the medium. At a higher speed of stirring the beads have been found to come down towards the bottom of the container, but they show a tendency to move by the side of the container wall without being distributed throughout the liquid medium. However, with a further increase in stirring speed the turbulence at the surface of the liquid has been found to be severe. As such the liquid motion has been found to be interrupted and the beads have been found again to join the vortex by the side of the container wall.

The initiation of exposure of the impeller during stirring has been found to occur at different stirring speed with a change in d/D ratio of the impeller. It may be noted that at this stirring speed a sudden incorporation of beads into water has been observed. A correlation between the size

of the impeller and the speed of stirring at the beginning of exposure of the impeller surface has been shown in the Fig. 4.17. It has been observed that the exposure of the impeller starts at a higher speed of stirring for an impeller having lower d/D ratio.

With the increase of stirring speed the suction of air has also been found to increase along with the plastic beads through the forced vortex region. The air has been observed to enter into the liquid as a thin envelope surrounding the plastic beads or being trapped in the cluster of beads during the sudden incorporation of large number of beads. However, at a stirring speed beyond a critical value the air bubbles have been found to be attracted towards the bottom of the impeller when the impeller of d/D ratio 0.66 has been used. This behaviour has been clearly observed in Fig. 4.15 where the air bubbles have been found to accumulate in the vortex below the impeller. In case of using the smaller impeller of d/D=0.48, at a very high speed of stirring the air bubbles sucked through the forced vortex region has been found to move out to the vortex by the side of the container wall.

4.2.4   DISCUSSION

In the present investigation it should be noted that the particle retention has been measured from the microstructure of the solidified metal particulate composite and so it is not truly characteristic of only the mixing

process in the slurry because a part of the particles incorporated in the slurry might have been rejected during solidification in the mould. However, the particle rejection in the mould is expected to be negligible because the growth of already solidified' phase results in a network entrapping the remaining liquid containing the dispersed particles. Also, the use of a permanent metallic mould results in a velocity of the solidification front far greater than the critical velocity above which the particles are entrapped by the advancing solidification front [126]. In any case the particles finally incorporated in the solid alloy is the parameter of our interest.

The cold model experiment carried out to study the behaviour of the incorporation of plastic beads into water through the vortex under different mixing parameters have revealed the nature of the vortex and the importance of the exposure of the impeller vis-a-vis the retention of the beads in the liquid. The mechanism of incorporation of solid in the agitated liquid has been understood from the model experiments as shown in Fig. 4.14, Fig. 4.15 and Fig. 4.16. In a concentrically agitated mixing process the height of the liquid surface comes down at the center during stirring as the speed of the stirrer increases. Beyond a certain stirring speed a part of the stirrer becomes exposed and the particles floating on the liquid surface are drawn towards the center by the extended free vortex region and fall on the exposed rotating stirrer. These particles get scattered by
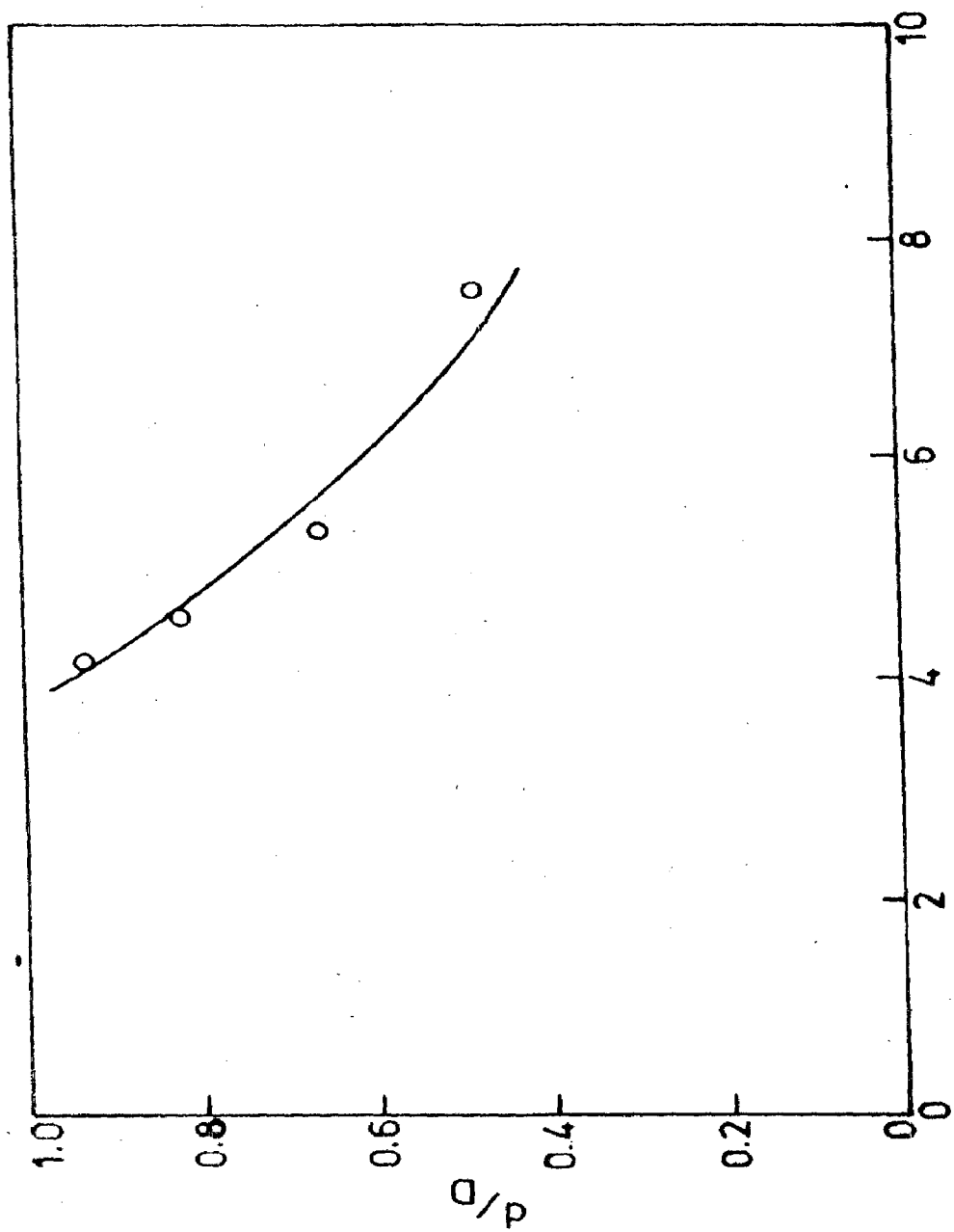
FIG. 4.17 THE CRITICAL SPEED FOR INCORPORATION AT IMPELLERS WITH DIFFERENT d/D RATIOS.

the stirrer and thus gain an inertial centrifugal force
enabling them to enter the liquid. Under this inertial force
the particles may even impinge on the surface of the container
and get■ distributed throughout the liquid under the influence.
of its turbulent flow as shown in Fig. 2.3.

The schematic diagram of the impeller (Fig. 3.4)
shows that the impellers used in this investigation are having
a central zone of radius, r_3, extending to the blades. With
the increase of stirring speed when the increasing value
of r_c exceeds the value of r_3 as it is presented schematically
in Fig. 4.18 then a large size bubble forms due to the
existance of a low pressure at the boundary of the forced
vortex region as it is observed in Fig. 4.15. Under these
circumstances a considerable amount of air bubble is sucked
inside the liquid and these bubbles rise to the vortex region
at the bottom of the impeller. The beads already incorporated
inside the water carried eventually by the flow of liquid
to the vortex below the impeller as shown in Fig'.2.3 and
Fig. 4.15 thereby minimising the retention of beads in the
matrix. It is suspected that the beads may have entered
the liquid with an air envelope due to its low wettability.

During stirring of water with a bigger impeller of
the size d/D=0.82 the vortex has not been observed to come
down below the impeller (Fig. 4.14) at any stirring
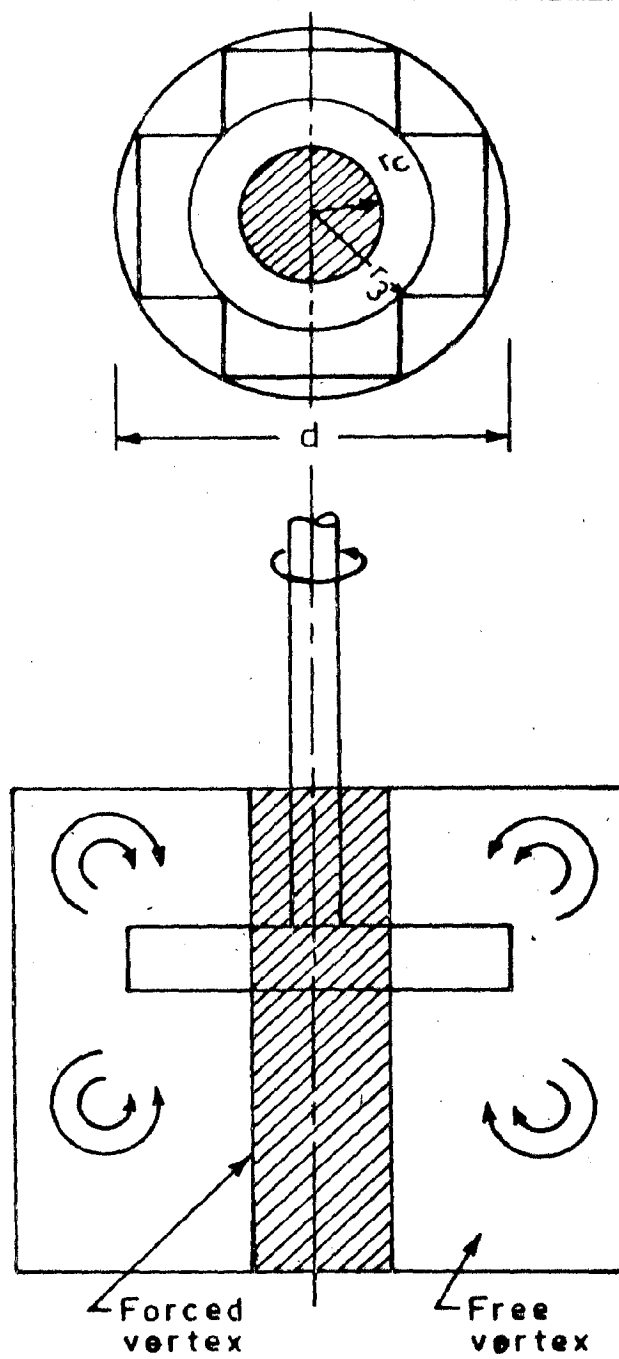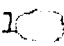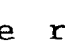
FIG. 4.18 SIMPLIFIED FLOW MODEL OF A CON-
CENTRICALLY AGITATED MIXING SYSTEM
IN A CYLINDRICAL VESSEL.

speed used in this investigation because of a comparatively larger r_3 than the value of r_c achieved. At a given stirring speed the Reynold's number is more in case of an impeller of higher d/D ratio as it follows from equation (2.28) and it results in a larger value of r_c as obtained from equation (2.29). Thus, in case of stirring with a bigger impeller at a fixed stirring speed the value of Z_0 as estimated from equation (2.26) will be lower than that estimated for a smaller impeller. So it can be inferred that during stirring with an impeller of higher d/D ratio the impeller will be exposed at a lower stirring speed than that for an impeller of lower size. As a result the incorporation of beads will take place at a lower speed of stirring where a bigger impeller is used as it has been shown in Fig. 4.17. Similar observations have been made while stirring with a big impeller (d/D=0.82) and a comparatively small impeller (d/D=0.66) in cold model experiments as evident in Fig. 4.14 and Fig. 4.15 respectively. However, while stirring with an impeller of higher d/D ratio r_c is increasing with an increase in the stirring speed but the volume of liquid under turbulence is decreasing adversely affects mixing. Moreover, at higher stirring speeds the beads strike the vessel wall at a higher kinetic energy due to which the particles could not be deflected enough downwards to go into the region below the impeller. This may have caused the beads to come back to the vortex after getting scattered by the container wall to strike eventually the stirrer again. Thus, for a higher speed of

stirring with a stirrer of d/D=0.82 the incorporation is lowered as it is observed in Fig. 4.14. Also, it has been observed that the beads which are incorporated enter the vortex region and get accumulated at the bottom of the impeller as shown in Fig. 4.14.

In the cold model experiment during stirring at a lower speed with the help of a smaller impeller (d/D=0.48) the axial velocity of the discharge flow is low. It increases the thickness of the stagnant layer of liquid adjacent to the vessel wall as it has been described in Fig. 2.4 so the beads incorporated inside the liquid have been observe to float out by the side of the vessel wall as it has bee observed in Fig. 4.16. Due to lower r_3 of this impeller, at a certain value of increasing stirring speed the r_c has exceeded the value of r_3 where the accumulation of air bubble and the particles have been found to occur at the bottom of the impeller as it has been discussed earlier. However, the bubbles become unstable due to the accumulation of air and floats out above the impeller along with the accumulated beads. With further increase of stirring speed a substantial part of the impeller (d/D=0.48) surface becomes exposed and r_c becomes much higher than r_3. Under this circumstance the air bubble accumulating at the bottom of the impeller comes out frequently with the growth of its size. This process along with the severity of turbulence disturb the entire discharge flow system. Thus the beads already inside the

liquid float out of the liquid by the side of the vessel wall.

In the present investigation during stirring of the molten metal under different mixing conditions imposed by changing the impeller size, the impeller position and the holding temperature of the melt, the critical stirring speed at which the impeller starts to get exposed are estimated as follows.

The Reynold's number of the agitated slurry, Re_{slurry}, has been estimated with the help of the relation

$$Re_{slurry} = \frac{d^2 n \, \rho_{slurry}}{\eta_{slurry}} \qquad .. \qquad (4.1)$$

The average density of the partially solid Al-4wt% Mg alloy, ρ_{slurry}, has been evaluated as [127].

$$\rho_{slurry} = \emptyset \, \rho_s + (1 - \emptyset) \, \rho_L \qquad .. \qquad (4.2)$$

where, $\emptyset$ is the volume fraction of primary solid particles in the slurry, ρ_s is the density of the primary solid particles and ρ_L is the density of the remaining liquid. The volume fraction of primary solid particles, $\emptyset$, in partially solid Al-4wt% Mg alloy has been estimated by well known Scheil's equation [128] as

$$C_s = K_O \, C_O \, (1 - \emptyset)^{K_O - 1} \qquad .. \qquad (4.3)$$

where, K_O is the partition ratio of the solute expressed as $K_O = C_S/C_L$, C_O is the magnesium content of the alloy, C_S and C_L are the magnesium content in the solid and in the liquid respectively at a given temperature within the partially solid range of the alloy. The co-efficient of viscosity of the partially solid Al-4wt.% Mg alloy, η_{slurry}, has been estimated by using the expression given by Thomas [129] as,

$$\eta_{slurry} = \eta_L \left[1 + 2.5\, \emptyset + 10.05\, \emptyset^2 + 0.00273\, \exp\,(16.6\emptyset) \right]$$

$$.. \quad (4.4)$$

where, η_L is the coefficient of viscosity of the liquid matrix in partially solid Al-4 wt.%Mg alloy.

One can find out the value of r_c/r_1 by using the equation (2.29). For a given size of impeller the value of r_c has been calculated from the ratio of r_c/r_1. Thus from the known value of the radius, r_2, of the crucible the ratio $r_c/r_2=y$ has been evaluated. The stirring speed corresponding to the vortex touching the surface of the impeller has been estimated graphically in Fig. 4.19, Fig. 4.20 and Fig. 4.21 for various mixing conditions. After putting $Z_O = h$ in equation (2.26) it becomes

$$\left(\frac{H-h}{r_2^2}\right)\left(\frac{g}{\omega^2}\right) = y^2 - y^4 \left[2.303 \log\left(\frac{1}{y}\right) + 0.75 \right] .. \quad (4.5)$$

The right hand side and the left hand side expressions of the equation (4.5) are denoted as two functions

$$f_1 = y^2 - y^4 \left[2.303 \log\left(\frac{1}{y}\right) + 0.75 \right] \qquad .. \quad (4.6)$$

$$f_2 = \left(\frac{H-h}{r_2^2}\right)\left(\frac{g}{\omega^2}\right) \qquad .. \quad (4.7)$$
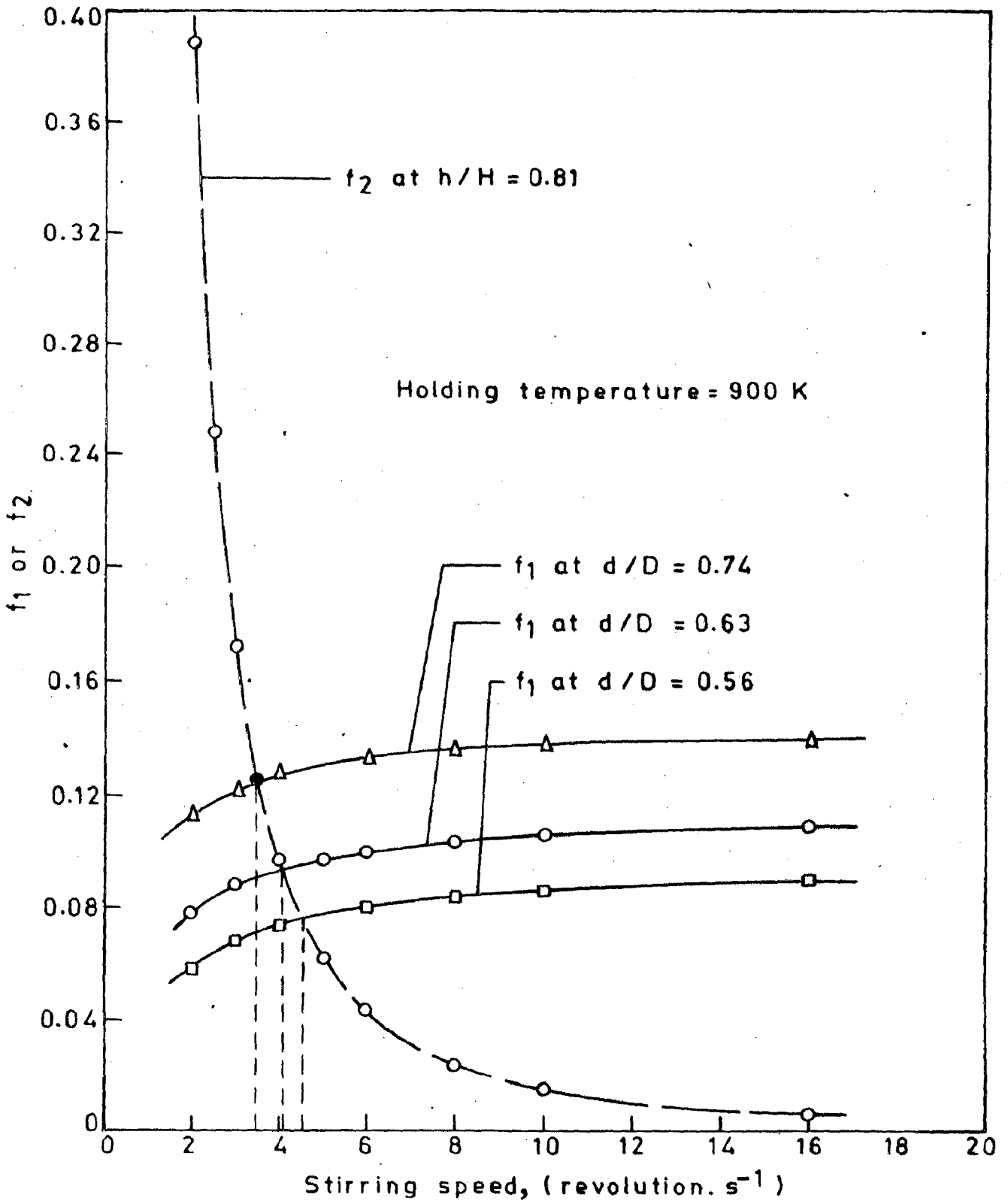
FIG. 4.19 GRAPHICAL SOLUTION FOR CRITICAL STIRRING
SPEED FOR EXPOSING THE IMPELLER OF DIF-
FERENT SIZES; HOLDING TEMPERATURE = 900 K
AND h/H = 0.81
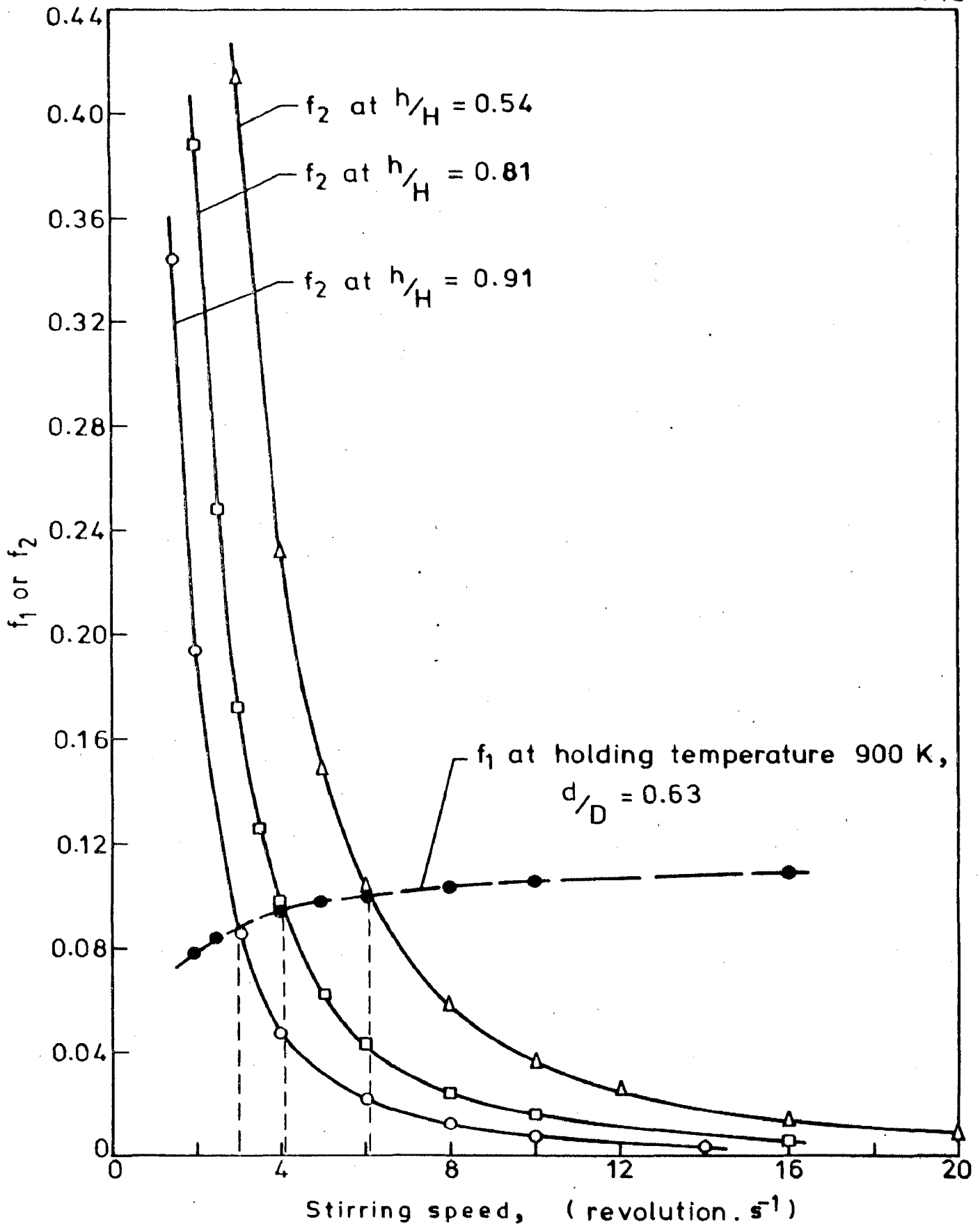
FIG. 4.20 GRAPHICAL SOLUTION FOR CRITICAL STIRRING
SPEED FOR EXPOSING THE IMPELLER PLACED
AT DIFFERENT POSITIONS INSIDE THE SLURRY;
HOLDING TEMPERATURE = 900 K AND d/D = 0.63
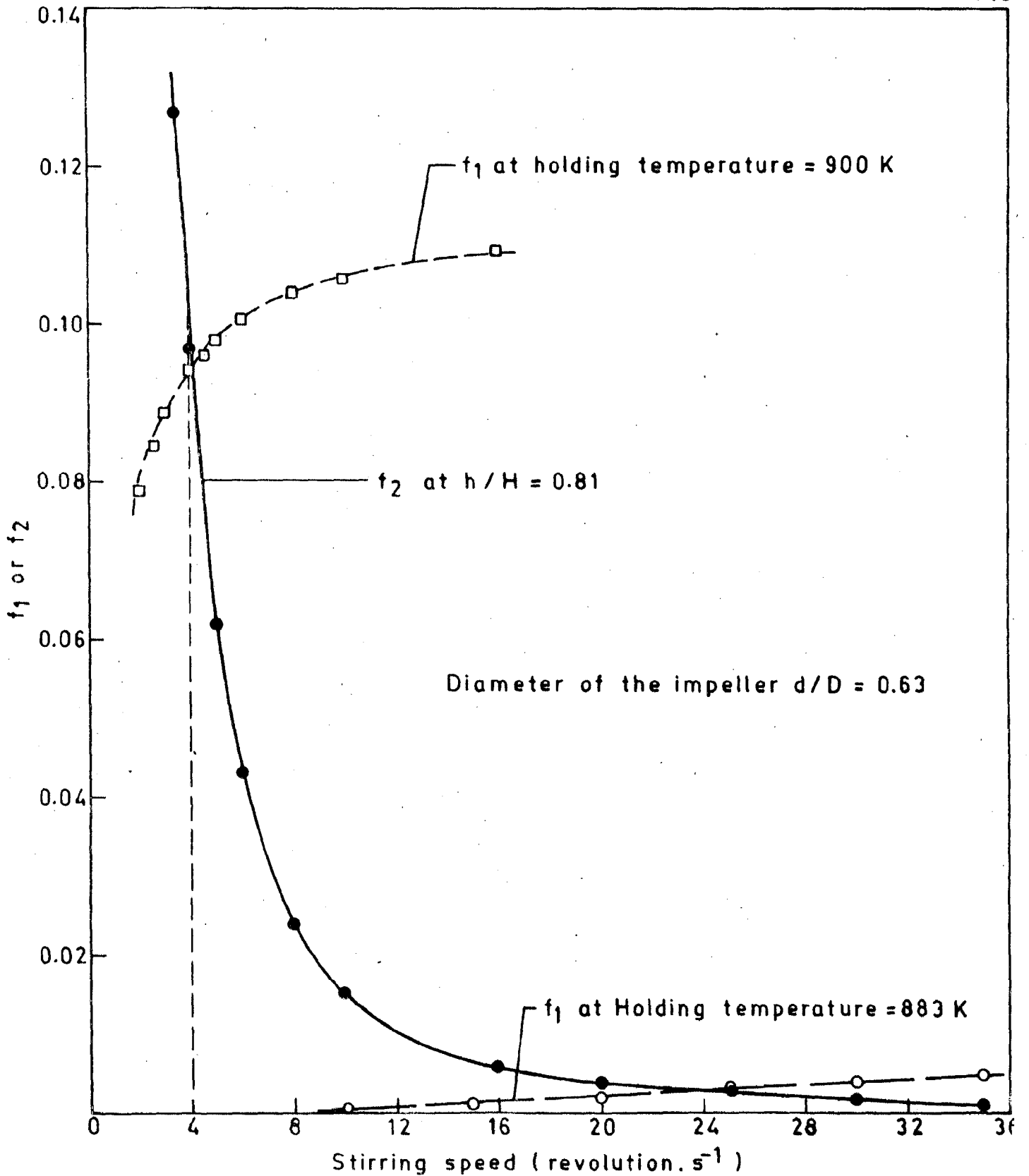
FIG. 4-21 GRAPHICAL SOLUTION FOR CRITICAL STIRRING SPEED FOR EXPOSING THE IMPELLER AT DIFFERENT HOLDING TEMPE RATURES; d/D = 0.63 AND h/H = 0.81

Now from the values of f_1 and f_2 for the variation of the stirring speed, n, one gets the graphical solution of the stirring speed where the impeller gets exposed under a given condition of mixing. Fig. 4.19 shows the graphical solution for the critical speed at which the impeller of various sizes gets exposed and Fig. 4.20 shows the solution for the critical speeds for different position of the impeller inside the partially solid melt. It has been observed that in all these cases the impellers have been exposed at the high speed of stirring (16 revolution.s^{-1}) used in the present investigation. So the range of our investigation falls within the effective limits indicated by the cold model experiments in respect of exposing the stirrer for effective incorporation. Fig. 4.21 shows that the impeller has been exposed at the stirring speed of 16 revolution.s^{-1} when the holding temperature of the melt has been kept at 900 K but when the holding temperature is reduced to 883 K, at the same stirring speed the stirrer remains inside the melt due to an increase in the viscosity, η_{slurry} caused by the solid phase in the melt.

While investigating the effect of holding temperature on the retention of alumina particles in the casting (Fig. 4.1) it has been estimated by equation (4.3) that at the holding temperatures of 883 K and 900 K the Al-4 wt.% Mg slurry contains about 78% and 57% primary solid particles respectively. During the addition of alumina

particles in a vigorously agitated partially solid aluminium alloy melt the added particles collide with the particles of the primary solid phase imparting kinetic energy and momentum in random directions. The residence time of the alumina particles in the slurry is enhanced due to successive collisions. Thus the incorporation of these particles in the slurry is increased giving rise to a better mixing. Though at the holding temperature of 883 K the impeller has not exposed during stirring with a speed of 16 revolution.s^1 (Fig. 4.21) yet the increase in the retention of the alumina particles in the slurry at this holding temperature (Fig. 4.1) is observed. The retention of a significant amount of particles in the matrix of a cast composite fabricated by stirring partially solid Al-4wt.% Mg slurry at a holding temperature of 883 K is revealed in the micrographs presented in Fig. 4.2 (i) and (ii). With an increase in the holding temperature to 900 K the amount of primary solid particles in the slurry falls down and the retention of alumina particles in the composite also become less as shown in Figs. 4.2 (iii) and (iv). The decrease in the amount of alumina retention in the casting with an increase in the holding temperature clearly establishes the helpful role of the proeutectic primary solid in the slurry whose amount decreases with an increase in the holding temperature. At a holding temperature beyond the liquidus point of the alloy (915 K) no primary solid particles are there. Thus at a holding temperature beyond 915 K a

comparatively lower retention of alumina particles is observed in the casting as shown in Fig. 4.1 and a variation in holding temperature in this range has not influenced the amount of retention of alumina particles significantly. A comparatively lower retention of alumina particles in the matrix of a composite made at a holding temperature of 958 K is shown in the micrographs presented in Figs. 4.2 (v) and (vi).

In Fig. 4.1 it has been observed that at a holding temperature of 900 K no significant difference exists between the alumina content at the bottom and the top of the casting as it has been revealed in the micrographs of Fig. 4.2 (iii) and Fig. 4.2 (iv) respectively. However, at a holding temperature of 883 K though the slurry has a primary solid particles content as high as 78%, still, a relative difference of ~ 1.5 wt.% in the retention of alumina at the bottom and at the top of the casting is observed in the micrograph shown in Fig. 4.2 (i) and Fig. 4.2 (ii) respectively. The difference in the particle distribution at the top and the bottom of the castings should depend on the extent of particle incorporation and the motion of the particles after collisions. If the particle content is large the random collisions may not be able to disperse the colliding particles to a larger distance and the distribution may become poor. This may be the reason for observing larger segregations of the particles between the top and the bottom of an ingot cast at a holding temperature of 883 K compared to that at 900 K although the particle retention is higher in case of the former holding temperature.

At a given holding temperature (900 K), the size of the impeller (d/D=0.63) and the position of the impeller (h/H=0.81) the annular flow of liquid under secondary circulation touches the higher region of the vortex with an increase in the stirring speed as shown in Fig. 2.5. It may be noted that the particles fall at the center as well as all along the surface of the vortex during addition of the alumina particles from the top in the vortex. The annular flow provides a substantial down flow of the slurry from the higher region of the vortex and it drags alumina particles lying on the surface of the vortex along with slurry towards the impeller. An increase in the stirring speed enhances this annular flow resulting in an increase in the retention of alumina inside the slurry as observed in Fig. 4.3 and revealed in comparison of the micrographs presented in Fig. 4.4 (i,ii) and Fig. 4.2 (iii,iv), during increase of stirring speed from 7.5 revolution.s^{-1} upto 16 revolution.s^{-1} respectively. The r_c increases with the increase of stirring speed and upto a stirring speed of 16 revolution.s^{-1} the value of r_c remains lower than the value of r_3 = 15.25 mm for d/D=0.63. But with further increase of stirring speed the value of r_c exceeds the value of r_3 as shown in Fig. 4.22 and results in suction of air bubbles as discussed earlier. The alumina particles entering inside with an air envelope cannot be wetted by the slurry and accumulate at the bottom of the impeller resulting in a reduction in retention of particles at the stirring speed
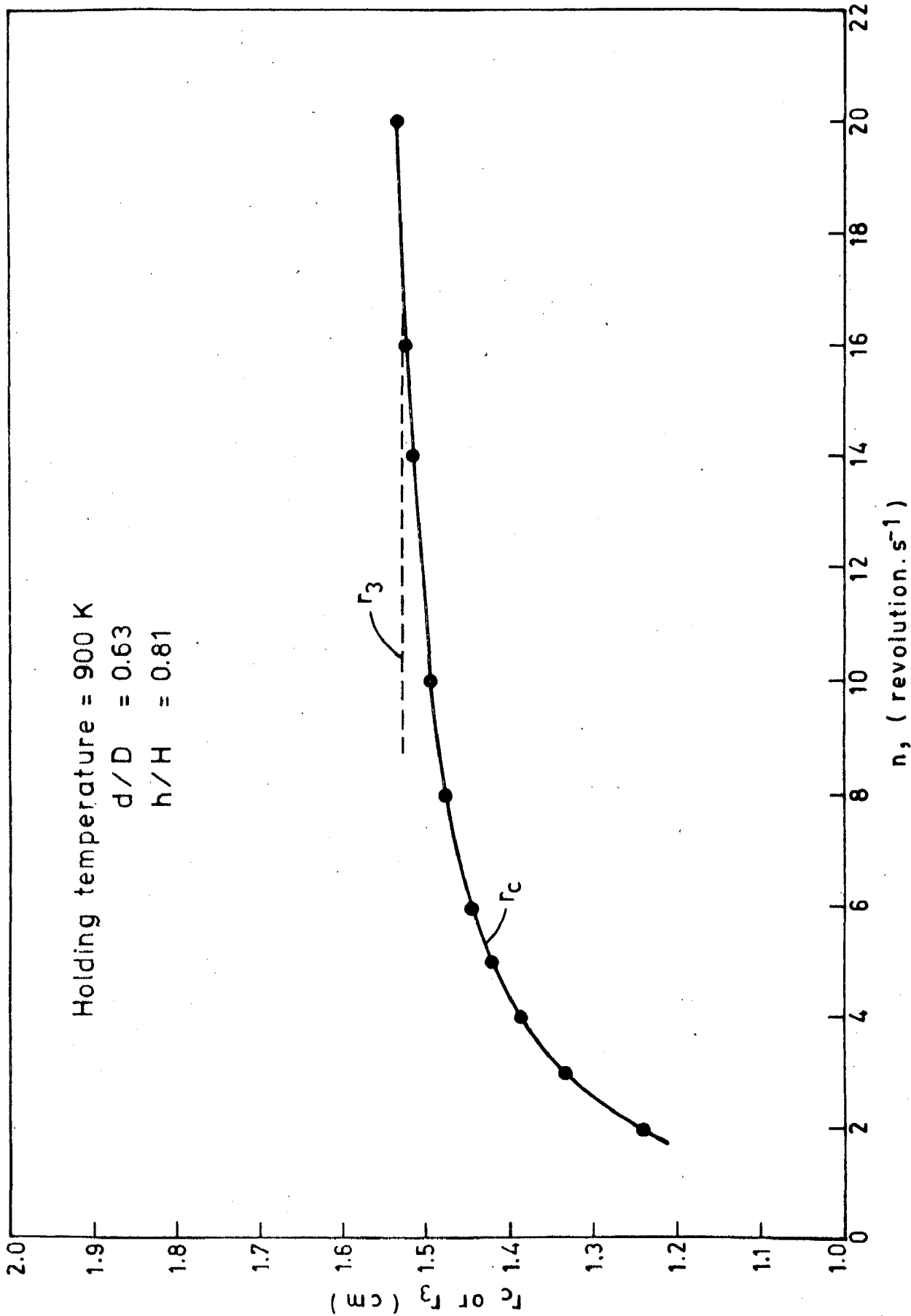
FIG. 4.22 CRITICAL SPEED FOR r_c TO CROSS THE r_3 AT A GIVEN HOLDING TEMPERATURE = 900 K; d/D = 0.63 AND h/H = 0.81

beyond 16 revolution.s^{-1} as shown in Fig. 4.3. The clustering of alumina particles in the micrographs of the top of the casting made at 23 revolution.s^{-1} shown in Fig. 4.4 (iv) is in agreement to the accumulation of particles at the bottom of the impeller. However, a further increase in stirring speed to 25 revolution.s^{-1} has drastically reduced the retention of the particles in the casting as revealed in the micrographs shown in Fig. 4.4 (v and vi) may be due to enhancement in the suction of air bubble. In Fig. 4.23 it is interesting to note that under a given holding temperature (900 K), size of the impeller (d/D=0.63), and the position of the impeller (h/H=0.81) the retention of alumina in the composite increases as the ratio r_c/r_1 increases upto 0.605 with the increase of stirring speed from 7.5 revolution.s^{-1} to 16 revolution.s^{-1}. However, with further increase of r_c/r_1 by the increase of stirring speed beyond 16 revolution.s^{-1} upto 25 revolution. s^{-1} a sharp fall in the retention of alumina takes place. It is important to note that the retention of particles between the bottom and the top of the casting is again minimum at a retention level of 12.7 wt.% alumina, as revealed in the micrographs shown in Fig. 4.2 (iii and iv).

The vertical motion of the liquid during its annular flow is largely dependent on the speed of stirring. So at a given holding temperature (900 K), size of the impeller (d/D=0.63), and stirring speed (16 revolution.s^{-1}), the extent of the annular flow above the impeller is fixed
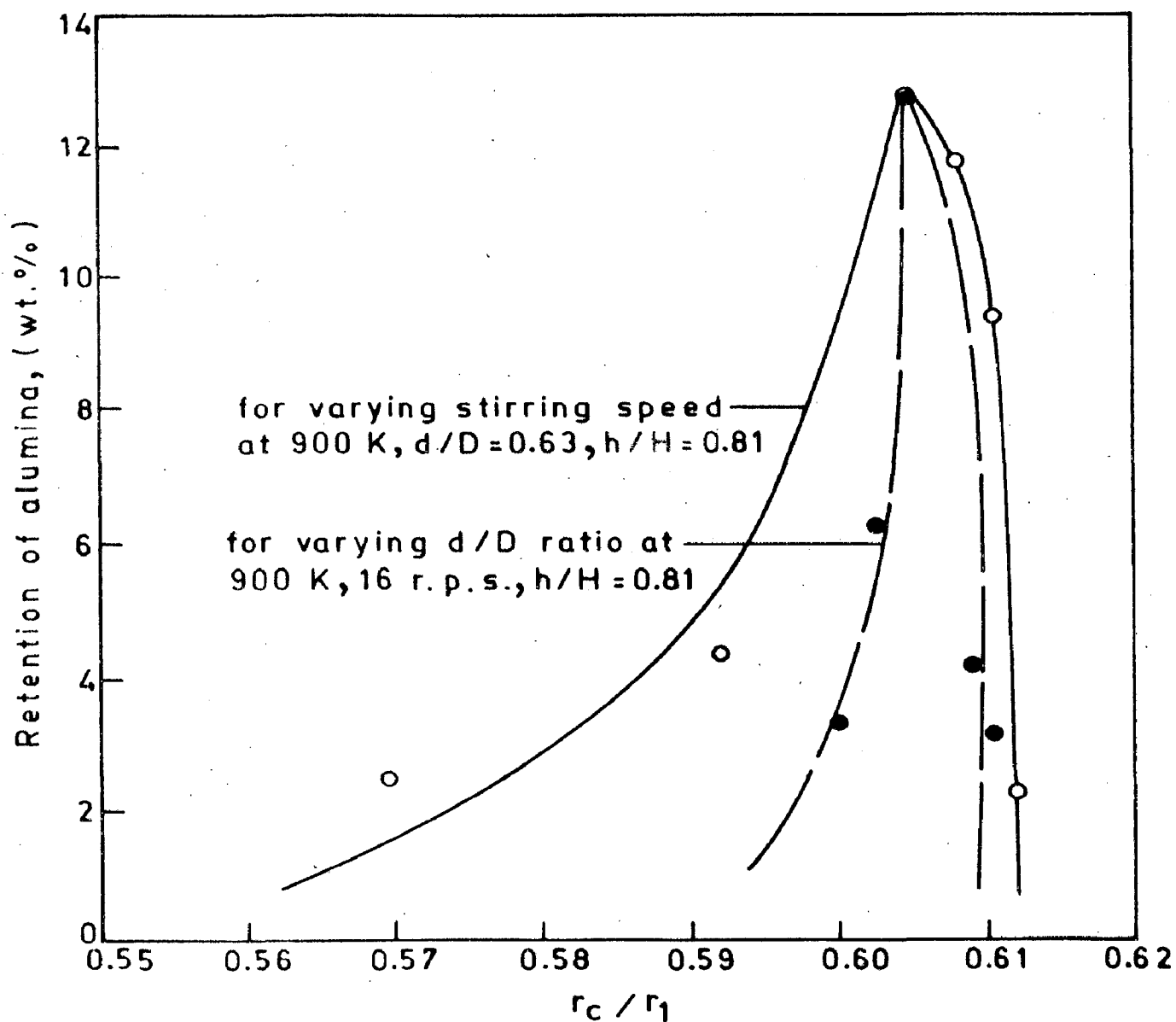
FIG. 4.23 EFFECT OF r_c / r_1 VARYING WITH STIRRING SPEED AND SIZE OF THE IMPELLER ON THE RETENTION OF ALUMINA IN THE COMPOSITE.

for a given position of the impeller. Thus under the mixing condition mentioned above when the impeller is placed at a larger depth (h/H=0.54) inside the slurry the annular flow at the vortex surface is reduced significantly. The particles lying in the upper region of the vortex have been observed to remain to a large extent and not enter the slurry resulting into a lower retention of alumina in the casting when the impeller is placed at h/H=0.54 as shown in Fig. 4.5 and revealed in the micrographs presented in Fig. 4.6 (i and ii) . With the increase in value of h/H the retention of particles in the casting has increased upto 12.7 wt.% at h/H=0.81 as it is observed in Fig.4.5 and depicted in Fig. 4.2 (iii and iv), because at higher h/H ratio the depth of the vortex is decreased and thus the annular flow of the slurry has been effective to draw in the particles from the surface of the vortex. However, with further increase in value of h/H beyond 0.81, the turbulence in the vortex region becomes very large and the particles remain confined in the region of the slurry above the impeller adversely affecting the particle retention. As such the alumina content of the casting is lowered as it is observed in Fig. 4.5 and evident in Fig. 4.6 (iii and iv) for h/H=0.91.

At a given holding temperature of 900 K, the stirring speed of 16 revolution.s^{-1} and the position of the impeller of h/H=0.81 the value of r_c has been found to increase linearly with the increase in the size of the impeller as shown in Fig. 4.24. In Fig. 4.24 it has been observed that
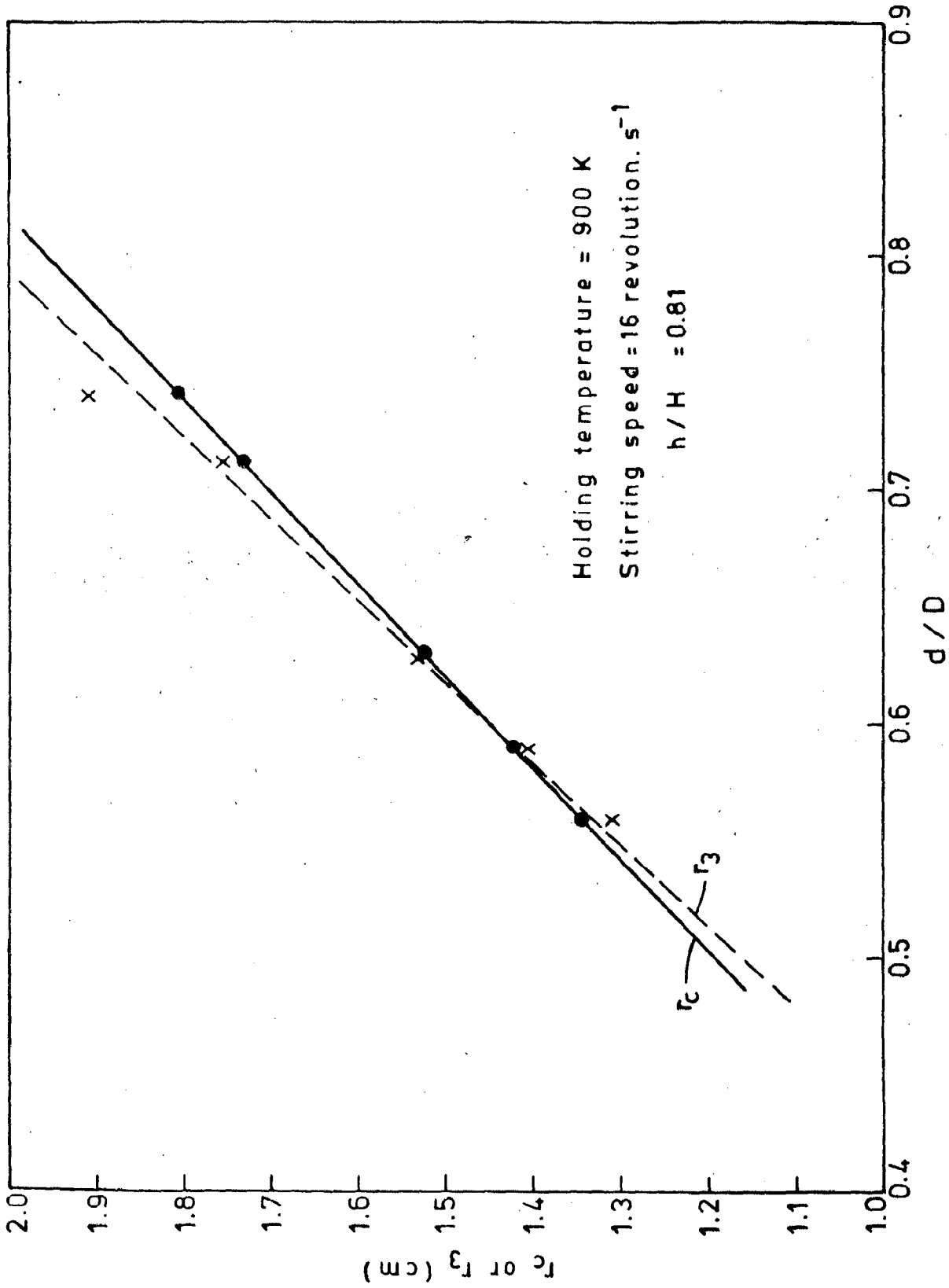
FIG. 4.24 CRITICAL SIZE OF THE IMPELLER WHEN r_c CROSSES OVER THE r_3 AT A GIVEN HOLDING TEMPERATURE = 900 K; STIRRING SPEED = 16 r.p.s. AND h/H = 0.81

Holding temperature = 900 K

Stirring speed = 16 revolution. s^{-1}

h/H = 0.81

r_c

r_3

d/D

r_c or r_3 (cm)

the values of r_c are higher than the values of r_3 for the impellers of d/D=0.56 and d/D=0.59. Thus, in view of the similar phenomena discussed earlier for the case of $r_c>r_3$ it can be inferred that in both the above cases alumina particles along with the air bubble have entered and accumulated at the bottom of the impeller without mixing with the slurry resulting into a reduction in the retention of particles in the castings as revealed in Fig.4.8(i) and (ii) from casting made at d/D=0.56. However, with the increase in size of the impeller from d/D=0.56 to d/D=0.59,due to increase of r_c the difference in size between $r_c$and r_3 is reduced (Fig.4.24)and as a result the retention of alumina particles in the casting has increased as it is shown in Fig.4.7.The value of r_c has been found to be a little lower than the value of r_3 when the stirring of partially solid melt has ben carried out by an impeller of d/D=0.63. Thus no accumulation of air bubble have taken place at the bottom of the impeller and a large amount of retention of alumina in the casting is obtained as shown in Fig.4.7 and evident in the micrographs presented in Fig.4.2 (ii and iv). The reason for this retention of large amount of alumina in the casting has been attributed to the helpful role of the expo$\overset{su}{\underset{k}{r}}$e of the impeller on the retention of particles. With further increase in size of the impeller upto d/D=0.74 the difference in r_c and r_3 has been found to increase continuously having r_c always less than r_3 as depicted in Fig.4.24. In these

cases though the r_c is lower than r_3 still the retention of alumina has been found to be ~~lowered~~ reduced with the increase in the value of d/D as shown in Fig. 4.7 and revealed in the micrographs (Fig. 4.8 iii and iv) of the cast composite made by using an impeller of d/D=0.74 . It is attributed to a decrease in volume of liquid under turbulence with the increase of r_c and the effect of back reflection of beads from the vessel wall during the use of large size impeller as it has been explained earlier. As a result when large impellers of d/D lying between 0.72-0.74 are used , retention of alumina at the top of the castings have been found to be significantly higher than that observed in the bottom of the castings as shown in Fig. 4.7 and in the microphotographs in Fig. 4.8 (iv) and Fig. 4.8 (iii) for the top and the bottom of the castings respectively. For a given holding temperature (900 K), stirring speed (16 revolution.s^{-1}) and position of the impeller (h/H=0.81), as the value of r_c/r_1 increases upto a value of r_c/r_1=0.605 with the increase in size of the impeller (d/D), the amount of retention of alumina in the casting is also enhanced followed by a sharp fall in retention of alumina with further increase in r_c/r_1 as shown in Fig. 4.23. It is interesting to note in Fig. 4.23 that the retention of alumina is more sensitive to the ratio r_c/r_1 during the variation in impeller size (d/D) than that observed in case of variation in stirring speed (n).

The porosity in castings may result either from the presence of air bubbles sucked in the melt or due to the evolution of gases during solidification in the mould. The lower porosity content in the composites cast at the holding temperatures above the liquidus point (915 K) as compared to those cast from that found in the partially solid state (Fig. 4.9) shows the role of the sucked bubbles in the overall porosity content of the casting. The cold model experiment with water and plastic beads confirms the phenomena of suction of bubbles in the forced vortex region of the stirred liquid. However, the bubbles incorporated due to suction in forced vortex region have enough scope to go out of the slurry during its stirring and casting. This has been reflected in Fig. 4.10, where at a higher stirring speed beyond 19.2 revolution.s^{-1} inspite of the increased suction the porosity level of the composites has been found less which shows that the bubbles incorporated freely has not posed any significant problem by increasing the porosity in the composite.

It is interesting to note that variation in porosity content of the composites with a change in holding temperature stirring speed and the values of h/H and d/D as presented in Fig. 4.9 to Fig. 4.12 respectively follow a similar behaviour to that of the retention of alumina shown in Figs. 4.1, 4.3, 4.5 and 4.7 respectively. These results indicate a simultaneous suction of air and alumina in the vortex.

The cold model experiments have shown that the air may also enter the liquid as a thin envelope surrounding the solid particles. These particles undergo collisions with the primary α -particles and help the particle to get detached from its air envelop. Now, the particle surface may be wetted by the melt. However, some of the particles may not be able to get rid of its air envelope and cast as such resulting into a void containing particles in the composite as shown in Fig. 4.13.

The entire porosity content, thus, consists of (a) sucked air bubbles and (b) the evolved gas pores. The linear variation of porosity with alumina content irrespective of the levels of process variables as shown in Fig. 4.25 indicates that the latter contribution is negligible or, at best, causing minor scatter (correlation co-efficient $\sim$ 0.87) in the observed results. The sucked air bubbles are entering the slurry either independently or as an envelope to the alumina particles. The suction of independent bubbles will depend on the suction pressure existing at the forced vortex region. The incorporation of the alumina particles will also depend on the same variable. The suction of alumina particles with an air envelope and their subsequent retention will enhance the particle and the porosity content in the same way. The particles getting detached from the air bubble will increase the population of independent air bubbles and the particles, resulting in a proportinate in- crease. The rejection of the air bubbles and the
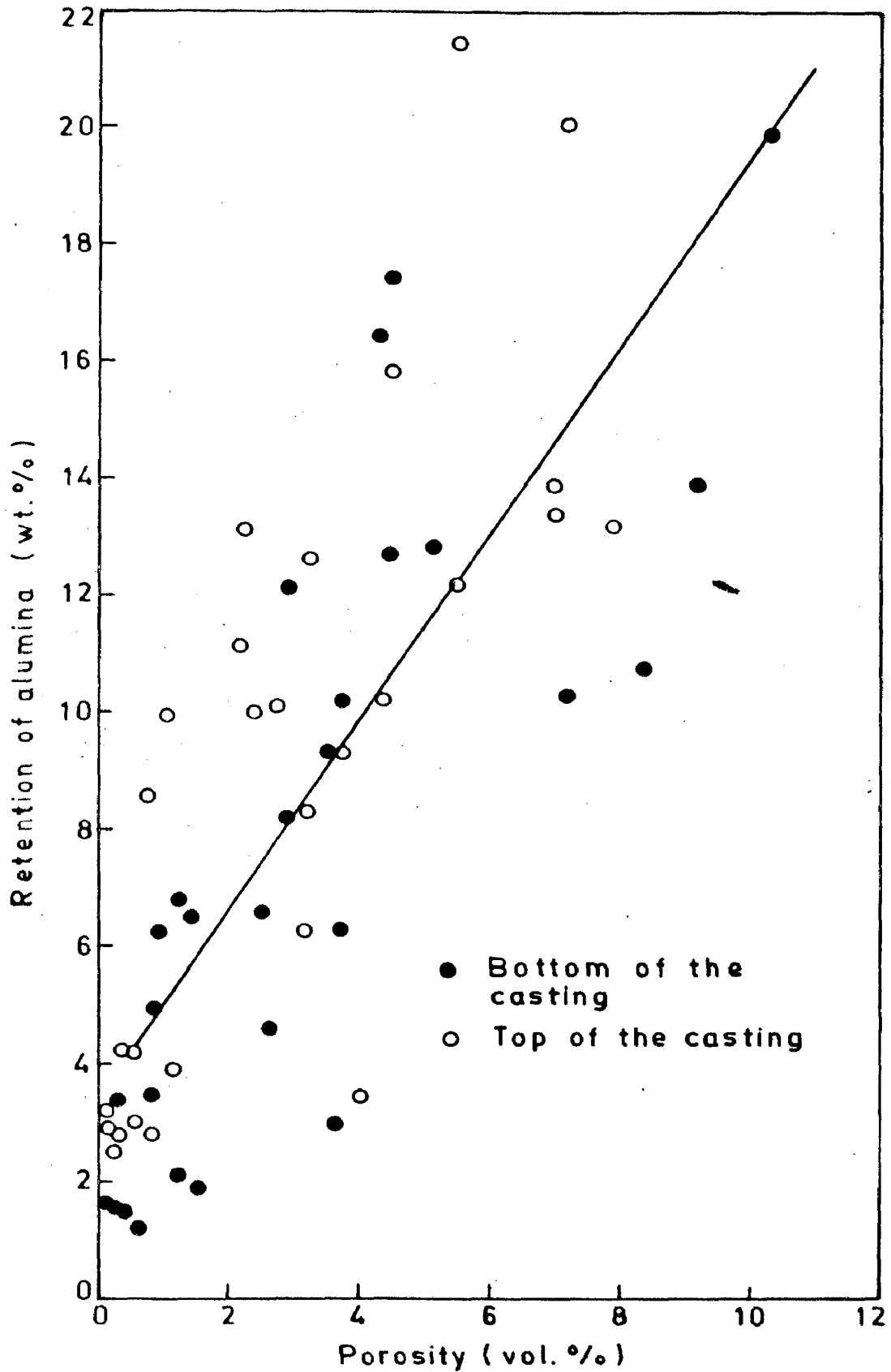
FIG. 4.25 VARIATION OF POROSITY IN CASTING
WITH AN INCREASE IN RETAINED
ALUMINA OF WIDE SPECTRUM OF SIZES.

particles must be controlled by the same mechanisms so that the observed trend of their proportional retention could have been explained. It appears that the mechanical blocking of the particle and the air bubbles by the primary solid particles is the controlling steps in the rejection process.

Further it has been observed (Fig. 4.26) that the porosity content of the composite increases linearly with the increase of the standard deviation of distribution of particles in the composite containing different levels of particles between ~ 1.6-14.6 vol %. The characteristics of Fig. 4.26 indicates that there is also a possibility of clustering of particles in the matrix where a significant amount of porosity exists. This behaviour indicates a special tendency of coagulation or clustering of particles with air envelope inside the mould. However, the clustering of particles in the matrix may also arise from the accumulation of particles over a big bubble formed at the bottom of the impeller when the stirring has been carried out beyond the optimum level of process parameters as discussed earlier.

Further, it is interesting to note that the proportionality of the retention of alumina with porosity does not depend on the size of the particle as indicated in Fig. 4.27. If the incorporation is assumed to take place by independent particles with an air envelope the finer particles should show a relatively
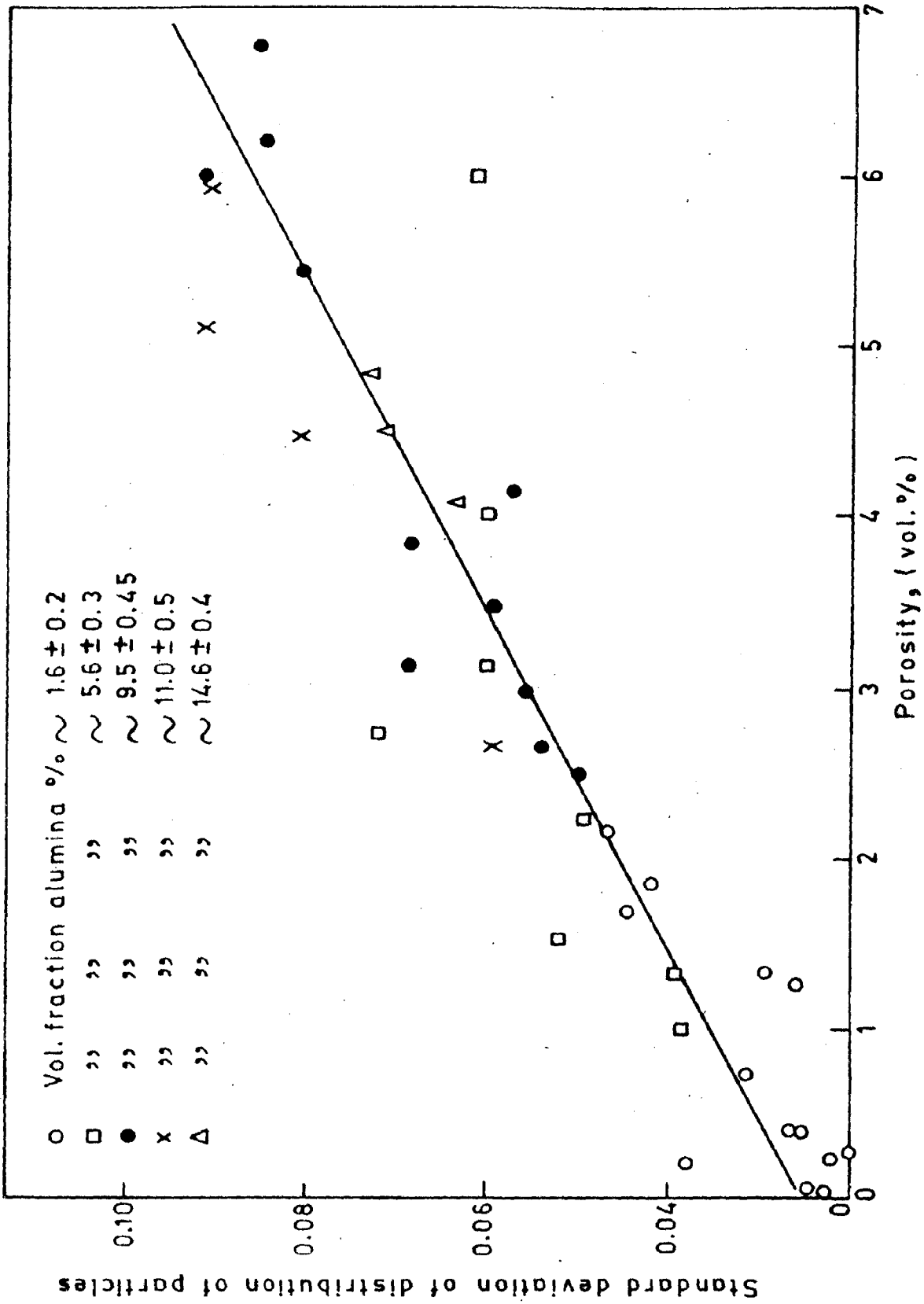
FIG. 4.26 EFFECT OF STANDARD DEVIATION OF DISTRIBUTION OF PARTICLES ON THE POROSITY CONTENT OF THE COMPOSITE.
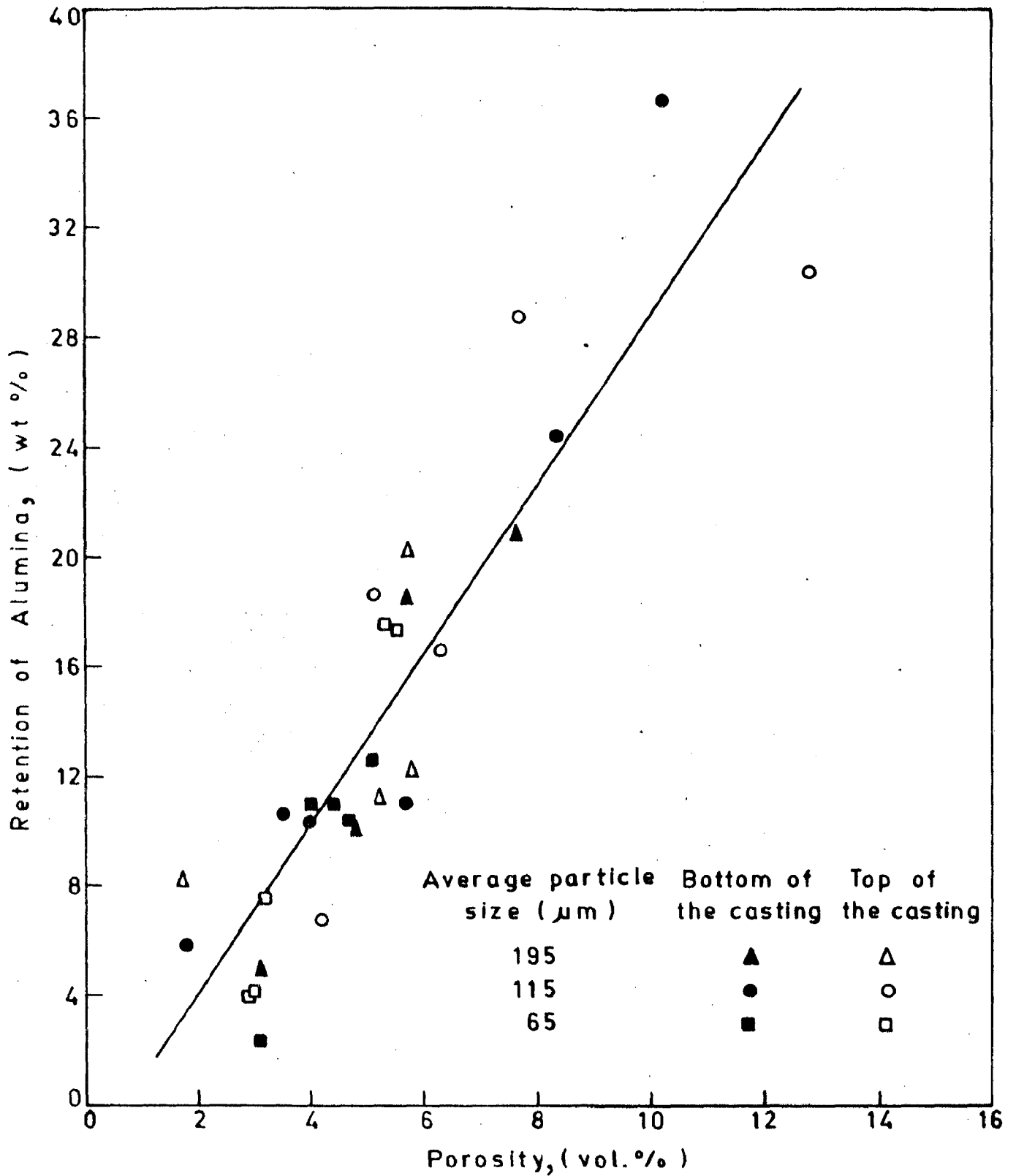
FIG. 4.27 VARIATION OF POROSITY IN CASTING WITH AN INCREASE IN RETAINED ALUMINA OF SPECIFIC SIZE RANGES.

.higher proportion of voids due to a high surface to volume ratio. The experimental results are not in conformity with this idea. Still, the assumed nature of incorporation is not ruled out because the observed trend of the increased clustering with decreasing particle size as shown in the micrographs presented in Fig. 4.28 may have caused the observed independence of particle size.

4.3 MICROSTRUCTURES OF THE COMPOSITES

4.3.1 RESULTS : INFLUENCE OF PROCESS PARAMETERS ON THE MICROSTRUCTURES OF THE CAST COMPOSITES.

The microstructures of the bottom and the top of the cast composite fabricated at a holding temperature of 883 K have been shown in Fig. 4.29 (i) and Fig. 4.29 (ii) respectively where the stirring speed was maintained at 16 revolutions.s^{-1}, with an impeller of d/D=0.63 placed inside the slurry at h/H=0.81. In both the figures the presence of primary solid particles along with an extent of dendritic overgrowth has been observed in the matrix. However, the tendency for the dendritic solidification has been found more at the top (Fig. 4.29 (ii)) of the casting as compared to that observed in its bottom (Fig. 4.29 (i)). Changing the holding temperature to 900 K and keeping other process parameters fixed at the previous levels the extent of dendritic solidification is reduced as shown in the micro structures in Figs. 4.29 (iii) and (iv). Still, the top

(i)   65 μm   (ii)   115 μm
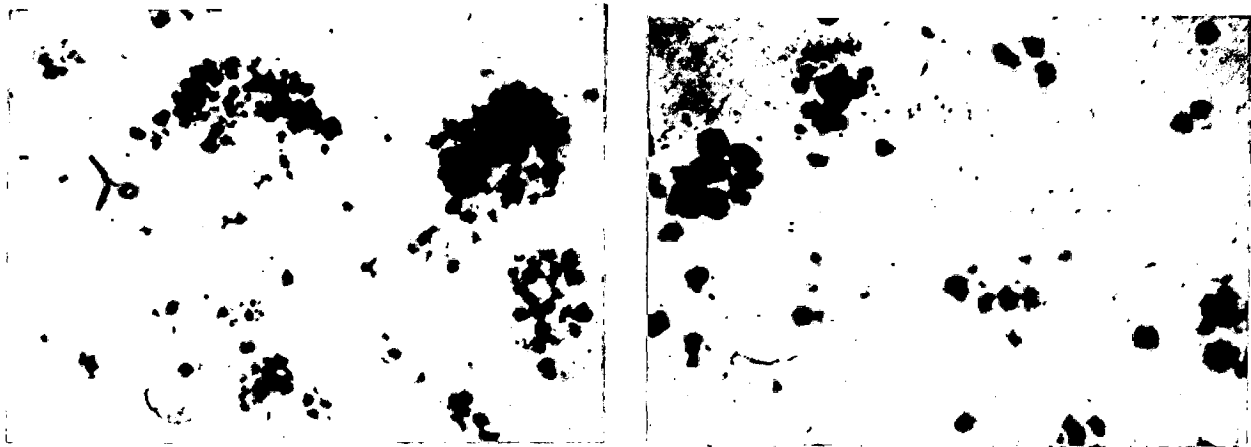
(iii)   195 μm

FIG. 4.28 MICROGRAPHS SHOWING THE EFFECT OF PARTICLE SIZE ON THEIR CLUSTERING IN THE COMPOSITE. X 60

of the casting is more prone to dendritic solidification (Fig. 4.29 (iv)) in comparison to the bottom (Fig. 4.29 (iii)).When the temperature is raised to 958 K the presence of a fully dendritic cast structure is observed both at the bottom and the top of the cast composites as revealed in Fig. 4.29(v) and Fig. 4.29(vi) respectively.

Decreasing the stirring speed to 7.5 revolutions.s^{-1} and keeping all other variables fixed at the levels mentioned in the context of Figs. 4.29 (iii) and (iv) the tendency of dendritic formation is enhanced particularly at the top of the casting as shown in Figs. 4.30 (i) and (ii). When the stirring speed has been increased to 25 revolutions.s^{-1} keeping the other parameters same it was observed that the microstructures mainly consist of primary solid particles as shown in Figs. 4.30 (iii) and (iv). However, a small amount of dendrites has been observed at the top of the casting (Fig. 4.30, iv).

The position of the impeller inside the slurry influences the microstructures of various zones of the cast composites as shown in Fig. 4.31. The Fig. 4.31 (i) and Fig. 4.31 (ii) show the microstructures of the bottom and the top of the samples respectively, cast using a stirrer at h/H=0.54. In both the figures there is a tendency to form dendrites in the matrix along with large primary solid particles. The microstructures of the bottom and the top

BOTTOM TOP

(i) 883 K (ii) 883 K

(iii) 900 K (iv) 900 K

(v) 958 K (vi) 958 K
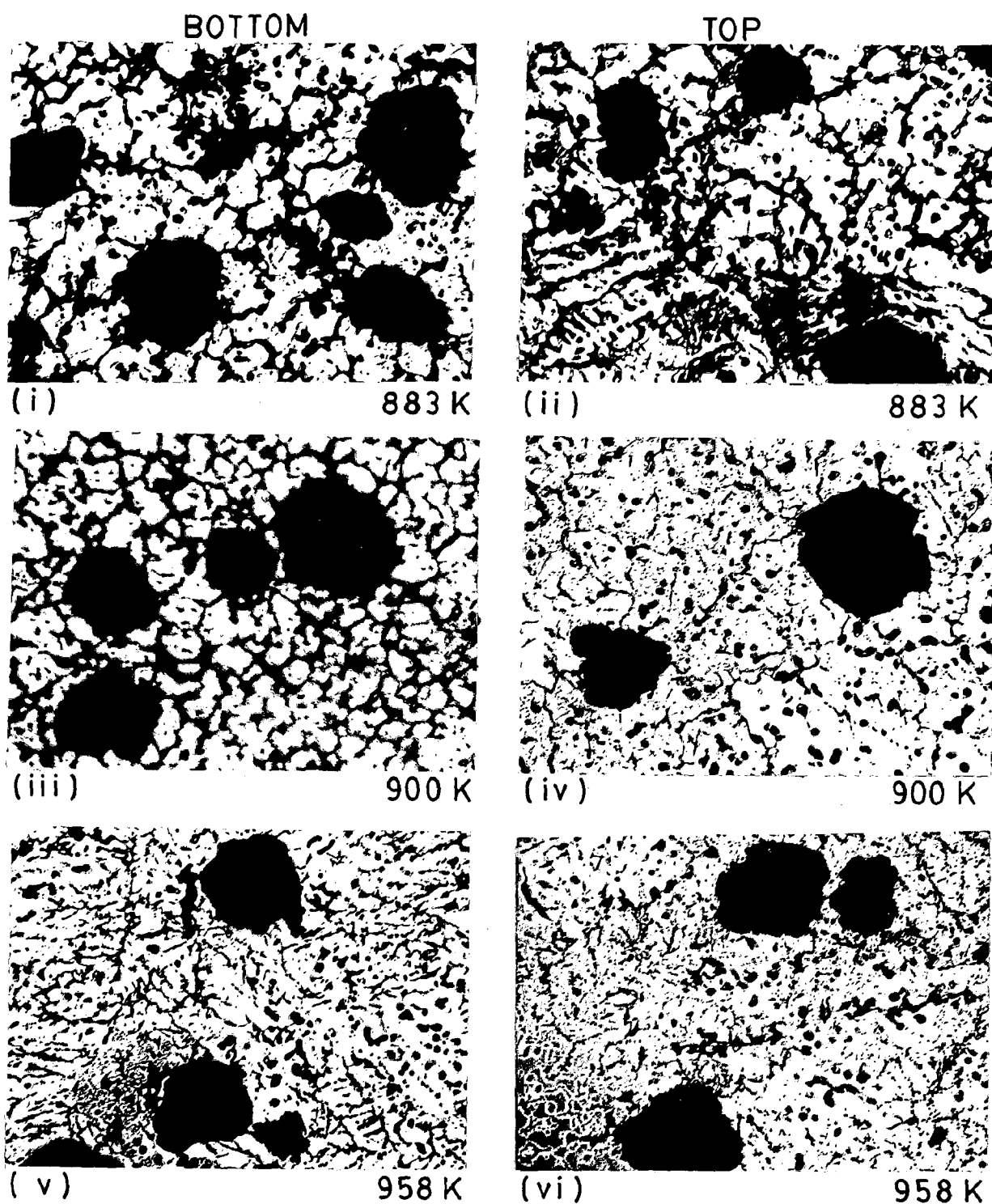
FIG. 4.29 THE EFFECT OF HOLDING TEMPERATURE ON THE MICROSTRUCTURES AT THE TOP AND THE BOTTOM OF THE CASTINGS; STIRRING SPEED = 16 r. p. s., d/D = 0.63 AND h/H = 0.81; X 250

BOTTOM   TOP

(i)   7.5 r. p.s.   (ii)   7.5 r. p.s.

(iii)   25 r. p. s.   (iv)   25 r. p. s.
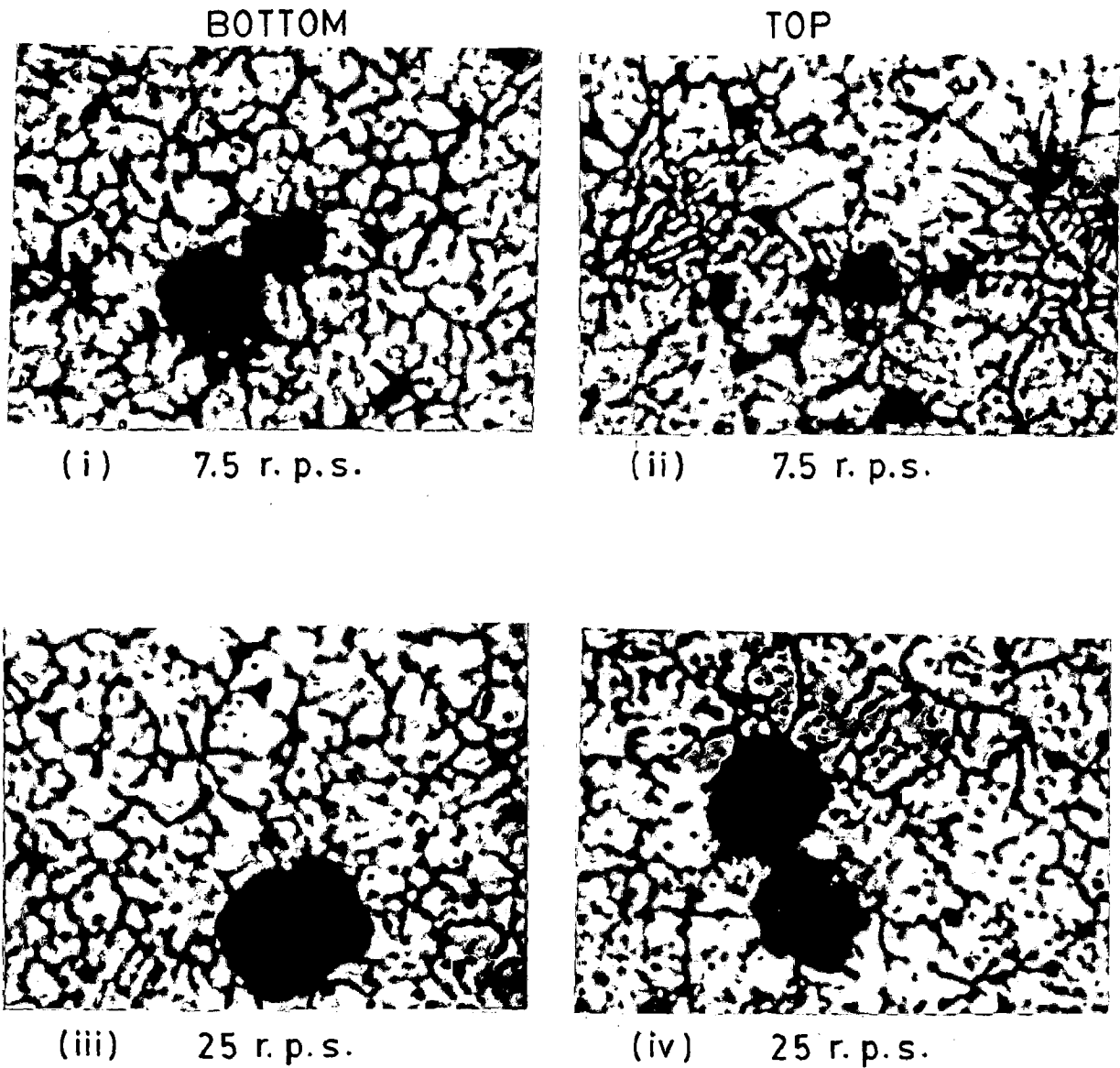
FIG. 4.30 THE EFFECT OF STIRRING SPEED ON THE MICROSTRUCTURES AT THE TOP AND THE BOTTOM OF THE CASTINGS; HOLDING TEMPE- RATURE = 900 K, d/D = 0.63 AND h/H = 0.81; X 250
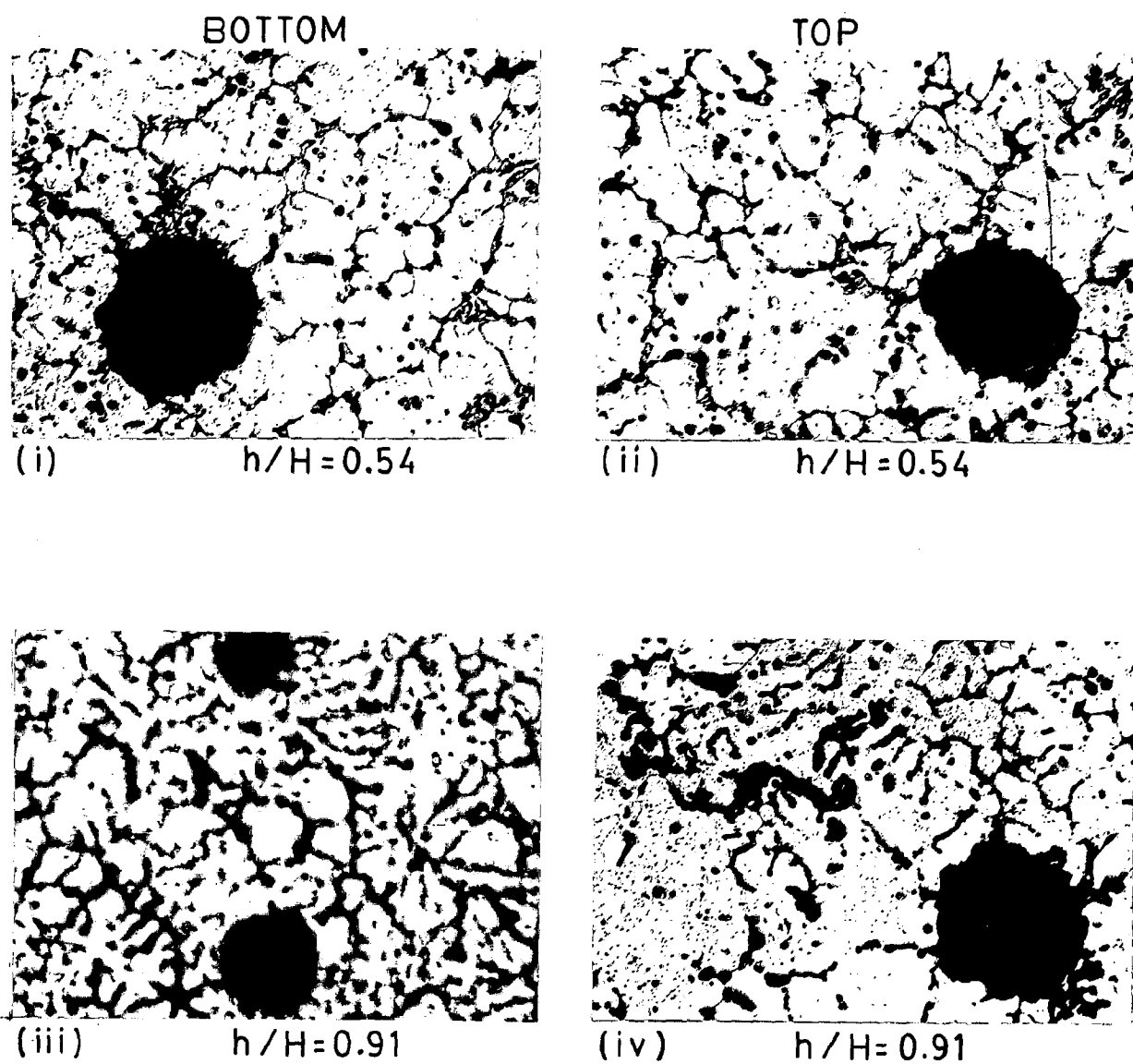
FIG.4.31 THE EFFECT OF POSITION OF THE IMPELLER IN-
SIDE THE SLURRY ON THE MICROSTRUCTURES
AT THE TOP AND THE BOTTOM OF THE CASTINGS;
HOLDING TEMPERATURE = 900 K, STIRRING SPEED
= 16 r. p. s., AND d/D = 0.63; X 250

of the sample cast using a stirrer at h/H=0.81 are shown in Fig. 4.29 (iii) and Fig. 4.29 (iv) respectively and explained earlier. At a still higher value of h/H=0.91 it has been observed that the microstructure of the bottom of the casting is having finer dendrites along with the formation of primary solid particles as shown in Fig. 4.31 (iii). However, in the microstructure of the top of the same casting coarse dendrites and certain regions with large solid particles has been observed as shown in Fig. 4.31 (iv).

The effect of stirring with various sizes of impellers on the microstructure of the bottom and the top of the cast composites are shown in Fig. 4.32. The microstructures of the bottom and the top of the composite cast by using an impeller of d/D=0.56 have been presented in Fig. 4.32 (i) and Fig. 4.32 (ii) respectively. The microstructure of the bottom of the casting shows the presence of primary solid particles in the matrix where there is a significant tendency to form dendrites especially at the top of the casting. In the microstructure presented in Fig. 4.32 (iii) showing the bottom of the composite cast with the help of an impeller of d/D=0.74 the presence of a comparatively finer primary solid particles has been observed with a limited tendency for the formation of dendrites. But the microstructure of the top of the same casting is having a significant tendency towards dendritic growth as revealed in Fig. 4.32 (iv).

BOTTOM TOP

(i)   d/D = 0.56   (ii)   d/D = 0.56

(iii)   d/D = 0.74   (iv)   d/D = 0.74

FIG. 4.32 THE EFFECT OF SIZE OF THE IMPELLER ON
THE MICROSTRUCTURES AT THE TOP AND THE
BOTTOM OF THE CASTINGS; HOLDING TEMPE-
RATURE = 900 K, STIRRING SPEED = 16 r. p. s.
AND h/H = 0.81; X 250

The microstructures presented in Fig. 4.33 (i) and Fig. 4.33 (ii) show that the zone having large (primary) solid particles does not contain any alumina particles. It has also been observed that the dendrites have not entrapped any alumina particles (Fig. 4.33 (iii)). These features have been observed in the castings made at a lower holding temperature (883 K) of the slurry, where the stirring has been carried out at a speed of 16 revolution.s^{-1} with the help of an impeller of d/D=0.63 placed at a depth of h/H= 0.81.

Typical microstructures of the matrix observed under scanning electron microscope on various composites fabricated at different stirring speeds of 7.5 revolution. s^{-1}, 16 revolution.s^{-1} and 25 revolution.s^{-1} have been shown in Figs. 4.34 (i), (ii) and (iii) respectively, where other process parameters as holding temperature, d/D and h/H have been kept constant at 900 K, 0.63 and 0.81 respectively. The microstructures reveal the presence of a considerable amount of oxides at the boundary of the primary solid particles when the stirring speed has been maintained at 7.5 revolution. s^{-1} and its amount has gradually reduced with an increase in the stirring speed upto 25 revolution.s^{-1}. It has also been observed that in composites the voids have formed at the boundary of the primary/solid particles as well as inside it. At a higher stirring speed of 25 revolution.s^{-1} the alumina
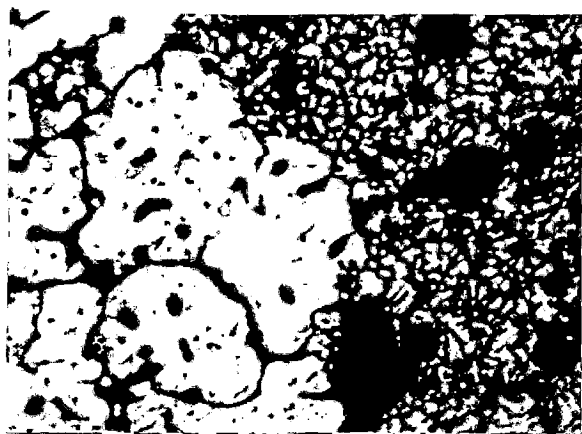
(i)

(ii)
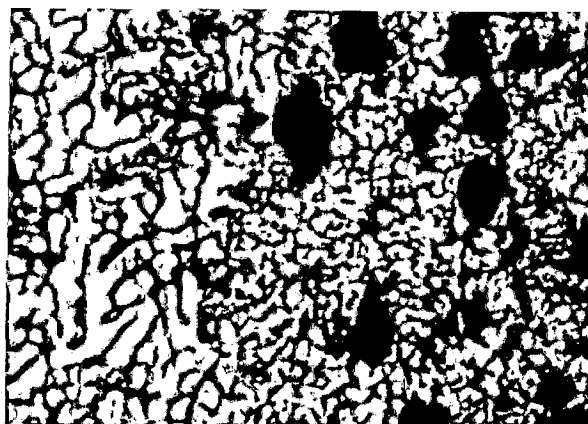
(iii)

FIG. 4.33 (i) OPTICAL MICROGRAPH SHOWING THE
ABSENCE OF ALUMINA PARTICLES IN THE
ZONE OF LARGE α-PARTICLES; X 125

(ii) SCANNING ELECTRON MICROGRAPH OF THE
SAME REGION AS OBSERVED IN (i); X 450

(iii) OPTICAL MICROGRAPH SHOWING NO ALU-
MINA PARTICLES ENTRAPPED IN THE
DENDRITES; X 125
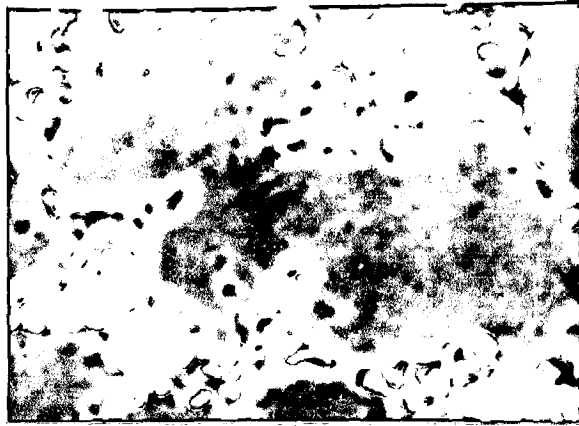
(i)   7.5 r. p. s.   (ii)   16 r. p. s.

(iii)   25 r. p. s.

FIG. 4.34 SCANNING ELECTRON MICROGRAPHS OF THE MATRIX OF COMPOSITES FABRICATED AT DIF-FERENT STIRRING SPEEDS; HOLDING TEMPE-RATURE = 900 K, d/D = 0.63 AND h/H = 0.81; X 3500

particles added or formed are observed within the primary particles as shown in Fig. 4.34 (iii) but at lower speeds the oxide particles are in the inter particle region. The matrix of the composites fabricated at different holding temperature of 883 K and 958 K have been observed under SEM as shown in Figs. 4.35 (i) and (ii) respectively, where the other parameters such as the stirring speed and d/D and h/H have been fixed at 16 revolution.s^{-1}, 0.63 and 0.81 respectively. In both these microstructures formation of voids at the boundary and within the primary particles has been observed but the extent of formation has been comparatively less at a higher holding temperature of 958 K as revealed in Fig. 4.35 (ii). The matrix of the composites having different volume percent of porosity as 0.4, 1.5 and 5.2 have been observed under SEM at a lower magnification as shown in Figs. 4.36 (i), (ii), and (iii) respectively. In the micrographs presented in Fig. 4.36 a significant amount of void has only been revealed in the composite containing 5.2 vol.% of porosity, where it is present at the boundaries of both the primary particles and the alumina particles.

4.3.2   DISCUSSION

The presence of dendrites in the microstructures of the cast particulate composites results primarily from the solidification of the liquid component of the slurry inside the mould. In a vigorously agitated semi solid casting

(i)   883 K
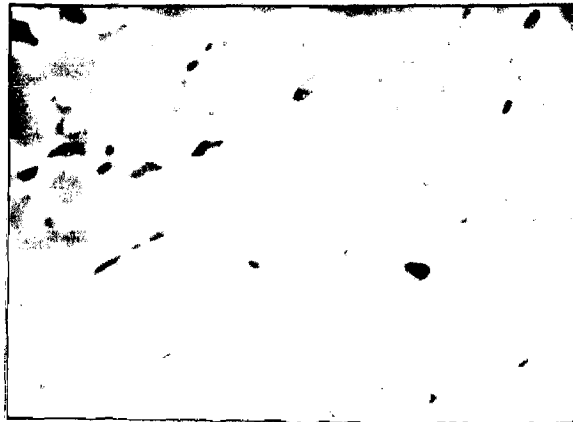
(ii)   958 K

FIG. 4.35 SCANNING ELECTRON MICROGRAPHS OF THE
MATRIX OF COMPOSITES FABRICATED AT DIF-
FERENT HOLDING TEMPERATURES; STIRRING
SPEED = 16 r. p. s., d/D = 0.63 AND h/H = 0.81;
X 3500
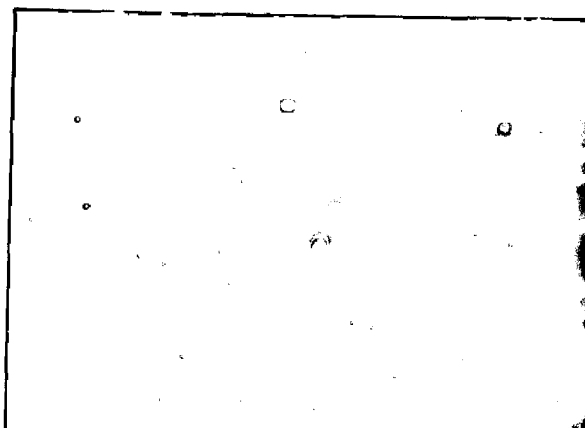
(i)   0.3 Vol.% POROSITY   (ii)   1.5 Vol.% POROSITY

(iii)   5.2 Vol.% POROSITY

FIG. 4.36 MICROGRAPHS SHOWING THE DIFFERENT POROSITY CONTENTS IN COMPOSITES (i) 0.3 Vol.% , (ii) 1.5 Vol.% AND (iii) 5.2 Vol.% ; X 500

process [130-132] the primary particles transform into spheroidal shape in absence of constitutional super cooling. The extent of dendritic solidification at different locations inside the mould is dependent on the relative amount of liquid present prior to its solidification there. The volume fraction of the liquid in the slurry is dependent on the holding temperature.

It has been mentioned earlier in section 2.2.2(a) that in a concentrically agitated cylindrical vessel the circumferential velocity of the liquid is reduced as one goes away from the boundary of the cylindrically rotating zone (C.R.Z.) to the vessel wall [74] as shown in Fig. 2.4. Adjacent to the wall there exists a stagnant boundary layer of liquid. In the presence investigation the stirring of partially solid Al-4 wt.% Mg slurry has been carried out concentrically in a cylindrical crucible, where a stagnant layer of slurry has always been present by the side of the crucible wall. In absence of the shear field there may have been a limited growth of dendrites in the slurry of this region by interface instability due to constitutional super cooling. In the present process the constitutional supercooling exists inside the mould, infront of the primary solid particles and it results in a dendritic solidification over the spheroidal or dendritic primary particles . Thus, an extent of dendrite has always been observed in the composites as shown in the micrographs presented under the Figs. 4.29 (i-iv), 4.30, 4.31 and 4.32.

The presence of a fully dendritic matrix in the composite cast at a holding temperature of 958 K i.e. above the liquidus point of Al-4 wt.% Mg alloy, as shown in Figs. 4.29 (v,vi), has resulted from the solidification of the liquid metal entirely inside the mould.

In all the compocast composites the extent of dendrite has been more at the top of the ingots as shown in various micrographs in Figs. 4.29, 4.30 and 4.31 and 4.32. It has been mentioned in section 3.3 that the stirring has been continued during pouring and so, there is a downward pressure in the central region of the crucible even during pouring to result in an early exit of the slurry from this region to the mould as compared to that present at the side of the crucible wall, which comes out subsequently at the top of the mould. The slurry coming from the side of the crucible wall will contain primary particles of dendritic morphology resulting from the stagnant boundary layer and these particles subsequently grow further dendritically inside the mould. Thus, there are more dendrites of primary Solid phase at the top of the ingot as compared to that at its bottom.

From the above discussion it can be realised that the extent of dendritic solidification and the morphology of primary particles at the top of the ingot is substantially governed by the extent of the stagnant layer at the crucible wall, which is dictated by the Reynold's number (Re)

of the slurry [74]. The increase in Re reduces the thickness of the boundary layer in an agitated cylinder. The equation (2.28) indicates that the Reynold's number of the slurry varies directly with the size of the impeller and the speed of stirring but inversely with the viscosity of the slurry. As such the increase in stirring speed to 25 revolution. s^{-1} from 7.5 revolution.s^{-1} or the size (d/D) of the impeller to 0.74 from 0.56 decreases the thickness of the boundary layer at the crucible wall, resulting in a reduced dendrite formation at the top of the ingot as shown in Figs. 4.30 (iv) and 4.30 (ii) for a variation in stirring speed, and in Figs. 4.32 (iv) and 4.32 (ii) for a variation in the size of the impeller. The thickness of the stagnant boundary layer increases with a decrease in holding temperature within the partially solid range of the alloy. The lowering of holding temperature from 900 K to 883 K has increased the extent of dendrite formation at the top of the ingot as shown in Fig. 4.29 (iv) and Fig. 4.29 (ii). During compocasting at a lower holding temperature of 883 K the viscosity of the Al-4wt.% Mg slurry increases significantly due to an increase in the volume fraction of pro-eutectic particles in it and it has hindered the process of mixing creating zones of very low shearfield in the agitated slurry where dendritic solidification has taken place. So dendrites form extensively even at the bottom of the ingot fabricated at a holding temperature of 883 K as shown in Fig. 4.29 (i) .

The weakening of the annular flow in the slurry caused by shifting the impeller from h/H=0.91 to h/H=0.54 results in an insufficient shearing in a larger region of the slurry above the impeller and extended primary solid particles form dendritically. When the impeller is placed close to the bottom of the crucible the slurry flows out from the bottom to the top of the impeller [133] quickly and there is (not) much ( ) residence in a strong shear field. As a result there has been hardly any fine primary solid particles in the microstructure even at the bottom of the ingot as shown in Fig. 4.31 (i). A more or less similar microstructure showing a comparatively coarser dendrite Fig. 4.31 (ii) at the top of the ingot has been observed. When the impeller is placed close to the surface of the slurry (h/H=0.91) the increase in turbulence as discussed in section 4.2.4 may have weakened the discharge flow resulting in the formation of solids of non-spheroidal morphology. The weakening of discharge flow enhances the extent of dendritic growth leading to a comparatively coarser dendrites at the top and fine dendrites at the bottom of the casting as shown in Figs. 4.31 (iii) and (iv) respectively.

The lowering of holding temperature of the slurry increases the volume fraction of primary ( ) solid particles in it and so, in a stirred slurry at a lower holding temperature, an increased collision of particles followed by possible coalesence may take place. As a result

primary particles of a larger radius are also observed at
a holding temperature of 883 K as shown in Figs. 4.33 (i)
and (ii). The absence of alumina in the regions of dendrites
and large primary particles observed in the composite made
at a holding temperature of 883 K as shown in Fig. 4.33
(i) to (iii) may indicate weaker flow in the regions of
its origin preventing entry of particles.

The air bubbles sucked inside the slurry has oxidised
the aluminium and the magnesium and the reacted products
have accumulated at the boundary of the primary/particles as
discrete particles as shown in the Fig. 4.34 (i). In Fig.
4.10 it has been observed that the porosity content of the
composite increases with an increase in stirring speed upto
16 revolution.s^{-1} followed by a reduction with a further
increase in stirring speed upto 25 revolution.s^{-1} as indicated
in the microstructure of composites fabricated at a stirring
speed of 16 revolution.s^{-1} (Fig. 4.34 (ii)) as compared to
those in the composites fabricated at a stirring speeds
of 7.5 revolution.s^{-1} (Fig. 4.34 (i)) and 25 revolution.
s^{-1} (Fig. 4.34 (iii)). A higher void content in the
microstructure of the composite prepared at a lower holding
temperature of 883 K (Fig. 4.35(i)) has been observed in
comparison to that fabricated at a higher holding temperature
of 958 K (Fig. 4.35(ii)) The porosity content of the
composite has been found to reduce with an increase in
the holding temperature of the slurry as shown in Fig. 4.9.

It appears that a correlation exists between the void and alumina content in a composite. This question has been explored in section. 4.2.4 during a discussion on the porosity content in composites.

In the micrographs presented in the Figs. 4.34 and 4.35 the voids are present at the boundaries of the primary particles and the dendrites (Fig. 4.35, ii). The shrinkage porosities observed in the matrix are considerably fine in the composites having a porosity content of even upto 1.5 vol.% and these porosities are not revealed at a lower magnification under SEM as shown in Fig. 4.36 (i) and (ii). But in the composites having higher amount of porosity (Fig. 4.36 (iii)) of the order of 5.2 vol.% the voids are coarser.

4.4   PARTICLE-MATRIX INTERACTION AND THEIR INTERFACE

4.4.1   RESULTS : PARTICLE-MATRIX INTERFACE

During fabrication of particulate composite a reacted layer has been formed on the alumina particles affecting the bonding between the particle and the matrix. However, the thickness of reacted layer on alumina particles has significantly changed with a variation in process parameter such as stirring speed and holding temperature. The effect of stirring speed on the reacted layer at the particle-matrix interface has been revealed under scanning electron microscope and is shown in Figs. 4.37(i), (ii) and (iii) for
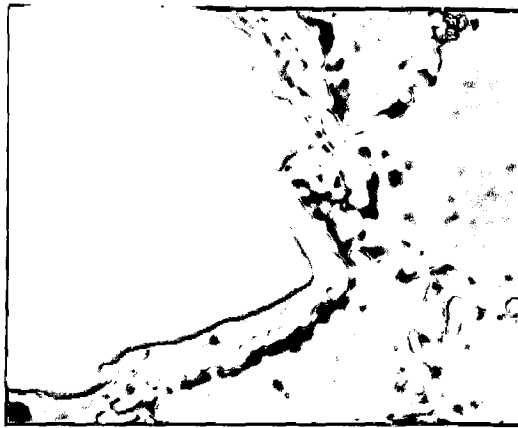
(i) 7.5 r. p. s.

(ii) 16 r. p. s.
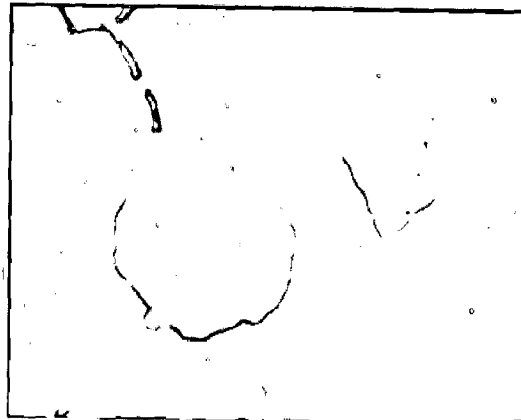
(iii) 25 r. p. s.

FIG. 4.37 SCANNING ELECTRON MICROGRAPHS SHOWING
THE PARTICLE-MATRIX INTERFACES IN THE
COMPOSITES FABRICATED AT DIFFERENT STIR-
RING SPEEDS; HOLDING TEMPERATURE = 900 K,
d/D = 0.63 AND h/H = 0.81; X 3500

stirring speeds of 7.5 revolution.s^{-1}, 16 revolution.s^{-1} and 25 revolution.s^{-1} respectively, where other parameters such as holding temperature, the d/D and h/H ratios have been kept constant at 900 K, 0.63 and 0.81 respectively. It is interesting to note that increase in stirring speed minimises the thickness of reacted layer on alumina particles and at a stirring speed of 25 revolution.s^{-1} the alumina particles do not have almost any reacted layer on it as shown in Fig. 4.37 (iii). The thickness of the reacted layer on alumina particle has been found to be considerable in a composite fabricated at a holding temperature of 883 K as shown in Fig. 4.38 (i) and becomes thinner with an increase in the holding temperature to 900 K and 958 K as revealed in Figs. 4.37 (ii) and 4.38 (ii) respectively. The microstructures presented in Figs. 4.39 (i) and (ii) show a non – uniformity in thickness of reacted layer around an alumina particle present in the composites fabricated at holding temperatures of 900 K and 958 K by stirring the slurry with a speed of 16 revolution.s^{-1}.

The non – uniformity is large at higher holding temperatures. It has sometimes been observed that some alumina particles have joined together through the reacted layer as shown in Fig. 4.40.

In the composites fabricated in this investigation at different process parameters, the presence of particles of irregular shape different from those of alumina particles

(i)   883 K

(ii)   958 K

FIG. 4.38 SCANNING ELECTRON MICROGRAPHS SHOWING
THE PARTICLE-MATRIX INTERFACES IN THE
COMPOSITES FABRICATED AT DIFFERENT HOL-
DING TEMPERATURES; STIRRING SPEED =16 r. p.s.,
d/D = 0.63 AND h/H = 0.81; X 3500

(i)   900 K   X 1050
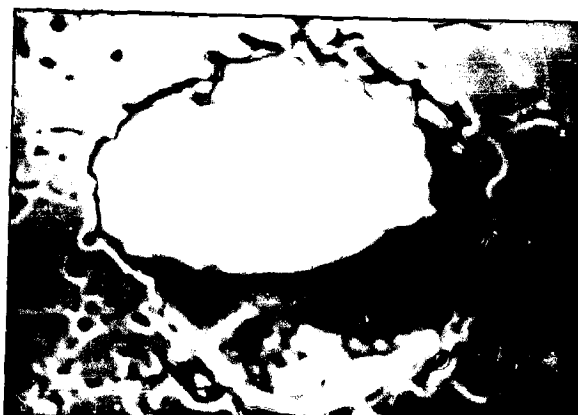
(ii)   958 K   X 1800

FIG. 4.39 SCANNING ELECTRON MICROGRAPHS SHOWING
          THE NON-UNIFORMITY IN THICKNESS OF
          REACTED LAYER AROUND THE ALUMINA PARTI-
          CLES; STIRRING SPEED = 16 r. p. s., d/D = 0.63
          AND h/H = 0.81

FIG. 4.40 SCANNING ELECTRON MICROGRAPH SHOWING
THE COALESCENCE OF ALUMINA PARTICLES
IN A COMPOSITE FABRICATED AT A HOLDING
TEMPERATURE OF 900 K ; X 1800

have been observed in the matrix as shown in the microstructures presented in Figs. 4.41 (i) and (ii). These particles are presumably the crystals of the reacted product with or without alumina present inside it. Sometimes there are cracks in these particles as shown in Fig. 4.41 (i).

4.4.2 RESULTS : X-RAY DIFFRACTION ANALYSIS

The interplanar spacings ($\bar{d}$) obtained from the X-ray diffraction analysis of the compocast composites have been listed in Table 4.1. A comparison with ASTM chart reveals the presence of magnesium aluminate ($MgAl_2O_4$) in the composite apart from aluminium and α -Al_2O_3. The existance of $MgAl_2O_4$ is presumed because of the observed peaks corresponding to $\bar{d}$-values of 2.8029 and 0.9324 where, no other peak from the phases present are interfering.

4.4.3 DISCUSSION

During fabrication of particulate composites by foundry process the reacted products form as observed in the microstructures presented in Figs. 4.37 to 4.41. It has been observed by other workers [28,49] also. The X-ray diffraction analysis as carried out by us indicates that the compound is $MgAl_2O_4$ apart from α -Al_2O_3 formed due to inevitable oxidation of aluminium. The oxide particles so formed could not be confirmed by X-ray diffraction due to the presence of the alumina particles added externally.

(i)   900 K, 7.5 r. p. s.

(ii)   958 K, 16 r. p. s.

FIG. 4.41 SCANNING ELECTRON MICROGRAPHS OF A
COMPOSITE SHOWING THE PRESENCE OF
REACTED PRODUCT OF IRREGULAR SHAPE
AND SOMETIMES CRACKED ; X 3500

TABLE 4.1

X-RAY DIFFRACTION ANALYSIS OF THE COMPOSITES

Radiation CuK_α

Sin θ_2	$\bar{d}$	(hkl)
0.2748	2.8029	$(220)_{MgAl_2O_4}$
0.3297	2.3362	$(222)_{MgA_2O_4}$ $(111)_{Al}$
0.3806	2.0238	$(400)_{MgAl_2O_4}$ $(200)_{Al}$
0.5365	1.4357	$(220)_{Al}$
0.5471	1.4078	$(124)_{\alpha-Al_2O_3}$
0.6289	1.2247	$(311)_{Al}$
0.657	1.1724	$(444)_{MgAl_2O_4}$ $(306)_{\alpha-Al_2O_3}$
0.7584	1.0156	$(400)_{Al}$ $(800)_{MgAl_2O_4}$ $(402)_{\alpha-Al_2O_3}$
0.8261	0.9324	$(751)_{MgAl_2O_4}$
0.8476	0.9087	$(324)_{\alpha-Al_2O_3}$ $(420)_{Al}$ $(840)_{MgAl_2O_4}$

But these reacted oxide particles are of a different size class and so can easily be identified in the microstructure. There is also no confusion between these particles and $MgAl_2O_4$ especially under SEM due to different levels of charging. The formation of magnesium aluminate at temperatures between 873 K to 923 K in the aluminium alloy composite having magnesium in the range of 4 wt.% have been marked earlier by several workers [28,61].

In the present investigation before addition of magnesium the slurry undergoes stirring for a considerable length of time where the formation of fine alumina particles inside the slurry in presence of air sucked through the vortex is obviously favoured. Under this condition of readily available oxygen inside the slurry the magnesium inoculated in it should also form MgO following the reaction given in equation (2.13). However, it is interesting to note that the X-ray diffraction analysis does not show the existence of MgO in the composite. It may, thus, be inferred that the entire MgO formed inside the slurry has possibly reacted giving rise to the formation of $MgAl_2O_4$ following the chemical reactions mentioned in equations (2.11) and (2.12).

The reacted product of $MgAl_2O_4$ observed on the surface of the externally added alumina particles and shown in Figs. 4.37 (i), (ii) and 4.38 may have resulted by the following possible mechanisms. The added alumina particles may have undergone a chemical reaction with available magnesium

inside the slurry following the equations (2.9) and/or (2.8) and an uniform layer of reacted products containing either $MgAl_2O_4$ and/or MgO may form. Different charging characteristics of these compounds from that of Al_2O_3 under scanning electron microscope will help in identifying these compounds as shown in Figs. 4.37 (i) and 4.38 (i). It is reported that the formation of MgO by reduction of Al_2O_3 with magnesium following equation (2.8) is favoured at a higher concentration of magnesium (>4 wt.%) [28] and in the present investigation a magnesium concentration of $\sim$ 4 wt.% has been used. The absence of MgO as evident from X-ray diffraction analysis indicates that the reaction (2.8) is not taking place. It may be argued that the reactions (2.8) and (2.11) or (2.12) occurring simultaneously may have consumed the intermediate product MgO. But it is unlikely because (2.12) is a solid-solid reaction and the reaction (2.11) also requires Al-diffusion in solid. In a similar system of Al-4 wt.% Mg-Al_2O_3 the reaction (2.9) has been ruled out as an origin for the formation of $MgAl_2O_4$ by Levi et al [28] on the basis of a larger extent of alumina consumption in this reaction and a smaller thickness of $MgAl_2O_4$ layer observed. This argument is hardly convincing because a smaller thickness of reacted product indicates that the kinetics of reaction (2.9), if at all it takes place, is slow and has nothing to do with the extent of Al_2O_3 consumption in the reaction. The observed uniform thickness of reacted   layer on alumina

(Figs. 4.37 (i) and 4.38 (i)) could not have been possible unless the other reacting constituent is in liquid phase. The formation of MgO which is solid at the temperature under consideration could have reacted only locally with the alumina particles giving rise to reacted zones. The discrete small particles of $MgAl_2O_4$ may have formed by the reaction of magnesium or MgO with aluminium or internally formed fine alumina particle [28,61] and later on, may have clustered around the externally added alumina particles during stirring as observed in Fig. 4.37 (i).

At a given holding temperature of 900 K the extent of the reacted product at the boundary of the incorporated alumina reduces with an increase in stirring speed from 7.5 revolution.s^{-1} to 25 revolution.s^{-1} as shown in the micro structures presented in Fig. 4.37. The kinetics of formation of $MgAl_2O_4$ should have been helped by stirring if diffusion in liquid is the slowest step. If the rate controlling step is solid state diffusion or interfacial process the kinetics should not be affected significantly by stirring. The observed reduction in the boundary layer thickness of the reacted product can only be explained by presuming a process of mechanical removal of these products at higher stirring speeds. This assumption is further strengthened by the reduction of the reacted layer thickness with an increase in holding temperature of the slurry from 883 K to 958 K as revealed

in the microstructures in Figs. 4.38 (i), 4.37 (ii) and 4.38 (iii). At a given stirring speed of 16 revolution.s^{-1} the thickness of the reacted layer on the incorporated alumina particles should, in general, increase with the increase in holding temperature of the slurry if its formation is governed by a general Arrhenius law. The contrary observations are attributed to an increased mechanical removal of the reacted layer at higher stirring speed. At higher temperatures the strength of reacted layer reduces and thus, enhances its rate of removal. Further, the increase in stirring speed or holding temperature of the slurry increases the Reynold's number resulting in an increased number of random collisions between the particles inside the slurry which increases the erosion of the reacted products from the surfaces of the incorporated alumina particles. So, the thickness of the reacted layer reduces as shown in Figs. 4.37 (ii) and 4.38 (ii) at high stirring speed of 16 revolution.s^{-1} and at a high holding temperature of 958 K respectively. The non uniformity in thickness of the reacted layer around the alumina particles as shown in Figs. 4.39 (i) and (ii), lends additional support to the assumption of a mechanical reduction of reacted layer thickness on the particles. At a high stirring speed of 25 revolution.s^{-1} when the reacted product has almost been removed from the boundary of the alumina, a few alumina particles have been trapped within the primary solid particles

as shown in Figs. 4.37 (iii) and 4.34 (iii). At a holding temperature of 900 K the alumina particles (Fig. 4.40 (i)) have joined through the reacted layers. Sometimes, reacted products in the form of stringers are observed as shown in Fig. 4.41 (ii) and cracks have been observed in the reacted layer due to differential expansion as shown in Fig. 4.41 (i).

4.5   SUMMARY

Compocast Al-4 wt.% Mg-Al$_2$O$_3$ composites have been fabricated by varying the holding temperature from 883 K to 958 K, the stirring speed from 7.5 to 25 resolution.s^{-1}, the size of the impeller expressed as a ratio of the diameter of the impeller (d) and the surface of the melt (D), from 0.56 to 0.74 and the position of the impeller expressed as a ratio of the height of the impeller from the bottom of the crucible (h) to the depth of the melt (H), from 0.54 to 0.91. The experiments show that a lowering of holding temperature increases the alumina retention in the slurry. The retention of alumina increases with the increase in stirring speed and the values of d/D and h/H upto a certain level followed by a reduction with a further increase in the values of the above parameters. The maximum retention of alumina with a better distribution is achieved by keeping the holding temperature, the stirring speed, d/D and h/H at 900 K, 16 revolution.s^{-1}, 0.63 and 0.81 respectively. Cold model experiments have been carried out to find out

the reasons of the above behaviour of stirring speed and
d/D ratio on alumina retention. The regions of large primary solid
particles and coarse dendrites observed at lower holding
temperature, create inhomogenity in distribution by restricting
entry of externally added alumina particles in these zones.

The porosity content of the composite increases
linearly with particle retention and its clustering but does
not show dependence on particle size.

The incorporated alumina particles react with the
matrix and form a thick layer of reacted product. around.
X-ray diffraction analysis confirms the reacted product as
$MgAl_2O_4$. The thickness of the reacted product on alumina
reduces with the increase in stirring speed from 7.5 to 25
revolutions.s^{-1} and also with the increase in holding
temperature due to enhanced mechanical erosion.

CHAPTER V

RESULTS AND DISCUSSIONS: MECHANICAL PROPERTIES OF THE PARTICULATE COMPOSITES

5.1   INTRODUCTION

The mechanical properties of cast materials are well known to deteriorate considerably in presence of porosity as a common defect inherent in castings. Thus the mechanical properties of compocast particulate composites also suffer from its sensitiveness to the negative role of porosity. The volume fraction of porosity and reinforcing particles along with their shape, size and distribution in cast composites play a major role in controlling the mechanical properties of the composite.

It is a common practice to correlate the mechanical properties of castings directly to the volume fraction of total porosity. Besides reduction in effective cross sectional area, the weakening of a material containing pores essentially happens by the damage caused to the local load bearing capacity of the material due to stress concentration near the pores. To examine the role of such weakened zones around the pores in determining the

strength of Al-4wt.% Mg—Al$_2$O$_3$ particulate composite a phenomenological model proposed earlier [134] has been used. The equation below shows the strength of a composite containing a given amount of particle, σ_p, at a porosity level of P (volume percentage) as given below

$$\sigma_p/\sigma_0 = 1 - \alpha P \qquad \qquad (5.1)$$

where, σ_0 is the ultimate tensile strength at zero porosity and α is the weakening factor due to the pores.

In this chapter the validity of the model equation (5.1) has been examined on the basis of experimental data for Al-4wt.% Mg - Al$_2$O$_3$ particulate composite. The effects of size and volume fraction of alumina particles on the tensile strength of Al-4wt.% Mg - Al$_2$O$_3$ compocast particulate composite have been determined by taking particles with a narrow and a wide spectrum of sizes (as mentioned in Table 3.1) respectively. The contribution of porosity in reducing the strength has been estimated at different levels of alumina content and the projected ultimate tensile strength at zero porosity level has been determined. The variation of this strength with alumina content has been reported.

The mechanical properties of Al-4wt.% Mg - Al$_2$O$_3$ compocast particulate composite at elevated temperatures have also been reported and discussed in this chapter .

The role of porosity in reducing the high temperature strength of a composite at given levels of alumina content and at different temperatures have been determined to project ultimate tensile strength at zero porosity level. The variation in this strength with a change in temperature and with a variation in alumina content have been estimated. The effect of temperature and volume fraction of particles on the projected tensile strength at zero porosity in composites having a definite amount of alumina have been reported.

The role of porosity on the fracture characteristic in these composites, at ambient and elevated temperatures, have been examined. The effect of particle content on the formation of new voids in the matrix under strain has been analysed.

5.2   MECHANIAL PROPERTIES AT AMBIENT TEMPERATURE

5.2.1   RESULTS: EFFECT   OF   POROSITY,   PARTICLE   SIZE
                      AND   PARTICLE   CONTENT   ON   THE   TENSILE
                      STRENGTH.

To examine the validity of the model equation (5.1) on the basis of experimental data obtained for various Al-4wt.% Mg—Al_2O_3 particulate composites having a wide spectrum of particle size mentioned in Table 3.1, the values of ultimate tensile strength σ_p

has been plotted against volume percent of porosity, P, and extrapolated to zero porosity level to get the values of σ_o for each alumina content. The values of σ_p/σ_o for each alumina content have been calculated and its behaviour against porosity level were examined. The typical nature of σ_p/σ_o versus P plots for composites containing 0.8, 2.0, 8.1 and 18.0 volume percent of alumina are depicted in Fig. 5.1. The figure shows that the tensile strength of these composites is a linear function of porosity content having a co-efficient of correlation in the range of 0.7-0.9. The slopes of these curves give the values of α contained in equation (5.1) and it is a measure of the weakening effect of the pore. Fig. 5.1 also reveals that the value of α decreases with an increase in alumina content in the composite. The variation of α with a change in alumina content of composite has been estimated following the procedure mentioned above and has been shown in Fig. 5.2. It has been observed that the value of α decreases significantly with an increase in alumina content in a composite.

The relationship between the particle content and the tensile strength at zero porosity, σ_o, for different composites containing alumina particles having a wide range of sizes as given in Table 3.1, has been shown in Fig. 5.3. The value of σ_o has been found to decrease with the increase in the volume fraction of alumina. The rate of
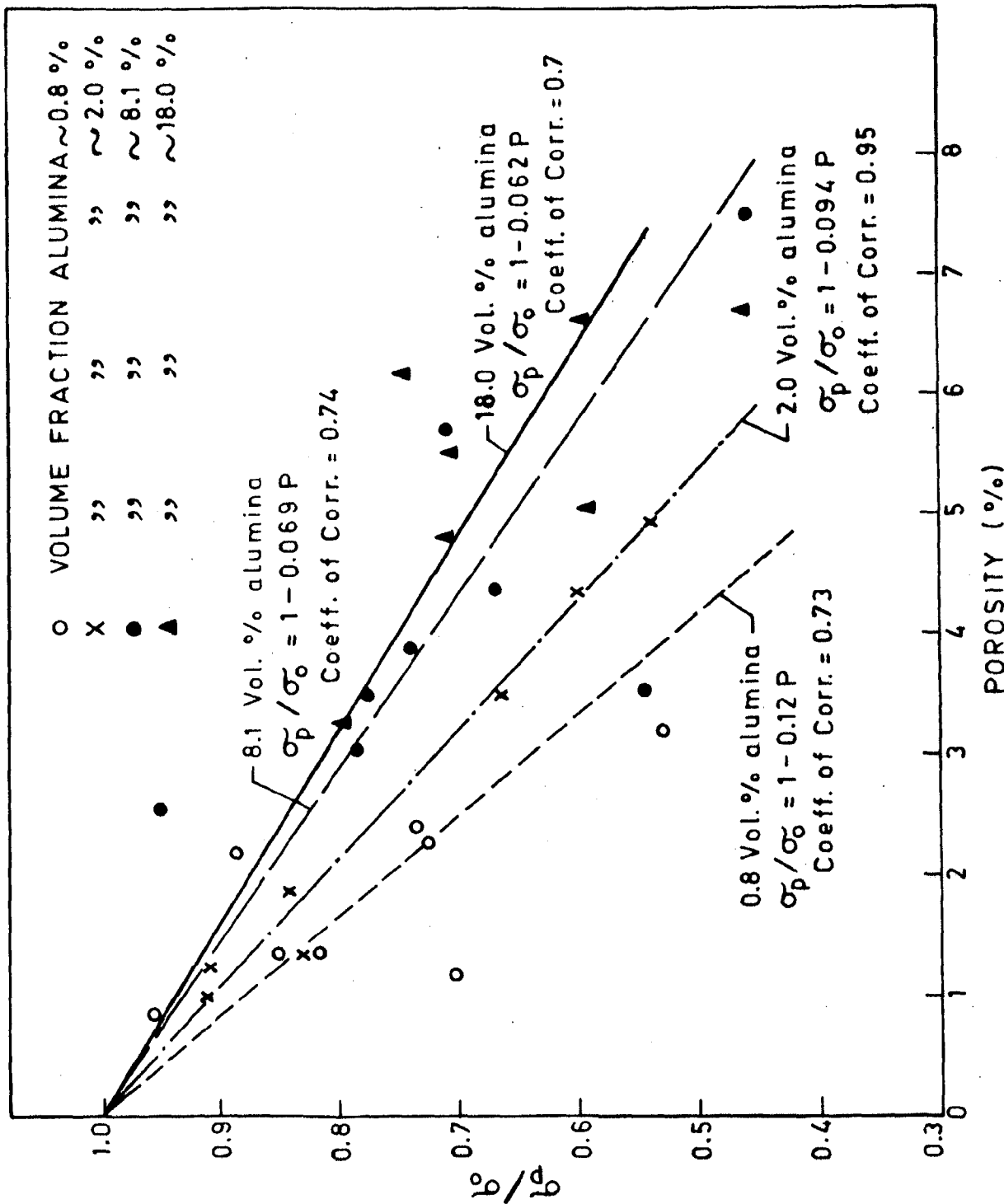
FIG. 5.1 EFFECT OF POROSITY ON THE AMBIENT TEMPERATURE TENSILE STRENGTH RATIO, σ_p/σ_o, OF THE COMPOSITES CONTAINING DIFFERENT AMOUNTS OF Al
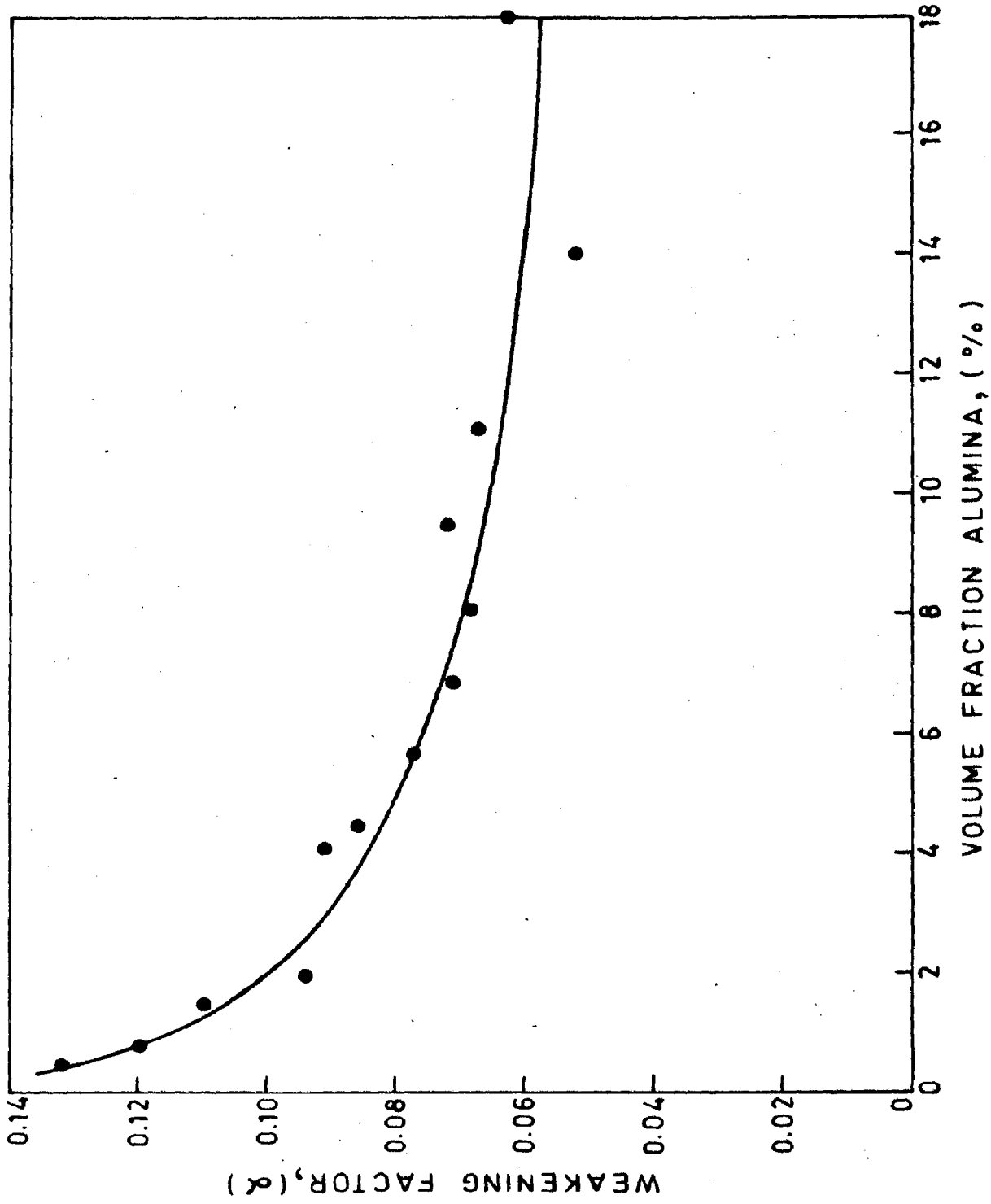
FIG.5.2 VARIATION OF WEAKENING FACTOR WITH ALUMINA CON-
TENT OF THE COMPOSITES AT AMBIENT TEMPERATURE.

200
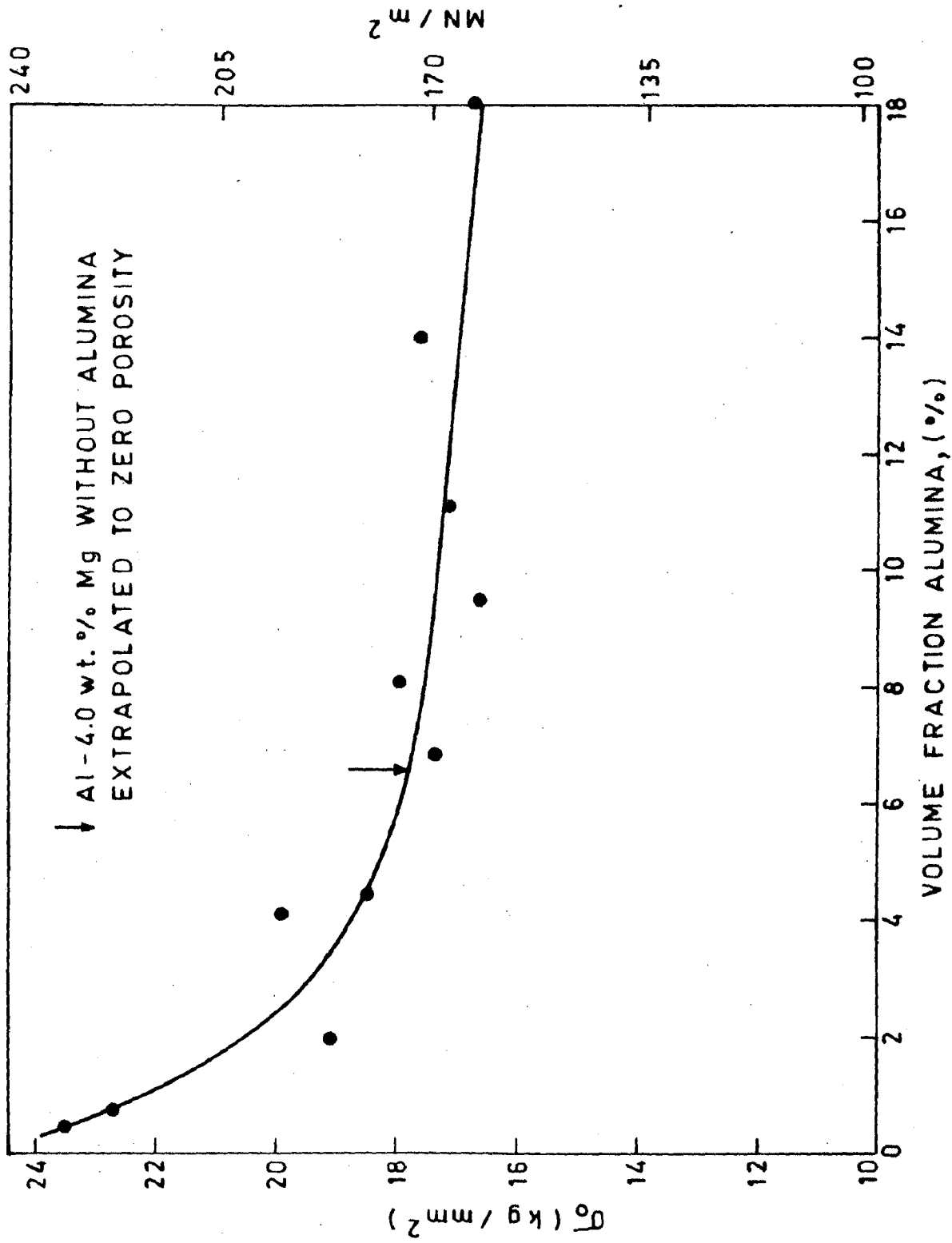
FIG.5.3 EFFECT OF PARTICLE CONTENT ON THE AMBIENT TEMPE -
RATURE TENSILE STRENGTH OF THE COMPOSITES AT ZERO
POROSITY.

decrease of σ_o with the increase of alumina content of the composite is quite significant at lower alumina level upto $\sim$ 7 vol.%. The variation in ultimate tensile strength of the composite with an increase in its alumina content having a wide spectrum of sizes has been shown in Fig. 5.4. The different curves correspond to different volume percent of porosities — 0.76, 1.6 and 2.98. The figure shows that the tensile strength of the composite decreases with an increase in alumina content in the composite but beyond a certain level of alumina content no significant variation has been observed. The alumina level, upto which a considerable decrease in tensile strength of the composite takes place with an increase in alumina content, decreases with an increase in the level of porosity in the composite. It has been observed that at a given volume fraction of alumina the increase of porosity decreases the tensile strength of the composite. The variation of σ_o is similar to that of the ultimate tensile strength with the alumina content observed in the composites.

The effect of porosity content on the behaviour of engineering tensile stress-strain curve of the composite having $\sim$ 1.92 vol.% of alumina has been shown in Fig. 5.5. The curves show considerable serration during deformation of the specimen. However, the serrations are more pronounced at a lower porosity content of $\sim$ 0.06 vol.% where the tensile specimen has been found to fracture at higher strain
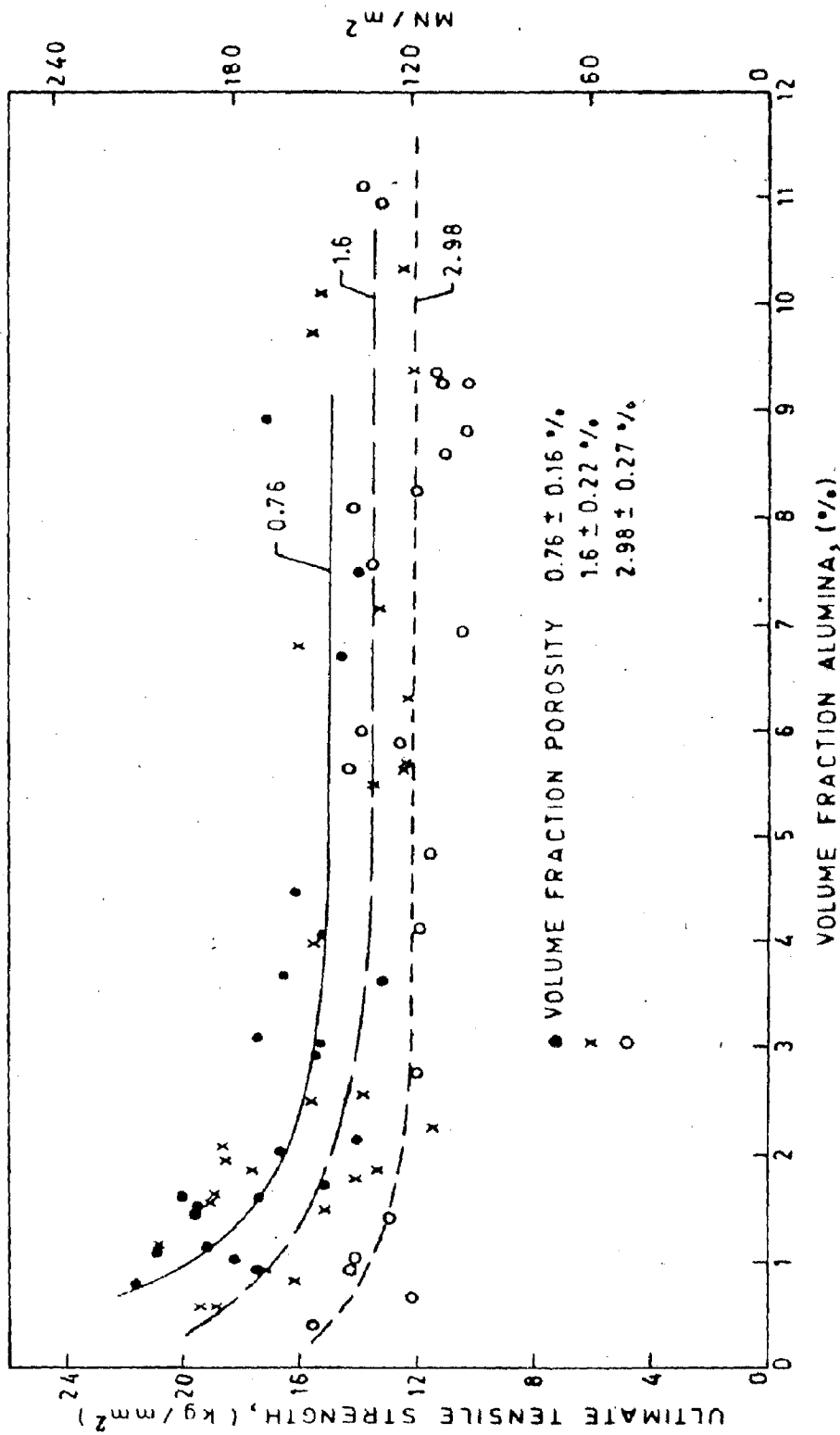
FIG.5.4 EFFECT OF PARTICLE CONTENT ON THE AMBIENT TEMPERATURE TENSILE STRENGTH OF THE COMPOSITES CONTAINING DIFFERENT LEVELS OF POROSITY.
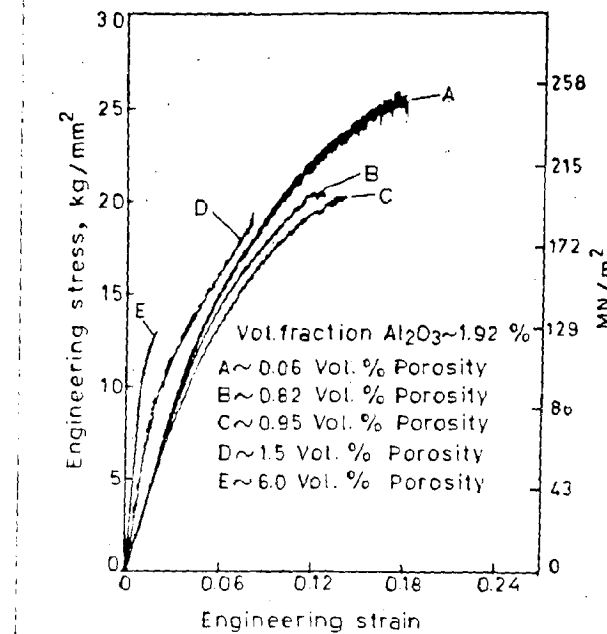
FIG. 5.5 EFFECT OF POROSITY CONTENT OF ENGI-
NEERING STRESS – STRAIN CURVE OF A
COMPOSITE AT AMBIENT TEMPERATURE.

level. The tensile specimen containing higher amounts
of porosity of the order of ~ 6.0 vol.% has been found
to fracture at a low strain level without showing any
significant serration in the stress-strain curve.

The value of σ_o has been found to decrease with
an increase in the average particle size from 22 μm upto
195 μm for composites containing a fixed amount (~ 8.62
vol.%) of alumina as shown in Fig. 5.6. The magnitude
of the corresponding weakening factor c has been found
to increase a little with an increase in the average particle
size from 22 μm to 115 μm followed by a significant decrease
with a further increase in particle size to 195 μm as shown
in Fig. 5.7. The ultimate tensile strength of the composite
having volume fraction of alumina and porosity of the order
of ~ 9.0% and ~ 4.26% respectively, has been found to
decrease with an increase in the average particle size
in the composite (Fig. 5.8) following a similar trend as
it has been observed earlier in Fig. 5.6 for a variation
of σ_o with the size of the particle.

The effect of stirring speed on the tensile strength
of a composite fabricated by maintaining other process
parameters constant as the holding temperature of 900
K, d/D=0.63 and h/H=0.81, has been presented in Table 5.1
for different combination of alumina and porosity content
of the composite. In the table it has been observed   that
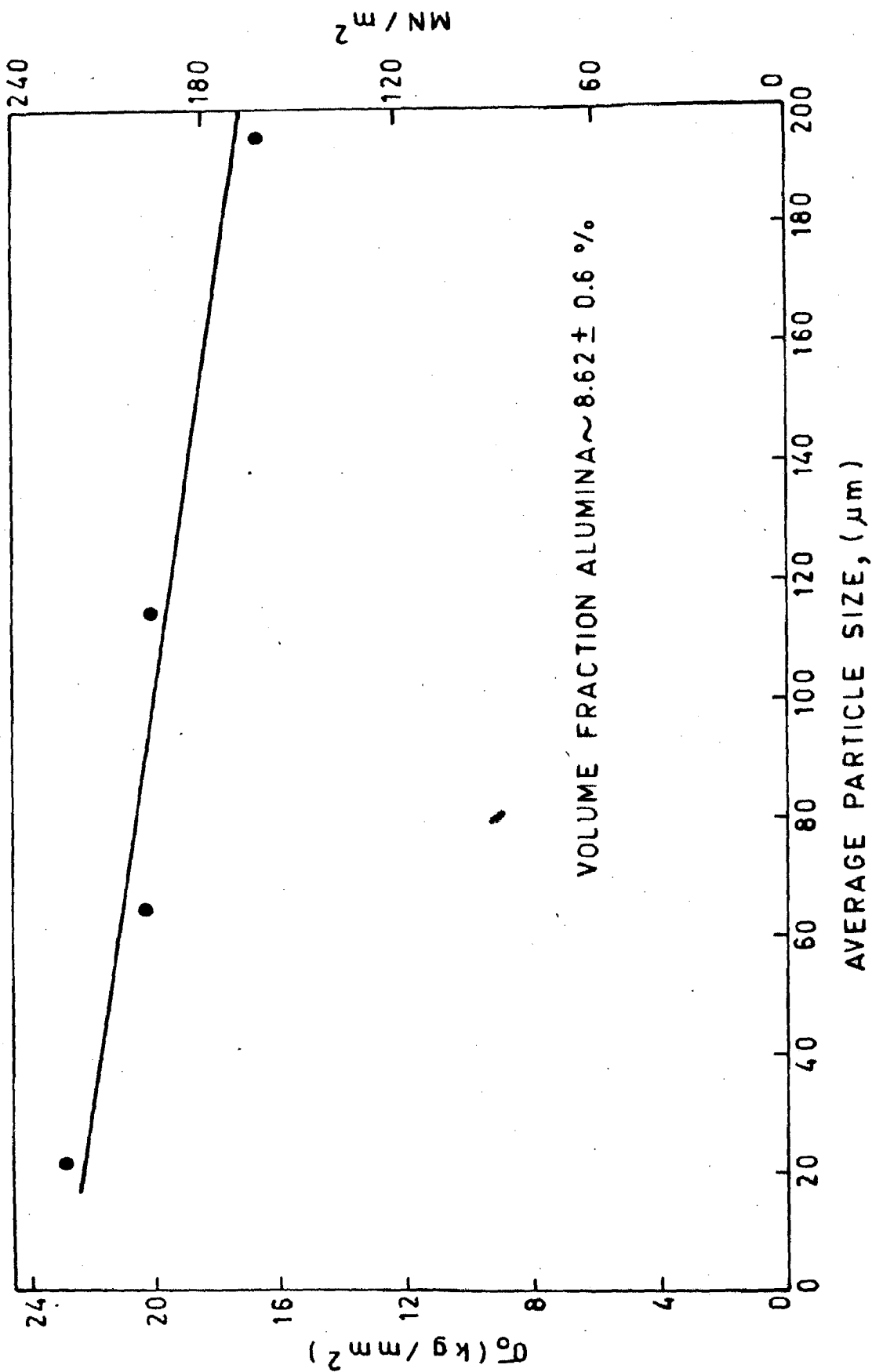
FIG.5.6 EFFECT OF AVERAGE PARTICLE SIZE ON THE AMBIENT TEMPE-
RATURE TENSILE STRENGTH OF THE COMPOSITES AT ZERO
POROSITY.
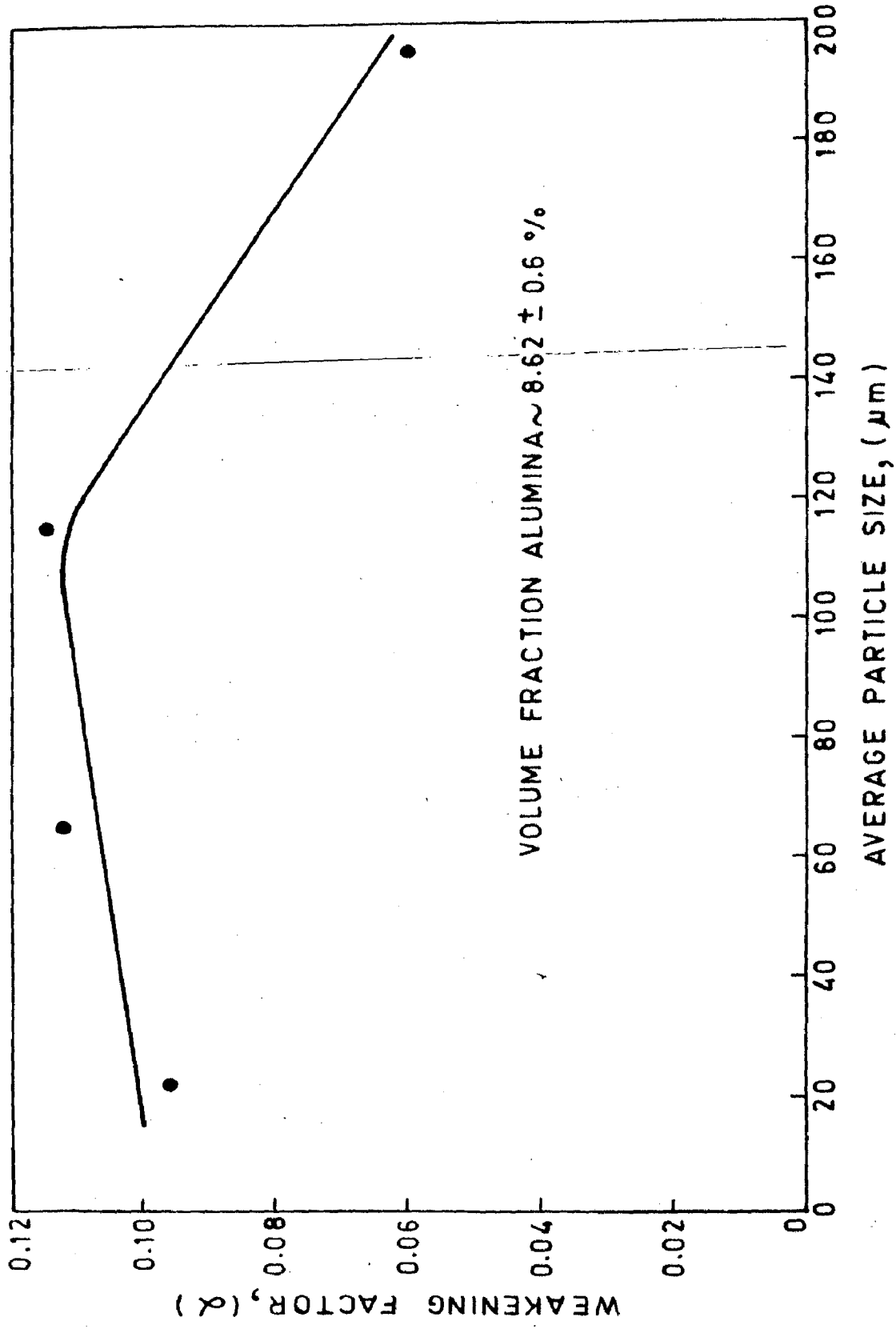
FIG.5.7 VARIATION OF WEAKENING FACTOR WITH AVERAGE PARTICLE SIZE IN THE COMPOSITES AT AMBIENT TEMPERATURE.
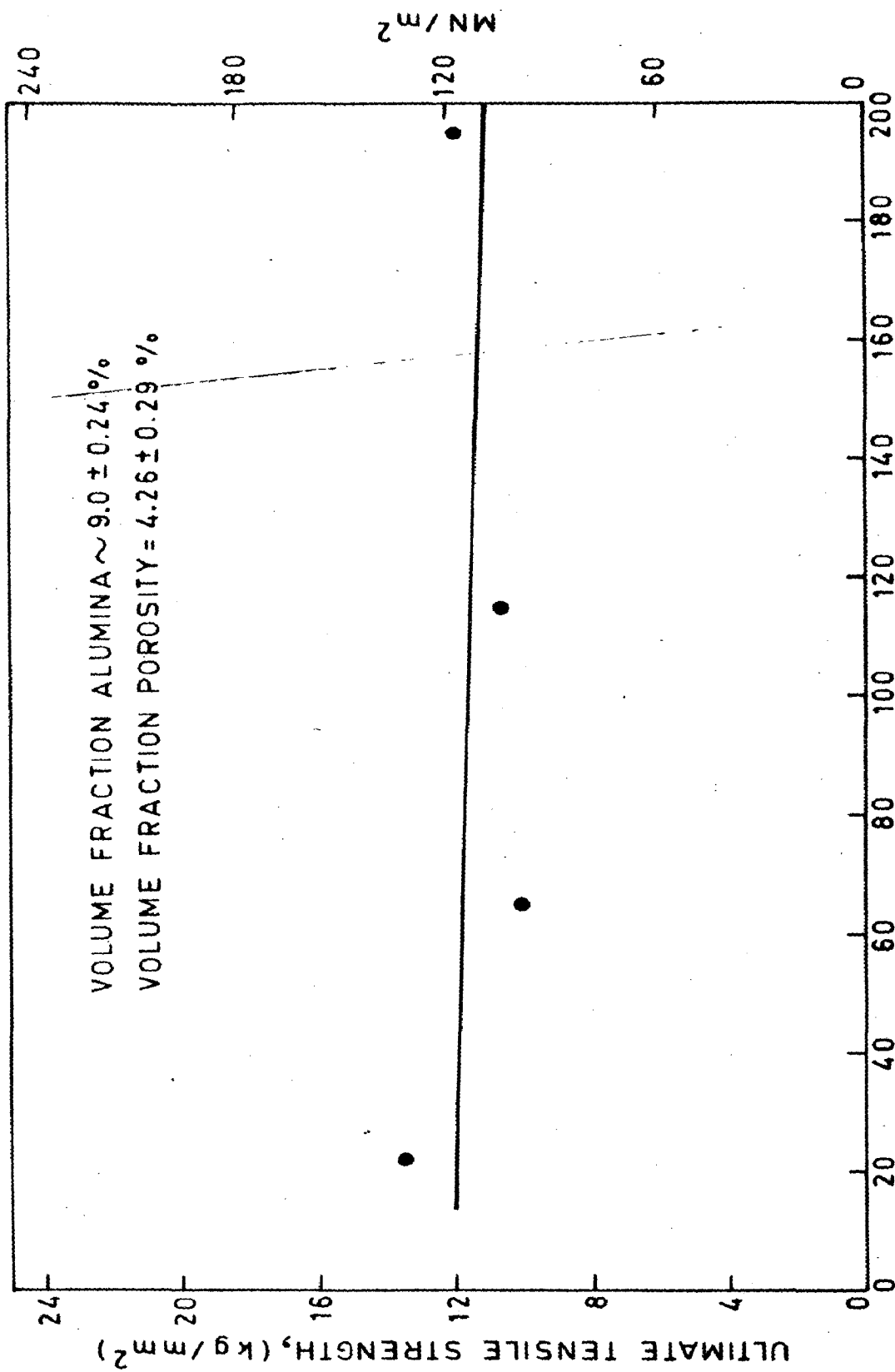
FIG. 5.8 EFFECT OF AVERAGE PARTICLE SIZE ON THE AMBIENT TEMPE-RATURE TENSILE STRENGTH OF THE COMPOSITES.

TABLE - 5.1

EFFECT OF STIRRING SPEED ON THE TENSILE STRENGTH OF A COMPOSITE
(HOLDING TEMPERATURE 900 K, d/D=0.63, h/H=0.81)

Vol.fraction porosity (%)	Vol.fraction alumina (%)	Ultimate tensile strength (MN/m^2) at various stirring speed					
		7.5 rps	9.7 rps	16 rps	17.7 rps	22.5 rps	25 rps
0.54 ± 0.16	1.46 ± 0.2	193.62	-	179.29	-	-	153.78
0.7 ± 0.17	3.78 ± 0.2	-	178.8	162.9	-	149.65	-
3.68 ± 0.29	8.8 ± 0.45	-	-	134.44	123.94	119.04	-
4.49 ± 0.18	8.3 ± 0.12	-	-	127.57	118.35	104.41	-

there is a significant trend of decreasing ultimate tensile strength of a composite with an increase in stirring speed in the range of 7.5 revolution.s^{-1} to 25 revolution.s^{-1}.

5.2.2   RESULTS: FRACTURE BEHAVIOUR

(a)   Effect of Porosity Content on Fracture Strain

In specimens with a definite amount of alumina particles with a broad spectrum of sizes, as given in Table 3.1 the nature of variation in engineering fracture strain, e_f, with variation in the reciprocal of the percentage of porosity content in the composites has been presented in Fig. 5.9. The fracture strain, e_f, of the composites increases linearly with a decrease in porosity only upto a limit. The linear behaviour of fracture strain can approximately be described by an equation as given below

$$e_f = m/P + c \qquad .. \qquad (5.2)$$

where, m and c are constants. The slope of the equation (5.2), m, has been found to increase with an increase in alumina content of the composite as shown in Fig. 5.10. However, the intercept, c, has been found to decrease as observed in Fig.5.11, with an increase in alumina content. The linear nature of the fracture strain, e_f, versus inverse porosity 1/P, curve is violated when the porosity is reduced below a critical level depending on the alumina content.
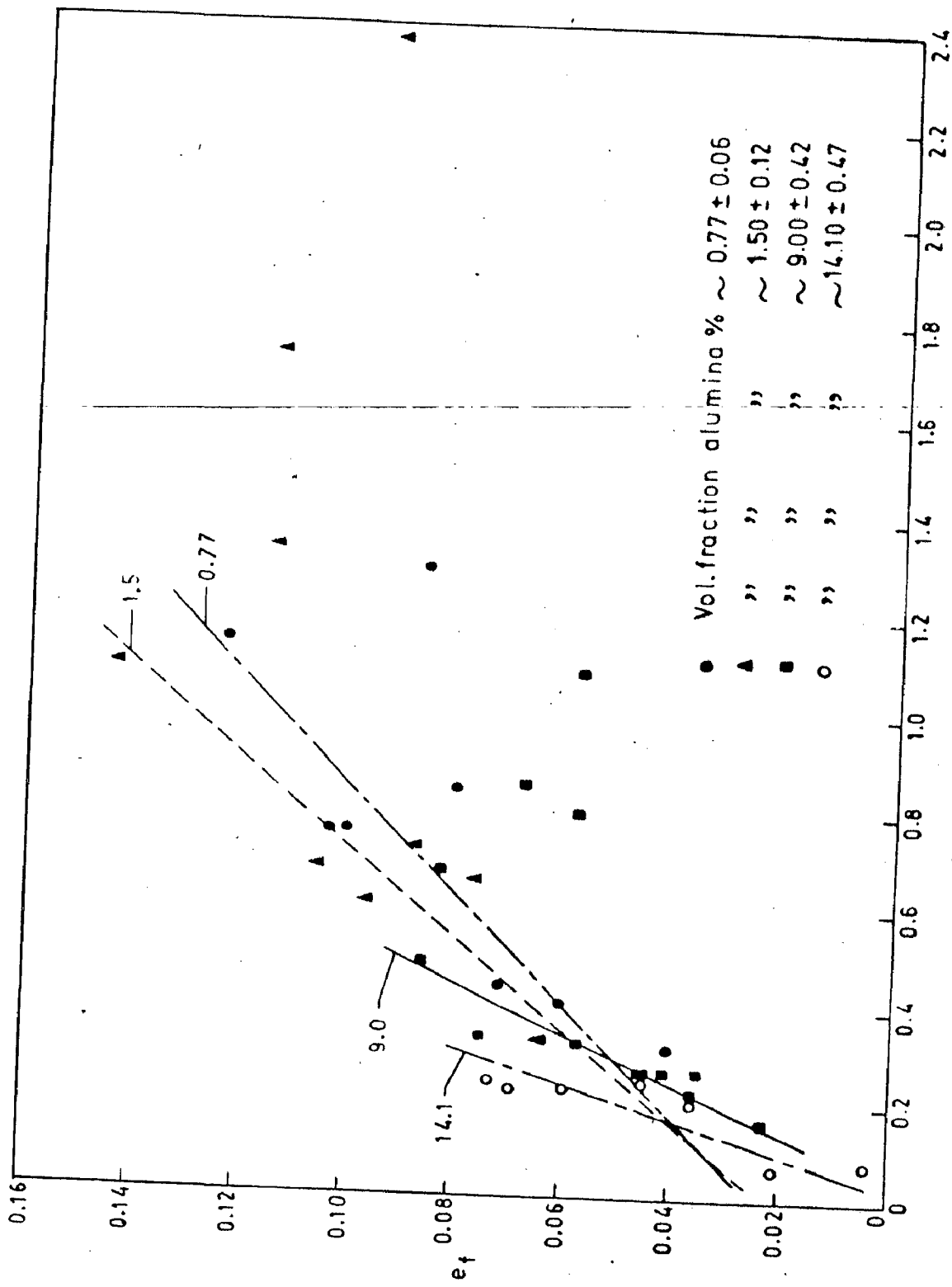
FIG.5.9 EFFECT OF THE INVERSE VOLUME PERCENT OF POROSITY ON THE ENGINEERING FRACTURE STRAIN AT AMBIENT TEMPERATURE OF THE COMPOSITES CON-TAINING DIFFERENT VOLUME FRACTIONS OF ALUMINA.
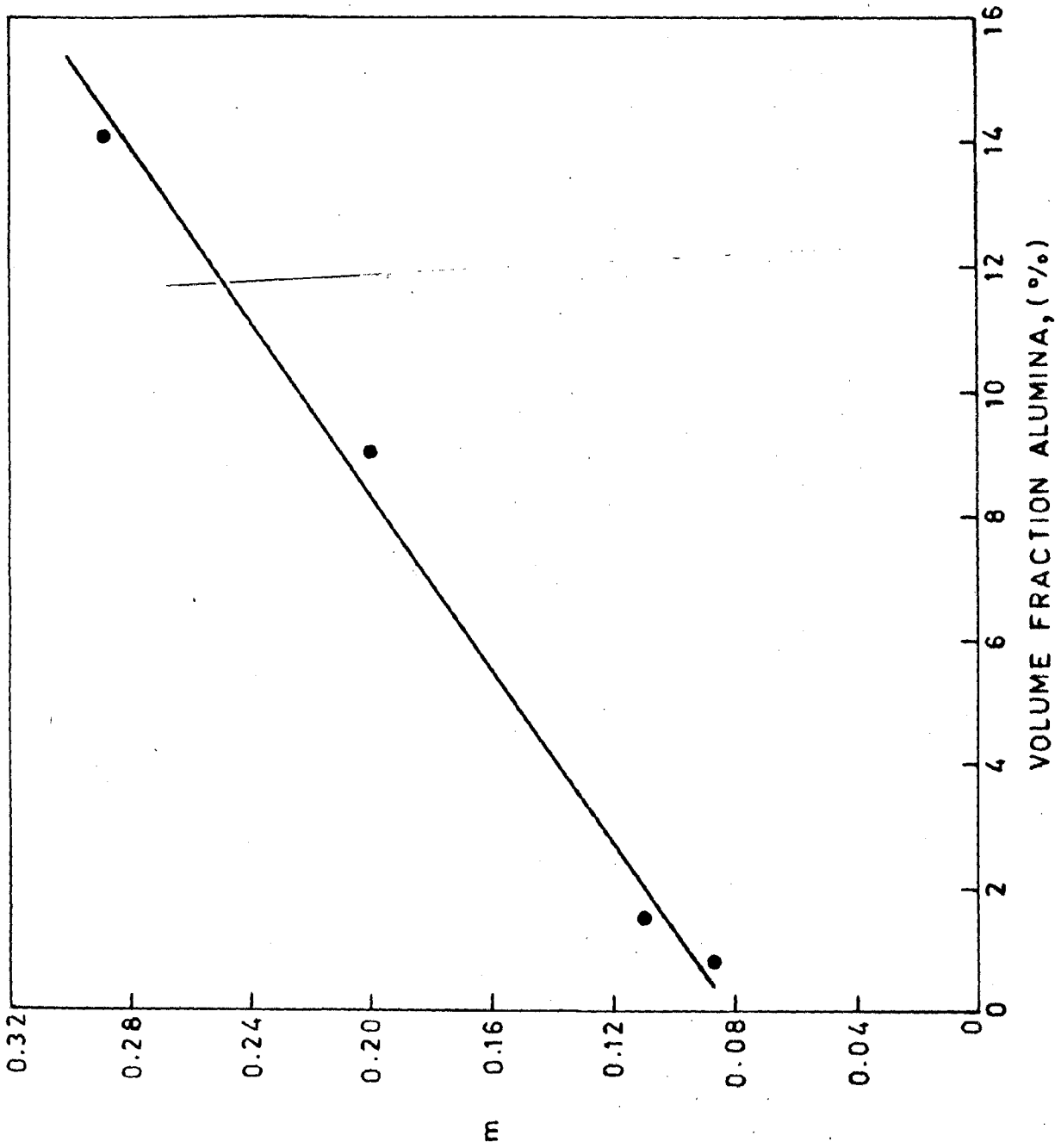
FIG. 5.10 EFFECT OF ALUMINA CONTENT OF THE COMPO-
SITE ON THE SLOPE, m, OF EQUATION (5.?)
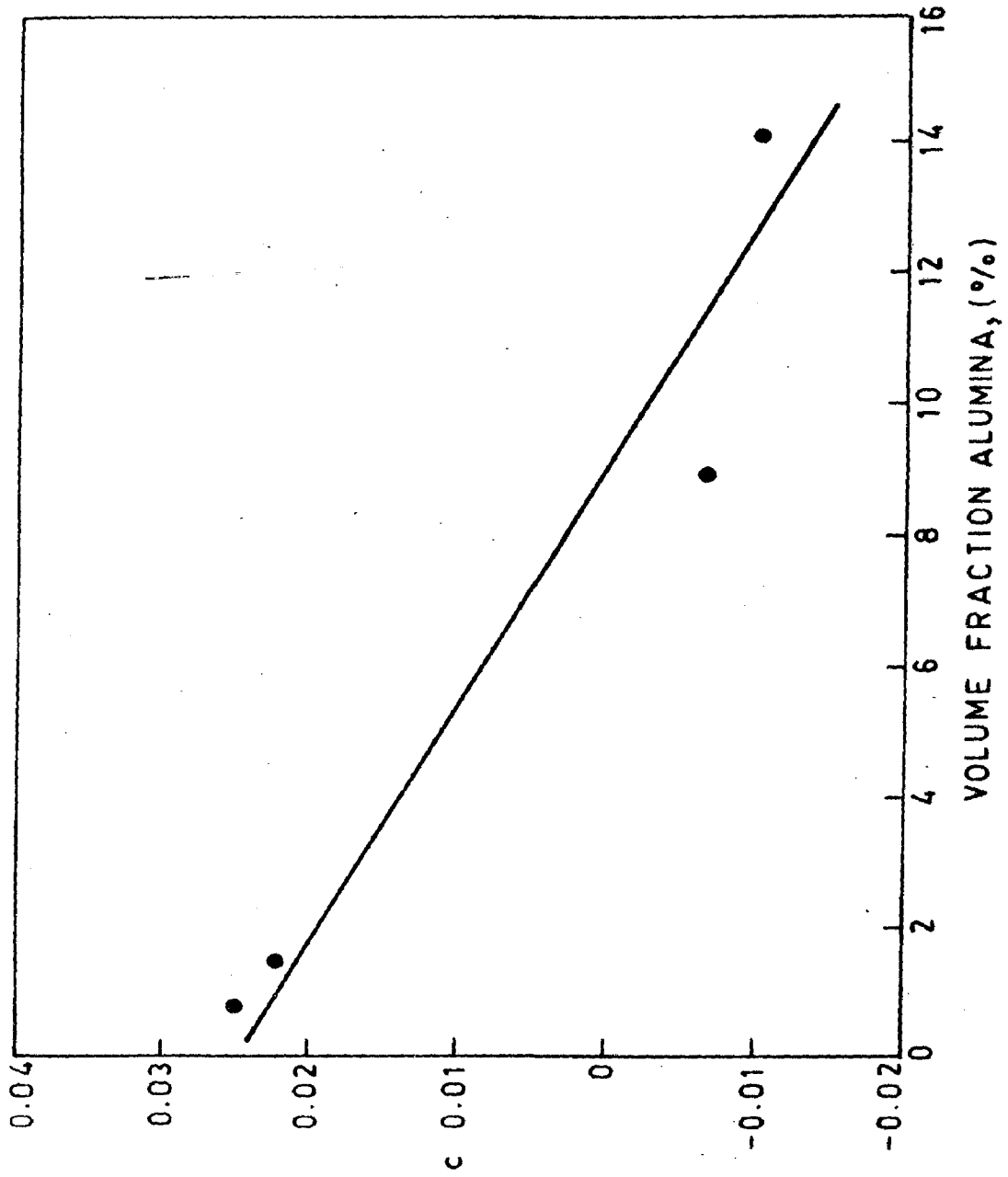
FIG.5.11 EFFECT OF ALUMINA CONTENT OF THE COMPOSITE
ON THE VALUE OF, C, OF EQUATION (5.2)

A further reduction in porosity does not influence the value of e_f significantly as it is evident for the composites containing 0.77, 1.5 and 9.0 volume percent of alumina. It is also interesting to note that the limiting porosity level for linear behaviour appears to increase with higher amount of alumina as it has been observed particularly for composites containing 9.0 and 1.5 vol.% alumina.

The fractographs of the composites having 0.35 Vol.% and 4.05 vol.% of porosity as presented in Figs. 5.12 (i) and (ii) respectively show the presence of larger voids in the latter than the size of that exists in the former one.

(b)   Void Nucleation in the Matrix

The strain levels for void nucleation, ϵ_N, in the matrix of the tensile specimens having 2.95 vol.% and 8.9 vol.% of alumina have been shown in Fig. 5.13. The figure shows that in both the specimens having different level of porosity and alumina content the volume percent of voids increases quite slowly with strain till a critical value is reached. At the critical strain the rate of increase in volume percent of voids has been found to enhance significantly and it is attributed to the nucleation of new voids and their subsequent growth in the matrix. Thus, the critical strain at which the crossover has taken place is identified as the nucleating strain, ϵ_N. The ϵ_N in the composites having 8.9 vol.% and 2.95 vol.% of alumina have been found as 0.26 and 0.272 respectively. It has also been
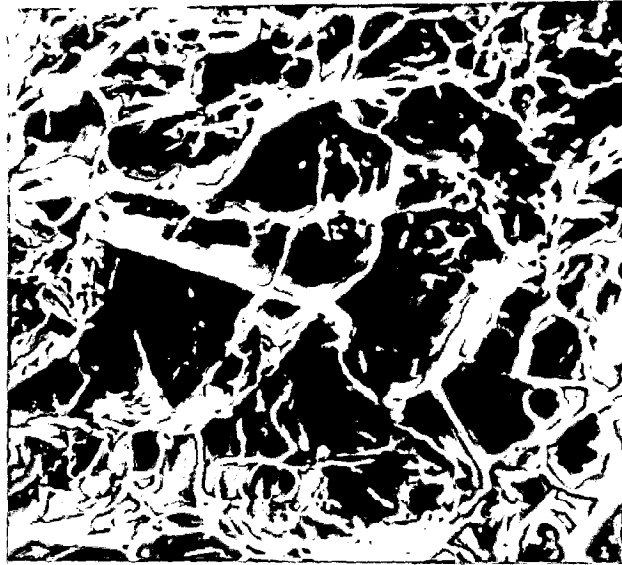
(i)   0.35 Vol. % POROSITY
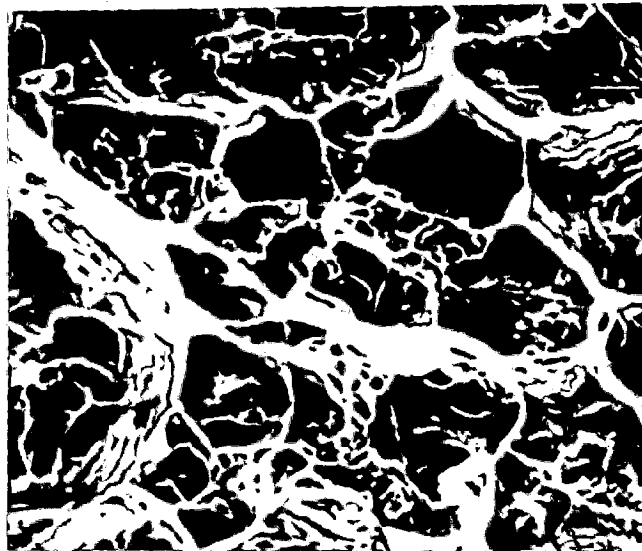
(ii)   4.05 Vol. % POROSITY

FIG. 5.12 FRACTOGRAPHS SHOWING THE DIFFERENCE IN
         SIZE OF VOIDS PRESENT IN THE COMPOSITES
         CONTAINING (4.5 Vol.% Al_2O_3) AND DIFFERENT
         LEVELS OF POROSITY FRACTURED UNDER
         TENSION; X 830
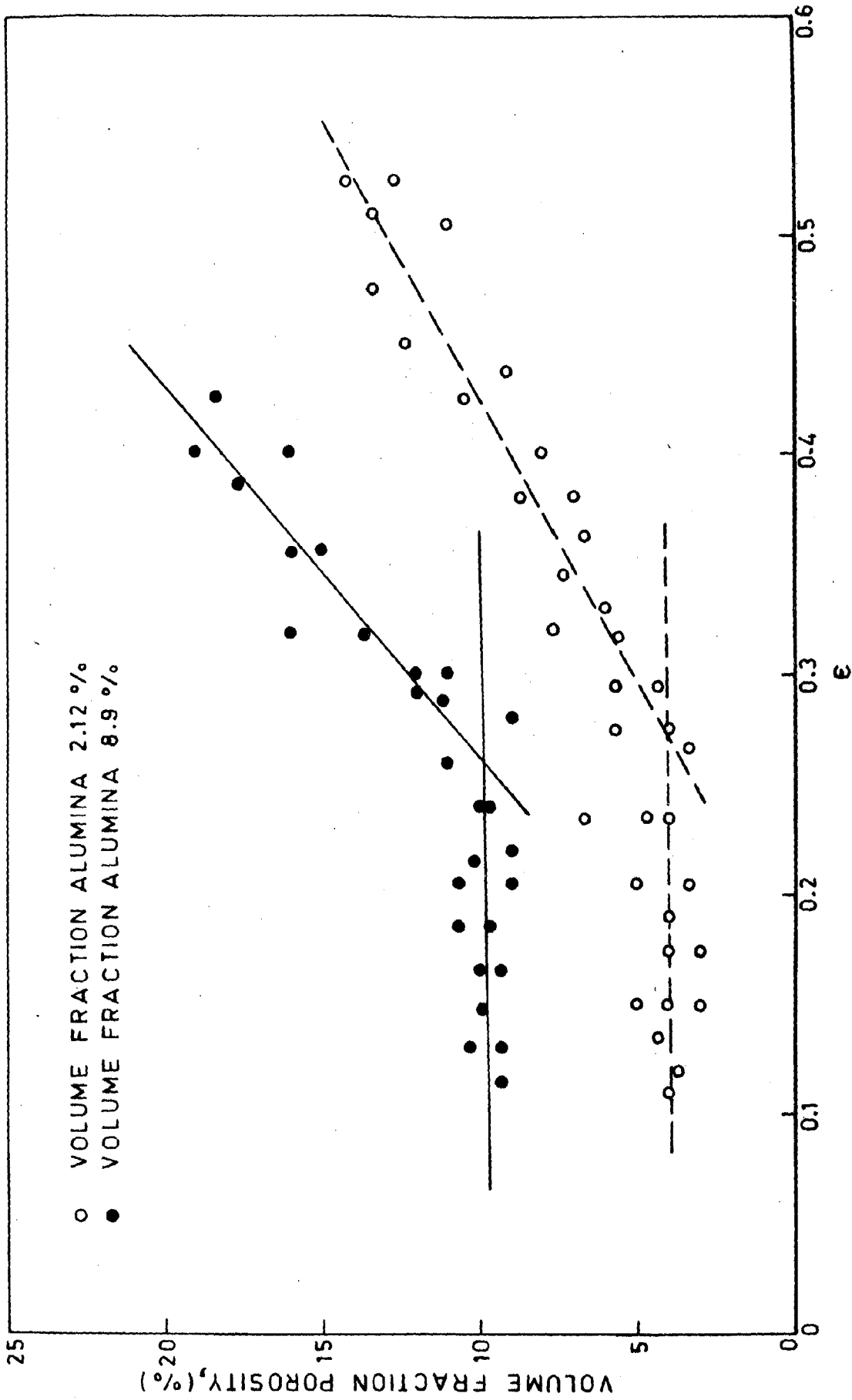
FIG.5.13 VARIATION OF VOLUME FRACTION OF VOIDS WITH APPLIED TENSILE STRAIN AT AMBIENT TEMPERATURE FOR COMPOSITES WITH DIFFERENT ALUMINA CONTENTS.

o VOLUME FRACTION ALUMINA 2.12 %
• VOLUME FRACTION ALUMINA 8.9 %

VOLUME FRACTION POROSITY,(%)

ε

observed that the rate of increase in volume percent porosity with an increase in strain beyond ϵ_N is more in the composite having 8.9 vol.% of alumina than that observed in the composite with lower (2.95 vol.%) alumina content.

(c)   Crack Propagation in the Matrix

A typical void formation by debonding particle-matrix interface identified as A has been shown in Fig. 5.14. In the same figure it has also been observed that a large number of voids (marked as B) have been nucleated in the matrix of the composite, at a true strain level of about ϵ = 0.325, during tensile deformation. In the same specimen at the region near the fracture surface having a true strain around 0.4 the existing and the nucleated voids in the matrix have been found to grow and coalesce leading to initiation and propagation of cracks causing fracture of the composite as shown in Fig. 5.15. It has been observed that during tensile testing the cracks originated from the sharp corners of reacted products of irregular shape have been spread in the matrix as revealed in Fig. 5.16.

The fractured surface of a composite having 8.6 vol.% of alumina and 3.0 vol. % of porosity has been presented in Fig. 5.17. The figure shows a typical indication of initiation of crack from a shrinkage porosity (E) and debonding of alumina particle-matrix interface (F).
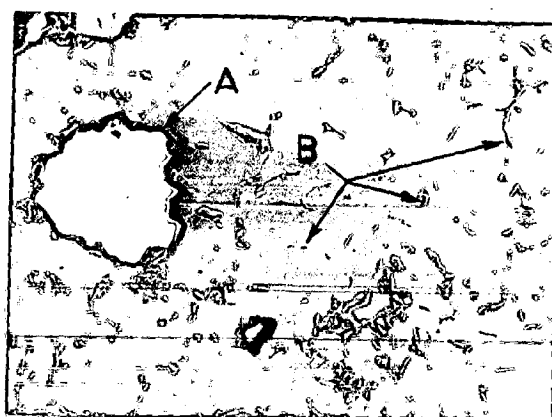
FIG.5.14 SCANNING ELECTRON MICROGRAPH SHOWING
DEBONDING OF PARTICLE-MATRIX INTERFACE
(A) AND PRESENCE OF VOIDS IN THE
MATRIX (B); X 480
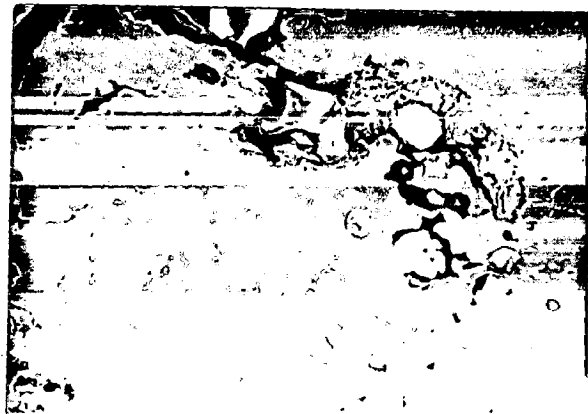
FIG. 5.15 NATURE OF CRACK PATH IN A COMPOSITE
FRACTURED UNDER TENSILE LOADING; X 550

FIG. 5.16 SCANNING ELECTRON MICROGRAPH SHOWING
THE CRACKS GENERATED AT THE SHARP
CORNERS OF REACTED PARTICLES OF
IRREGULAR SHAPE ; X 850

FIG. 5.17 FRACTOGRAPH SHOWING THE INITIATION OF
CRACK AT THE SHRINKAGE CAVITY (E) AND
THE DEBONDING THE PARTICLE -MATRIX
INTERFACE (F); X 650

5.2.3   DISCUSSION

The observed variation of porosity with the particle content in a composite has been attributed earlier to an identical mechanism of incorporation for both these constituents as discussed in section 4.2.4. Further the level of porosity also depends on the inhomogeneity in particle distribution. The separated particles do not generally have voids at the interface but a cluster of particles often has voids. These voids affect the mechanical properties of a composite more adversely than that observed in the case of metals and alloys.

The contribution of porosity on the tensile strength of a material has been estimated grossly as a weakening effect caused by the formation of a weakened zone around a spherical pore and is expressed by the model equation (5.1). In the model [135] a specimen of cross-sectional area A_O contains randomly distributed pores of average effective radius R_V and is subjected to a tensile force F. The number of pores per unit area, N_A, on a planar section equals $3V_p/2 \pi R_V^2$ where V_p is the volume fraction of pores. The total number of pores on the cross-section of the specimen is therefore equal to $3V_pA_O/2 \pi R_V^2$.

It is assumed that the cross-section of the specimen is divided into the same number of cells as the number of pores with an average cell radius R such that

each cell shares a pore of average effective radius r_p' in the plane of cross-section considered. The schematic diagram of such a cell is depicted in Fig. 5.18. It is assumed that the pore has a damaging effect on the load bearing capacity of a material upto a certain distance $R_p = n_1 r_p'$ from the pore where, n_1 is a constant having a value exceeding one and defines the weakened zone around the pores. The value of n_1, is primarily dependent on the mechanical characteristics of the material. The weaking of the material also depends on the geometry of the pore and on pore distribution. The average stress at $r' = r_p'$ is $k\ \sigma_m''$ where, k is a constant factor and σ_m'' is the stress in region unaffected by the pore. The averaging has been done over the size distribution of the pores and the angles around the axis of loading. The weakening of the material limits the value of k in the range of $0 < k < 1$. Satisfying the physical criteria described above the functional form of the force $f(r')$ carried by unit area of the material is explained as

$$ f(r') = \sigma_m''\ k\ \exp.(-\ln k \cdot \frac{r' - r_p'}{R_p - r_p'}\ ) \qquad .. \qquad (5.3) $$

From equation (5.3) the total load has been calculated by integrating over a single cell and multiplying it by the number of weakened cells. Assuming the material fails when σ_m'' equals σ_0, the tensile strength of pore free material. The tensile strength of the material containing pore, σ_p, is expressed as
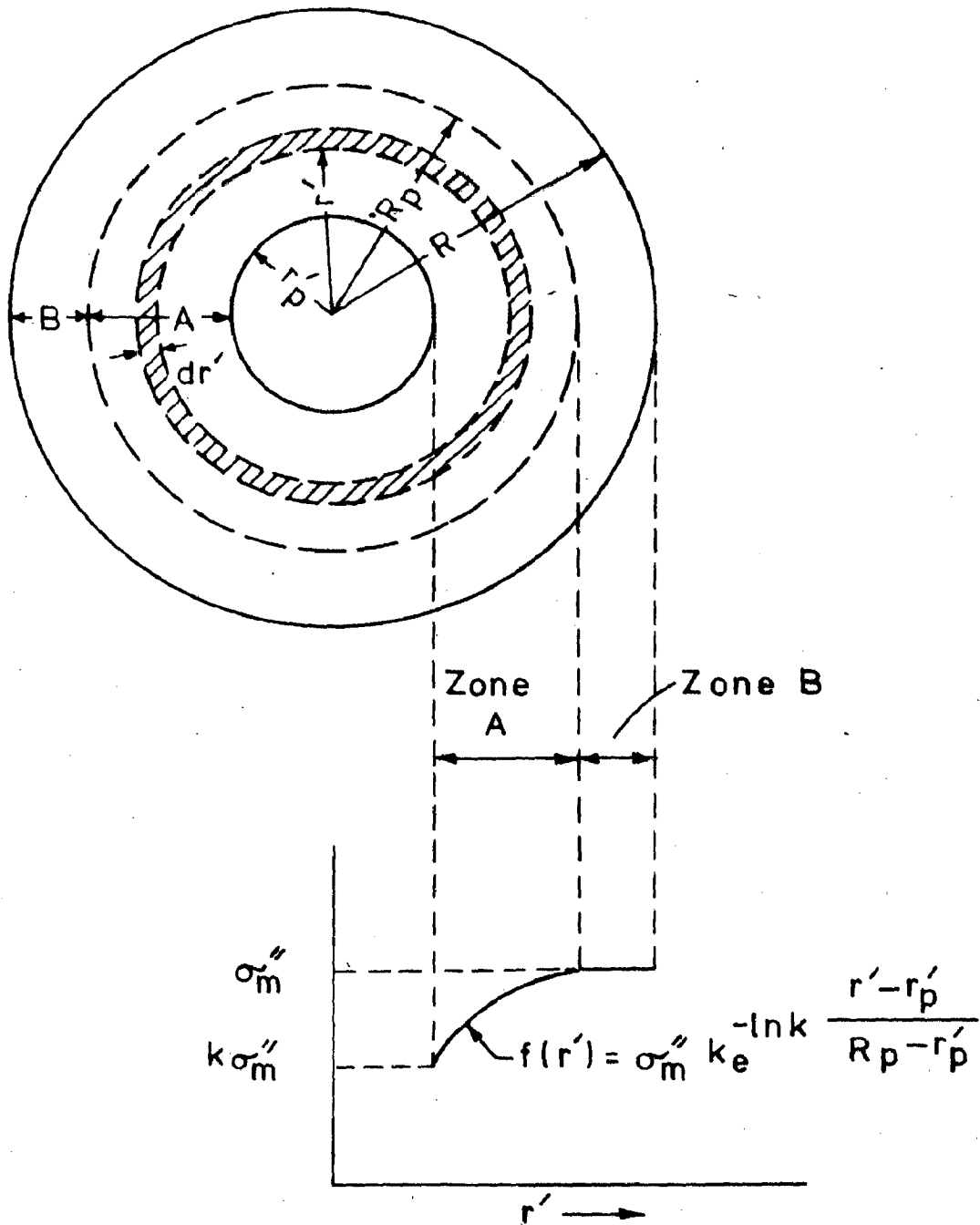
FIG. 5·18 VARIATION OF LOAD BEARING CAPACITY OF MATERIAL NEAR A PORE ON A PLANAR SECTION PERPENDICULAR TO THE DIRECTION OF APPLIED FORCE [135].

$$\frac{\sigma_p}{\sigma_o} = 1 - [n_1^2 - 2(n_1-1)(\frac{k-1}{lnk}) - 2(n_1-1)^2 (\frac{k-1}{(lnk)^2} - \frac{1}{lnk})] \frac{P}{100}$$

.. . (5.4)

where, P is the total porosity in percent. Denoting the co-efficient of porosity term of equation (5.4) by α a two-parameter formal equation (5.1) is obtained. The weakening factor α is a function of both the parameters, n_1 and k. The equation (5.1) is capable of estimating the contribution of pore in the linear regime upto a porosity level P_C which can be expressed as,

$$P_C = 100/n_1^2$$ .. (5.5)

obtained by imposing the condition of $R_p=R$. At a higher porosity level the equation (5.1) is not valid because the stress distribution around pore start interfering mutually to result into an effective pore-pore interaction term when R_p is greater than the radius of the average volume of material per pore R.

The linear variation of σ_p/σ_o with P for composites containing 0.8, 2.0, 8.1 and 18.0 vol.% alumina presented in Fig. 5.1 establish the validity of equation (5.1) and confirm that the tensile strength of these composites is a linear function of the porosity. The scattering in the experimental results presented in Fig. 5.1 is

attributed to the fact that the tensile test specimens have been collected randomly from the cast composites irrespective of its fabrication process parameters which has been found to influence its tensile strength as shown in Table 5.1, possibly due to a variation in reacted layer thickness as revealed in Fig. 4.37. The value of α estimated as a slope of these curves (Fig. 5.1) reduces with an increase in alumina content in the composite which is further revealed in Fig. 5.2. Since the particles with the same broad spectrum of sizes has been used, an increase in its volume fraction indicates an increase in the number of particles per unit area of the matrix. The spatial recovery of the load bearing capacity shall be affected by the presence of foreign particles due to a modification in the stress distribution around it. Thus, both n_1 and k may get modified to cause the observed lowering of the weakening factor α . However, the reduction of α becomes less marked at higher particle content in the composites (Fig. 5.2) because of enhanced particle-particle interaction caused by a lowering of interparticle spacing at higher alumina content of the composites.

The lowering of the projected tensile strength at zero porosity, σ_0, with an increase in volume fraction of reinforced particles is shown in Fig. 5.3 and is attributed to nucleation of voids by debonding of particles from the matrix as typically observed in Fig. 5.12

The void initiates in the particle-matrix interface at early stages of plastic deformation [106] and damages the load bearing capacity of the material. This phenomenon starts at a strain reducing with an increase in alumina content. Moreover, $MgAl_2O_4$ [27] formed in extended irregular shapes with sharp corners often gives rise to cracks as shown in Figs. 4.41 (i),(ii) and 5.16. However, the observed σ_0 of the composites is superior to the strength of the matrix at zero porosity level upto about 6.5 volume percent alumina. Beyond this level a further incorporation of alumina on debonding may transfer a load to the matrix which is sufficient to cause ✓. its immediate failure and thus, the room temperature strength is reduced. The similarity in the trend of variation in the ultimate tensile strength at different porosity level (Fig. 5.4) and the variation of σ_0 (Fig. 5.3) with alumina content of the composite provides an amount of confidence in our analysis.

From a consideration of the growth of voids under stress Brown and Embury[119] has given the criteria for estimating the critical strain, ϵ_g, at which the necking instability in the material between two growing voids will cause the joining of voids. This strain together with the nucleating strain, ϵ_N, for the voids will constitute the fracture strain. The same authors proposed that,

$$1+ \epsilon_g = 1/2 (\sqrt{2 \pi /3V_p} - \sqrt{8/3}) \qquad .. \qquad (5.6)$$

where, V_p is the volume fraction of particles keeping the size of the particles constant. It is expected that ϵ_g and the corresponding stress will decrease non-linearly with the volume fraction of particles as it has been observed for σ_0 shown in Fig. 5.3. However, it must be remembered that in the cast materials with porosity this picture will be modified by the growth of the already existing porosity for which the nucleating strain is zero.

For the same volume fraction of particles if the particle size is increased i.e. interparticle spacing is reduced one observes a reduction in strength as shown in Fig. 5.6. These results are in agreement with the earlier investigations [106, 136] and can be explained in terms of a lower ϵ_N for nucleation of voids around particles having a larger size and a larger initial size of the void. The effect of particle size on σ_0 of the composites having $\sim$ 8.62 vol.% alumina (Fig. 5.6) is similar to that observed in a composite having $\sim$ 9.0 vol.% of alumina and 4.26 vol.% porosity (Fig. 5.8), and thus confirms the validity of the analysis.

A little initial enhancement of weakening factor α with an increase in average particle size upto $\sim$ 115 µm as shown in Fig. 5.7 is possibly caused by an enhanced debonding of particles due to a lower strain required for void nucleation.

But the subsequent decrease in the value of α_c with an increase in particle size beyond $\sim$ 115 μm indicates a significant reduction in stress concentration in the matrix.

The true fracture strain has been correlated to the inverse of volume fraction of porosity by several authors [120, 137, 138]. The engineering fracture strain observed in the present investigation has been plotted against the inverse of porosity content (Fig. 5.9) to identify the influence of porosity on fracture behaviour. When the porosity is above a critical level depending on the alumina content of the composite the correlation of inverse of as cast porosity with engineering fracture strain shows a linear behaviour with a correlation co-efficient exceeding 0.9 as shown in Fig. 5.9. In these ranges of porosity the failure is caused primarily by the growth and coalescence of the existing pores in the matrix either isolated or in the cluster of particles as typically observed in Fig. 4.36(iii). The voids nucleated during deformation at the boundary between the well bonded particles and the matrix are not primarily responsible for the fracture of these composites. The Fig. 5.14 clearly demonstrates extension and linkage of pre-existing pores at the boundary of alumina particles and at micro porosities (see Fig. 5.17) away from the particles during tensile deformation. However, Fig. 5.15

showing the microstructure of the transverse section near the fractured surface demonstrates the void growth and coalescence being confined to the inhomogeneous regions containing particle clusters with voids. The matrix away from these weak zones is relatively free from damage. The fractograph of the composite (4.5 vol.% Al_2O_3) containing porosity of 4.05 vol.%, which falls within the linear regime of e_f versus P^{-1} curve, shows the presence of large voids being created by the growth of pre-existing pores as shown in Fig. 5.12 (ii). It confirms the assumed fracture mechanism of the composite at its higher porosity level.

The serrated nature of tensile stress-strain curve as observed in Fig. 5.5 is an indication of continuing void coalescence over the range of strain. From the above discussion it is inferred that although the debonding at the alumina-matrix interface might have taken place but the failure is primarily caused by the existing voids as evident in Fig. 5.14. So the present approach to explain the tensile properties of the particulate composite on the basis of a model incorporating the role of pre-existing pores is thus justified. The particles are assumed to exert only a secondary influence by modifying the parameters of the model equation (5.1) for ultimate tensile strength.

In the regime of porosity content above the critical level, the variation of fracture strain with

porosity has been represented by equation (5.2) and the particle content has been found to influence both m and c as shown in Fig. 5.10 and Fig. 5.11 respectively. These figures indicate that the engineering fracture strain is higher for composites with higher alumina content resulting in higher values of m. The factor c which makes a smaller contribution on e_f compared to m/P and is distributed around zero may have appeared due to a random error introduced by the limitations of the measurement.

The critical level of porosity content above which the fracture is controlled by porosity increases with the increase of alumina content of the composite (Fig. 5.9). This is a clear demonstration of a helpful role of the particles in suppressing the deleterious effect of porosity by modifying the stress distribution. However, the particles are soon made ineffective by nucleation of voids by debonding of the particles from the matrix. A larger particle content leads to a higher rate of nucleation of voids as indicated in Fig. 5.13 and causes fracture at lower level of strain. The present observation on the variation in void nucleating strain (ϵ_N) of the composites with a change in its alumina content showing a minor increase in value of ϵ_N in case of lower alumina content ($\sim$ 2.12 vol.%) than that of the higher alumina content ($\sim$ 8.9 vol.%) composite is in agreement to the earlier observations of Brown et al [119] and Le Roy et al [118].

At a porosity content below the critical level the composites having 1.5 and 9.0 vol.% of alumina show no significant variation of fracture strain with the reduction in porosity as shown in Fig. 5.9. This may have been possible because at a lower porosity level the failure of the composite is primarily caused by the normal fracture mechanism by nucleation of voids, its growth and linkage occurring independently of pre-existing porosities. This is in agreement to the observations presented in the fractographs (Figs. 5.12 (i) and (iii)) of the composites containing 4.5 vol.% of alumina and with a porosity content of 0.35 vol.% (< critical level of porosity) where the fracture due to growth and linkage of nucleated voids are evident from the existance of considerably smaller size of voids (Fig. 5.12 (i)) compared to these observed in Fig. 5.12 (ii).

5.3 MECHANICAL PROPERTIES AT ELEVATED TEMPERATURE

5.3.1 RESULTS: EFFECT OF POROSITY AND PARTICLE CONTENT ON THE TENSILE STRENGTH

The validity of the model equation (5.1) for the the elevated temperature tensile strength of Al-4wt.% Mg - Al_2O_3 particulate composite having a wide spectrum of particle sizes as mentioned in Table 3.1 have been examined. The values of σ_p and σ_0 are estimated

following the procedure mentioned in section 5.2.1. For low alumina contents of 2.0, 2.5 and 2.6 vol.% the typical nature of σ_p/σ_0 versus P plots for composites tested at the temperatures of 298 K, 473 K and 573 K have been shown in Fig. 5.19. The same behaviour for composites having higher alumina contents of 9.2 and 10.5 vol.% tested at temperatures of 473 K and 573 K have also been given in Fig. 5.19. The tensile strength of the composites at elevated temperature can justifiably be represented as a linear function of porosity in view of high values of co-efficient of correlation in the range of 0.88 to 0.97. The slope of these curves as it has been indicated earlier in section 5.2.1 is the weakening factor, α, of the pore. It has been observed in Fig. 5.19 that for a given close range of alumina content the value of α increases with the increase of temperature and at a given temperature, the value of α decreases with the increase in the alumina level in the compoiste.

Following the model equation (5.1), the effect of alumina content of the composite on the weakening factor, α, at elevated temperatures of 473 K and 573 K have been determined and presented in Fig. 5.20 along with the behaviour of α at ambient temperature. At the temperatures under investigation the values of α have been found to decrease with the increase in volume fraction of alumina in the composite.
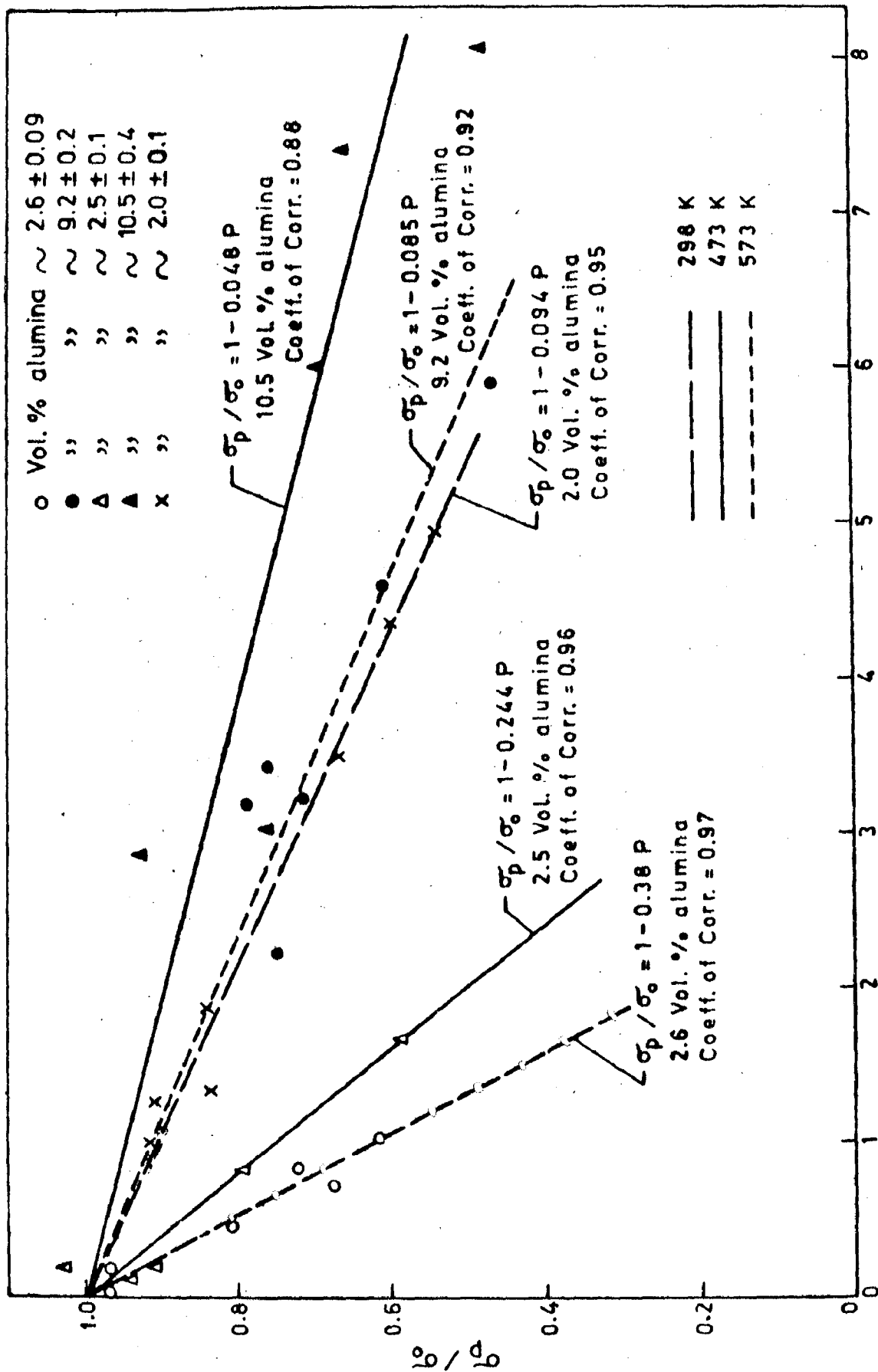
FIG. 5.19 EFFECT OF POROSITY ON THE TENSILE STRENGTH RATIO (σ_p/σ_o) IN COMPOSITES CONTAINING DIFFERENT AMOUNTS OF ALUMINA AND TESTED AT DIFFERENT TEMPERATURES.
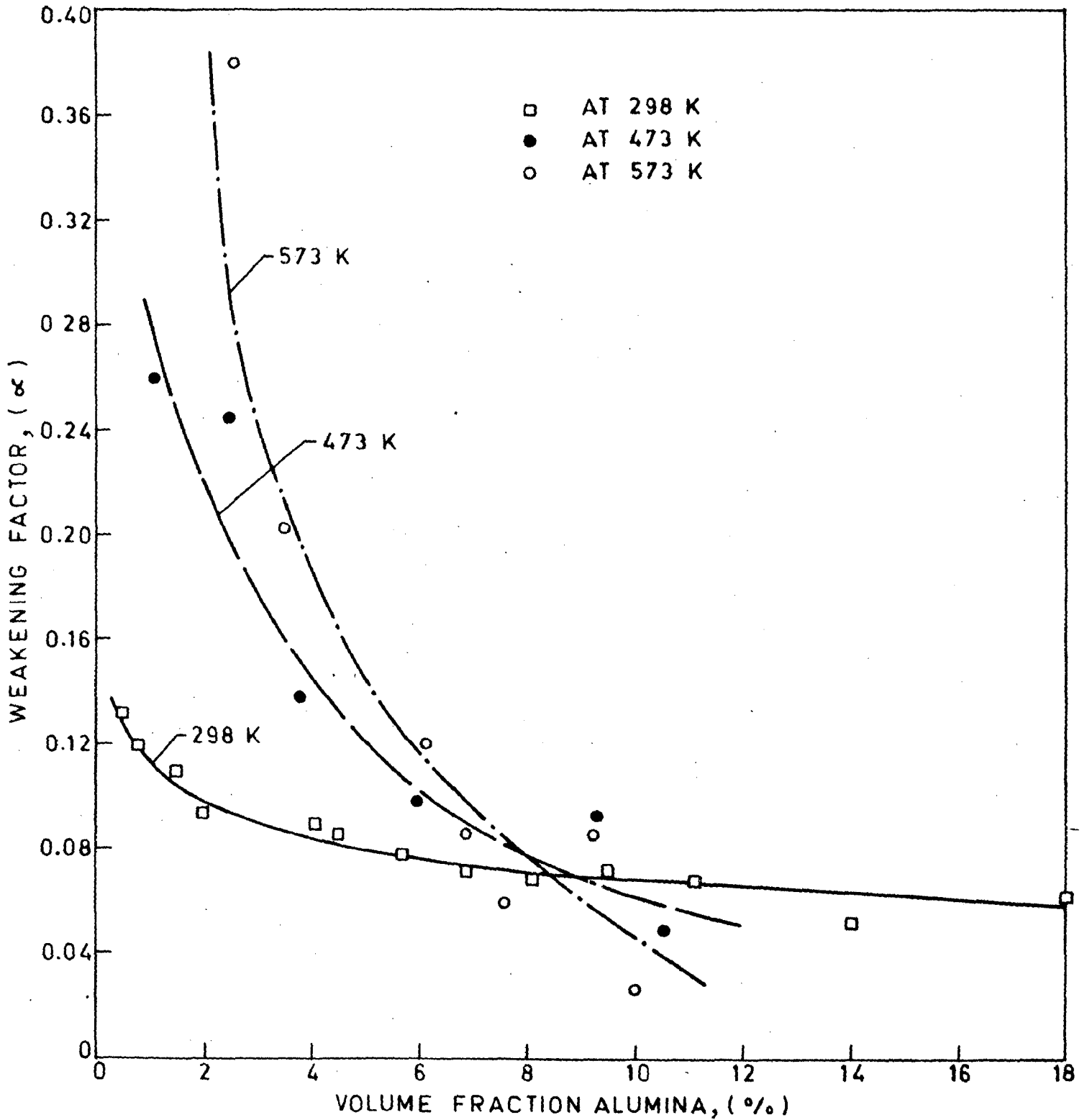
FIG. 5.20 VARIATION OF WEAKENING FACTOR WITH ALUMINA CONTENT OF THE COMPOSITES AT DIFFERENT TEMPERATURES.

At elevated temperatures the weakening effect of the
composite at a given alumina content has been found more
at 573 K than that observed at 473 K or ambient temperature
where the alumina content of the composite is below $\sim$ 7.0-
8.0 vol.%. In an effort to find a power law relation
between α and the volume fraction of alumina in the
composite at 298 K, 473 K, and 573 K the observed values
of α and volume fraction of alumina have been plotted
on a log-log scale and an almost linear behaviours have
been observed as shown in Fig. 5.21. The nature of the
curves can be described empirically by the equation

$$In \, \alpha \quad = \quad m \, \ln V_{Al_2O_3} + c \qquad \qquad .. \qquad (5.7)$$

where, m and c are constants. The correlation co-efficient
of this linear fit is more than 0.92. Rewriting equation
(5.7) one gets

$$\alpha \quad = \quad A(V_{Al_2O_3})^m \qquad \qquad .. \qquad (5.8)$$

when, $c = \ln A$. It is observed that the exponent m of
the composite is negative and increases with the increase
in temperature as shown in Table 5.2. The value of $\ln A$
is negative at 298 K and 473 K and it increases with
the increase in temperature (Table 5.2).

The effect of particle content of the composite
on its tensile strength at zero porosity, σ_0, at 298K,
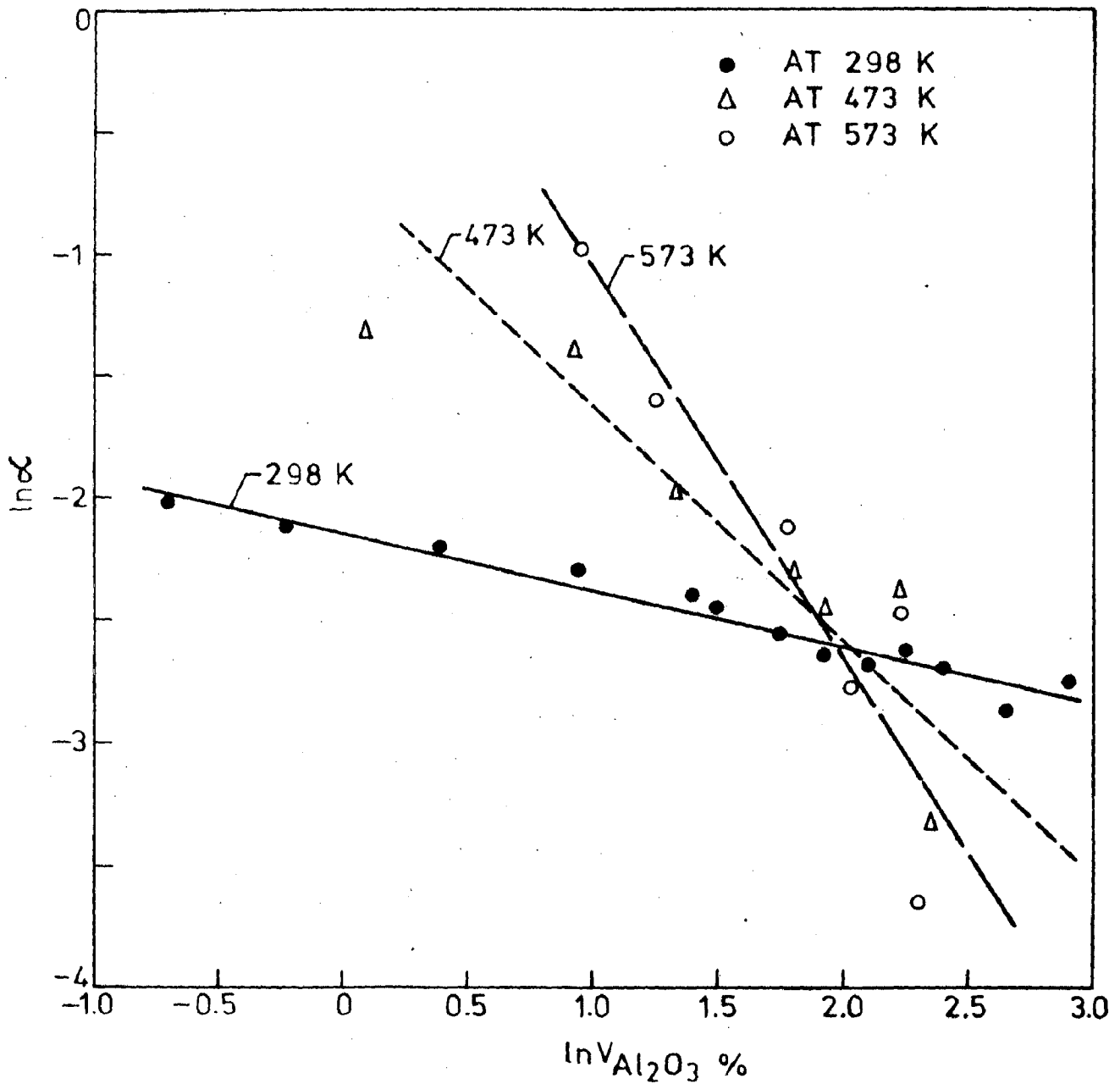
FIG. 5.21 VARIATION OF WEAKENING FACTOR WITH VOLUME PERCENT OF ALUMINA IN COMPOSITES AT DIFFE- RENT TEMPERATURES.

TABLE 5.2

THE VARIATION IN THE VALUES OF CONSTANTS OF EQUATION (5.7)
WITH THE INCREASE IN TEMPERATURE OF THE TENSILE TESTS

Temperature (K)	Values of constants		Correlation co-efficient
	m	lnA	
298	-0.233	-2.144	0.98
473	-0.975	-0.642	0.92
573	-1.6	0.547	0.93

473 K and 573 K are shown in Fig. 5.22. At both ambient and elevated temperatures the σ_0 have been found to decrease with an increase in the volume fraction of alumina in the composite. For a given alumina content the values of σ_0 has been found to be higher at lower temperatures compared to that observed at 573 K. The values of σ_0 reduces drastically beyond $\sim$ 9.0-9.5 vol.% alumina at elevated temperatures. It has been observed that the extent of reduction in σ_0 with temperature is quite small upto 473 K for an alumina content of <4.0 vol.% but, between $\sim$ 4.0-9.0 vol.% of alumina the composite shows higher values of σ_0 at 473 K than those observed even at ambient temperature of 298 K.

Fig. 5.23 shows the variation of α with test-temperature for composites having different amount of alumina varying from $\sim$ 2.6 vol.% to $\sim$ 10.3 vol.%. At alumina level between $\sim$ 2.6 vol.% to $\sim$ 9.3 vol.% the value of α have been found to increase with an increase in temperature. But the weakening factor, α, becomes relatively insensitive to temperature as the alumina content is increased. Finally at 10.3 vol.% alumina the nature of variation of α with temperature is reversed and it reduces with an increase in temperature.

At a given alumina content of the composite, the values of σ_0 shows a minor decrease with an increase
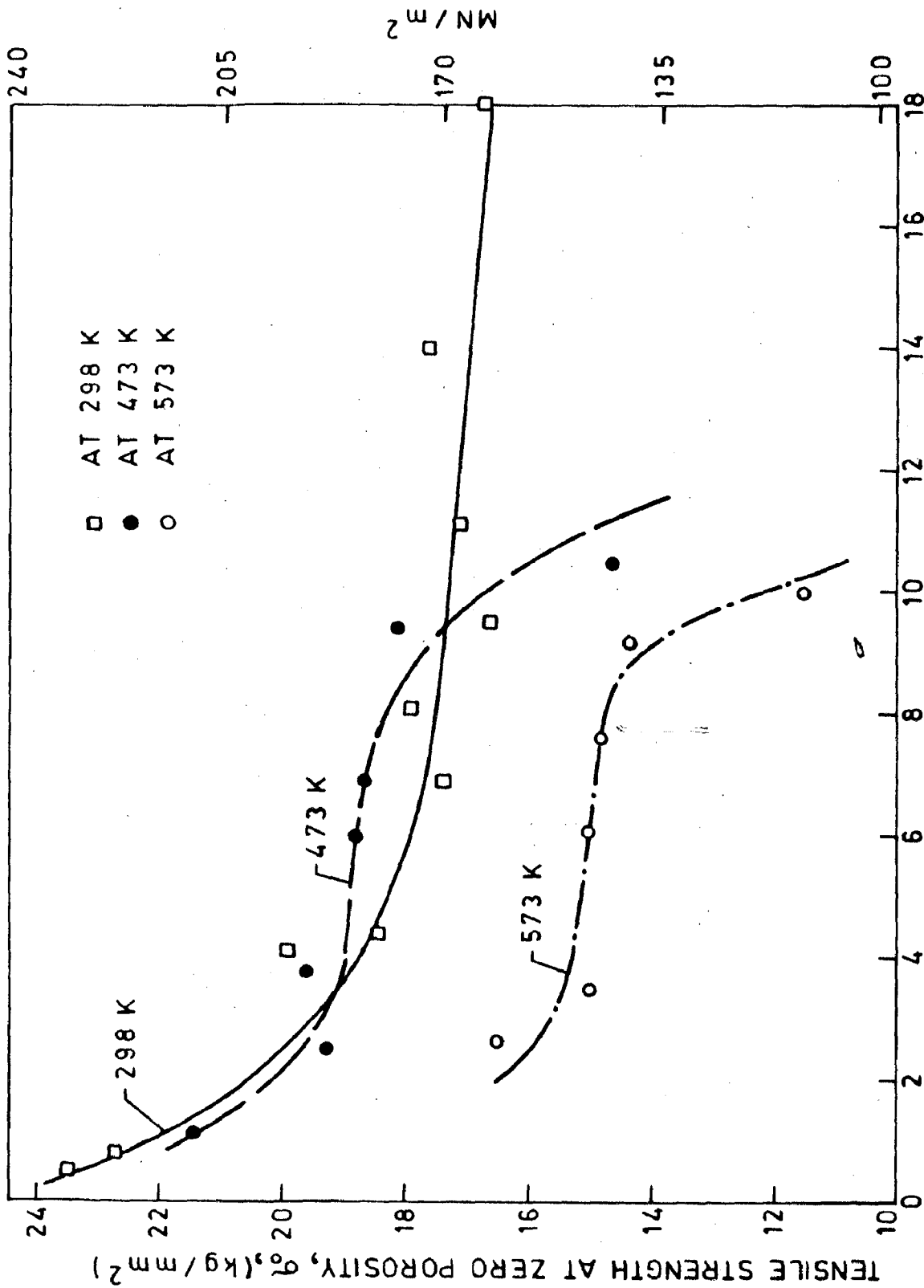
FIG.5.22 EFFECT OF PARTICLE CONTENT ON THE PROJECTED TENSILE STRENGTH AT ZERO POROSITY FOR COMPOSITES AT DIFFE-RENT TEMPERATURES.
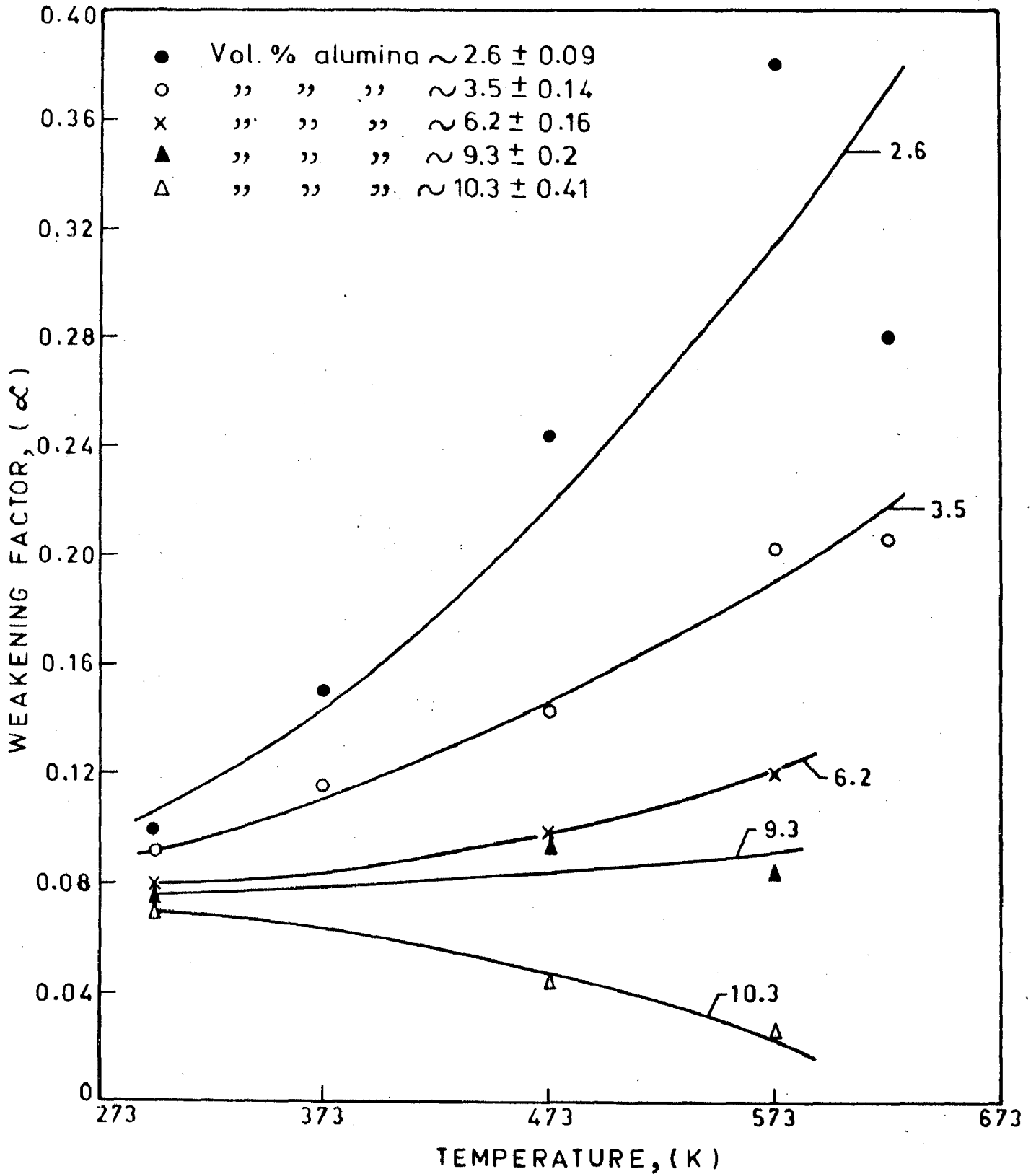
FIG. 5.23 VARIATION OF WEAKENING FACTOR WITH TEMPE-
RATURE FOR COMPOSITES CONTAINING GIVEN
LEVEL OF ALUMINA PARTICLES.

in temperature upto 473 K followed by a rapid drop with a further increase in temperatures as it has been commented earlier and further evident in Fig. 5.24. At any given temperature the values of σ_0 have been found to be higher at lower alumina content. The variation in ultimate tensile strength of composites having a given alumina content with an increase in temperature has been shown in Fig. 5.25. The figures shows a minor reduction in tensile strength with the increase of temperature upto 473 K followed by a sharp fall with a further rise of temperature. At a given temperature the tensile strength of a lower alumina content composite is more than that of one having a higher amount of alumina.

The effect of temperature on the engineering tensile stress-strain behaviour of the composite having alumina and porosity content ~ 2.4 vol.% and ~ 0.14 vol.% respectively has been shown in Fig. 5.26. It has been observed that with the increase of temperature from the ambient temperature (298 K) to 623 K the failure of the composite takes place at a lower stress level but the fracture strain in general is enhanced. Upto a temperature of 473 K the curves have been found to maintain a similar trend where the strain increases continuously with the rise of stress. However, at the temperature of 573 K and 623 K, beyond a certain strain level the composite
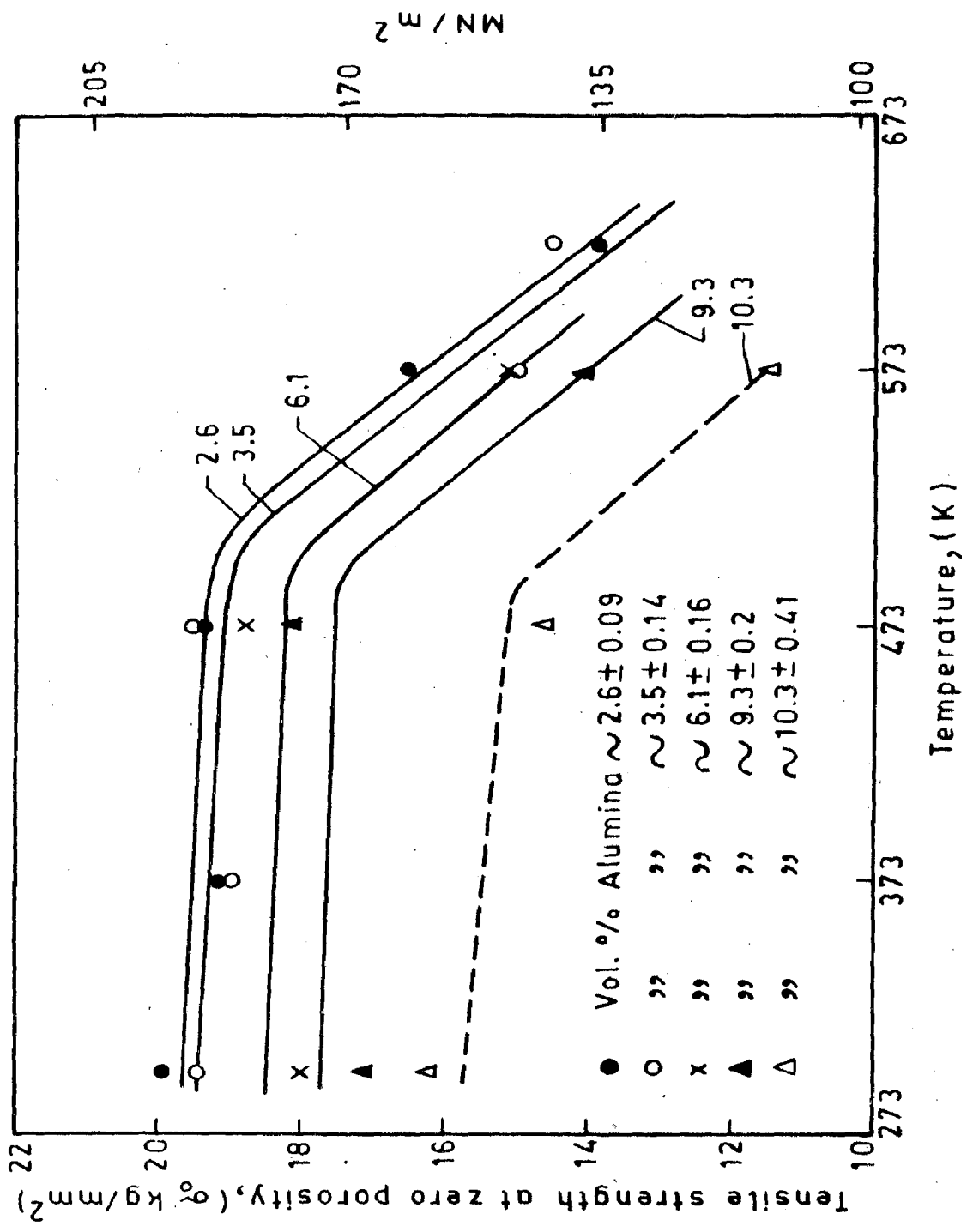
FIG.5.24 EFFECT OF TEMPERATURE ON THE PROJECTED TENSILE STRENGTH AT ZERO POROSITY FOR COMPOSITES WITH GIVEN LEVEL OF ALUMINA PARTICLES.
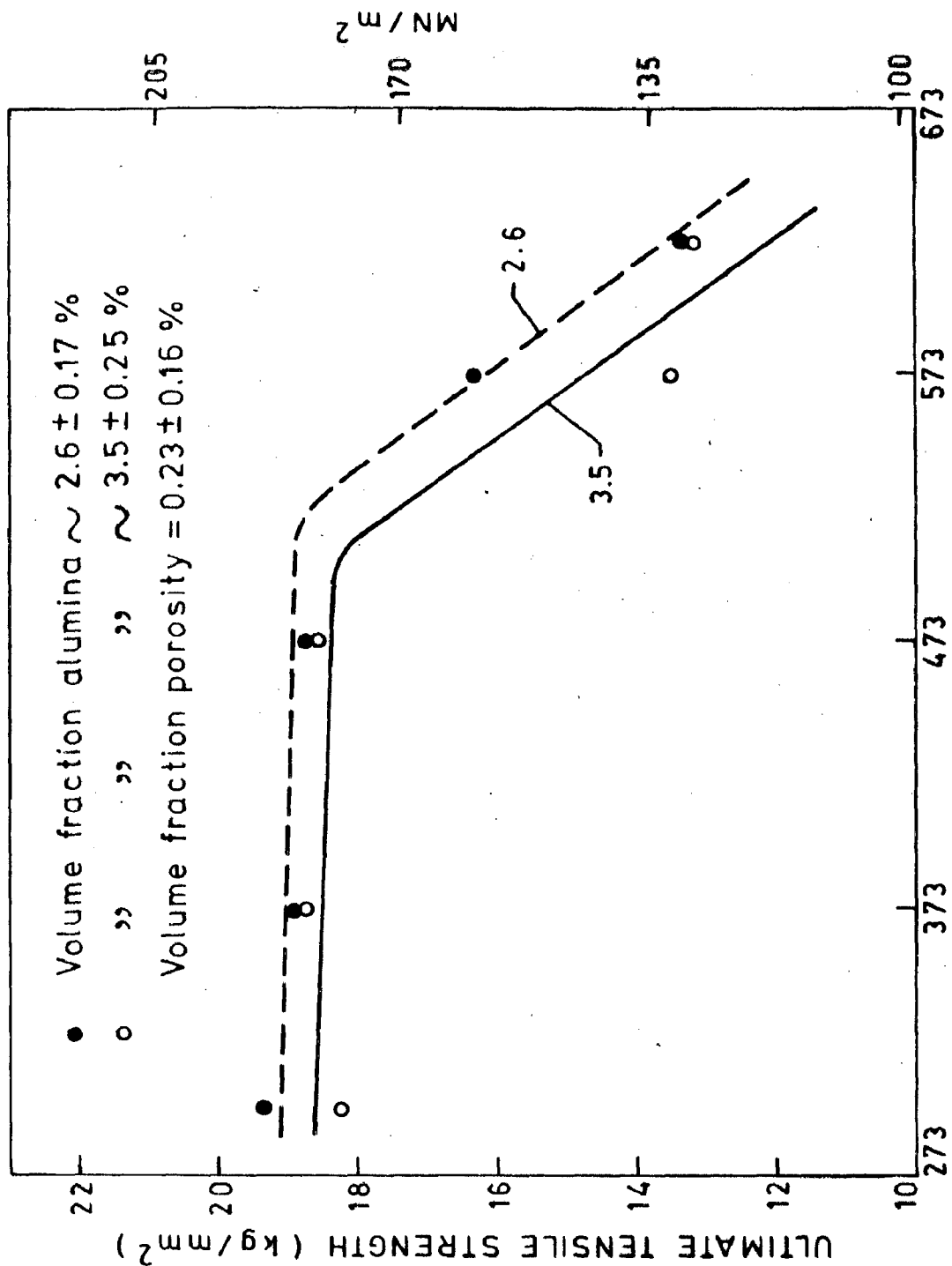
FIG.5.25 EFFECT OF TEMPERATURE ON THE ULTIMATE TENSILE STRENGTH OF COMPOSITES WITH GIVEN ALUMINA CONTENT.
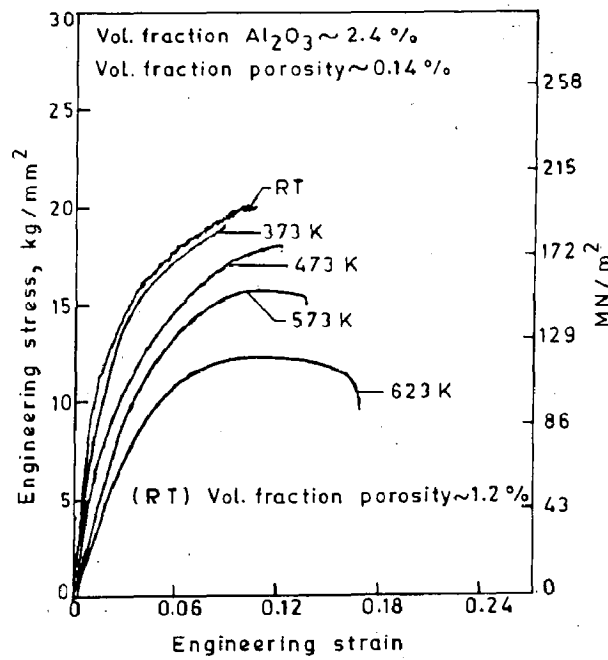
FIG.5.26 EFFECT OF TEMPERATURE ON ENGINEERING
        STRESS-STRAIN CURVE OF COMPOSITES
        WITH GIVEN ALUMINA CONTENT.

has been found to deform continuously without showing any appreciable change in stress. The strain characterising the onset of this trend has been observed to reduce with an increase in temperature.

5.3.2   RESULTS : FRACTURE BEHAVIOUR

(a)   Effect of Porosity Content on Fracture Strain

The variation in average fracture strain (e_f) with the increase in temperature from 373 K upto 623 K of the composites having different amount of alumina at a given volume fraction of porosity has been given in Table 5.3. The table shows that at the lower levels of alumina content below $\sim$ 8.98 vol.% the fracture strain of the composites increases with the increase of temperature. However, in case of higher alumina content beyond the amount mentioned above the fracture strain of the composite has been found to decrease with the increase of its temperature.

The relation between the fracture strain, e_f, and the reciprocal of percentage of porosity, P^{-1}, observed at various temperatures in a composite containing $\sim$ 9.4 vol.% of alumina has been shown in Fig. 5.27. The curves are the least square straight lines fitted to the experimental points with correlation co-efficient of 0.89 and more. The straight lines drawn for the data at elevated

TABLE 5.3

VARIATION IN AVERAGE FRACTURE STRAIN (e_f) WITH TEMPERATURE IN DIFFERENT COMPOSITES

Volume fraction porosity (%)	Volume fraction alumina (%)	Average fracture strain (e_f) at elevated temperature			
		373 K	473 K	573 K	623 K
0.117 ± 0.08	2.64 ± 0.17	0.106	0.117	0.131	0.147
	2.51 ± 0.19	0.08	0.09	–	0.097
0.47 ± 0.08	3.59 ± 0.29	0.09	0.122	–	0.164
	3.69 ± 0.29	0.082	–	–	0.107
1.43 ± 0.26	6.07 ± 0.17	–	0.048	0.064	–
	3.53 ± 0.3	–	0.04	0.058	0.085
3.17 ± 0.48	8.98 ± 0.39	–	0.0475	0.047	–
	10.33 ± 0.28	–	0.049	0.036	–
7.26 ± 1.5	9.97 ± 0.68	–	0.0396	0.032	0.026

248
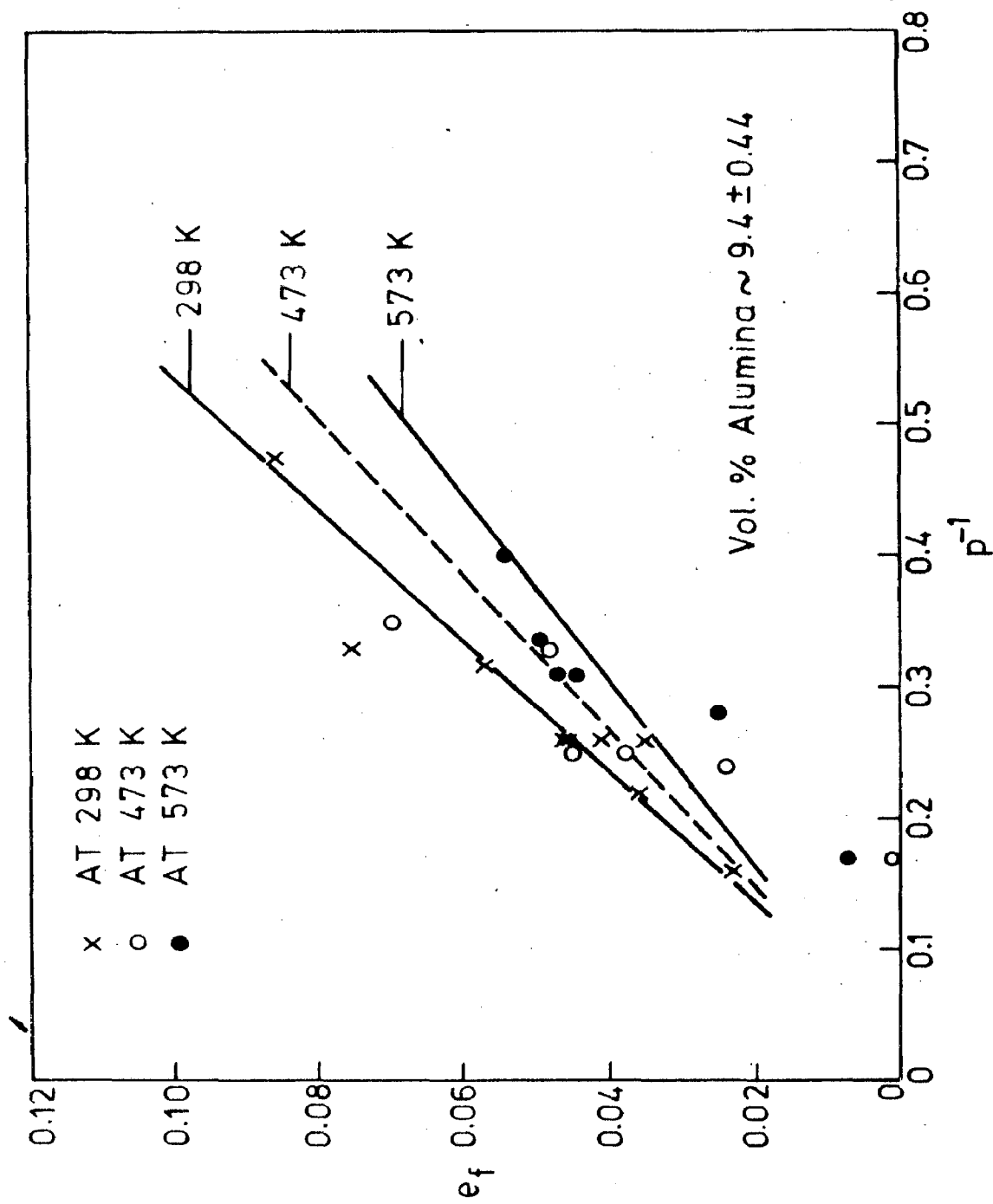
FIG.5.27 EFFECT OF INVERSE VOLUME PERCENT POROSITY ON ENGINEERING FRACTURE STRAIN OF COMPO-SITES TESTED AT DIFFERENT TEMPERATURES.

temperatures have been forced towards origin by including (0,0) as a data point with a weightage of three. ~~~~~~ The values of constants in equation (5.2) are given in Table 5.4. At a given porosity level the e_f of a composite containing ~ 9.4 vol.% of alumina has been found to decrease with an increase of temperature.

(b)   Void Nucleation in the Matrix

The longitudinal section of the tensile specimens having ~ 3.6 vol.% alumina and ~ 0.45 vol.% of porosity tested at 373 K, 473 K and 623 K near the fractured surface reveals under scanning electron microscope that the voids have primarily been nucleated in the matrix along the boundary of the primary particles as shown in Figs. 5.28 (i),(ii) and (iii). In these figures it has been observed that before fracture the extent of growth and linkage of voids have been extensive at higher temperature of 623 K (Fig. 5.28 (iii)) giving rise to propagating cracks. The void nucleation and growth in the matrix even away from the fractured surface in the tensile specimen tested at the temperature of 623 K has enhanced considerably as shown in Fig. 5.29.

(c)   Fractography

Fig. 5.30 shows the path of propagation of a crack initiated from a particle-matrix interface as observed in the fractured surface of a composite having 10.0 vol.%

TABLE 5.4

THE VARIATION IN THE VALUES OF CONSTANTS OF EQUATION (5.2) WITH AN INCREASE IN TEST-TEMPERATURE

Temperature (K)	Values of constants		Correlation co-efficient
	m	c	
298	0.2	-0.008	0.94
473	0.17	-0.004	0.89
573	0.14	-0.003	0.91
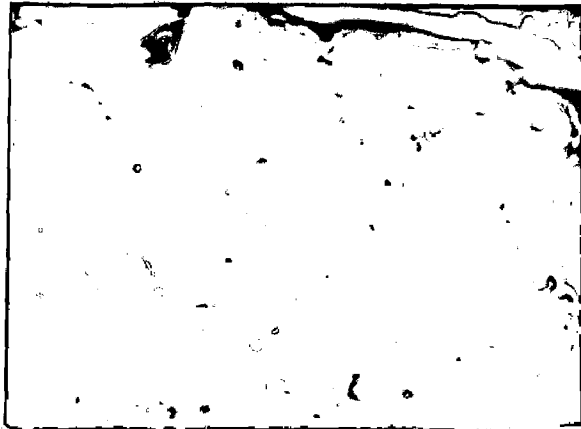
(i)   373 K

(ii)   473 K
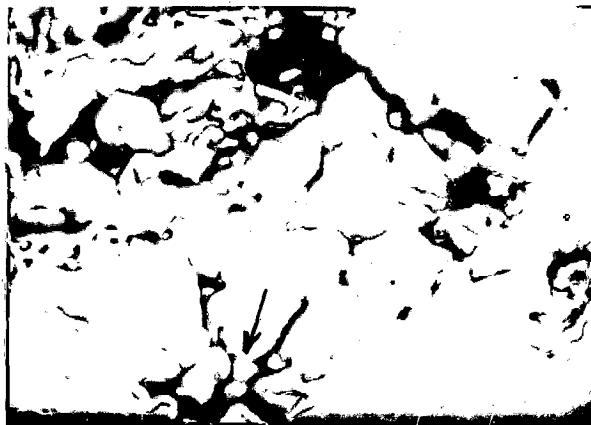
(iii)   623 K

FIG.5.28 SCANNING ELECTRON MICROGRAPHS SHOWING
THE FRACTURED SURFACE OF COMPOSITES
TESTED AT DIFFERENT TEMPERATURES RE-
CRSTALLISED GRAINS (marked by arrow);
X 900

FIG.5.29 SCANNING ELECTRON MICROGRAPH SHOWING
THE RECRYSTALLIZATION (marked by arrow)
AND THE PRESENCE OF VOIDS IN THE MATRIX
AWAY FROM THE FRACTURED SURFACE OF A
COMPOSITE TESTED AT 623 K ; X 900
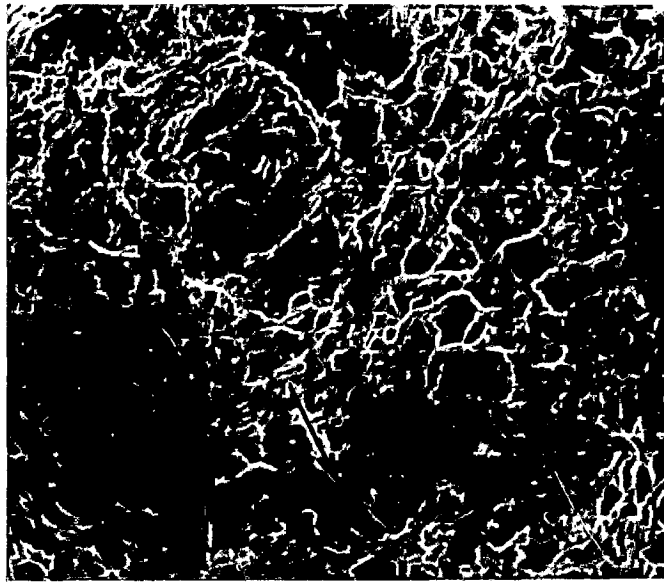
FIG.5.30 FRACTOGRAPH SHOWING THE PATH OF PROPA-
GATION OF A CRACK INITIATED FROM A VOID
CREATED BY PARTICLE-MATRIX DEBONDING
AT 473 K; X 650

of alumina and 3.0 vol.% of porosity tested under tension at a temperature of 473 K. In the same specimen there are also cracks originating from the shrinkage porosities within the primary solid particles as shown in Fig.5.31.

The fracture characteristics of the composites having 9.8 ± 0.8 vol.% of alumina and 2.9 ± 0.05 vol. % of porosity, fractured under tension at various temperatures of 298 K, 473 K and 573 K are shown in Figs. 5.32 (i), (ii) and (iii) respectively. The Fig. 5.32 (i) shows that at 298 K the failure of the composite has taken place by a mixed mode of ductile and clevage fracture. However, the fractographs of the composites failed at the elevated temperatures of 473 K and 573 K show that the size of the dimples become comparatively larger at higher temperature (573 K) as revealed in Fig. 5.32 (iii) than that observed at a lower test temperature of 473 K (Fig. 5.32 (ii)). It is interesting to note that a number of considerably small dimples (marked by arrow) along with the larger one are also present in the fractured surface of the composite tested at 573 K as shown in Fig. 5.32 (iii).

To find out the reason for the change in fracture characteristics of the composites with the rise in test temperature as mentioned above investigations have been carried out on the microstructures of the longitudinal

FIG. 5.31 SCANNING ELECTRON MICROGRAPH SHOWING A
CRACK ORIGINATING FROM A SHRINKAGE PORO-
SITY WITHIN THE PRIMARY SOLID PARTICLES;
X 2450
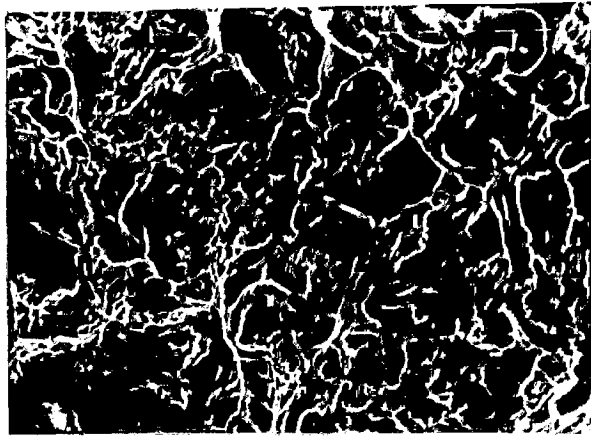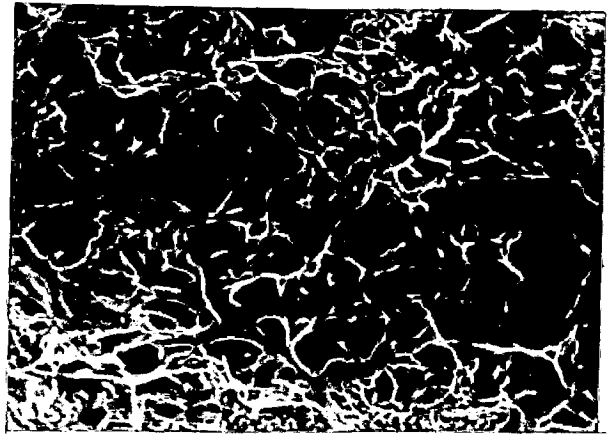
(i) 298 K   (ii) 473 K
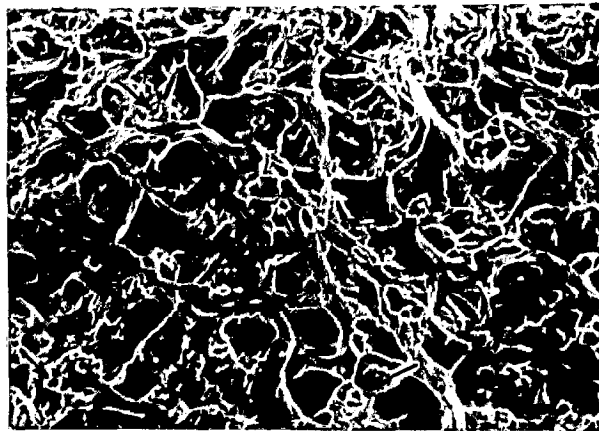
(iii) 573 K

FIG. 5.32 FRACTOGRAPHS OF THE COMPOSITES SHOWING
AN INCREASING EXTENT OF DUCTILE FRACTURE
WITH TEMPERATURE AND A NUMBER OF FINE
DIMPLES (marked by arrow) APPEARING WHEN
TESTED AT 573 K ; X 900

section near the fractured surface of the tensile specimens tested at different temperatures. The optical micrographs of the specimens containing ~ 3.17 vol.% of alumina and ~ 0.2 vol.% of porosity tested at 373 K, 473 K, 573 K and 623 K are shown in Figs. 5.33 (i), (ii), (iii) and (iv) respectively. The microstructures of the specimens tested at 373 K and 473 K show the presence of as cast equiaxed primary particles even after testing as shown in Figs. 5.33 (i) and (ii) respectively. However, in the microstructures of the specimens tested at 573 K and 623 K a large number of newly formed fine grains have been found to exist surrounding the primary solid and alumina particles as shown in Figs. 5.33 (iii) and (iv) respectively. It has also been revealed in Fig. 5.33 (iv) that the newly formed grains become coarser at 623 K than that observed at 573 K as depicted in Fig. 5.33 (iii). The enhanced coarsening of newly formed grains at higher test temperature of 623 K than that observed at 573 K at the particle-matrix interfaces (marked by arrow) have been revealed under the scanning electron microscope as shown in Figs. 5.34 (ii) and (i) respectively.

Figs. 5.28 (iii) and 5.29 show the micrographs of the matrices near and also away from the fractured surface respectively where the coarse recrystallized grains in the region away from the alumina particles (marked by arrow) in a composite tested at 623 K are observed.
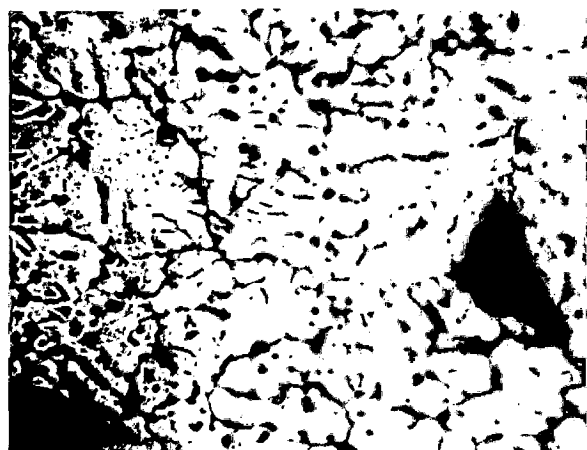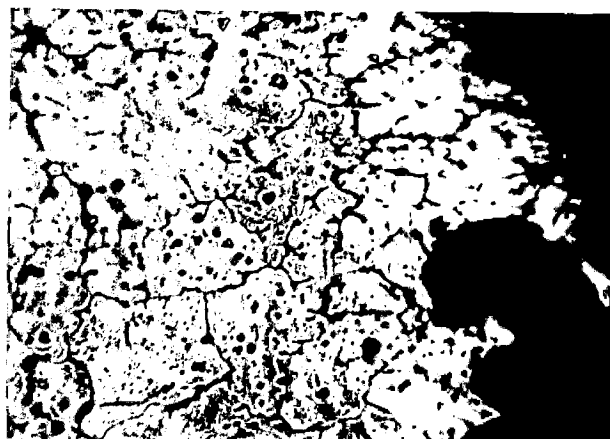
(i)   373 K   (ii)   473 K
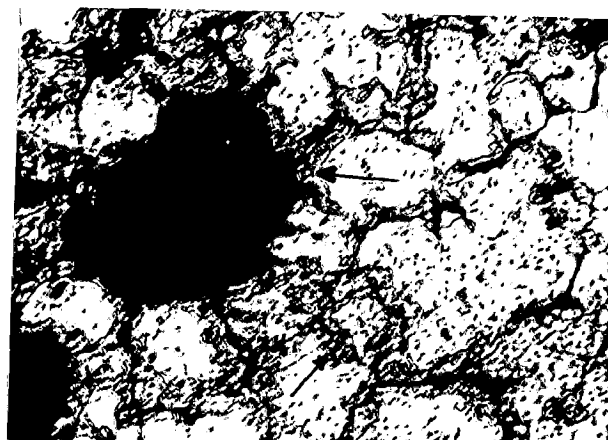
(iii)   573 K   (iv)   623 K

FIG.5.33 OPTICAL MICROGRAPHS OF THE MATRIX NEAR
THE FRACTURED SURFACE OF THE COMPOSITES
SHOWING NO SIGNIFICANT CHANGE WHEN TES-
TED AT 373 K AND 473 K BUT RECRYSTALLI-
ZATION AND GRAIN GROWTH (marked by arrow)
AT 573 K AND 623 K RESPECTIVELY; X 250
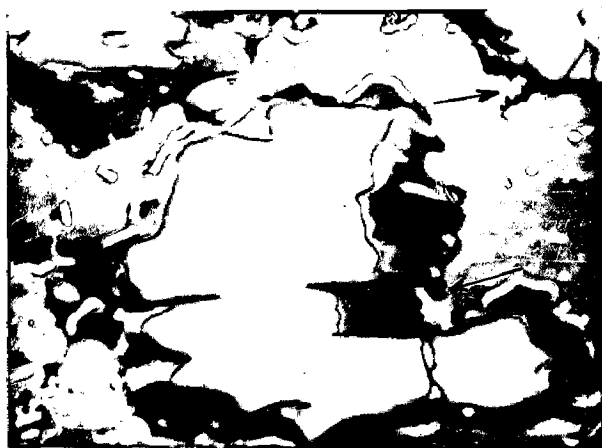
(i)   573 K
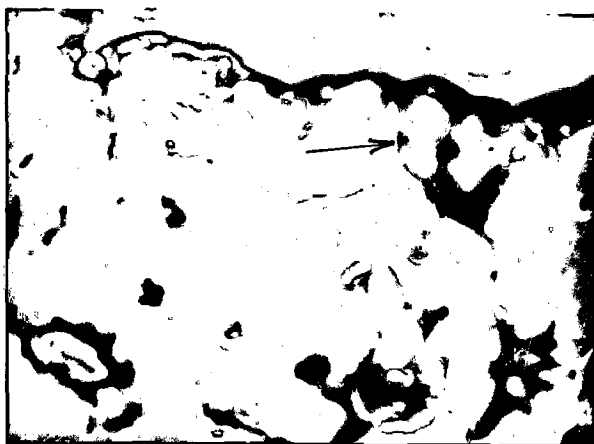
(ii)   623 K

FIG.5.34 SCANNING ELECTRON MICROGRAPH SHOWING
RECRYSTALLIZATION AND GRAIN GROWTH AT
THE PARTICLE -MATRIX INTERFACE (marked
by arrow) AT TEST TEMPERATURES OF 573 K
AND 623 K RESPECTIVELY; X 900

5.3.3　　　DISCUSSION

The linear nature of the ratio of ultimate tensile strength at porosity P to that at zero porosity, σ_p/σ_o, versus volume fraction of porosity plots as shown in Fig. 5.19, for composites containing different volume fraction of alumina lying in the range of 2.0-10.5% tested at elevated temperatures of 473 K and 573 K confirms the applicability of the model equation (5.1) for estimating the contribution of porosity on the elevated temperature tensile strength of the composite. At a given close range of alumina (2.0-2.6 vol.%) content the change in weakening factor, α, of porosity with the increase in test temperature is shown in Fig. 5.19 and is attributed to a modification in plastic flow characteristic of the composite with a change in temperature.

The damaging effect of porosity to the tensile load bearing capacity as discussed earlier in section 5.2.3 takes place by the development of a stress field around and due to it during loading and its extent is governed by the mechanical characteristics of the matrix. The distribution of stress is controlled by the magnitude of flow stress and the dispersion of pores in the matrix. The presence of particles in a composite helps to reduce the deleterious effect of porosity as observed in section 5.2.3. This is accompanied by a lowering of total

elongation causing a reduction in the extent of particle-matrix debonding.

A rise in temperature reduces the flow stress and the material undergoes a substantial plastic flow even around the particles giving rise to a wide spread particle-matrix debonding . Thus, the particles reinforce the weakening effect of porosity at larger elongations observed with the rise of temperature as shown in Fig. 5.20 and also in Fig. 5.23 at the alumina levels below ~ 9.0 vol.%. However, the weakening factor, c , still decreases with an increase in particle content (Fig. 5.20) which indicates the continuing helpful role of particles in modifying the stress distribution around the pores in a positive manner even at elevated temperatures. But a lower weakening factor at elevated temperatures is observed as compared to that at ambient temperature beyond ~ 9.0 vol.% of alumina as shown in Figs. 5.20 and 5.23. A lower c also corresponds to a lower fracture strain at elevated temperatures in comparison to that observed at ambient temperature as shown in Fig. 5.27. The power law relationship between $\ln c$ and $\ln V_{Al_2O_3}$ given in Fig. 5.21 bearing a co-efficient of correlation of the curves in the range of 0.92-0.98 (Table 5.2) further confirms the trends of variation in c with the change in temperature observed in the composites ntaining a given level of alumina lying below and above 9.0 vol.%. From these observations it is clear that c

has a close dependence on the manner of variation of fracture strain. In particulate composites the debonding of the particles from the matrix takes place easily and at ultimate tensile strength the weakening is caused both by the porosity and the voids created by debonding. The extent of debonding is also controlled by the amount of plastic strain the material can undergo and this is again influenced by the particle content. Thus, the particle content helps to reduce the weakening effect and all the factors contributing to an increase in fracture strain enhances the weakening factor.

The nucleation of voids at the particle-matrix interface and its growth leading to the formation of a crack as shown in Fig. 5.30 and causing a progressive deteriotion in load bearing capacity of a composite gets delayed at higher temperature due to lower flow stress causing an extensive plastic flow at the tip of crack to result in its blunting. This delay at higher temperature is reflected in the observed absence of serrations in the tensile stress-strain curve with the rise of temperature as shown in Fig. 5.26. Thus, with an increase in alumina content upto about 9.0 vol.% σ_0 of the composites has been found to reduce slowly at higher temperatures of 473 K and 573 K than that observed at 298 K. As such in the range of alumina content between 4.0-9.0 vol.% σ_0 of the

Composites show a comparatively higher value at 473 K than those obtained when they are tested at 298 K as shown in Fig. 5.22. However, at elevated temperatures of 473 K and 573 K the abrupt lowering of σ_o with the increase of alumina beyond $\sim$ 9.0 vol.% may have been caused by the particles restraining plastic flow in its surrounding zone as it is indicated by a lower fracture strain. This effect may have been further accentuated at higher temperature due to a higher compressive stress around the particles originating from a difference in thermal expansion in the matrix and the particle.

The increase in temperature reduces the strain hardening exponent due to thermally activated deformation leading to flattening-out [139] of stress-strain curve (Fig. 5.26) and gives rise to an improvement in ductility of the composites as revealed in the fractographs presented in Fig. 5.32 where it is observed that the fracture is characterised by the formation of dimples (Fig. 5.32 (ii)) whose size have increased (Fig. 5.32 (iii)) with the rise of temperature from 473 K to 573 K. This may be attributed to the occurrence of recrystallization near the fractured surface observed as the newly formed fine grains [124] in the matrix as revealed in the micrographs presented in Figs. 5.33 and 5.34 and subsequent grain growth at 623 K as shown in Figs.5.33

(iv) and 5.34 (ii). The presence of a significant amount of fine dimples in the fractograph (marked by arrow) as shown in Fig. 5.32 (iii) have possibly resulted from the fracture of recrystallized grains in the composite formed at 573 K. The recrystallization has also contributed to a considerable improvement in ductility of the composites observed at temperatures 573 K and above. An increase in test temperature also enhances the grain boundary sliding giving rise to the formation of voids at the grain boundary at a lower stress. This void formation is further favoured in presence of second phase particles at the grain boundary [140] and initiate grain boundary cracks by the growth and coalesence of voids under a joint action of vacancy diffusion and grain boundary sliding. Due to grain boundary sliding wedge-shaped cracks also initiate at the points of stress concentration as a grain boundary triple points. As a result there is an increase in the extent of nucleation and growth of voids leading to generation of cracks with the rise of test temperature as revealed in the microstructure of matrix near the fractured surface and even in the region away from it at a temperature of 623 K, observed in a composite having ~ 3.6 vol.% alumina as shown in Figs. 5.28 and 5.29 respectively. Further the zones having recrystallization and grain growth at higher temperatures will have a considerably lower

strength but there will be no grain boundary shearing in it. These factors taken together may have caused a drastic fall of σ_0 with the rise of temperature to beyond $\sim$ 500 K. This trend of variation is similar to that of ultimate tensile strength with the rise of its test temperature for a composite with a given alumina content as shown in Fig. 5.25. However, at a given alumina content a slow reduction of σ_0 with an increase in temperature upto 473 K as observed in Fig. 5.24 has been caused by a lowering of flow stress in the matrix.

The recrystallization and grain boundary migration accomodates the stress concentration introduced by straining near grain boundaries and improves the ductility of the composites with the increase of its temperature giving rise to a higher fracture strain (e_f) as shown in Table 5.3. However, this variation of e_f with temperature is particularly marked at lower alumina contents (< 8.98 vol.%) but in composites with higher amounts of alumina an opposite trend of variation of e_f with the rise in temperature is observed due to the resistance of larger number of particles to plastic flow as mentioned earlier in this section.

5.4   SUMMARY

The weakening effect of porosity estimated by the weakening factor, α , on the tensile strength of the composites at ambient and elevated temperatures are analysed by a model equation. The tensile strength of a porosity free given alumina content composite (σ_0) is estimated by extrapolation of its ultimate tensile strength with porosity plot upto zero porosity.

At both the ambient and elevated temperatures the model equation can be safely applied as evident from the linear behaviour of tensile strength ratio (σ_p/σ_0) with porosity. The weakening factor determined from the slope of these tensile strength ratio-porosity plots varies with alumina content of the composite and the temperature used. The increase in alumina content reduces α comparatively slowly at ambient temperature but more rapidly with an increase in test temperature. The increase in test temperature of a composite with given alumina content ($<$ 9.0 vol.%) enhances α but its extent reduces with increasing alumina content. At an alumina content beyond 9.0 vol.% α reduces with the rise of temperature. At ambient temperature with the increase in particle size upto $\sim$ 120 µm α gradually increases but beyond it there is a rapid fall in α with particle size.

The increase of particle content reduces the σ_0 at ambient and elevated temperatures. However, at elevated temperatures the increase of alumina content beyond ~ 9.0 vol.% σ_0 reduces drastically. At a given alumina level the σ_0 decreases slowly with the rise of temperature upto 473 K followed by a rapid fall with a further increase in temperature. The increase in average particle size also reduces σ_0 at ambient temperature.

At ambient temperature the decrease in porosity upto a limit increases linearly the fracture strain, e_f, linearly. A further reduction in porosity does not influence the fracture strain significantly. At higher alumina content the linear behaviour is observed upto a higher porosity and lower fracture strain. At elevated temperature the fracture strain increases when the alumina content is below ~ 9.0 vol.% but beyond this limit it decreases with the rise of temperature.

The fracture of the composite is associated with the particle-matrix debonding and nucleation and coalescence of voids. The higher alumina content favours the extent of void formation.

CHAPTER 6

CONCLUSION

In the present investigation the cast Al-4.0 wt.% Mg-Al$_2$O$_3$ particulate composites have been prepared by vortex method adding superheated alumina particles of wide spectrum of sizes and also of specific sizes into the vortex formed in concentrically stirred freshly alloyed molten Al-4.0 wt.% Mg alloy. The composites fabricated by the vortex method contain different amounts of particles and porosities depending on the levels of process parameters maintained. In this respect the parameters of particular importance are (i) the holding temperature of the melt, (ii) the stirring speed, (iii) the size of the impeller and (iv) the position of the impeller inside the melt whose influence on particle incorporation and porosity content of the composite have been investigated.

The increase in stirring speed, the ratio of the diameter of the impeller (d) to the diameter of the surface of the melt at rest (D) and the ratio of the position of the impeller from the bottom of the crucible(h) to the depth of the melt at rest (H) increases the level of retention of alumina upto a certain limit followed by a reduction with a further increase in the level

of these process parameters. An increase in holding temperature within the partially solid range of the Al-4.0 wt.% Mg alloy reduces the alumina retention in the casting but a further increase beyond the liquidus temperature of the alloy (915 K) does not affect the retention of alumina significantly. For the given design of impeller used in this investigation a maximum retention of alumina in cast composites has been obtained when the process parameters are maintained at the following levels: a stirring speed of 16 revolution.s^{-1}, d/D=0.63, h/H=0.81 and a holding temperature of 900 K. A deviation in these parameters from the optimum values causes a significant difference in alumina retention between the top and the bottom of the ingot. The tendency to clustering of alumina particles increases with the rise in its level of retention. Also, the decrease in particle size increases the tendency to cluster.

The cold model experiment carried out by mixing plastic beads in water confirms the observed trend of retention with stirring speed and size of the impeller. It has also been observed that the exposure of the impeller surface significantly enhances the extent of incorporation of beads into agitated water because the beads fall on the rotating surface of the impeller and enter the liquid after being scattered by the stirrer.

The exposure of the impeller starts at a higher speed of stirring for an impeller of lower d/D ratio. When the stirring speed is lower than its optimum level there is no transfer of beads into water due to non-exposure of the impeller. At a stirring speed higher than the optimum one particles are rejected and sometimes, accumulates at the bottom of the impeller when the vortex comes down below it.

Analysis of the mixing process shows that for all the choices of process parameters in this work the impeller surface has been exposed except during mixing at a holding temperature of 883 K where a large retention of alumina in the slurry has been observed inspite of non-exposure of the impeller possibly due to widespread mechanical entrapping of alumina particles by the primary solid particles in the slurry. The radius of the cylindrically rotating zone (c.r.z.), r_c, of the liquid under a concentric stirring plays an important role over the retention of alumina particles in the slurry. The retention of particles in the slurry increases so long as r_c remains below r_3, the radius of the central solid region of the impeller excluding the blades, because at $r_c > r_3$ the vortex reaches below the impeller due to suction and the particles accumulate there to lower its retention.

The porosity in the composites increases initially with the increase in stirring speed and the values of d/D and h/H ratios upto a certain value followed by a decrease with a further increase in the levels of these variables. The increase in holding temperature reduces the porosity content of the composite. The porosity in the composites increases linearly with the level of retention of alumina indicating that the incorporation of alumina and pores can be attributed to similar processes. The porosity in the composites has primarily resulted from the air bubbles entering the slurry either independently through the suction existing at the vortex or as an envelope to alumina particles. Porosity in the composites exists primarily at the boundary of the primary solid particles caused by evolution of gases and shrinkage during solidification. Sometimes pores have also been observed inside the primary solid particles and at the alumina particle-matrix interface.

The cast structure of the composite is marked by a tendency to form dendrites particularly at the top of the ingot due to solidification of liquid in the slurry inside the mould. The extent of dendritic growth at the top of ingot is controlled by the extent of stagnant layer existing at the crucible wall and it increases with the lowering of holding temperature, stirring speed and size of the impeller. A low holding temperature (883 K) gives rise to formation of large primary solid particles and

coarse dendrites in certain regions where there is hardly any incorporation of alumina particles.

The alumina particles react with the matrix and forms a reacted layer of $MgAl_2O_4$ at particle surface as confirmed by microscopy and X-ray diffraction analysis. The thickness of the reacted layer reduces with an increase in stirring speed and the holding temperature which has been attributed to mechanical removal of these products by agitated melt and by random collisions between the particles. The reacted layers sometimes assume irregular shape under these forces and often have cracks in it generated by differential expansion during cooling.

The tensile strengths of different amount of alumina and porosity content composites confirm the validity of the model linear equation (5.1) between the tensile strength ratio, σ_p/σ_o , and porosity, P , at ambient (298 K) and elevated (473 K, 573 K and 623 K) temperatures where, σ_p, is the tensile strength of a composite with porosity P; σ_o is the tensile strength of pore free composite; α termed the weakening factor is the slope of this equation.

The alumina particles play a helpful role in modification of stress distribution around a pore. An increase in alumina content of the composite upto $\sim$ 7.0 vol.% reduces α significantly. A further increase

in alumina does not affect α in the same manner because an enhanced particle-matrix debonding creates increasing number of voids reinforcing the role of porosities.

The variation of σ_0 with alumina content in a composite also show a similar trend of variation as observed in case of the weakening factor α. The reduction in σ_0 with an increase in alumina content has been explained also on the basis of nucleation of voids by debonding of particle-matrix interface. But, upto 6.5 vol.% of alumina σ_0 of the composite shows a superior strength to that of the matrix. At a given level of porosity the ultimate tensile strength of a composite varies in a similar fashion like that of σ_0 with the alumina content.

At a given alumina content the increase in average particle size from 22 μm to 115 μm increases the value of α a little due to an increase in the extent of particle-matrix debonding due to void nucleation at lower strain. The lowering of α with a further increase in particle size to 195 μm has resulted due to a reduction in stress concentration in the matrix around the particle in bonded or unbonded state . σ_0 of the composites decreases with an increase in particle size possibly because the voids even if nucleated has a lower associated stress concentration due to its larger size. At a given level of alumina content and porosity the ultimate tensile strength of the

composites also varies similarly to σ_0 with the average particle size.

The stress-strain curves at different porosity levels of the composites having $\sim$ 1.92 vol.% alumina show that the composites with a lower porosity content (0.06 vol.%) fails at higher strain than that for composites with a higher porosity content. The observed serrations in the stress-strain curve for composites with lower porosity content indicate that void coalescence takes place over a range of strain. But, at higher porosity content particle-matrix debonding leads to immediate failure.

The presence of a large number of particles leads to a higher rate of nucleation of voids with the increase of strain beyond a critical level (ϵ_N) and causes fracture at lower level of strain. The void nucleating strain, ϵ_N, of a composite with a higher alumina content ($\sim$ 8.9 vol.%) is comparatively lower than that observed in a composite with lower alumina content ($\sim$ 2.12 vol.%).

When the porosity is above a critical level depending on the alumina content of the composite, the engineering fracture strain increases linearly with a decrease in porosity. The critical level of porosity increases with an increase in alumina content in a composite. The fracture strain increases with a decrease

in alumina content and a low fracture strain results in a better correlation with porosity by limiting the contributions of voids due to a reduced extent of debonding at lower fracture strain. The fracture strain reduces more with a lowering cf porosity in a composite with a higher alumina content which reflects ~~still~~ the presence and role of voids created by debonding but the failure of the composite is caused primarily by the growth and coalescence of the existing pores. Below the critical level the fracture strain does not correlate with porosity possibly because at lower porosity level the failure of the composite is primarily caused by nucleation, growth and linkage of voids created by debonding.

At elevated temperatures of 473 K and 573 K the weakening factor, α , falls more sharply with an increase in alumina content in comparison to that observed at ambient temperature (298 K) for composites having alumina varying from 1.0 to 10.5 vol.%. This may have been possible because there is an increase in fracture strain at elevated temperature and the particles cause a larger reduction in fracture strain than that at ambient temperature. Thus, the presence of particles becomes more effective at higher temperature due to a reduction in the extent of particle-matrix debonding and α reduces with the increase of alumina more quickly at higher temperature.

The substantial plastic flow due to lower flow stress at higher temperature giving rise to a wide spread particle-matrix·debonding enhances α_c with a rise in temperature from 298 K to 623 K for a composites having alumina below ~ 9.0 vol.%. As mentioned earlier α_c has a close dependence on the variation of fracture strain. The fracture strain of a composite increases or decreases with temperature when the alumina content lies below or above ~ 9.0 vol.% of alumina respectively. Accordingly, α_c also increases or decreases depending on alumina content below or above ~ 9.0 vol.% because the extent of particle-matrix debonding is determined by the plastic strain in the matrix.

At higher temperature there is an increase in uniform strain and the coalscence of voids to result in cracks may take place at higher strain. Thus, the rate of reduction of σ_0 with alumina content should be lower than that observed at ambient temperature. However, with the increase of alumina beyond ~ 9.0 vol.% the fracture strain reduces with temperature and σ_0 falls abruptly. It may have been caused by restraints to plastic flow imposed by a stress arising due to a difference in thermal expansion between the particle and the matrix.

An increase in test temperature flattens-out the stress-strain curve due to a reduction in strain

hardening exponent of the matrix. This flattening behaviour is significant at temperatures above 573 K where a recrystallization of the matrix takes place.

In a composite with a given alumina content σ_0 reduces slowly with the rise of temperature upto 473 K due to a lowering of flow stress and other high temperature effects like grain boundary sliding. But at a further higher temperature of 573 K and above recrystallization drastically reduces σ_0.

In the vortex method the influence of various process parameters on the retention of alumina particles in the cast particulate composite may help in identifying the critical parameters for control in large scale production of cast particulate composite. The required amount of alumina in a $Al-4.0\,wt.\%\,Mg-Al_2O_3$ composite can be obtained by maintaining suitable levels of process variables like the holding temperature, stirring speed, size of the impeller and the position of the impeller inside the melt. However, the level of porosity, as it appears can not be independently controlled. Also, the distribution of particles characterized by its tendency of clustering can not be varied independently. The mechanical properties of these composites will be determined by particle content, its distribution and the porosity

content. Since the particle content decides the levels of the other variables it is not possible to obtain a broader range of mechanical properties which could have been possible if these variables could have been varied independently.

REFERENCES

1. Dexter, H.B., "Composite Components on Commercial Air Craft", AGARD NATO, (CP-288), p. 22, April (1980).

2. Levitt, A.P., "Whisker Technology", 1st ed., Wiley Interscience, N.Y., p. 245, (1970).

3. Rack, H.J. and Niskanen, P.W., "Extrusion of Discontinuous Metal Matrix Composites", Light Met. Age, Vol. 42, p. 9, Feb. (1984).

4. Kiuchi, M., Sugiyama, S. and Endo, N., "Experimental Study of Metal Forming in Mashy State, VI-Production and Working of Particle Reinforced Clad Metals by Mashy State Process", J. Jpn. Soc. Technol. Plast., Vol. 24 (274), p. 1113, Nov. (1983).

5. Rohatgi, P.K. and Surappa, M.K., "Deformation of Graphite During Hot Extrusion of Cast Aluminium/Silicon/Graphite Particle Composites", Mater. Sci. Eng., Vol. 62, p. 159, Feb. (1984).

6. Riggs, D. M. and Gillis, P., "The Effect of Mechanical Working on SiC Whisker Reinforced Aluminium Alloy", US Army Materials and Mechanics Research Center, AD-AO 87565, p. 19, April (1980).

7. Yuasa, E. and Morooka, T., "Hot Extrusion of an Aluminium Composite Containing Dispersed Graphite Particles", J. Jpn. Soc. Technol. Plast., Vol. 22 (244), p. 482, May (1981).

8. Kiuchi, M. and Sugiyama, S., "Production and Mechanical Property of Clad Metals Laminated with Particle-Reinforced Composite Metal and Ceramic Powder", Proc. Conf., Mechanical Behaviour of Materials-IV, Stockholm, Sweden, 15-19 Aug., Vol. 2, p. 10 23, (1983).

9. Kainer, K.U., Bergmann, H.W. and Mordike, B.L., "Powder Metallurgically Produced Metal-Glass Composites", Powder Metallurgy, Vol. 26, No.1, p. 30, (1984).

10. Jangg, G., Kutner, F., and Huppmann, W.J., "Sintering-forging Dispersion Hardened Aluminium Materials", Proc. Conf., 7th Int. Light Metals Congress, Looben/Vienna, 22-26 June (1981).

11. Misra, P.S. and Upadhyaya, G.S., "Properties of Sintered Aluminium Dispersed with Titanium and Tungsten Carbides", The Int. J. of Powder Metallurgy and Powder Technology, Vol. 11, No. 4, p. 129, (1975).

12. Demisenko, E.T. et al., "Mechanical Properties of Dispersion Strengthened Cu-Al₂O₃ Materials", Sov. Powder Metall. Met. and Ceram., Vol.19, No.4, p. 265, (1980).

13. Sablet de, P. and Accary, A., "Comparison Between Powder Metallurgy and Competitive Process for the Mass Production of Structural Parts", Powder Metallurgy Int., Vol. 9, No. 3, p. 131, (1977).

14. Schreiner, H., "A Comparison of Potential and Limits of Foundry and Sintering Technology", Powder Metallurgy Int., Vol.10, No. 3, p. 140, (1978).

15. Ray, S., "Fabrication of Aluminium-Alumina Particulate Composite by Foundry Technique", M.Tech. Dissertation, Indian Institute of Technology, Kanpur, (1969).

16. Williams, D.N., Roberts, J.W. and Jaffe, R.I., "Modern Castings", Vol.37, p. 81, (1960).

17. Mehrabian, R., Rick, R.G. and Flemings, M.C., "Preparation and Casting of Metal Particulate Non-metal Composites", Met. Trans., Vol.5, p. 1899, (1974).

18. Mehrabian, R., Sato, A. and Flemings, M.C., "Cast Composites of Aluminium Alloys", The Light Metals, Vol. II, p. 177, (1975).

19. Rohatgi, P.K., Ranganathan, N. and Shetty, H.R., "The Use of Metal Coated Refractory Powders to Make Particulate Composites by Infiltration", Composites, Vol. 9, No.3, p. 153, (1978).

20. Surappa, M.K. and Rohatgi, P.K., "Preparation and Properties of Cast Aluminium/Ceramic Particle Composites", J. Mater. Sci., Vol.16, No.4, p. 983, (1981).

21. Deonath, N.I. and Rohatgi, P.K., "Cast Aluminium Alloy Composites Containing Copper Coated Ground Mica Particles", J. Mater. Sci., Vol.16, No.6, p. 1599, (1981).

22. Krishnan, B.P., Surappa, M.K. and Rohatgi, P.K., "The UPAL Process: A Direct Method of Preparing Cast Aluminium Alloy/Graphite Particle Composites", J. Mater. Sci., Vol 16, No.5, p. 1209, (1981).

23. Abdul-Lattef, N.I., Khedar, A.R.I., Goel, S.K., "Preparation of Al-Al₂O₃-MgO Cast Particulate Composites Using MgO Coating Technique", J. Mater. Sci., No.4, p. 385, (1985).

24. Badia, F.A. and Rohatgi, P.K., "Dispersion of Graphite Particles in Aluminium Castings Through Injection of the Melt", Trans. of AFS, Vol.77, p. 402, (1969).

25. Goetzel, C.G., "Cermets", edited by S.R. Tinkelpough and W.B. Crandell, Reinhold Publishing Corporation, p. 73, (1960).

26. Chandra, K., Ray, S. and Goel, D.B., "Development of Al-base Cast Composites by Internal Oxidation", Proc. Solidification and Casting of Metals, Dept. of Metallurgical Engineering, University of Roorkee, India, p. 21, Oct. (1984).

27. Quigley, B.F., Abbaschian, G.J., Wunderlin, R. and Mehrabian, R., "A Method for Fabrication of Aluminium-Alumina Composites", Met. Trans., Vol.13A, p. 93, (1982).

28. Levi, C.G., Abbaschian, G.J. and Mehrabian, R., "Interface Interactions During Fabrication of Aluminium Alloy-Alumina Fiber Composites", Met. Trans., Vol.9A, p. 697, (1978).

29. Flemings, M.C., and Mehrahian, R., "Casting Semi-solid Metals", Transactions of the International Foundry Congress, Moscow 1973, Trans. of AFS, Vol.81, p. 81, (1973).

30. Flemings, M.C., Rick, R.G. and Young, K.P., "Rheocasting Processes", AFS Int. Cast Metals Journal, Vol.1, No.3, p. 11, Sept., (1976).

31. Mehrabian, R., Hosking, F.M., Protillo, F.F. and Wunderlin, R., "Structure and Deformation Characteristics of Rheocast Metals", Illinois University, AD-A086469, p. 95, March, (1980).

32. Zantout, B., Das, A.A. and Franklin, J.R., "Squeeze-cast Aluminium Matrix Composite: Strength at Higher Temperature", Proc. Conf. The Metallurgy of Light Alloys, Loughborough University, England 24-26, March, p. 215, (1983).

33. Hosking, F.M., Portillo, F.F., Wunderlin, R. and Mehrabian, R., "Comosites of Aluminium Alloys: Fabrication and Wear Behaviour", Jl. of Materials Science, Vol.17, No.2, p. 477, (1982).

34. Bhansali, J.K. and Mehrabian, R., "Abrasive Wear of Aluminium-matrix Composites", Jl. of Metals, Vol. 34, No.9, p. 30, (1982).

35. Pai, B.C., Ray, S., Prabhakar, K.V. and Rohatgi, P.K., "Fabrication of Aluminium-alumina (Magnesia) Particulate Composites in Foundries Using Magnesium Additions to the Metls", Materials Science and Engineering, Vol. 24, p. 31, (1976).

36. Semenchenko, V.K., "Surface Phenomena in Metals and Alloys", Edited by R. Kennedy (English translation), Pergamon Press, p. 61, (1961).

37. Ermenko, V.N., "Physiocochemical Bases of the Formation of Cermets", Proc. Conf., The Role of Surface Phenomena in Metallurgy, edited by V.N. Ermenko, Consultants Bureau, New York, p. 1, (1963).

38. Verwey, E., in Coll: "Semi Conducting Materials", Edited by V.I. Tuchkevich (Russian translation), IL, p. 201, (1954).

39. Mott, N., and Gurney, R., "Electronic Process in Ionic Crystals", IL, (1950).

40. Vol'kenshtein, F.F., "Electrical Conductivity of Semi Conductors" (in Russian), Gostekhizdat, (1947).

41. Semenchenko, V.K., "Surface Phenomena in Metals and Alloys", Edited by R. Kennedy (English translation), Pergamon Press, p. 303, (1961).

42. Semenchenko, V.K., "Surface Phenomena in Metals and Alloys", Edited by R. Kennedy (English translation) Pergamon Press, p. 152, (1961).

43. Semenchenko, V.K., "Surface Phenomena in Metals and Alloys", Edited by R. Kennedy (English Trannslation), Pergamon Press, p. 312, (1961).

44. Ermenko, V.N., Soc. J. of Powder Metallurgy, p. 208, (1965).

45. Brewer, L. and Searcy, A.W., "Gaseous Species of the $Al-A_2O_3$ Systems", J. American Chemical Society, Vol. 73, No.11, p. 5308, (1951).

46. Carnahan, R.D., Johnson, T.L. and Li, C.H., "Some Observations on the Wetting of Al_2O_3 by Aluminium", J. Amer. Ceram. Soc., Vol.41, p. 343, (1958).

47. Champion, J.A., Keene, B.J. and Sillwood, J.M., "Wetting of Aluminium Oxide by Molten Aluminium and Ohter Metals", J. of Materials Science, Vol. 4, p. 39, (1969).

48. Brennan, John J. and Pask, Joseph, A., "Effect of Nature of Surfaces on Wetting of Sapphire by Liquid Aluminium", J. American Ceramic Society, Vol.51, p. 569, (1968).

49. Wolf, S.M., Levitt, A.P., and Brown, J., "Whisker-metal Matrix Bonding", Chem. Eng. Progr., Vol.62, No.3, p.74,(1966).

50. Kubaschewski, O., and Hopkins, B.E., "Oxidation of Metals and Alloys", Butterworths, London, (1962).

51. Mykura, H., "Solid Surfaces and Interfaces", Routledge and Kegan Paul, London, (1966).

52. Munitz, A., Metzger, M. and Mehrabian, R., "The Interface Phase in $Al-Mg/Al_2O_3$ Composites", Met. Trans., Vol. 10A, No.10, p. 1491, (1979).

53. Semenchenko, V.K., "Surface Phenomena in Metals and Alloys", Edited by R. Kennedy (English translation) Pergamon Press, p. 371, (1961).

54. Tressler, R.E., "Composite Materials", 1st ed., Vol. I, Academic Press, New York, (1974).

55. Golland, D.I., and Beevers, C.J., "An Aluminium-α-Alumina Composite", J. Mater. Sci.,Vol. 7, p. 716, Letters (1972).

56. Champion, A.R., Kreuger, W.H., Hartmann, H.S., and Dhingra A.K., "Fiber Reinforced Metal Matrix Composites", Second Int. Conf. on Composite Materials, Toronto, Canada, (1978).

57. Löhberg, K., Procd. Conf., Second European Symposium on Material Sciences in Space, Frascati, Italy, April, p. 375, (1976).

58. Imich, G., "Method of Preparing Composite Products Containing Metallic and Non-metallic Materials", U.S. Patent No.2, 793, 949, May 28, (1957).

59. Herald, C.D., and Seruggs, D.M., "Method of Producing Dispersion Strengthened Metals", U.S. Patent No.3, 468, 658, September 23, (1969).

60. Goddard, D.M., "Interface Reactions During Preparation of Aluminium-matrix Composites by the Sodium Process", J. Mater. Sci., Vol.13, No. 9, p. 1841, (1978).

61. Haginoya, I., and Fukusako, T., "Oxidation of Molten Al-Mg Alloys", Trans. Japan Inst. of Metals, Vol. 24, No. 9, p. 613, (1983).

62. Badia, F.A., "Dispersion of Oxides and Carbides in Aluminium and Zinc Alloy Castings", Trans. of AFS, Vol. 79, p. 347, (1971).

63. Badia, F.A., Macdonald, D.F., and Pearson, J.R., "Graphitic-Al New Method of Production and Some Foundry Characteristics", Trans. AFS, Vol 79, p. 265, (1971).

64. Mahar, R.L., Jakes, R., and Bruch, C.A., "Behavior or Study of Saphire Wool Aluminium and Aluminium Alloy Composites, Technical Report AFML-TR-68-100, May, (1968).

65. Mehan, R.L., and Feingold, E., J. of Materials, Vol. 2, p. 239, (1967).

66. Mehan, R.L., "Metal Matrix Composites", STP 438, ASTM, p. 29, (1968).

67. Mehan, R.L., "Fabrication and Mechanical Properties of Sapphire Whisker/Aluminium Composites", J. Composite Materials, Vol. 4, No.1, p. 90, (1970).

68. Presnov, V.A.,"Physicochemical Nature of Bonds Between Dissimilar Materials", Procd. Conf., The Role of Surface Phenomena in Metallurgy, edited by V.N. Ermenko, Consultants Bureau, New York, p. 92, (1963).

69. Levitt, A.P., "Whisker Technology", 1st ed., Willey Intr. Science, N.Y., p. 245, (1970).

70. Weyl, W.A., Proc. No. 46, ASTM, p. 506, (1946).

71. Katz, G.,"Thin Solid Films", Vol. 33, p. 99, (1976).

72. Metcalfe, A.G., and Klein, M.J., "Composite Materials", 1st ed., Vol. I, p. 125, Academic Press, New York, (1974).

73. Nagata, S., "Mixing Principles and Applications", John Wiley & Sons, New York, p. 1, (1975).

74. Nagata, S., "Mixing Principles and Applications", John Wiley & Sons, New York, p. 125, (1975).

75. Nagata, S., "Mixing Principles and Applications", John Wiley & Sons, New York, p. 250, (1975).

76. Rushton, J.H. and Oldshue, J.Y., Chem. Engg. Progr. Symp. Series, Vol. 55, No. 25, p. 181, (1955).

77. Spencer, D.B., Mehrabian, R., and Flemings, M.C., "Rheological Behaviour of Tin-15% Lead in the Crystallization Range", Met. Trans., Vol. 3, p. 1925, (1972).

78. Mehrabian, R., and Flemings, M.C., Trans. AFS, Vol. 80, p. 173, (1972).

93. Devies, R.G., "The Deformation Behaviour of a Vanadium Strengthened Dual Phase Steel", Met. Trans. Vol. 9A, p. 41, (1978).

94. Devies, R.G., "The Mechanical Properties of Zero Carbon Ferrite-Plus-Martensite Structures", Met. Trans., Vol. 9A, p. 451, (1978).

95. Devies, R.G., "Influence of Martensite Composition and Content on the Properties of Dual Phase Steels", Met. Trans., Vol. 9A, p. 671, (1978).

96. Koo, J.Y., Young, M.J. and Thomas, G., "On the Law of Mixtures in Dual-Phase Steels", Met. Trans., Vol. 11A, p. 852, (1980).

97. Öström, P., "Deformation Models for Two-Phase Materials", Met. Trans., Vol. 12A, p. 355, (1981).

98. Ashby, M.F., "Work Hardening of Dispersion-Hardened Crystals", Phil. Mag., Vol. 14, p. 1157, (1966).

99. Ashby, M.F., Z. Metallk., Vol. 55, p. 5, (1964).

100. Balliger, N.K. and Gladman, T., "Work Hardening of Dual-Phase Steel", Metal Science, Vol. 15, p. 95, (1981).

101. Brown, L.M. and Stobbs, W.M., "The Work Hardening of Copper-Silica Equilibrium Plastic Relaxation by Secondary Dislocations", Phil. Mag., Vol. 34, p. 351.

102. Lanzilloto, C.A.N. and Peckering, F.B., "Structure-Property Relationship in Dual Phase Steels", Metal Science, Vol. 16, p. 371, (1982).

103. Fisher, J.R. and Gurland, J., "Void Nucleation in Spheroidized Carbon Steels Part 2: Model", Metal Science, Vol. 15, p. 193, (1981).

104. Hippsley, J.R. and Druce, S.G., "The Influence of Phosphorous Segregation to Particle-Matrix Interface on Ductile Fracture in a High Strength Steel", Acta. Met., Vol. 31, p. 1861, (1983).

105. Goods, S.H. and Brown, L.M., "The Nucleation of Cavities by Plastic Deformation", Acta. Met., Vol. 27, p. 1, (1979).

106. Tanaka, K., Mori, T. and Nakamura, T., "Cavity Formation at the Interface of a Spherical inclusion in Pastically Deformed Matrix", Phil. Mag., Vol. 21, p. 267, (1970).

107. Palmer, I.G. and Smith, G.C., "Oxide Dispersion Strengthening", Gordon and Breach, New York, ed. G.S. Ansell et. al., p. 253, (1968).

108. Edolson, B.I. and Baldwin, W.M., Trans. ASM, Vol. 55, p. 230, (1962).

109. Gurland, J. and Plateau, J., "The Mechanism of Ductile Rupture of Metals Containing Inclusions", Trans. ASM, Vol. 56, p. 442, (1963).

110. Inoue, T. and Kinoshita, S., "Mechanism of Void Initiation in the Ductile Fracture Process of a Spheroidized Carbon Steel", Procd., The Microstructure and Design of Alloys, 3rd Int. Conf. on the Strength of Metals and Alloys, Cambridge, England, 20-25 Aug., Vol. I, p. 159, (1973).

111. Rogers, H.C., "Ductility", ASM, Ohio, p. 31, (1968).

112. Lindley, T.C., Oates, G. and Richards, C.E., "Effect of Second-Phase Particles on the Mechanical Properties of Steel", Iron and Steel Institute, London, (1971).

113. Easterling, K.E.., Fischmeister, H.F. and Navara, E., Met. Sci., Journal, Vol. 6, p. 211, (1972).

114. Pickering, F.B., Int Conf. on Toward Improved Ductility and Toughness, Kyoto, Japan, p. 9, (1971).

115. McClintock, F.A., "Ductility", ASM, Ohio, p. 255, (1968).

116. McClintock, F.A., "A Criterion for Ductile Fracutre by the Growth of Holes", J. Appl. Mech., Vol. 35, p. 363, (1968).

117. Rice, J.R. and Tracey, D.M., "On the Ductile Enlargement of Voids in Triaxial Stress Fiels", J. Mech. Phys. Solids, Vol. 17, p. 201, (1969).

118. LeRoy, G., Embury, J.D., Edward, G. and Ashby, M.F., "A Model of Ductile Fracture Based on the Nucleation and Growth of Voids", Acta. Met., Vol. 29, p. 1509, (1981).

119. Brown, L.M. and Embury, J.D., "The Initiation and Growth of Voids at Second Phase Particles", The Microstructure and Design of Alloys (Procd. ICSMA 3), Inst. Metals, London, Vol. 1, p. 164, (1973).

120. Gladman, T., Holmes, B. and McIvor, I.D., "Effect of Second Phase Particles on the Mechanical Properties of Steel", Iron & Steel Institute, London, (1971).

121. Schmitt, J.H. and Jalinier J.M., "Damage in Sheet Metal Forming-I Physical Behaviour", Acta Met., Vol. 30, p. 1789, (1982).

122. Hunn, D.L., "SEM Fractographic Analysis of Metal/Matrix Composites Exposed to Elevated-Temperature, Short Duration Environments", Mechanical Behaviour of Metal/Matrix Composites, Proc. Conf., Dalas, Tex., USA, Dr. Warrendale; Pa. 15086, p. 83, (1983).

123. Mondolfo, L.F., "Aluminium Alloys Structure and Properties", Butter Worths, London-Boston, p. 314, (1979).

124. Takasugi, T. and Izumi, O., "High Temperature Strength and Ductility of Polycrystalline Co_3Ti" Acta Metall., Vol. 33, No.1, p. 39, (1985).

125. Kent, R. Van Horn, "Aluminium", Vol I, 4th ed., ASM, p. 280, (1971).

126. Chalmers, B., "Principles of Solidification", John Wiley & Sons, (1964).

127. Nagata, S., "Mixing Principles and Applications", John Wiley & Sons, p. 63, (1975).

128. Mukherjee, P.C., "Fundamentals of Metal Casting Technology", Oxford & IBH, p. 234, (1979).

129. Govier, G.W. and Aziz, K., "The Flow of Complex Mixtures in Pies", Van Nostrand Reinhold Company, p. 98, (1972).

130. Kievits, F.J. and Prabhakar, K.V., "Rheocasting (stir-casting) of Aluminium Alloy", Proc. Symposium on Quality Control of Engineering Alloys and the Role of Metal Science", Delft., p. 203, (1978).

131. Apaydin, N., Prabhakar, K.V. and Doherty, R.D., "Special Grain Boundaries in Rheocast Al-Mg", Mater. Sci. and Engg., Vol. 46, p. 145, (1980).

132. Vogel, A., Doherty, R.D. and Cantor, B., "Stir-Cast Microstructure and Slow Crack Growth", Proc. Conf. Solidification and Casting of Metals, Sheffield, p. 518, (1979).

133. Nagata, S., Mixing Principles and Applications, John Wiley and Sons, New York, p. 251, (1975).

134. Prasad, P.R., "Microstructure and Mechanical Properties of Rheocast Aluminium-Copper Alloys", Ph.D. Thesis, Deptt. of Met. Engg., University of Roorkee-247 667, India, (1983).

135. Ghosh, P.K., Prasad, P.R. and Ray, S., "Effect of Porosity on the Strength of Particulate Composites", Z. Metallkde., Vol. 75, H. 12, p. 934, (1984).

136. Sergeenkova, V.M., Dubinin, V.P. and Osasyuk, V.V., Poroshkovaya Met., No.6, p. 81, (1969).

137. Knott, J.F., Fundamentals of Fracture Mechanics, Chap. 8, Butterworths, London, (1973).

138. Edelson, B.I. and Baldwin, W.M., Trans. Am. Soc. Metals, Vol. 55, p. 230, (1962).

139. Dieter, G.E., "Mechanical Metallurgy", 2nd ed., McGraw Hill Kogakusha, p. 355, (1976).

140. Dieter, G.E., "Mechanical Metallurgy", 2nd ed., McGraw Hill Kogakusha, p. 241, (1976).

APPENDIX

COPY OF PAPERS PUBLISHED FROM THIS INVESTIGATION

1. Ghosh, P.K., Ray, S., Rohatgi, P.K., "Incorporation of Alumina Particles in Aluminium-Magnesium Alloy by Stirring in Melt", Trans. Japan Inst. Met., Vol. 25, No.6, p. 440, (1984).

2. Ghosh, P.K., Prasad, P.R., Ray, S., "Effect of Porosity on the Strength of Particulate Composites", Z. Metallkde., p. 934, December (1984).

3. Ghosh, P.K., Ray, S., "Effect of Porosity and Alumina Content on the Mechanical Properties of Compocast Aluminium Alloy-Alumina Particulate Composite.", J. Mater. Sci., Vol. 21, No.5,, p. 1667, (1986).

Incorporation of Alumina Particles in
Aluminium-Magnesium Alloy by Stirring in Melt*

By P. K. Ghosh**, S. Ray** and P. K. Rohatgi***

The impact of process parameters like temperature, the dimension and the position of an impeller on the incorporation of Al_2O_3 particles in cast Al-Mg alloy has been investigated. The maximum incorporation level of Al_2O_3 particle is achieved by dispersing the Al_2O_3 particles in the semi-solid alloy by the impeller with a diameter 0.63 times as large as that of the crucible at stirring speed of 16 revol. s^{-1}. The optimal position of the impeller has been found to be 0.81 times as large as the depth of the liquid at rest from the bottom of the crucible. Incorporation of Al_2O_3 particles increased with the decrease of melt temperature between the solidus and the liquidus temperature under given stirring speed, dimension and position of the impeller. Model experiments have been conducted with water and poorly wetting plastic beads, in order to find an explanation for the role of the above variables. An estimate of the porosity in the cast alloy indicates a linear increase with the amount of Al_2O_3 particles incorporated.

I. Introduction

The foundry technique of making alloy particulate composite is a more direct and simpler process than the other techniques of making composites by mechanical mixing and sintering or infiltration. In the foundry technique the particles are directly added to the molten base alloy, and the resulting slurry is cast by a suitable process. The major difficulty of this process is poor wettability of most of the ceramic particles (e.g. alumina, graphite etc.) due to the molten alloy which makes the incorporation and retention of the particles in the liquid extremely difficult. Prior coating[1] of the ceramic particles and the introduction of wetting agents[2][3] in the molten metal prior to the addition of particles have improved the wettability. A number of experiments[4][5] of contact angles as a function of temperature in the aluminium-alumina system indicate that the temperature of aluminium melt will above the liquidus improves the wettability of alumina

* This work form s a part of Ph D. Thesis work of P. K. Ghosh.
** Department of Metallurgical Engineering, University of Roorkee, Roorkee-247667, India.
*** Regional Research Laboratory, Bhopal-462026, India.

by molten aluminium. Preheating of ceramic particles prior to addition into the melt has been found [6][7] effective in retaining the particles into the melt by improving wettability. However, in all previous attempts[1][2][6][7] it has been observed that a significant amount of particles is not retained in the liquid metal at temperature above the liquidus due to rejection of the particles to the surface of the aluminium alloy melt. It has been observed[8] that when the particles are added in vigorously agitated partially solid aluminium alloy melt the added particles collide with the particles of primary solid phase imparting kinetic energy and momentum in random directions. Thus the residence time of the ceramic particles is enhanced due to successive collisions, and the incorporation of these particles in liquid metal increases giving rise to a better mixing.

A systematic investigation of the parameters influencing the mixing has not yet been undertaken. In earlier studies of making composites by the foundry technique, maintenance of suitable mixing conditions has been found important for incorporation of particles or short fibres inside the melt. In this work an effort has been made to optimise the mixing parameters for the incorporation of alumina particles in partially solid aluminium alloy melt so as to achieve the maximum incorpora-

tion of the particles in the melt and a homogeneous dispersion.

II. Experimental

1. Apparatus and procedure

Stirring speed, impeller diameter, position of the impeller inside the melt and the holding temperature are the process variables whose impact on the amount of incorporation and distribution of alumina particles in the composite is under investigation. The schematic diagram of the experimental set-up used in this investigation is shown in Fig. 1. It consists of a graphite crucible inside a resistance heating verticle muffle furnace having a bottom pouring arrangement. The crucible has a bottom hole 12 mm in diameter plugged with a graphite stopper. A stirrer having capacity to rotate up to 66.6 revolution·s^{-1} has been used. The speed of the stirring is varied as per requirements by controlling the voltage. Flat four blades mild steel impellers of different diameters

Fig. 1   Schematic diagram of the experimental set-up.

having a thickness of 3.0 mm are used. The impellers are threaded to the mild steel shaft 9.8 mm in diameter.

The speed of the stirrer is measured with a strobometer. The surface diameter of the melt with the stirrer dipped into it is measured by a divider. The position of the impeller inside the melt is varied by adjusting the shaft length of the stirrer. The depth of the impeller from the surface of the melt and the depth of the liquid are estimated by dipping a graduated scale into the melt. The temperature of the melt is measured using a potentiometer and by a chromel-alumel thermocouple placed 15–20 mm inside the melt.

Commercially pure aluminium of about 500 g is melted in the crucible and heated to 1005 K. Magnesium is added to the melt at different temperatures between 980–1005 K according to the variation in pouring temperature. The surface of the melt is cleaned by skimming. To minimise the dissolution of the impeller by way of precaution, the stirrer is introduced into the melt, when the melt temperature comes down to 20–30 K above the pouring temperature. The melt is agitated vigorously at different speeds as per requirements. The temperature of the furnace is allowed to drop slowly until the melt reaches the desired pouring temperature. Alumina particles approximately round in shape with the size range, mentioned in Table 1, preheated to 1072 K are added to the vortex formed on the melt surface at the rate of 1.66–2.5 g/s. Stirring is continued for 225–240 s after the addition of particles to the melt. During this period the temperature of the slurry is kept within ±5 K of the pouring temperature. The slurry is poured in a 25 mm × 30 mm × 300 mm steel mould by removing the graphite stopper from the bottom of the crucible, and the ingot is quenched immediately by spraying water. During pouring the
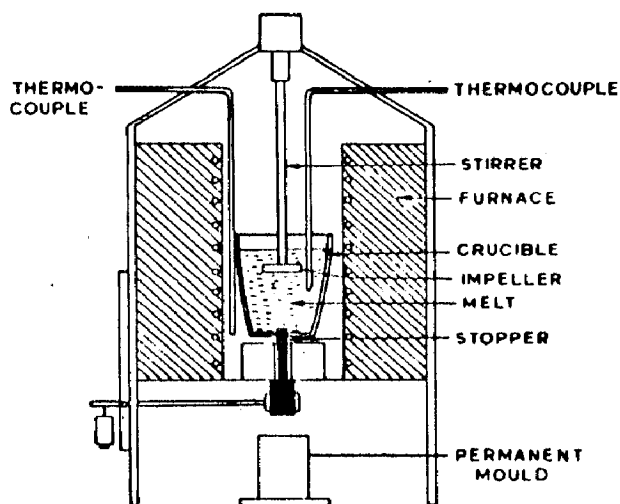
Table I   Distribution of various sizes of particles in the alumina powder used.

	Size of the alumina particles (μm)								
	+212	+180, −212	+125, −180	+106, −125	+75, −106	+63, −75	+53, −63	+45, −53	−45
Amount mass%	0.31	49.37	13.90	31.56	1.87	1.73	0.33	0.15	0.78

stirring is continued.

2. Metallography

Metallographic specimens are prepared both from the bottom and the top of the castings obtained to observe the distribution of the alumina particles on the matrix. Dark spots observed on the matrix of the composite are the alumina particles and the voids. The area fraction of the particle and the voids is measured under optical microscope at $\times 50$ magnification by the point counting method. For a random distribution of particles and voids the area fraction is numerically equal to volume fraction, V_a.

3. Estimation of particle and void content

The density of the cast particulate composite, ρ_{mes}, is determined by the usual weight loss method, and the density of Al–4 mass%Mg, ρ_{Al-Mg}, is taken[9] as 2.65 g/cm³. The theoretical density of the composite, ρ_{Th}, is defined assuming that there are no voids in the composite.

$$\rho_{Th} = V_a\rho_{Al_2O_3} + (1 - V_a)\rho_{Al-Mg}, \qquad (1)$$

where, $\rho_{Al_2O_3}$, is the density of alumina. The value of $\rho_{Al_2O_3}$ is measured to be 3.012 g/cm³. The measured density of the particulate composite can be expressed as

$$\rho_{mes} = (1 - V_a)\rho_{Al-Mg} + V_{Al_2O_3}\rho_{Al_2O_3}, \qquad (2)$$

where $V_{Al_2O_3}$, is the volume fraction of alumina in the composite. Since V_a includes both voids and alumina particles,

$$V_a = V_{Al_2O_3} + V_v, \qquad (3)$$

where V_v is the volume fraction of void. Combining the eqs. (1), (2) and (3), the following equation for estimating V_v is obtained as below.

$$V_v = \frac{\rho_{Th} - \rho_{mes}}{\rho_{Al_2O_3}}. \qquad (4)$$

Substituting the value of V_v for eq. (3), the value of $V_{Al_2O_3}$ is obtained. From $V_{Al_2O_3}$ the weight fraction of alumina in the composite is calculated.

III. Results and Discussion

In the present investigation it should be noted

that the particle incorporation has been measured from the microstructure of the solidified metal-particulate composite and so it is not truly characteristic of the mixing process taking place in liquid metal because a part of the particles incorporated might have been rejected during solidification in the mould. However, the particle rejection in the mould is observed to be minimum, because the growth of already solidified phase results in a network entrapping the remaining liquid containing the dispersed particles. Also, the use of permanent metallic mould results in a velocity of the solidification front far greater than the critical velocity, above which the particles are entrapped by the advancing solidification front. In any case the particles finally incorporating in the solid alloy is the parameter of our interest. Figure 2 shows the variations of incorporated alumina with the speed of stirring for a definite position of the impeller at a height ratio, $h/H = 0.81$, when h is the position of the impeller from the bottom of the crucible and H is the depth of the liquid at rest in the crucible. It is observed that increasing the speed of the stirrer leads to a larger suction at the vortex and the incorporation of alumina increases up to about 16 revolution·s⁻¹. But increasing the speed further leads to a lowering of incorporation up to 25 revolution·s⁻¹. Figure 3 shows the variation of porosity in casting with the increase in incorporated alumina. An almost linear increase in porosity is observed with the increase in incorporated alumina. This result indicates a
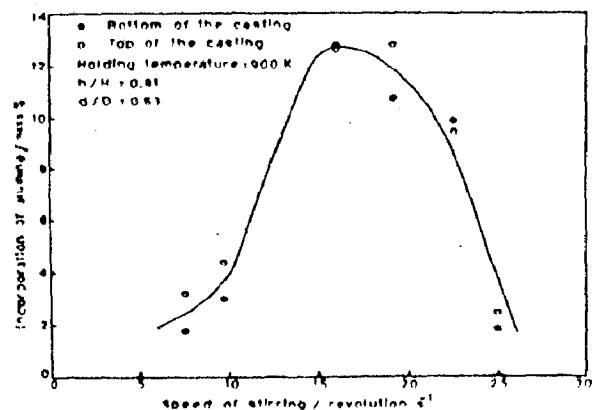

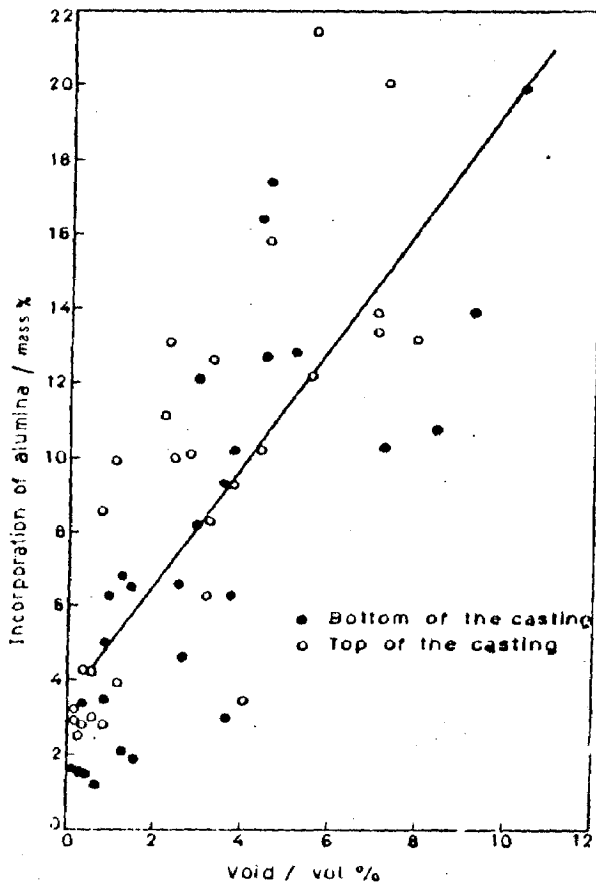Fig. 2 Variation of alumina incorporation with the speed of stirring.

Fig. 3 Variation of porosity in casting with the increase of alumina incorporation.

Fig. 4 Variation of alumina incorporation with the position of the impeller.

simultaneous suction of air and alumina in the vortex. A cold experiment with water and solid particles indicates that air may be incorporated by the suction of bubbles in the forced vortex region when the speed of the stirrer exceeds a critical value. However the air may also enter the liquid as a thin envelop surrounding the solid particles. Since the present investigation has been conducted using a different range of speed of the stirrer, it is not clear as to which mechanism is causing the increase in void with speed. However, a linear correlation between the extent of void and the particle incorporation tends to indicate that probably the formation of air envelop is responsible for the creation of voids. It is also interesting to note in Fig. 2 that the alumina incorporated at the top and that at the bottom of the castings indicated
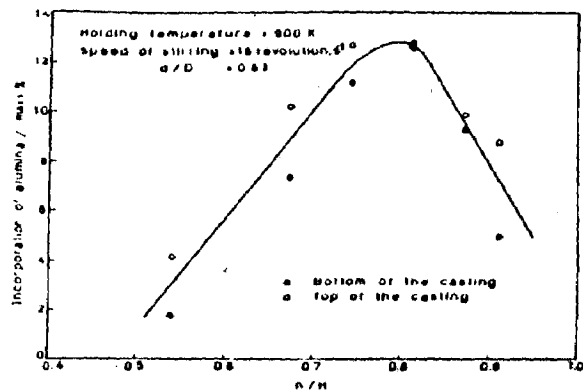
respectively by open and close circles does not differ significantly at the point of maximum incorporation. Figure 4 shows the variation of incorporated alumina with the position of the impeller. As h increases, the incorporation also increases till $h/H = 0.81$ is achieved, but beyond it the incorporation drops. The difference in distribution of alumina between the top and the bottom of the castings increases, as we go away from the optimum position where the maximum incorporation has been achieved. Experiments conducted with poorly wetting plastic beads and water indicate that the height of the liquid at the centre falls as the speed of the stirrer increases. If the speed is enhanced to the extent in which a part of the stirrer is exposed, the particles floating on the liquid surface are drawn towards the centre and fall on the exposed rotating stirrer. These particles thus gain an inertial centrifugal force enabling them to enter the liquid. This inertial force is so high that the particles impinge further on the surface of the container and get distributed throughout. However, if the speed of the stirrer is further increased so that the liquid surface appears below the stirrer, a fluid motion carrying the particles towards this surface of the liquid is observed to occur along the vertical axis and to result in particles getting attached to this rotating interface contributing to a sharp decrease in particle incorporation. Figure 5 shows that with the increase in holding temperature of the melt between the solidus and the liquidus temperature of Al–4.0 mass%Mg
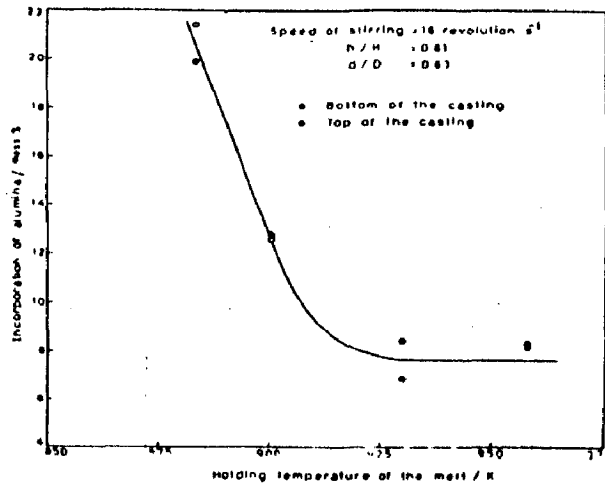
Fig. 5 Varia'ion of alumina incorporation with the holding temperature of the melt.
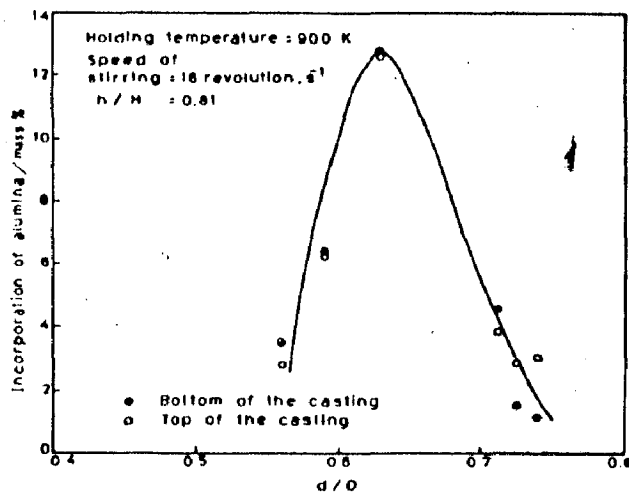

Fig. 6 Variation of alumina incorporation with the diameter of the impeller.

alloy the incorporation of alumina reduces. This clearly establishes the helpful role of the proeutectic α-solid in the slurry whose amount decreases with the increase in holding temperature. In an effort to optimise the diameter ratio,

d/D, where d is the diameter of the impeller and D is the diameter of the crucible at the surface of the melt, several impellers with varying diameter, d, have been used at 16 revolution·s^{-1} and at $h/H = 0.81$ to optimise the amount of incorporation. Figure 6 shows that at an optimum $d/D = 0.63$, a maximum incorporation of alumina of about 12.78 mass% has been achieved. In model experiments using impellers of various d/D values it has been observed that the partial exposure of the impeller leading to incorporation of plastic beads inside the water is achieved at higher speed of stirring with the decrease of d/D value for a given position of the impeller inside the water. But for a given speed of stirring the extent of incorporation of plastic beads decreases, when d/D deviates from an optimum value. For large d/D the particles are observed to strike the wall of the vessel and to reflect back to the surface of the vortex reducing the incorporation in the bulk of the liquid.

REFERENCES

(1) F. A. Badia and P. K. Rohatgi: Trans. Am. Foundrymen's Soc., 79 (1969), 402.
(2) B. C. Pai, S. Ray, K. V. Prabhakar and P. K. Rohatgi: Mat. Sci. and Eng., 24 (1976), 31.
(3) A. R. Champion, W. H. Kreuger, H. S. Hartman and A. K. Dhingra: 2nd Int. Conf. on Composite Materials, Toronto, Canada, (1978).
(4) John J. Brennan and Joseph A. Pask: J. Am. Ceramic Soc., 5 (1968), 569.
(5) J. A. Campion, B. J. Keene and J. M. Sillwood: J. Mater. Sci., 4 (1969), 39.
(6) V. Agarwal and D. Dixit: Trans. Japan Int. Metals, 22 (1981), 521.
(7) Shiv Omkar Singh: M. E. Thesis, Deptt. of Met. Eng., University of Roorkee, India, (1980).
(8) R. Mehrabian, A. Sato and M. C. Flemings: The Light Metals, II (1975), 177.
(9) Kent R. Van Horn: Aluminium, I, 4th ed. ASM, (1971), p. 280.

Effect of Porosity on the Strength of Particulate Composites

Prakriti K. Ghosh*, Priya R. Prasad**, and Subrata Ray*

(* Department of Metallurgical Engineering, University of Roorkee, Roorkee – 247667, India, and ** Department of Metallurgical Engineering, Bihar Institute of Technology, Sindri, India)

Theoretical analysis of the effect of uniformly distributed spherical pores on the tensile strength has been presented. The analysis predicts a linear dependence of tensile strength on porosity in the low porosity regime and provides a two parameter formal equation suitable for fitting experimental data. The experimental data for Al-4% Mg alloy plus alumina particulate composites confirm the theoretical findings. Increasing the alumina content in these composite has been found to decrease the weakening effect of pores due to decrease in the size of weakened zone around the pores in the matrix.

Einfluß der Porosität auf die Festigkeit von Teilchenverbunden

Es wird eine theoretische Analyse des Einflusses gleichmäßig verteilter spherischer Poren auf die Zugfestigkeit vorgestellt. Die Analyse sagt eine lineare Abhängigkeit der Zugfestigkeit von der Porosität im Bereich niederer Porosität voraus und liefert eine formale Zweiparameter-Gleichung zur Anpassung experimenteller Werte. Die experimentellen Daten für einen Teilchenverbund aus Al-4%Mg-Legierung mit Aluminiumoxid bestätigen die Theorie. Es wurde gefunden, daß eine Erhöhung des Aluminiumoxidgehalts in diesen Verbunden den Schwächungseffekt der Poren erniedrigt, weil die Größe der geschwächten Zonen um die Poren in der Matrix verringert wird.

Porosity is a common defect inherent to castings and composite materials and is known to cause considerable deterioration of mechanical properties. The quantitative influence of porosity on mechanical properties is governed by its shape, size, distribution and volume fraction. The shape, size and distribution are usually not fully controllable during processing and therefore, it is a common practice to correlate the mechanical properties directly to the volume fraction or the total porosity[1] to [4]).

Besides reduction in the effective cross sectional area, an important effect by which a material is weakened by the presence of pores is the damage caused to the local load-bearing capacity of the material due to stress concentration near the pores. In the development of a quantitative relationship between porosity and material strength the need to examine the role of such weakened zones around the pores cannot be over-emphasized. The mathematical modelling of the problem will require at least three parameters to represent (i) the reduction in the cross section due to absence of the material, (ii) the geometry of the pore determining the extent of reduction in the capacity of load bearing in the layer next to the pore, and (iii) the ability of the material to recover its load bearing capacity as reflected in the size of the weakened zone. This study assumes special significance in case of two-phase materials, such as composite materials, due to possible interaction of the second phase with the weakened zones in the matrix. In this communication therefore, a theoretical analysis of material weakening vis-a-vis weakened zones around uniformly distributed pores of volume equal to that of the equivalent sphere has been presented and the validity of the analysis has been examined on the basis of experimental data for Al-4% Mg alloy + alumina particulate composites.

Theoretical Analysis

Consider a specimen of cross-sectional area A_0 subjected to a tensile force F. If the specimen contains randomly distributed pores of average effective radius R_v, the number of pores per unit area, N_A, on a planar section equals $3V_p/2\pi R_v^2$, where V_p is the volume fraction of pores. The total number of pores on the cross-section of the specimen is therefore equal to $3V_pA_0/2\pi R_v^2$.

Now, let the cross-section of the specimen be divided into the same number of cells as the number of pores with an average cell radius R such that each cell shares a pore of average effective radius r_p in the plane of cross-section considered. Figure 1 depicts the structure of such a cell. It has been assumed that beyond a distance R_p, the damage by the pore has no influence and the material is bearing as much load as it would have done without the pore. It is generally not possible to define R_p precisely but in order to construct a workable model it is assumed that $R_p = n\,r_p$. The parameter n is greater than one and depends largely upon the inherent ability of the material to recover its load bearing capacity away from the pore.

The load bearing capacity of the material decreases as one approaches closer to the pore. Also, the functional form of the force $f(r)$ carried by unit area of the material should be so chosen that it satisfies the condition, $f(r) = k\sigma_m$ at $r = r_p$ and $f(r) = \sigma_m$ at $r = R_p$ (fig. 1), where σ_m is the uniform stress outside the weakened zone, k is a weakening factor and r is the radial vector from the origin of the pore on the plane of interest perpendicular to the applied load. The magnitude of k is limited to $0 < k < 1$ which depends upon the geometry of the pore. Within the weakened zone, the $f(r)$ should have a cylindrical symmetry due to the nature of application of force in the tensile test. The following mathematical form chosen for $f(r)$ satisfies the physical criteria outlined above,

$$f(r) = \sigma_m\, k\, \exp\left(-\ln k \cdot \frac{r-r_p}{R_p-r_p}\right) \tag{1}$$

From eq. (1) the force df carried by an element dr within zone A may be calculated as,

$$df = 2\pi r \, dr \, \sigma_m \, k \, \exp(-\ln k \cdot \frac{r-r_p}{R_p-r_p}) \tag{2}$$

Integration of eq. (2) within the limits $r = r_p$ to $r = R_p$ gives the total force f_A carried by zone A. Thus,

$$f_A = 2\pi \, \sigma_m \, r_p^2 \left[(n-1) \, (\frac{k-1}{\ln k}) + (n-1)^2 \left\{ \frac{k-1}{(\ln k)^2} - \frac{1}{\ln k} \right\} \right] \tag{3}$$

The force f_B carried by zone B of the cell is given by,

$$f_B = \sigma_m \, \pi \, (R^2 - R_p^2) = \sigma_m \, \pi \, (R^2 - n^2 r_p^2) \tag{4}$$

The total force F applied to the specimen is obtained by adding eq. (3) and (4), and multiplying by the total number of cells on the cross section. Thus,

$$F = 3V_p \, A_o \, \sigma_m \, \frac{r_p^2}{R_v^2} \left[(n-1) \, (\frac{k-1}{\ln k}) + (n-1)^2 \left\{ \frac{k-1}{(\ln k)^2} - \frac{1}{\ln k} \right\} \right]$$

$$+ \frac{3}{2} \, V_p A_o \, \sigma_m \, (\frac{R^2}{R_v^2} - n^2 \frac{r_p^2}{R_v^2}) \tag{5}$$

r_p^2/R_v^2 and R^2/R_v^2 can be determined experimentally. For a random distribution of equal sized pores, however, it can be shown that $r_p^2 R_v^2 = 2/3$ and $R^2/R_v^2 = 2/3V_p$. Putting these values in eq. (5) and rearranging we get,

$$\frac{F}{A_o} = \sigma_m - \sigma_m \left[n^2 - 2(n-1) \, (\frac{k-1}{\ln k}) - 2(n-1)^2 \right.$$

$$\left. \left\{ \frac{k-1}{(\ln k)^2} - \frac{1}{\ln k} \right\} \right] V_p \tag{6}$$

It is now assumed that the material fails when σ_m equals σ_o, the tensile strength of the pore free material. The tensile strength of the material containing pores is given by $\sigma_p = F/A_o$ and therefore eq. (6) may be rewritten as,

$$\frac{\sigma_p}{\sigma_o} = 1 - \left[n^2 - 2(n-1) \, (\frac{k-1}{\ln k}) - 2(n-1)^2 \right.$$

$$(\frac{k-1}{(\ln k)^2} - \frac{1}{\ln k}) \left] \frac{P}{100} \right. \tag{7}$$

Where P is the total porosity in percent.

If the coefficient of porosity term is represented by a, eq. (7) may be written as,

$$\frac{\sigma_p}{\sigma_o} = 1 - aP \tag{8}$$

a represents the magnitude of weakening for each percent of porosity and depends upon n and k. Figure 2 shows the iso-weakening diagram which reveals that for the same weakening effect i.e. same a value, a number of combinations of n and k values exist and therefore, it is not possible to obtain the values of n and k straightforward even if the value of a is experimentally known. Nevertheless, fig. 2 is significant in that it illustrates that for a given value of n the maximum weakening i.e. a_{max} is fixed and is independent of k.

The above analysis provides us with a two parameter formal equation for fitting the experimental data. This highly simplistic model equation predicts that the variation of tensile strength with porosity is linear because the non-linearity arising out of interaction between the pores have been neglected. The limiting porosity level upto which this model is valid can be readily found out by imposing the condition $R_p = R$. Since $r_p^2/R_v^2 = 2/3$ and $R^2/R_v^2 = 2/3V_p$, the limiting porosity level P_c for the validity of the equation (7 or 8) may be given by,

$$P_c = 100/n^2 \tag{9}$$

For the case $R_p > R$, the pore-pore interaction takes place and therefore for porosity greater than P_c, the model will not apply.
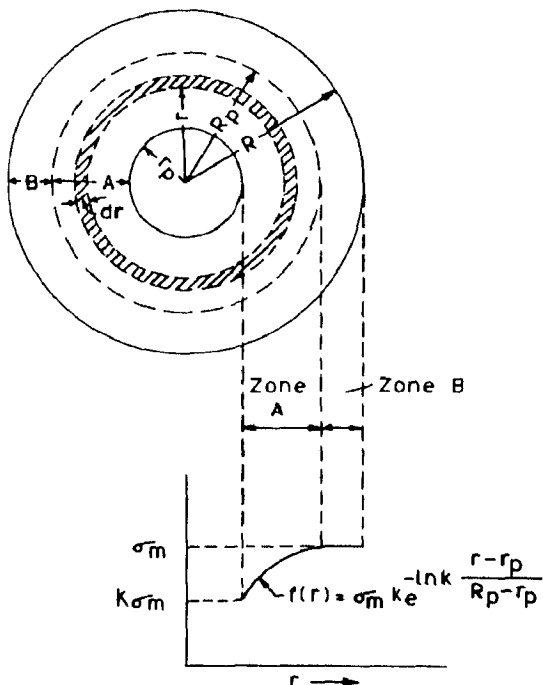

Fig. 1. Variation of load bearing capacity of material near a pore on a planar section perpendicular to the direction of applied force.
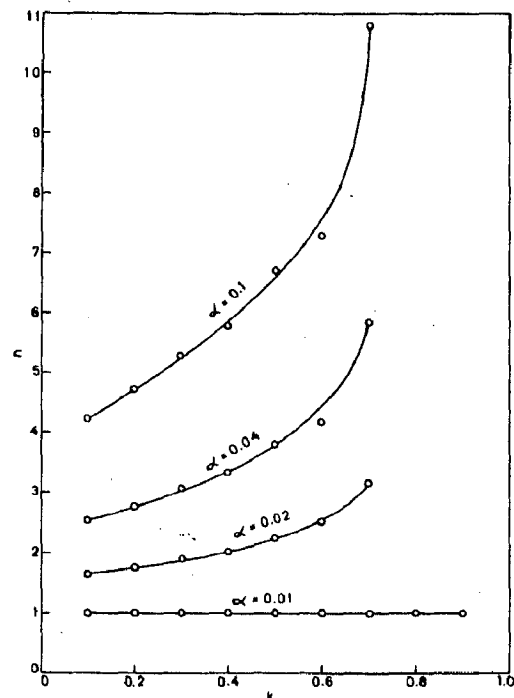

Fig. 2. Iso-weakening diagram.

Application of the Model

The validity of the model has been examined on the basis of experimental data obtained for various Al-4% Mg alloy + alumina particulate composites. For making the composites, commercial purity aluminium was melted in a graphite crucible and required amounts of magnesium chips were added to the melt. After all the magnesium dissolved, the melt was vigorously stirred with a mechanical stirrer at speeds varying from 400 to 1500 r.p.m. and the melt was allowed to cool through the solidification range of the alloy during stirring. At 900 K, within the liquidus and the solidus temperatures of the alloy, alumina particles of average 160 μm size preheated at 1072 K were added to the vortex formed in the melt due to stirring. After stirring for 240 s, the melt was cast by pouring it directly into a 25 × 30 × 300 mm³ laboratory scale ingot mould made of steel. A typical microstructure of the cast composite is shown in fig. 3. The chemical analysis of the Al-Mg alloy matrix revealed the average composition as 4.0 % Mg, 0.98 % Fe, 0.3 % Si, 0.05 % Mn, 0.01 % Ti and balance Al. The volume fraction of alumina particles was determined by "point counting" method with suitable modification to account for the amount for porosity[5]. Suitable tensile test specimens were machined out from each casting and the tensile tests were performed on a Hounsfield tensiometer.
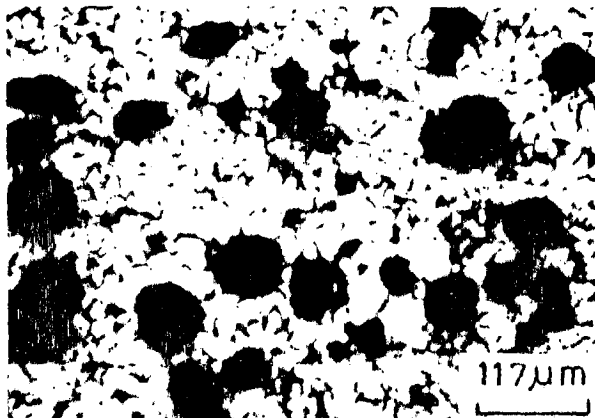

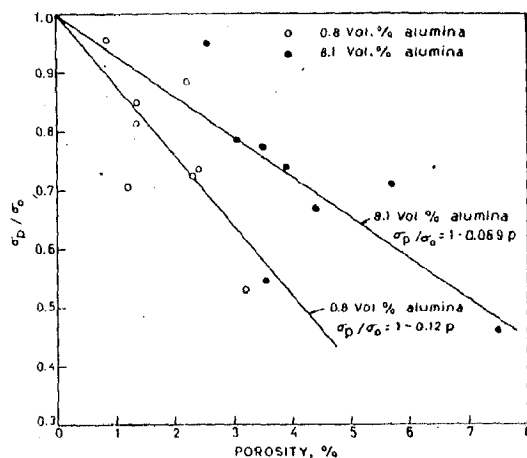Fig. 3.   Optical micrograph of Al-4% Mg alloy + alumina particulate composite.

On the basis of the data obtained as above, plots between ultimate tensile strength, σ_p, versus % porosity, P, were made and extrapolated to zero porosity value to get σ_0 values for each alumina content. σ_p/σ_0 values were then calculated and plotted against porosity values. Figure 4 depicts typical σ_p/σ_0 versus P plots for composites containing 0.8 and 8.1 vol.% alumina and shows that the tensile strength of these composites is a linear function of porosity content. The linear nature of these curves is in accordance with the model eq. (8) and therefore, the validity of the theoretical analysis presented in the preceding section is confirmed. The slope of these curves gives the values of a of eq. (8) and is a measure of the weakening effect of the pores.
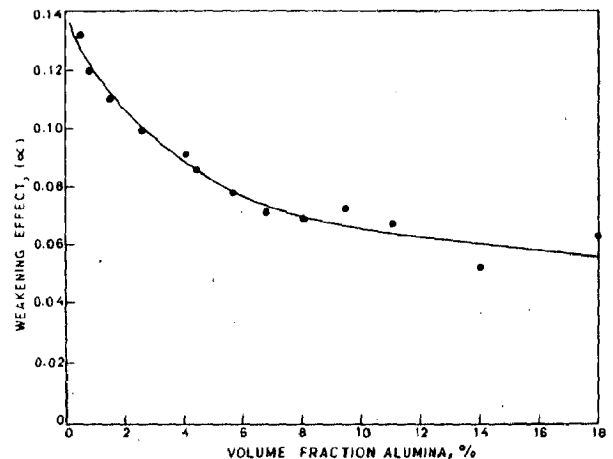

Fig. 5.   Effect of alumina content on the weakening effect of pores in Al-4% Mg alloy + alumina particulate composites.

Figure 4 further reveals that the value of a is lower for higher alumina content. In fig. 5, a values have been plotted against alumina content. It shows that increasing the alumina content lowers the weakening effect of pores. The role of alumina content in lowering the weakening effect may be explained in the light of iso-weakening diagram given in fig. 2. The weakening effect a is dependent upon both the parameters n and k, however, n being primarily dependent upon the inherent characteristics of the material, the change in alumina content of the composite may be assumed to cause change in the parameter n only. It follows therefore, that the decrease in the weakening effect a with increasing alumina content is related primarily to the decrease in parameter n. Such a result is obvious since each pore finds larger number of stronger alumina particles at closer distances limiting the weakened zone in the matrix if alumina content in the composite is increased.

Conclusions

1.   Theoretical analysis reveals that the tensile strength is a linear function of porosity content in the low porosity regime, the critical porosity level below which the analysis is valid being $100/n^2$ where n defines the weakened zone around the pores.

2.   Experimental data for Al-4% Mg alloy + alumina particulate composites confirm the linear dependence of strength on porosity.

Fig. 4.   Effect of porosity on the tensile strength of Al-4% Mg alloy + alumina particulate composites.

3. Increase in the alumina content decreases the weakening effect of pores by limiting the size of weakened zones around the pores in the matrix.

Literature

[1] L. J. COHEN and O. ISHAI, Compos. Mater. 1 (1967) 390.

[2] G. H. GESSINGER, H. MEITZLAR, P. ESPER, and H. E. EXNER, Third European Powder Metallurgy Symposium, Conference Suppl., Part I (1971) 298.

[3] K. RADHAKRISHNA, S. SESHAN, and M. R. SESHADRI, Trans. Ind. Inst. of Metals 34 (2) (1981) 169.

[4] J. K. MACKENZIE, Proc. Phys. Soc. B63 (1950) 2.

[5] P. K. GHOSH, S. RAY, P. K. ROHATGI, to be published, Trans. Japan Inst. Metals 6 (1984).

Effect of porosity and alumina content on the mechanical properties of compocast aluminium alloy–alumina particulate composite

P. K. GHOSH, S. RAY
Department of Metallurgical Engineering, University of Roorkee, Roorkee 247667, India

The effects of the size and volume fraction of alumina particles and of the porosity on the tensile strength of Al 4 wt% Mg alumina compocast particulate composite have been investigated. The contribution of porosity to the reduction in strength of the composite at various levels of alumina content is expressed as a linear function of porosity containing two experimentally determined parameters: σ_0, the ultimate tensile strength at zero porosity level, and x, a weakening factor. For a composite containing a lower level (< 7 vol %) of alumina particles, a rapid decrease in the value of σ_0 is observed with an increase in the volume fraction of alumina. The rate of reduction in strength slows down at higher alumina levels in the composite. An increase in particle size is found to reduce the value of σ_0. The value of x is found to decrease with an increase in the volume fraction of alumina in the composite. For a given alumina content the increase in average particle size from 22 to 115 μm is found to push the value of x up a little, followed by a significant decrease with an increase in particle size to 195 μm. The role of porosity in the engineering fracture strain e_f of the composite is found to increase almost linearly with the inverse of porosity above a critical level. For composites with a given level of porosity, e_f is found to increase with an increase in the alumina content of the composite.

1. Introduction

The mechanical properties of compocast particulate composites are very sensitive to the volume fraction of porosity, to the shape, size and distribution of the reinforcing particles, and to their content in the composite. The volume fraction of particles in the composite can be controlled by using suitable process parameters [1] but the porosity cannot be regulated during the process. So far, the mechanical properties of castings have been correlated with the volume fraction of porosity present through a phenomenological model, and verified experimentally for compocast aluminium alloy alumina composites with a given content of alumina particles [2].

In the present study we have investigated the effects of size and volume fraction of alumina particles with both narrow and wide spectra of sizes on the tensile strength of Al 4 wt% Mg alumina compocast particulate composite. The contribution of porosity in reducing the strength is estimated at different levels of alumina content and the projected ultimate tensile strength at zero porosity level is determined. The variation of the strength with alumina content is reported. The role of porosity in the initiation of fracture in these composites is examined.

2. Experimental details

Commercial-purity aluminium of about 500 g was melted in a graphite crucible and the required amount of about 25 g of magnesium lump was added to the melt. The melt was vigorously stirred mechanically at different speeds in the range of 400 to 1500 r.p.m. During stirring the melt was allowed to cool through the solidification range of the alloy until the desired pouring temperature was attained. In different castings, preheated alumina particles with the following size ranges: (+ 6, − 45), (+ 53, − 75), (+ 106, − 125), (+ 180, − 212) μm, and one with a broad spectrum of sizes as mentioned in Table I, were added at the pouring temperature which lies in the semi-solid region of the alloy at a temperature of 900 K. The alumina particles were preheated to 1072 K before adding to the vortex formed on the melt surface by stirring. After the addition of particles the slurry was continuously stirred for 3.75 to 4 min and the temperature was maintained within ± 5 K of the pouring temperature. The slurry was then poured into a 25 mm × 30 mm × 300 mm steel mould through the bottom of the crucible by removing the graphite stopper, and the ingot was cooled immediately by spraying water on it. The Al Mg alloy matrix had the following chemical composition: 4% Mg, 0.08% Fe, 0.3% Si, 0.05% Mn, 0.01% Ti and balance aluminium.

Suitable metallographic samples from both the bottom and top of each casting were prepared using standard metallographic procedures. The specimens were observed under an optical microscope for estimation of the alumina-particle and porosity contents of the composite. The particle matrix interface was examined under a scanning electron microscope.

Size of alumina particles (μm)	+212 +180	212 +125, 180 +106, -125	+75, -106	+63, -75	+53, -63	+45, -53	-45
Amount (wt %)	0.31	49.37	13.90	31.56	1.87	1.73	0.33	0.15	0.78

Tensile specimens of the dimensions shown in Fig. 1 were machined from each casting. The volume fraction of alumina particles in each specimen was determined by the point counting method and by using the observed density [1] to calculate the amount of porosity. Tensile tests were carried out on a Hounsfield tensometer at ambient temperature.

Polished and unetched sections perpendicular to the fractured surface of the tensile specimens were observed under a scanning electron microscope. The true strain, ε, at any location in the fractured specimen corresponding to the zone under observation was estimated by measuring the diameter of the specimen at that location as viewed under a scanning electron microscope.

3. Results

A typical distribution of alumina particles in a composite having about 13 vol% particles is shown in Fig. 2. The relation between the standard deviation of the measured volume percentage of particles in a given sample of composite having a specified amount of alumina particles and its porosity content is given in Fig. 3.

The reinforced alumina particles in the composites are found to be well bonded with the matrix, as shown in the scanning electron micrograph in Fig. 4. However, the debonding of alumina particles from the matrix is observed during tensile deformation of the composites. Typical void formation by debonding is depicted in Fig. 5. In this figure it is observed that a large number of voids have been nucleated in the matrix of the composite, at a strain level of about $\varepsilon = 0.325$, during tensile deformation. The path of a crack initiated in a specimen containing ~ 2.75 vol % alumina and fractured under tensile loading is shown in Fig. 6. The formation of a reacted layer of irregular shape around an alumina particle is shown in Fig. 7. The reacted layer is possibly $MgAl_2O_4$, which has been found to form under similar circumstances [3].

The effect of porosity content on the behaviour of the engineering stress–strain curve of a composite having ~ 1.92 vol % alumina is shown in Fig. 8.

The ultimate tensile strength, σ_p, at different volume percentages of porosity, P, was obtained for samples containing a known amount of alumina particles. Our earlier investigation [2] amply justifies the assumption

of linear behaviour of σ_p with P in this class of materials, in spite of the scatter observed. The scatter is attributed to the limitations of a one-parameter model in describing the shape and size distribution of the pores affecting the ultimate tensile strength. However, it should be noted that the correlation coefficient was found to be better than 0.85 in the earlier investigations. A linear least-squares fit of the observed σ_p with P was carried out following the model equation proposed earlier [2]:

$$\sigma_p/\sigma_0 = 1 - xP \qquad (1)$$

where σ_0 is the ultimate tensile strength at zero porosity for each alumina content and x is the weakening factor of the pores. The variation of x with alumina content is depicted in Fig. 9. It is observed that the value of x decreases with an increase in the volume fraction of alumina in the composite.

Fig. 10 shows the relationship between the particle content and the tensile strength at zero porosity, σ_0, for different composites containing alumina particles having a wide range of sizes as given in Table I. The value of σ_0 is found to decrease rapidly with an increase of the volume fraction of alumina, up to around 7% in the composite. A further increase in the volume fraction of alumina content up to around 18% is found to reduce the tensile strength of the composite very slowly.

The value of σ_0 is found to decrease with an increase in the average particle size from 22 up to 195 μm for composites containing a fixed amount (~ 8.62 vol %) of alumina, as shown in Fig. 11. The magnitude of the corresponding weakening factor x is found to increase a little with an increase in the average particle size from 22 to 115 μm, followed by a significant decrease with further increase in particle size to 195 μm as shown in Fig. 12.

In Fig. 13 the engineering fracture strain, e_f, is plotted against the reciprocal of the percentage of porosity content in composites with a given amount of volume fraction of alumina particles having a broad
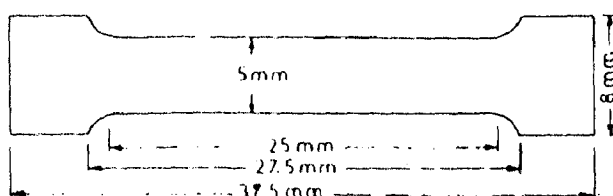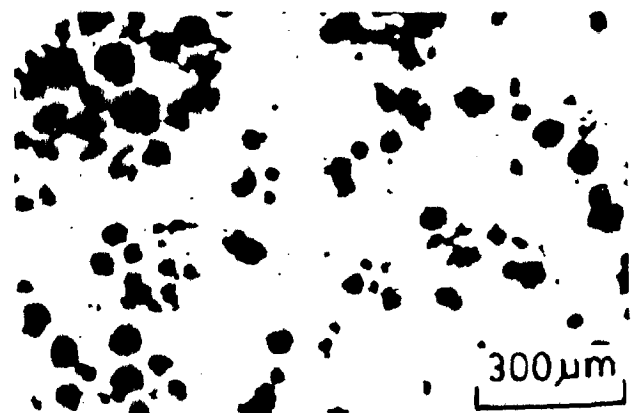

Figure 1 Dimensions of the tensile specimen.

Figure 2 Typical distribution of alumina particles in the composite.
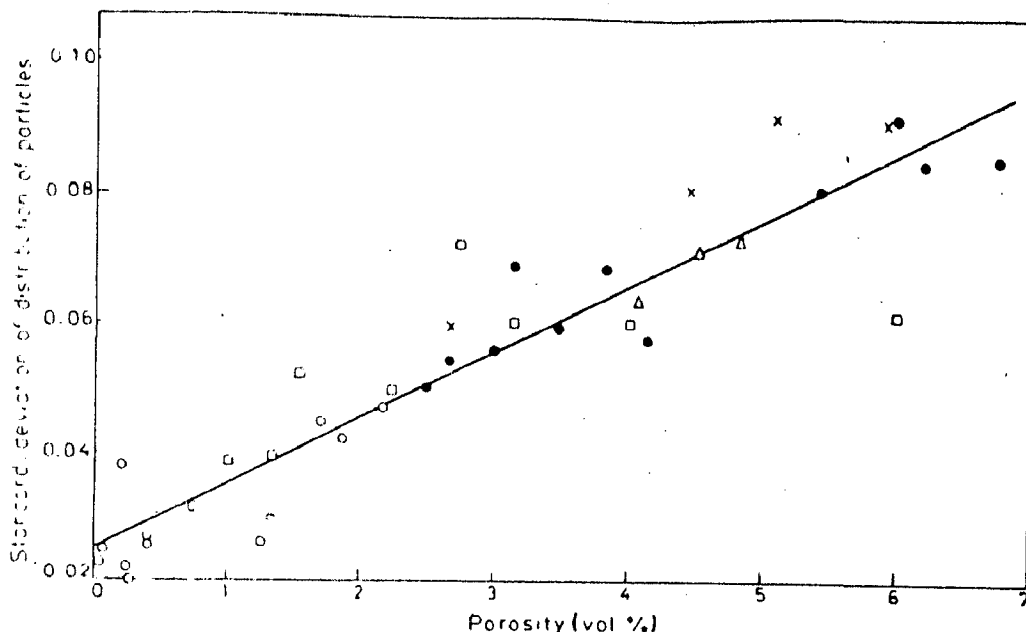
1668

Figure 3 Effect of standard deviation of distribution of particles on the porosity content of the composite. Approximate volume percentage of alumina (○) 1.6 ± 0.2, (□) 5.6 ± 0.3, (●) 9.5 ± 0.45, (×) 11.0 ± 0.5, (△) 14.6 ± 0.4

spectrum of sizes (as given in Table 1) The c_i of the composites increases linearly with a decrease of porosity content, but only up to a certain limit. The nature of the curves can approximately be described by the equation

$$c_i = c + m\,P \qquad (2)$$

where c and m are constants. The slope of the line, m, increases with an increase in the alumina content of the composite as shown in Fig. 14 However, the value of c decreases linearly with an increase in the alumina content as shown in Fig 15. The linear nature of the c_i against $1/P$ curve is violated when the porosity is reduced below a critical level depending on the alumina content. A further reduction in porosity lowers c_i, as is evident for the composites containing 0.77, and 1.5 and 9.0 vol % alumina.

4. Discussion

The level of porosity in a compocast composite is directly correlated with the inhomogeneity in particle distribution. It has been observed from microscopic investigations that a well-separated particle does not

generally have a void at the interface, but a cluster of particles often has voids. During particle addition in the semi-solid melt the stirring employed creates a negative pressure at the centre of the stirrer, and air bubbles are sucked into the melt along with a few particles. The particles may subsequently get transferred from the bubble to the melt and the bubble floats to the top. In the case of certain bubble-particle configurations, particle transfer from the bubble may not be dynamically feasible and clusters of particles are observed in the microstructure along with voids. There may be clusters without voids resulting from sintering together of the particles. However, the increase in porosity with a tendency for clustering shows the former mechanism of cluster formation to be the dominant one. It is evident from Fig. 3 that a higher level of porosity results from an increased tendency for particle clustering. In addition, these clusters with voids are creating inhomogeneous regions of weakness.

The contribution of porosity to the tensile strength of a material has been estimated grossly as a weakening effect caused by the formation of a weakened zone

Figure 4 Scanning electron micrograph showing bonding of alumina particle with the matrix

Figure 5 Scanning electron micrograph showing debonding of particle-matrix interface and presence of voids in the matrix.
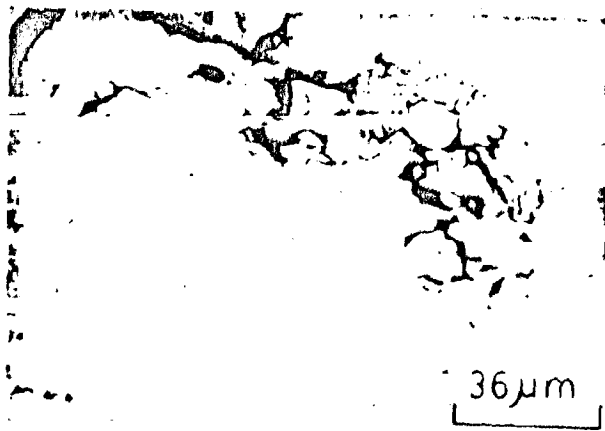
Figure 6 Nature of a crack path in a composite fractured under tensile loading

Figure 8 Effect of porosity content on engineering stress strain curve of a particulate composite. Approximate porosity (vol %). (A) 0.76, (B) 0.82, (C) 0.95, (D) 1.5, (E) 6.0. Content of $Al_2O_3 \sim 1.92$ vol %.

around a spherical pore, and is given by Equation 1. The equation is derived by assuming that the pore has no damaging effect on the load-bearing capacity of a material beyond a certain distance $R_p = nr_p$ from the pore, where r_p is the average effective radius of the pore and n is a constant having a value greater than unity which is primarily dependent on the mechanical characteristics of the material. The weakening of the material also depends on the geometry of the pore and on the the pore distribution. The average stress at $r = r_p$ is $k \sigma_m$ where k is a constant factor and σ_m is the stress in regions unaffected by the pore. The averaging is performed over the size distribution of the pores and the angles around the axis of loading. The weakening of the material will limit the value of k in the range $0 < k < 1$. The weakening factor x is a function of both the parameters n and k. Equation 1 is capable of estimating the contribution of the pore in the linear regime up to a porosity level P_c given by

$$P_c = 100/n^3 \qquad (3)$$

For a higher porosity level, Equation 1 is not effective because the stress distributions around pores start interfering with each other; this results in an effective pore–pore interaction term when R_p is greater than R, where R is the radius of the average volume of material per pore.
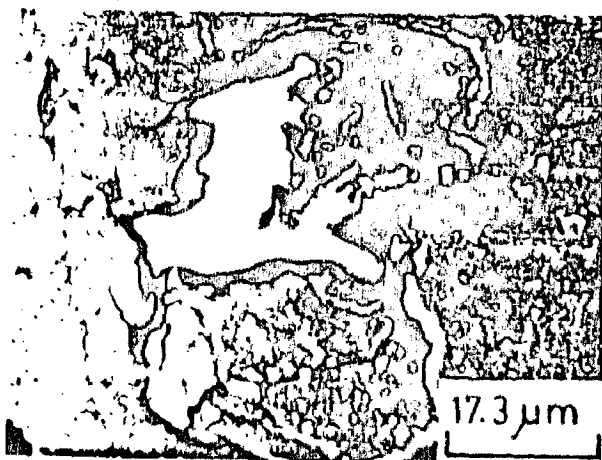

Figure 7 Scanning electron micrograph showing the formation of a reacted layer of irregular shape around an alumina particle.
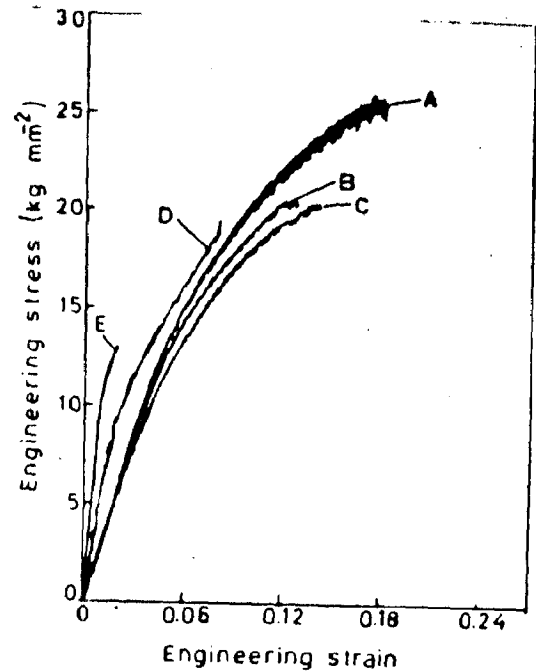
When the porosity is above a critical level depending on the alumina content of the composite, the correlation of the inverse of as-cast porosity with fracture strain shows a linear behaviour with coefficient exceeding 0.9, as shown in Fig. 13. In this range of porosity the failure is caused primarily by the growth and coalescence of pores confined primarily to the regions of particle cluster. The voids nucleated during deformation at the boundary between a well-bonded particle and the matrix are not responsible for the fracture of these composites. Fig. 5 clearly demonstrates extended voids created by the growth and linkage of pre-existing voids at the boundaries of alumina particles and microporosities away from the particles. However, Fig. 6 (showing the microstructure of a transverse section near the fractured surface) demonstrates that void growth and coalescence are confined to the inhomogeneous regions containing particle clusters with voids. The matrix away from this weak zone is relatively free from damage.

The serrated nature of the tensile stress–strain curve as given in Fig. 8 is an indication of continuing void coalescence over the range of strain. From the above discussion it is inferred that although debonding at the alumina–matrix interface might have taken place, the failure is primarily caused by existing voids as evident in Fig. 5. So the present approach to explaining the properties on the basis of a model incorporating the role of pre-existing pores is thus justified. The particles are assumed to exert only a secondary influence by modifying the parameters of the model Equation 1 for ultimate tensile strength.

The experimental observations presented in Fig. 9 show that the weakening factor α in a particulate composite decreases with the volume fraction of reinforcing alumina particles. Since the particles used for this set of experiments have the same broad

Figure 9 Variation of weakening factor with alumina content of the composite
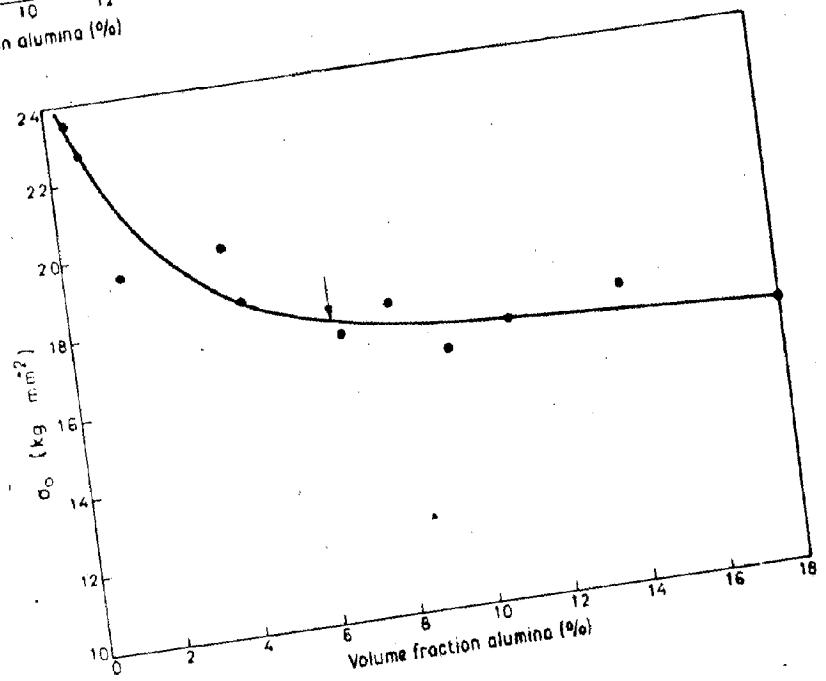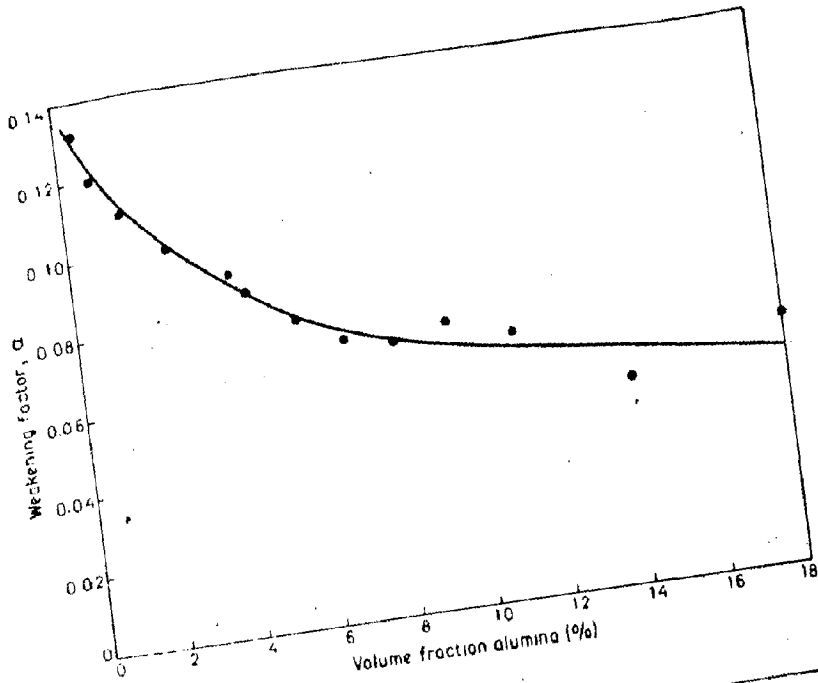

Figure 10 Effect of particle content on tensile strength of the composite at zero porosity. The arrow indicates the strength of Al-4.0wt% Mg without alumina, extrapolated to zero porosity.
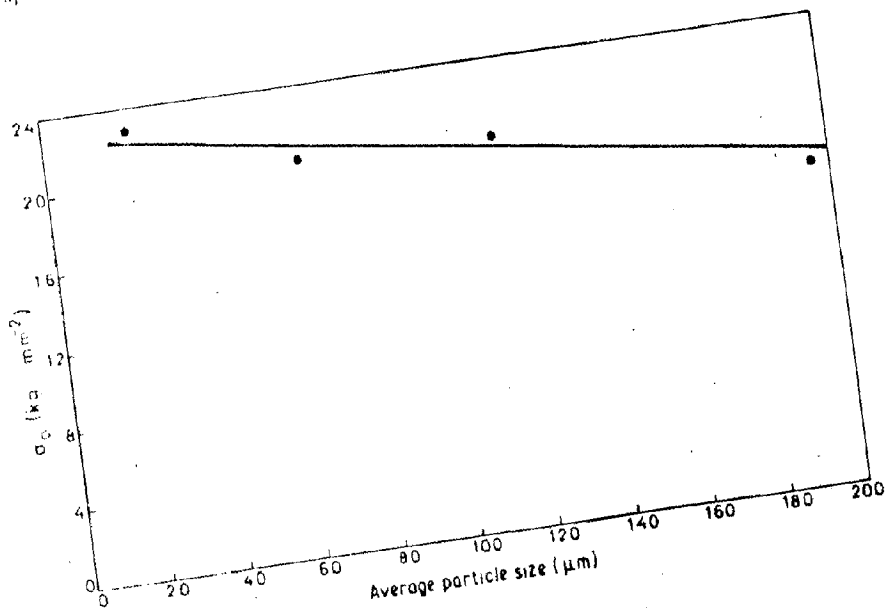

Figure 11 Effect of average particle size on tensile strength of the composite at zero porosity. Volume fraction of alumina ~8.62 ± 0.6%.
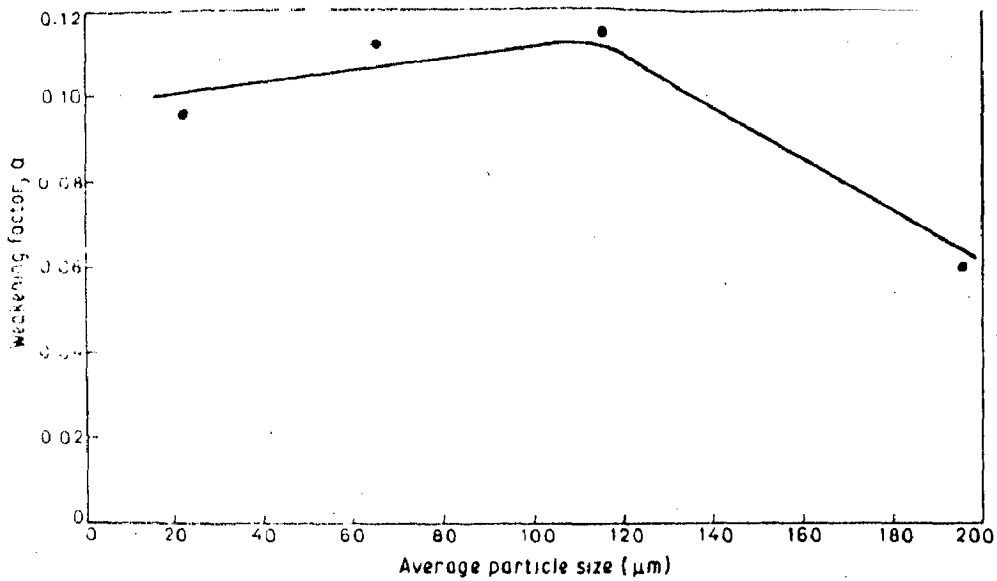
1671

Figure 12 Variation of weakening factor with average particle size in the composite. Volume fraction of alumina ~8.62 ± 0.6%.

spectrum of size distribution, so the increase in volume fraction indicates an increase in the number of particles per unit area of matrix. The spatial recovery of the load-bearing capacity will be affected by the presence of a foreign particle because of the modification in the stress distribution around it. Thus, both n and k may be modified to cause the observed lowering of the weakening factor α. However, this enhancement of α becomes less marked at higher particle content in the composites.

The lowering of tensile strength, σ_u, with an increase of the volume fraction of reinforced particles shown in Fig. 10 is caused by the nucleation of voids at the particle–matrix interface. The void is initiated in the particle–matrix interface at early stages of plastic deformation [4], and reduces the load-bearing

capacity of the material at a strain which falls with an increase in alumina content. Moreover the formation of $MgAl_2O_4$ [3] in irregular extended shapes with sharp corners is observed to create particularly susceptible areas for the generation of cracks as shown in Fig. 7. Fragmentation of brittle $MgAl_2O_4$ is commonly observed. However, the observed σ_0 of the composite is superior to the strength of the matrix at zero porosity level up to about 6.5 vol% alumina. Beyond this level of incorporation of alumina the room-temperature strength possibly degenerates.

From a consideration of the growth of voids under stress Brown and Embury [5] have given the criteria for estimating the critical strain, ε_u, at which the necking instability in the material between two growing voids will cause the joining of voids. This strain,
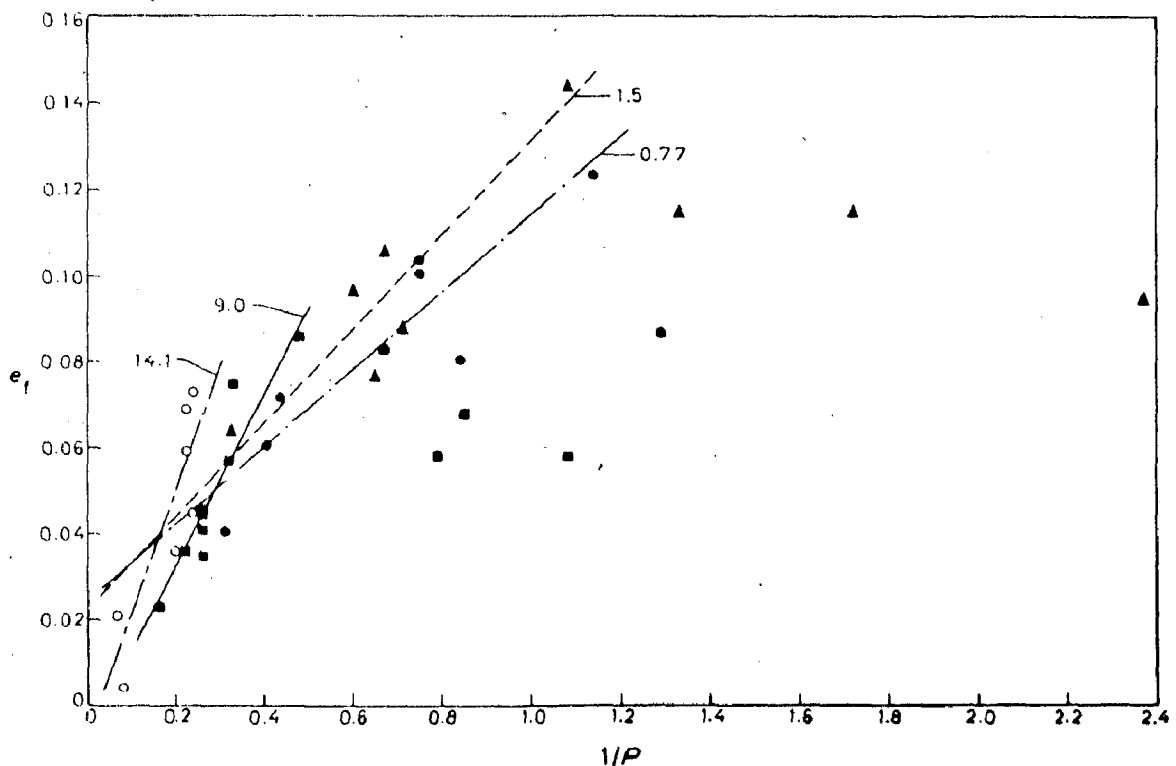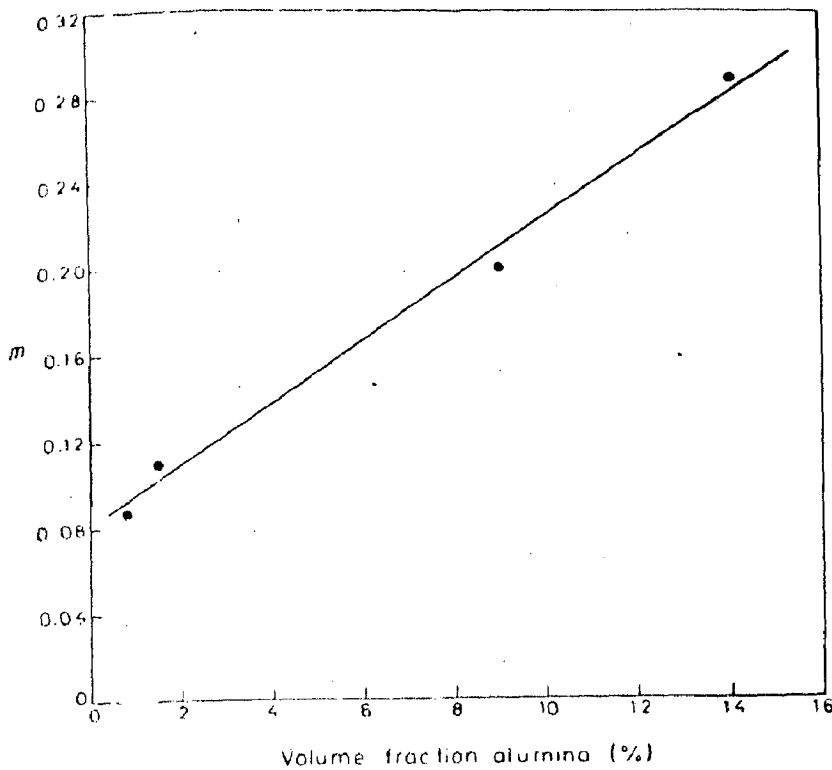

Figure 13 Effect of the inverse of volume percentage of porosity on engineering fracture strain for composites containing various volume fractions of alumina. Approximate volume percentage of alumina: (●) 0.77 ± 0.06, (▲) 1.50 ± 0.12, (■) 9.00 ± 0.42, (○) 14.10 ± 0.47.

together with the nucleating strain ε_n for the voids, will constitute the fracture strain. They proposed

$$1 + \varepsilon_p = \frac{1}{2}\left[\left(\frac{2\pi}{3f}\right)^{1/2} - \left(\frac{8}{3}\right)^{1/2}\right] \qquad (4)$$

where f is the volume fraction of particles, keeping the size of the particles constant. So it is expected that ε_p and the corresponding stress will decrease non-linearly with the volume fraction of particles, as observed in the behaviour of σ_u shown in Fig. 10. However, it must be remembered that in the cast materials with porosity this picture will be modified by the growth of already existing porosity, for which the nucleating strain is zero.

For the same volume fraction of particles, if the particle size is increased (i.e. interparticle spacing is reduced) one expects a delayed onset of the necking instability. However, the results shown in Fig. 11 show

a contrary trend which is in agreement with earlier investigations [4, 6] and can be explained in terms of a lower ε_n for the nucleation of voids around particles having a larger size. This effect, along with a larger initial size of the void, offsets the advantage gained by a larger interparticle spacing.

A small initial enhancement of the weakening factor x with an increase in the average particle size upto ~115 μm, as shown in Fig. 12, may be due to a decrease in the number of particles in the weakened zone. But the subsequent decrease in the value of x with an increase of particle size beyond ~115 μm indicates an important role of the particle in modifying the stress distribution of the weakened zone, thus resulting in a higher degree of recovery of the lost strength.

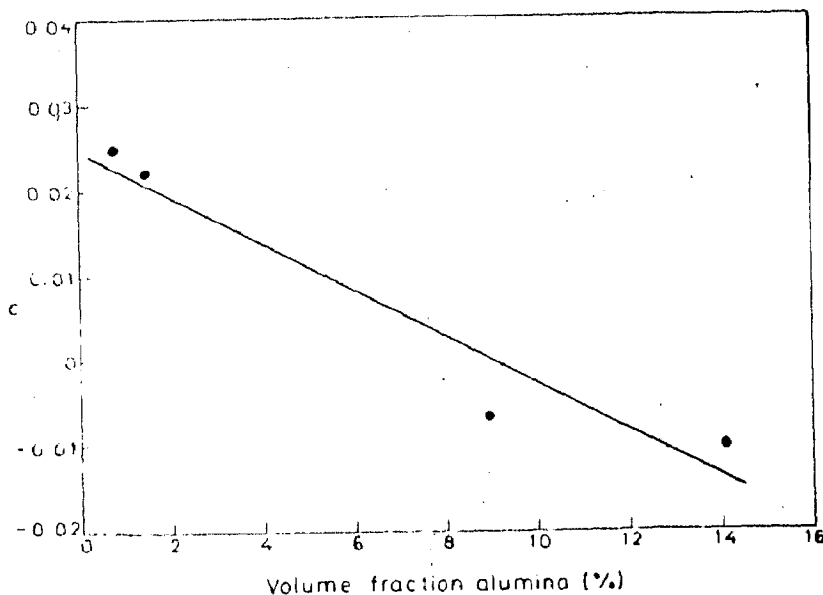The true fracture strain has been correlated with the inverse of the volume fraction of voids by several

authors [7 9]. The engineering fracture strain observed in the present investigation has been plotted against the inverse of porosity content (as shown in Fig 13) to identify the role of porosity in determining the fracture behaviour. Above a particular value of porosity the fracture strain increases almost linearly with the inverse of porosity. In this regime of porosity content, the variation of fracture strain with porosity has been represented by the Equation 2 and the particle content is found to influence both m and c as given in Figs 14 and 15, respectively. These figures indicate that the engineering fracture strain is higher for composites with a higher alumina content, resulting in higher values of m. The factor c, which makes a smaller contribution to e_i compared with m P and is distributed around zero, may have appeared because of a random error introduced by the limitations of our measurements.

References

1 P K GHOSH, S RAY and P K ROHATGI, *Trans. Jpn Inst. Metals* 25 (6) (1984) 440

2 P K GHOSH, P R PRASAD and S RAY, *Z. Metallkde* 75 (1984) 934

3 B F QUIGLEY, G J ABBASCHIAN, R WUNDERLIN and R WUNDERLIN and R MEHRABIAN, *Met. Trans.* 13A (1) (1982) 93

4 K TANAKA, T MORI and T NAKAMURA, *Phil. Mag.* 21 (1970) 267

5 L M BROWN and J D EMBURY, in Proceedings of 3rd International Conference on the Strength of Metals and Alloys, Cambridge, England, August 1973, "The Microstructure and Design of Alloys" (The Institute of Metals and Iron and Steel Institute, London, 1973) Vol. 1, p. 164

6 V M SERGUENKOVA, V P OLBINEN and V V OSASYEK, *Poroshkovaia Met.* 6 (1969) 81

7 T GLADMAN, B HOLMES and I D McIVOR, "Effect of Second-Phase Particles on the Mechanical Properties of Steel" (Institute of Metals, London, 1971) p. 68.

8 J F KNOTT, "Fundamentals of Fracture Mechanics" (Butterworths, London, 1973), Ch. 8.

9 B I EDELSON and W M BALDWIN, *Trans. Amer. Soc. Metals* 55 (1962) 230.

79. Onuki, J., Soeno, K. and Suwa, M., J. Japan Inst. of Metals, Vol.48, No.8, p. 765, (1978).

80. Dixit, D., and Agarwal, V., "Fabrication of Aluminium Base Composite by Foundry Technique", Trans. Japan Inst. of Metals, Vol.22, No.8, p. 521, (1981).

81. Keye, S., J. Vacuum Sci. Tech., No.11, p. 1114, (1974).

82. Berghezen, A., "Review of Composite Materials" Proc. Conf., Second Erupean Symposium on Material Sciences in Space, Frascati, Italy, p. 351, April, (1976).

83. Kelly, A., "Strong Solids", Clarendon Press-Oxford, (1973) .

84. Broutman, L.J. and Krock, R.H. (eds), "Modern Composite Materials", Addison - Wesley Publishing Co., (1967).

85. McG Tegart, W.J., "Principles of Composites", The J. of the Australian Inst. of Met., Vol. 16, No.4, p. 204, Dec. (1971).

86. Piggott, M.R., "Load-Bearing Fiber Composites", Pergamon Press, p. 141, (1980).

87. Chou, T.W. and Kelly, A., Annu. Rev. Mater. Sci., Vol. 10, p. 299, (1980).

88. Arsenault, R.J. and Fisher, R.M., "Microstructure of Fiber and Particulate SiC in 6061 Aluminium Composite", Scripta Met., Vol.17, No.1, p. 67, (1983).

89. Arsenault, R.J., "The Strengthening of Aluminium Alloy 6061 by Fiber and Platelet Silicon Carbide", Mater. Sci. and Engg., Vol.64, No.2, p. 171, (1984).

90. Piehler, H.R., "Plastic Deformation and Failure of Silver-Steel Filamentary", Trans. Metall. Soc. AIME, Vol. 233, p. 12, (1965).

91. Mileiko, S.T., "The Tensile Strength and Ductility of Continuous Fiber Composite", J. Mater. Sci., Vol. 4, No.11, p. 974, (1969).

92. Garmong, G. and Thompson, R.B., "A Theory for the Mechanical Properties of Metal-matrix Composites at Ultimate Loading", Met. Trans., Vol.4, p. 863, (1973).